

# **ON THE SPACE-TIME OCEAN CURRENT VARIABILITY AND ITS EFFECTS ON THE LENGTH-OF-DAY**

**N. T. CHRISTOU**

**September 1990**



**TECHNICAL REPORT  
NO. 148**

## PREFACE

In order to make our extensive series of technical reports more readily available, we have scanned the old master copies and produced electronic versions in Portable Document Format. The quality of the images varies depending on the quality of the originals. The images have not been converted to searchable text.

**ON THE SPACE-TIME OCEAN CURRENT  
VARIABILITY AND ITS EFFECTS ON THE  
LENGTH-OF-DAY**

Nikolaos Theodoros Christou

Department of Surveying Engineering  
University of New Brunswick  
P.O. Box 4400  
Fredericton, N.B.  
Canada  
E3B 5A3

September 1990

© N. T. Christou, 1990

## PREFACE

This technical report is a reproduction of a thesis submitted in partial fulfillment of the requirements for the degree of Doctor of Philosophy in the Department of Surveying Engineering, July 1990. The research was supervised by Dr. Richard B. Langley, and funding was provided by the Natural Sciences and Engineering Research Council of Canada.

As with any copyrighted material, permission to reprint or quote extensively from this report must be received from the author. The citation to this work should appear as follows:

Christou, N.T. (1990). *On the Space-Time Ocean Current Variability and its Effects on the Length-of-Day*. Ph.D. dissertation, Department of Surveying Engineering Technical Report No. 148, University of New Brunswick, Fredericton, New Brunswick, Canada, 333 pp.

## **ABSTRACT**

Earth Rotation (polar motion and length-of-day) studies have embarked on a new era with the contributions from space geodesy observation techniques (higher accuracy, higher temporal resolution) and the availability of new, global data bases of atmospheric and oceanic observables.

Irregular variations in the earth's rotation rate (length-of-day - LOD - variations) on time scales of 5 years or less are associated with changes in the angular momentum of the solid earth. The problem of transfer of angular momentum between the Earth System components (consisting of the solid earth, the oceans, and the atmosphere) has emerged today as a problem of great scientific interest, because of the geophysical and environmental implications associated with LOD variations.

This thesis research chiefly investigates the time-dependent perturbations of LOD on time scales of about two years or less, associated with the space-time fluctuations of the global ocean circulation. Estimates of the space-time variations of ocean currents were derived from both in-situ oceanographic data and two years of satellite altimetry observations from the GEOSAT Exact Repeat Mission.

A new technique for extracting ocean current variability from satellite altimetry was developed. The technique is based on the gradient operator and offers advantages over previously existing techniques on the recovery of oceanic variability in that it is conceptually simple and computationally efficient.

Through the analysis of ocean current variability, it is established that the oceanic excitation of LOD is at least at the level of 0.1 milliseconds. Variations in the oceanic excitation of  $\Delta LOD$  have been identified and quantified at periods of 1 year and 0.5 years. At the annual period, the results indicate that the oceanic excitation appears large enough to account for the existing discrepancy between the observed (non-tidal)  $\Delta LOD$  and the atmospheric contribution. No significant oceanic excitation of  $\Delta LOD$  is found at the semi-annual period. The results also indicate that there exist statistically significant higher frequency variations at approximately 121-day, 107-day, and 89-day periods.

The analysis of the GEOSAT altimetry data generated many new questions regarding the oceanic behaviour and its dynamical link to LOD variations that require further investigations.

# Table of Contents

Abstract.....	ii
List of Tables .....	vii
List of Figures .....	viii
Abbreviations .....	xii
Acknowledgements .....	xv
<b>Chapter 1: Introduction.....</b>	<b>1</b>
1.1. Earth Rotation and Length-of-Day .....	2
1.2. Atmosphere - Ocean - Solid Earth System .....	6
1.3. The Ocean Environment .....	8
1.3.1. The Dynamic Ocean.....	10
1.4. Research Objectives: The Problem at Issue.....	12
1.5. Research Contributions.....	15
1.6. Dissertation Outline .....	17
<b>Chapter 2: Earth Rotation - Length-of-Day Concepts .....</b>	<b>21</b>
2.1. Preamble.....	22
2.2. Basic Concepts and Relationships.....	23
2.2.1. Rotational Motion of a Deformable Earth-Fundamental Relations.....	24
2.3. Requirements for Precision LOD.....	33
2.4. Current Status of LOD Research .....	35
2.4.1. Contemporary LOD Observational Techniques.....	36
2.4.2. Short-Term Geophysical LOD Excitation: Current Status.....	40
2.4.3. Oceanic Excitation of Short-term LOD Variations.....	45
<b>Chapter 3: Ocean Dynamics - Oceanic Variability .....</b>	<b>50</b>
3.1. Preliminaries .....	50
3.2. General Ocean Circulation.....	52
3.3. Geostrophic Flow and Ocean Dynamic Topography.....	58
3.4. Classical Oceanographic Description of Oceanic Circulation.....	66
3.5. Oceanic Variability in Space and Time.....	70
3.6. Ocean Dynamics Modelling Techniques.....	76
3.7. Summary .....	80

<b>Chapter 4: Satellite Altimetry</b> .....	82
4.1. Preliminary Considerations .....	82
4.2. Radar Altimetry .....	85
4.2.1. Satellite Altimetry Errors .....	88
4.3. Satellite Altimetry Geometrical Considerations .....	92
4.4. Satellite Altimetry and Orbits.....	97
4.5. Ocean Dynamics Information from Satellite Altimetry.....	99
4.6. Techniques for Studying Temporal Variations of SST .....	107
4.6.1. Overlapping Pass Analysis.....	109
4.6.2. Mean Sea Surface Models.....	112
4.6.3. Cross-over Differences Method .....	113
4.6.4 New Developments .....	113
4.7. Summary .....	114
<b>Chapter 5: Oceanic Variability Results from Classical Oceanographic Descriptions</b>	116
5.1. Description of Specific Volume Data Sets.....	118
5.2. Data Processing and Analysis.....	120
5.2.1. Computation of Specific Volume Anomaly .....	120
5.2.2. Dynamic Topography Computations.....	130
5.3. Mean Seasonal Dynamic Topography Fields for the Global Ocean .....	131
5.4. Space-Time Variability of the Quasi-Permanent Ocean Dynamic Topography....	146
5.5. Mean Seasonal Geostrophic Currents Derived from the Quasi-Permanent Ocean Dynamic Topography Fields.....	152
5.6. Preliminary Conclusions .....	154
<b>Chapter 6: Ocean Surface Dynamics from GEOSAT / ERM Altimetry</b> .....	156
6.1. General Overview of the GEOSAT Mission .....	157
6.2. GEOSAT / ERM Geophysical Data Record (GDR).....	160
6.3. GEOSAT / ERM Data Base Used in This Thesis Work .....	164
6.4. Our Philosophy of How to Obtain Ocean Current Variability from Satellite Altimetry.....	165
6.5. GEOSAT GDR Pre-processing.....	173
6.6. Further Analysis of Orbital Errors.....	183
6.7. Data Analysis Techniques .....	186
6.8. Ocean Current Variability from the GEOSAT / ERM Data Set.....	196
6.9. Summary .....	206
<b>Chapter 7: The Estimation of Relative Oceanic Angular Momentum</b> .....	209
7.1. Basic Relationships .....	210
7.2. ROAM Estimates from the Quasi-Permanent Ocean Circulation.....	215
7.3. ROAM Estimates from the Time-Variable Ocean Circulation .....	222
7.4. The ROAM Time Series .....	225
<b>Chapter 8: The ROAM, RAAM, and LOD Time Series</b> .....	233
8.1. The LOD Time Series.....	234
8.2. The RAAM-Wind Time Series.....	235



8.3.	Comparison Between Observed LOD Fluctuations and Inferred Ones from the RAAM and ROAM Time Series .....	243
8.3.1.	Frequency Domain Comparisons.....	252
8.4.	Spectral Analysis Results and Intercomparisons .....	262
<b>Chapter 9:</b>	<b>Discussion, Conclusions, Future Considerations.....</b>	<b>273</b>
9.1.	Summary of Research Investigations .....	274
9.2.	Discussion of the Derived LOD Results .....	276
9.3.	Future Research Issues .....	280
<b>REFERENCES</b>	.....	<b>285</b>
<b>APPENDIX I</b>	.....	<b>301</b>
<b>APPENDIX II</b>	.....	<b>324</b>
<b>APPENDIX III</b>	.....	<b>326</b>

# List of Tables

<b>Table 5.1.</b>	Standard Depth Levels.....	119
<b>Table 6.1.</b>	Geophysical Data Record Contents .....	163
<b>Table 6.2.</b>	Cumulative Statistical Summary of Edited Records.....	177
<b>Table 7.1.</b>	Axial Relative Oceanic Angular Momentum (ROAM) Results .....	218
<b>Table 8.1.</b>	Differenced Time Series Spectral Analysis Results .....	263
<b>Table 8.2.</b>	Differenced Time Series Spectral Analysis Results .....	264
<b>Table 8.3.</b>	Spectral Analysis Results with Step-like Function Removed.....	265

# List of Figures

<b>Fig. 3.1.</b>	Graphical summary of the frequency - wavelength regions of some important dynamic processes in the ocean.....	55
<b>Fig. 4.1.</b>	Schematic illustration of fundamental geometric relations involved in satellite altimetry measurements .....	93
<b>Fig. 4.2.</b>	Graphical illustration of the inverse relationship between spatial and temporal resolution of satellite altimetry measurements.....	105
<b>Fig. 5.1a.</b>	Specific volume data-void grid cells at 500 dbar (level 14 of Table 5.1) for all four seasons .....	121
<b>Fig. 5.1b.</b>	Specific volume data-void grid cells for the 1000 dbar pressure surface .....	122
<b>Fig. 5.1c.</b>	Specific volume data-void grid cells for the 2000 dbar pressure surface .....	123
<b>Fig. 5.2a.</b>	Global Mean Seasonal Dynamic Topography Maps relative to 500 dbar .....	136
<b>Fig. 5.2b.</b>	Global Mean Seasonal Dynamic Topography Maps relative to 1000 dbar .....	137
<b>Fig. 5.2c.</b>	Global Mean Seasonal Dynamic Topography Maps relative to 2000 dbar.....	138
<b>Fig. 5.3a.</b>	Global Mean Annual Dynamic Topography Maps relative to 500 dbar computed from the mean seasonal maps (Figures 5.2) as the arithmetic average of the four seasons.....	139
<b>Fig. 5.3b.</b>	Global Mean Annual Dynamic Topography Maps relative to 1000 dbar computed from the mean seasonal maps (Figures 5.2) as the arithmetic average of the four seasons.....	140
<b>Fig. 5.3c.</b>	Global Mean Annual Dynamic Topography Maps relative to 2000 dbar computed from the mean seasonal maps (Figures 5.2) as the arithmetic average of the four seasons.....	141

Fig. 5.3d.	Annual Mean Dynamic Topography at 500 dbar relative to 1000 db.....	142
Fig. 5.3e.	Annual Mean Dynamic Topography at 1000 dbar relative to 2000 db.....	143
Fig. 5.4a.	Mean Seasonal Difference-Maps of Dynamic Topography for the global ocean relative to 500 dbar.....	148
Fig. 5.4b.	Mean Seasonal Difference-Maps of Dynamic Topography for the global ocean relative to 1000 dbar pressure surface.....	149
Fig. 5.4c.	Mean Seasonal Difference-Maps of Dynamic Topography for the global ocean relative to 2000 dbar pressure surface.....	150
Fig. 6.1.	GEOSAT GDR ground-track on Day 312 of ERM01 (November 8, 1986). Points on land and other dubious data records have been already removed.....	162
Fig. 6.2.	Five-day Average Significant Wave Height (SWH) Map.....	180
Fig. 6.3.	The figure displays the GEOSAT 5-day ground-track coverage that was used to generate the SWH maps shown in Figure 6.2.....	181
Fig. 6.4a.	Radial orbit differences between the NAG and GSFC/CCAR generated GEOSAT orbits for November 8, 1986, in units of metres.....	185
Fig. 6.4b.	The least squares spectrum of the NAG minus GSFC/CCAR radial orbital differences.....	187
Fig. 6.5.	Ascending/Descending pixel track geometry.....	194
Fig. 6.6a.	One-degree zonal average current variability during the first 22 ERMs.....	199
Fig. 6.6b.	One-degree zonal average current variability, for ERMs 22 to 44.....	200
Fig. 6.7.	Contour plot of the 2-year long 1-degree zonally averaged variability of ocean currents.....	201
Fig. 6.8.	Monthly mean values of the Tahiti - Darwin SOI for the period November 1986 - December 1988.....	204
Fig. 7.1.	Relative oceanic angular momentum (axial ROAM) budget computed for different integration limits for all seasons and the annual mean, in units of $10^{25} \text{ kg m}^2 \text{ s}^{-1}$ .....	217
Fig. 7.2a.	Global Axial Relative Oceanic Angular Momentum.....	226
Fig. 7.2b.	Monthly Values of Southern Oscillation Index (SOI).....	226
Fig. 7.2c.	Northern Hemisphere Axial Relative Oceanic Angular Momentum.....	227

<b>Fig. 7.2d.</b>	Southern Hemisphere Axial Relative Oceanic Angular Momentum.....	227
<b>Fig. 7.2e.</b>	North Tropics Axial Relative Oceanic Angular Momentum.....	228
<b>Fig. 7.2f.</b>	South Tropics Axial Relative Oceanic Angular Momentum.....	228
<b>Fig. 7.2g.</b>	ACC 65°S - 45°S Axial Relative Oceanic Angular Momentum.....	229
<b>Fig. 8.1a.</b>	VLBI $\Delta$ LOD Data Series : November 1986 - December 1988.....	236
<b>Fig. 8.1b.</b>	VLBI $\Delta$ LOD Data Series : November 1986 - December 1988 : Mean value removed .....	237
<b>Fig. 8.2a.</b>	NMC Wind Data : November 1986 - December 1988 : Axial Relative Atmospheric Angular Momentum : GLOBAL, NH, SH, (100 mbar) .....	240
<b>Fig. 8.2b.</b>	NMC Wind Data : November 1986 - December 1988 : Axial Relative Atmospheric Angular Momentum : GLOBAL, NH, SH, (50 mbar).....	241
<b>Fig. 8.2c.</b>	NMC Wind Data : November 1986 - December 1988 : Axial Relative Atmospheric Angular Momentum Differences (50 minus 100 mbar) .....	242
<b>Fig. 8.3a.</b>	Equivalent $\Delta$ LOD derived from RAAMW050 .....	244
<b>Fig. 8.3c.</b>	Equivalent $\Delta$ LOD derived from ROAM .....	245
<b>Fig. 8.3d.</b>	Equivalent $\Delta$ LOD derived from RAAMW050 minus RAAMW100.....	246
<b>Fig. 8.3e.</b>	Equivalent $\Delta$ LOD derived from RAAMW050 minus RAAMW100.....	247
<b>Fig. 8.3f.</b>	Equivalent $\Delta$ LOD derived from RAAMW050 minus RAAMW100.....	248
<b>Fig. 8.3h.</b>	Residual $\Delta$ LOD Data for the period November 1986 to December 1988. Residual = $\Delta$ LOD minus Equivalent $\Delta$ LOD computed from RAAM up to 50 mb .....	249
<b>Fig. 8.3g.</b>	Residual $\Delta$ LOD Data for the period November 1986 to December 1988. Residual = $\Delta$ LOD minus Equivalent $\Delta$ LOD computed from RAAM up to 100 mb.....	250
<b>Fig. 8.4a.</b>	Time Series Spectrum Following the Spectral Analysis of $\Delta$ LOD for the period November 1986 to December 1988 after the removal of bias and linear trend.....	254

<b>Fig. 8.4b.</b>	Time Series Spectrum Following the Spectral Analysis of RAAMW050 for the period November 1986 to December 1988 after the removal of bias and linear trend .....	255
<b>Fig. 8.4c.</b>	Time Series Spectrum Following the GEOSAT Analysis of 44 ERM's for the period November 1986 to December 1988 after the removal of bias and linear trend .....	256
<b>Fig. 8.4d.</b>	Time Series Spectrum Following the Spectral Analysis of ROAM Equivalent $\Delta$ LOD for the period November 1986 to December 1988 after the removal of 2 biases and a linear trend .....	257
<b>Fig. 8.4e.</b>	Time Series Spectrum Following the Spectral Analysis of SOI (Tahiti - Darwin) for the period November 1986 to December 1988 after the removal of bias and linear trend .....	258
<b>Fig. 8.5.</b>	Time Series Spectrum Following the Spectral Analysis Results (superposition plot) for the period November 1986 to December 1988 after the removal of bias, linear trend, and seasonal frequencies .....	266
<b>Fig. 8.6.</b>	Time Series Spectrum Following the Spectral Analysis of ROAM Equivalent $\Delta$ LOD for the period November 1986 to December 1988 after the removal of 2 biases, a linear trend, and seasonal frequencies .....	267

## Abbreviations

ACC	Antarctic Circumpolar Current
AGC	automatic gain control
AAM	atmospheric angular momentum
AM	angular momentum
BIH	Bureau International de l'Heure
CCAR	Colorado Center for Astrodynamics Research
CSTG	commission on international Coordination of Space Techniques for Geodesy and Geophysics
DTM	digital terrain model
$\Delta$ LOD	excess length-of-day
$\Delta$ RAAM	variations of relative atmospheric angular momentum
$\Delta$ ROAM	variations of relative oceanic angular momentum
EAMF	effective angular momentum functions
ECMWF	European Centre for Medium-range Weather Forecasting
EGCM	eddy-resolving general circulation model
EIS	earth integrated system
EKE	eddy kinetic energy
EM-bias	electromagnetic bias
ENSO	El Nino - Southern Oscillation
EOF	empirical orthogonal function
ER	earth rotation
ERM	Exact Repeat Mission
ERP	earth rotation parameters

ES	earth system
FNOC	Fleet Numerical Oceanographic Center
GCM	general circulation model
GDR	geophysical data record
GEOSAT	GEOdetic SATellite
GSFC	Goddard Space Flight Center
IAG	International Association of Geodesy
IEMSS	instantaneous electromagnetic mean sea surface
IERS	International Earth Rotation Service
IES'80	International Equation of State of 1980
IMSS	instantaneous mean sea surface
IPMS	International Polar Motion Service
IRIS	International Radio Interferometric Surveying
ISSH	instantaneous sea surface height
ISST	instantaneous sea surface topography
IUGG	International Union of Geodesy and Geophysics
JMA	Japanese Meteorological Agency
JPL	Jet Propulsion Laboratory
LLR	lunar laser ranging
LOD	length-of-day
LSSA	least squares spectral analysis
MERIT	Monitoring Earth Rotation and Intercomparison of Techniques of observations and analysis
MODE	Mid-Ocean Dynamics Experiment
NAG	Navy Astronautics Group
NH	northern hemisphere
NMC	National Meteorological Center (USA)
NOAA	National Oceanic and Atmospheric Administration (USA)



NODC	National Oceanographic Data Center (USA)
NSWC	Naval Surface Weapons Center
OAM	oceanic angular momentum
POD	precise orbit determination
PSS'78	Practical Salinity Scale of 1978
QBO	Quasi-Biennial Oscillation
Q-P SST	quasi-permanent sea surface topography
RAAM	relative atmospheric angular momentum
RISSH	residual instantaneous sea surface height
ROAM	relative oceanic angular momentum
SLR	satellite laser ranging
SOI	Southern Oscillation Index
SSH	sea surface height
SSt	sea surface temperature
SST	sea surface topography
SWH	significant wave height
TOGA	Tropical Ocean and Global Atmosphere
TOPEX	TOPographic EXperiment satellite
TTt	tropical tropospheric temperature
UKMO	United Kingdom Meteorological Office
VLBI	very long baseline interferometry
WOCE	World Ocean Circulation Experiment
XBT	eXpendable BathyThermograph

## Acknowledgements

The research reported here was financially supported in part by operating grants from the Canadian Natural Sciences and Engineering Research Council (NSERC) held by Prof. Dr. R. B. Langley.

Over the years of my graduate studies, I have also received financial assistance through contract research and other operating grants held by faculty members of the Surveying Engineering Department of U.N.B., as well as through graduate teaching assistantships. For all this long-lasting financial support, I am truly grateful to both the Department of Surveying Engineering and individual faculty members.

Dr. R. B. Langley, my research supervisor, deserves credit for his support during the years of my doctoral studies. I have enjoyed a lot of freedom in pursuing research off the main course of my dissertation. Sometimes he tolerated these excursions sometimes not. Overall, I owe him a big Thank You.

It would be unfair not to extend my sincere thanks to Dr. A. Kleusberg. He frequently served as a sounding board to my research thoughts. A lot of times I used as a sounding board the Surveying Engineering Geodesy/Hydrography Group. I wish that it will al-

ways be there as a forum for the SE graduate students to voice their research findings, struggles and frustrations. It has been a driving force for me.

There are also certain individuals that have directly or indirectly helped in the completion of this research by providing valuable data. Dr. J. R. Wilson and Mr. D. Spears of the Marine Environmental Data Service (MEDS) of the Department of Fisheries and Oceans made possible the acquisition and continuous flow of the GEOSAT/ERM altimetry data. Dr. D. Delikaraoglou of the Geodetic Survey of Canada made available the GEOSAT/ERM orbit replacement programs developed by GSFC/CCAR. Drs. D. Salstein of the Atmospheric Environmental Research Inc., Cambridge, MA, provided the atmospheric angular momentum and excess length-of-day VLBI data. The assistance and cooperation of the above individuals is gratefully acknowledged.

I owe a great deal to the UNB Computing Centre. Without the ample computing resources that were accessible to me, this research would have never been finished in a such a short time.

I am also indebted in many ways to many more men and women, who either through their books, or public lectures, or through their research articles extended my knowledge to where it stands today.

Deeper, however, than to anyone else is my debt to my wife Vassoula, my son Theodore and my daughter Anna. There is nothing that can compensate for all those priceless hours and days that I spent away from them in the pursuit of a personal goal

in my life. Thinking of them while being thousands of kilometres away was the only thing that kept me working even through the gray, early morning hours.

# Chapter 1: Introduction

Interactions between the earth and other astronomical bodies, as well as among the atmosphere, the oceans, the crust and the inner parts of the earth, perturb the earth's rotation (ER) to varying degrees from that of an ideal rigid body. Variations in earth rotation are detected by observing the apparent motion of objects in space from fixed points on earth.

Today, astronomic as well as geodetic extra-terrestrial observations have revealed a wide spectrum of time-dependent perturbations in earth rotation, which, without any loss of rigour, can be conveniently separated into polar motion and length-of-day (LOD) components. Commonly called the Earth Rotation Parameters (ERP), they correspond to: (a) the two coordinates of the earth's rotation axis in some earth-fixed reference frame with respect to the terrestrial pole of reference, and (b) to the value of an angle around the rotation axis [*Capitaine, 1986*].

In this research work we are chiefly interested in the latter aspect of the earth's rotation, i.e., the earth's rate of rotation and more specifically in its time variations. In simple words, we are interested in departures of the earth's rotation rate from uniformity, and more particularly in those variations associated with changes in the ocean circulation.

A thorough understanding of all aspects of the earth's variable rotation requires knowledge of a multitude of scientific fields such as geodesy, solid earth physics (geophysics), atmospheric physics (meteorology), ocean physics (oceanography), hydrology, fluid dynamics, theoretical mechanics, etc. Therefore, the study of the earth's variable rotation calls upon a considerable number of scientists and a variety of observation, analysis and interpretation methods and techniques in an attempt to elucidate the causes and mechanisms responsible for the variations. In all modesty, only a few of the above mentioned scientific fields will be addressed in this thesis in order to provide the necessary ties to our investigation. Mostly we will concentrate on geodesy and physical oceanography as the disciplines that can provide the essential observational information for our LOD investigations. Realistically, our problem will be 4-dimensional; we will tackle the problem of space-time ocean current variability and attempt to transform this information into associated changes in the earth's rotation rate.

## **1.1. Earth Rotation and Length-of-Day**

Until the 1930's the earth was universally considered as the best "time keeper"; in fact, its rotational velocity was taken as constant. It was the decisive contributions of Spencer Jones in the late 1930's which changed in a convincing manner the notion of the "best time keeper" [Mignard, 1986; Lambeck, 1980]. As accuracy of astronomical observations and clocks increased over the subsequent years, the ability to detect variations in the earth's angular speed and consequently variations in LOD, increased considerably too.

In the past 10 to 15 years, highly precise measurements of the ERPs and new global geophysical data bases have become available, thus allowing major advancements to be made toward the understanding of the various causes responsible for the irregularities in ER. Today's observational techniques for ERP determinations consist of classical astrometric methods, artificial satellite tracking techniques (Satellite Laser Ranging -SLR-, Doppler tracking), Lunar Laser Ranging -LLR- and Very Long Baseline Interferometry -VLBI-. These techniques provide observations suitable for investigating the short-term irregularities (few years and less) in ER. Observation of recent, historical and even ancient eclipses provide information about the long-term irregularities in ER (several years to centuries).

The accuracies of the results obtained from geodetic extra-terrestrial techniques indicate that LOD can be determined today at the level of 0.05 to 0.10 milliseconds (and 0.002 arcsec or better, for polar motion) from averages of 3-5 days, with further improvement expected when longer averaging times are used [Wahr, 1988].

Rotational dynamics of deformable bodies provide the theoretical foundation for writing the equations of motion of the rotating Earth System (ES) -atmosphere / ocean / solid earth (crust and mantle). The so-called *Liouville equations* are used to represent the dynamic earth, and to describe the conservation of angular momentum of the ES and to relate the departures of the ES from the behaviour of an ideal rigid body. It is common practice to decouple the departures in the rotation rate from uniformity ( $\Delta LOD$ ), from the motion of the rotation axis with respect to the surface of the earth (*polar motion*), thus modelling  $\Delta LOD$  separately.

The implication of the *Liouville equations* for LOD is that changes in earth rotation can be produced by external torques, by redistribution of mass within the ES, and by motion of material within the ES. The latter aspect, pertinent to the oceanic component of the ES, constitutes the heart of the problem set to be investigated in our research.

The behaviour of the observational results for the LOD fall into three (3) broad classes [Wahr, 1988; Lambeck, 1980; Munk & MacDonald, 1960]:

- (i) a linear increase in LOD of about 2 *ms/cy* (secular variations);
- (ii) irregular fluctuations of about 4 to 5 *ms* / 10 – 30 *yr* (decadal and longer period variations); and,
- (iii) those variations with periods shorter than about 5 to 7 years (short-term periodic with magnitudes of the order of 0.5 to 1.0 *ms* and short-term irregular variations with magnitudes sometimes exceeding 1.0 *ms*).

Models of the observed variability of the earth's rotation require an identification of the internal or external mechanisms driving the variability, plus knowledge of the transfer functions that describe the rotational response of the solid earth to the applied disturbances. Inferences about the source mechanism, or the transfer function, shed light on the dynamical behaviour of the earth and its environment. The observed LOD fluctuations then, can be used to learn more about the excitation process, which in turn can lead to better the understanding of the earth's deformational response, and this circular process can be carried on and on.

A very brief interpretation of the mechanisms associated with the LOD variations follows. Most of the observed linear trend in LOD is attributed to tidal action of the moon upon the solid earth and oceans; therefore, there is a perpetual transfer of spin angular momentum (AM) from the earth into orbital AM of the moon [Wahr, 1988; Lambeck,



1980; *Munk & MacDonald*, 1960]. The discrepancies of the observed LOD linear trend from the expected linear increase in LOD due to tidal dissipation, are today attributed to mechanisms internal to the earth, that cause an acceleration of the earth (i.e., decrease in LOD). The implicated mechanism is the one of post-glacial rebound, whereby the net transfer of material (uplift of land masses) within the earth modifies its polar moment of inertia (it decreases) and hence modifies the rotation rate of the earth (it increases).

Transfer of AM between the earth's fluid core and solid mantle is believed to be the source of the decadal fluctuations in the LOD. The mechanism by which AM is imparted from one to the other is still under debate. One mechanism put forth is electromagnetic forcing, an alternative being topographic coupling, caused by fluid pressure acting against topography at the core-mantle boundary.

The short-term variability spectrum of LOD is by far the richest one. There is a whole spectrum of tidal terms in LOD, from 5.64 days through 18.6 years [*Yoder et al.*, 1981]. The tidal action of the moon is the source of most of the observed amplitudes at the monthly and fortnightly periods, while the moon's and sun's tidal action is appreciable at the seasonal (annual and semi-annual) periodicities. This spectrum is enriched by large amplitude 6- and 12-month periodic terms and irregular variations such as the nearly biennial oscillation and the near 50-day oscillation due to atmospheric influences. Most of the annual and semi-annual variability due to atmospheric processes (about 70%), is associated with the action of the forcing winds. The interplay between the solid earth and atmospheric winds is accomplished by a combination of surface friction torques and mountain torques. Global atmospheric pressure also contributes

to the seasonal variations of LOD by modifying the atmospheric polar moment of inertia.

It appears that the atmosphere is responsible for most of the short-term irregular variations in LOD as well. This conclusion has been reached from analyses of atmospheric wind data and has been the main subject of interest in recent LOD studies. While global ground-water storage variations are believed to contribute negligibly to LOD seasonal variations, the contribution of ocean current variability (mostly attributed to the Antarctic Circumpolar Current - ACC) is believed to be only about 5 to 10 percent of the total observed LOD variability at the seasonal periods [*Lambeck & Hopgood, 1982; Wahr, 1983; Eubanks et al., 1985*]. However, no comprehensive observed ocean current variability data have been incorporated in the studies reported so far. This fact also constitutes one of the dominant motivations of the research conducted here.

In summary, there is at least some general understanding of what causes most of the various observed fluctuations in LOD. Some aspects are understood well, others have missing details. In this thesis we set out to illuminate some of the details regarding the oceanic component of the ES, and learn more about the earth and its wet fluid environment.

## **1.2. Atmosphere - Ocean - Solid Earth System**

Ever since primitive man started to ask questions about his living environment, he became interested in its form, structure and the natural phenomena he observed around him. In his myth-making stage of development he started to speculate about the origin

and integral components of the world surrounding him. Later on the speculation became a philosophical hypothesis until this was replaced by scientific theory in an effort to unravel the actual facts of creation and evolution of the Earth System.

The concept of the Earth System as an integral, composite system consisting of the atmosphere, the hydrosphere and the land masses (the “habitable world”), dates back to early civilizations. Thales of Miletus conceived the earth as a disk-like body floating in an infinite *Ocean* which bounds the habitable world. The Pythagorean school of philosophy upheld the spherical- as opposed to the flat-earth shape. Empedocles hypothesized that everything is made out of four eternal, indestructible and unchangeable elements: fire, air, earth and water. It is here that we see the Earth System in the form of “absolute elements”. It was Heraclitus who postulated that phenomena exist in a constant change of flux, always tending to assume new forms, a new state.

Earth science has traditionally advanced through studies of its individual components: atmosphere, hydrosphere / cryosphere, the earth's crust and interior, biosphere. The concepts of our planet's time history and evolution are undergoing unification as scientists explore and study the Earth System on scales from the global to the sub-microscopic.

Studies of the earth's components over the past 30 years or so have revealed an extremely complex and dynamic world. Recent research is clarifying the dynamic interactions that connect these components and combine them into an *Earth Integrated System* (EIS). These interactions are imperative to learning more about the Earth System in the present, explaining the past and predicting the future.

Global observations, new space technology and better, more elaborate quantitative models give us the capability to probe the complex, interactive processes and consequently move toward the science of *Global Change*. Moving towards this goal of *Global Change*, the study of the effect of oceanic current variability on the diurnal rotation of the earth gives additional impetus to our research.

### **1.3. The Ocean Environment**

In anticipation of deeper insights into the interactions among the Earth System components, we will take a system's analysis approach here. We will utilize global observing techniques together with conceptual and numerical modelling to bring forth an improved knowledge of ocean behaviour and study its interaction with other ES components.

The abundance of water in all three phases (clouds, oceans, ice) is a primary difference between the earth and other planets in the solar system and is critical in sustaining life on earth. Since a little more than two thirds of the earth's surface are covered by oceans, it is rightfully called the water planet.

The oceans profoundly affect the weather and climate and in turn they are affected by the atmosphere. They act both as a heat reservoir for storing, distributing and releasing solar energy and as the source for most atmospheric moisture. They interact with the bounding land and air over time scales ranging from seconds to hundreds of millions of years and over spatial scales from millimetres to the circumference of the earth. Without the oceans, climatic extremes on earth would be far more severe. The

ocean circulation modulates to a large extent the earth's climate and global weather. Although short period weather forecasting is today more or less a successful routine operation, it is becoming increasingly apparent that if longer period forecasting and climate prediction is desired, an improved knowledge of ocean dynamic behaviour will be required.

The transport of matter, momentum and energy across the atmosphere-ocean interface is chiefly due to solar radiation and wind stress. Such parameters as air-sea temperature difference, exchange of latent and sensible heat, the vector surface-wind field, are important observables for climatological, meteorological and oceanic processes. Observables that characterize ocean-solid earth interactions are storm surges, wind setup along the coast, tsunamis, water mass properties, tides, geostrophic currents, waves, ice melting, etc. The same observables, however, lead to an ocean surface that departs from an equilibrium surface (under gravitational and rotational forces) and thereby the relation of the ocean surface to the marine geoid becomes an extremely important issue in geodesy and oceanography.

Today, ocean remote sensing is no longer a futuristic endeavour. Artificial earth satellites have demonstrated conclusively that they are capable of measuring and recording a wide variety of information ranging from the chlorophyll content of the ocean to the ceaseless motion of the seas. Use of space platforms provides global and local explorations into the dynamics and resources of the oceans. The socio-economic impact of this information on the marine industries is tremendous. Such data provide early warning of severe wind, rain or wave conditions, an integral means of improving and

managing the resource yield in marine industries, improved navigation through ice and currents, etc.

By and large, satellite oceanography is confined to surface and near surface phenomena. This constraint is not as severe as it appears at first glance, because data taken from spacecraft will be appended to other conventionally derived surface and subsurface oceanic measurements in order to construct a nearly complete 3-dimensional view of the time varying ocean.

### **1.3.1. The Dynamic Ocean**

The variability of the oceans is a subject undergoing extensive research at present [Stewart *et al.*, 1986]. In addition, over the last decade there have been conceptual changes in the way we view the oceans. Our concept has changed from one of a steady-state ocean circulation perturbed by small-scale waves, to one of an ocean supporting a wide range of interacting phenomena occupying the full spectrum of time and space scales [Nova University, 1983].

The use of improved observational techniques during the past 15 years contributed to the change of the classical picture of a “smooth” oceanic circulation. In contrast to the oversimplified situation, recent observations have demonstrated that most regions of the world ocean are characterized by strong fluctuations with values often exceeding those of the mean flow [Duing, 1978]. One of the most important oceanographic discoveries of the last two decades is the existence of intense, time-dependent currents [Nova University, 1983]. Long-term current meter records from the eastern North

Atlantic suggest that eddy kinetic energy at all depths is principally a function of wind stress and stratification, generated during the winter and early spring, propagated to abyssal depths and decaying to a minimum in late summer [Dickson *et al.*, 1982]. Currents at a more energetic part of the North Atlantic, just south of the Gulf Stream, have been found to exhibit roughly a 50-day oscillation and have penetrated right to the ocean bottom [Malanotte-Rizolli, 1982; Rhines, 1979; Schmitz, 1978]. Baker *et al.* [1977] suggest that the observed variability of deep ocean currents in the Drake Passage (ACC) is correlated with atmospheric processes.

During the last decade, a large number of research articles have appeared in the literature dealing with the potential of satellite altimetric measurements of the ocean to provide quantitative information of its spatial and temporal variability on a world-wide scale. It is, however, difficult to cite here all of the voluminous literature that has appeared during these last ten years.

It has been demonstrated that it is possible to determine the large-scale ocean circulation and meso-scale eddies by using satellite altimetry (e.g., see Wunsch & Gaposchkin [1980]; Roemmich & Wunsch [1982]; Tai & Wunsch [1983]; Fu & Chelton [1984]). Obviously, satellite altimetry alone can only infer surface information on global oceanic circulation. Thus, in-situ oceanographic measurements and/or numerical ocean models are still needed to deal with a three-dimensional ocean.

Satellite altimetry derived ocean surface currents depict the combined barotropic and baroclinic ocean circulation, in contrast to the wind-driven circulation alone that has been assumed in previous studies of the oceans' effect on the LOD (e.g., see Wahr

[1983]). Moreover, analysis of existing satellite altimetry data sets (e.g., SEASAT derived data) has provided at the very least the “proof-of-concept” of establishing a global, synoptic picture of the oceans' variable circulation.

In this thesis work nearly synoptic oceanic variability has been obtained from satellite altimetry (from the analysis of over two years of data collected by the GEOSAT mission) and the long-term variable oceanic circulation has been extracted from a comprehensive analysis of long-term averaged relevant oceanographic data sets (analysis of mean seasonal statistics of specific volume).

#### **1.4. Research Objectives: The Problem at Issue**

If the non-tidal short-term changes in the LOD are due solely to AM exchange between the atmosphere and the solid earth, then the fluctuations in Atmospheric Angular Momentum (AAM) and LOD should be identical. Indeed the correlation between the two is very good qualitatively and quantitatively, indicating that a very high proportion is due to this excitation mechanism.

Armed with this argument it is very easy to rule out that the oceans have an appreciable effect on LOD. In addition, the difficulties associated with global synoptic observation of the oceans throughout the whole water column have discouraged the direct calculation of time series estimates of Oceanic Angular Momentum (OAM) and the oceans' contribution towards LOD fluctuations. These arguments were good enough reasons for labelling the possible oceanic contributions “insignificant” or “negligible” during the past 30 years.



The scene, however, has changed for the following reasons:

- (a) the oceans have proven to be more energetic than what was normally thought in the past;
- (b) today, we have the observational techniques and procedures to be able to start monitoring the oceanic variability on a global, nearly synoptic basis;
- (c) the accuracy with which LOD can be determined today from extra-terrestrial techniques, renders worthwhile the investigation of the oceanic contributions even if their magnitude remains at the currently supposed levels (at least at the annual and semi-annual periods);
- (d) it is universally accepted today that the ocean is the major modifier of global climate. Under these circumstances, its role becomes more important in the Earth System interaction processes with yet undiscovered implications.

It is logical therefore to launch a series of research investigations pertaining to the study of ocean current variability and in doing so elucidate further the aspect of LOD fluctuations.

One specific aim of this dissertation is to apply a comprehensive, interdisciplinary approach to solving problems in geodynamics. This approach includes understanding of

earth rotation concepts; ocean circulation and satellite geodesy basic principles; and observation, analysis and interpretation techniques.

If the objectives of this research are stated in point form, they read:

- (1) exploitation of satellite based geodetic observations and techniques useful for monitoring ocean surface dynamics both in space and time on a routine (operational) basis;
- (2) exploitation of in-situ oceanographic observations to provide information on the 3-dimensional structure of ocean dynamics as a reference frame for the synoptic ocean monitoring;
- (3) development of techniques for routine determination of axial relative oceanic angular momentum (ROAM) in the form of time series, in a manner similar to axial relative atmospheric angular momentum (RAAM) time series;
- (4) identification and quantification of periodic and irregular variations in ROAM at frequencies ranging from 1 month to 2 years; and
- (5) comparisons of the ROAM fluctuations with variations in LOD and RAAM to elucidate the role of the oceans in earth rotation.

To meet these objectives we have analysed a little over 2 years of GEOSAT/ERM altimetry data and have combined this analysis with long-term averaged in-situ

oceanographic information. Keeping up to date with the continual developments in all relevant fields of research and in pace with the computational requirements was by itself a daunting task.

## 1.5. Research Contributions

This research work represents the first documented systematic analysis and evaluation of the influence of the variable oceanic circulation on the length-of-day. Significant contributions have been made in terms of *improving our understanding* of ocean dynamics and also in terms of *quantifying* the role of the oceans in exciting LOD variations.

Three major areas of contributions stand out:

- (i) **Length-of-day Variations:** We have firmly established through our analyses of ocean current variability that the oceanic excitation of  $\Delta LOD$  is at least at the level of 0.1 ms. Furthermore, we have identified and quantified variations in the ocean current inferred  $\Delta LOD$  at periods of 1 year and 0.5 years, and identified statistically significant higher frequency variations with approximately 121-day, 107-day and 89-day periods.
- (ii) **Ocean Dynamics:** We have developed a new technique for extracting ocean current variability from satellite altimetry. The new technique has several advantages over the previously existing techniques on the recovery of oceanic variability from satellite altimetry. It is based on

the gradient operator and it is a conceptually simple, elegant and computationally efficient technique. It is sequential in nature and it allows for the direct observation of the sea surface slopes, rather than the sea surface heights, with the gradient operation acting as a high pass filter, thus reducing drastically the long wavelength radial orbit errors.

- (iii) **Geodesy-Oceanography:** We have derived a completely new set of mean seasonal dynamic topography maps of the global ocean from in-situ oceanographic measurements of specific volume, which, apart from their usefulness in the context of the present study, can potentially contribute new knowledge in the process of extracting the absolute sea surface topography from satellite altimetry and thus assist the sub-metre accuracy determination of the geoid over the oceanic regions.

There are several other contributions made in the course of this thesis research that are noteworthy, e.g., software development for all the stages and estimation procedures needed to complete the present thesis research; the establishment of a 3-year long satellite altimetry data base at UNB; software development for general satellite altimetry data editing and pre-processing; development of auxiliary software for a number of tasks, including graphics.

## 1.6. Dissertation Outline

Chapter 1 of this thesis serves to present the “opening arguments” for carrying out this research. The integral aspects of the earth's variable rotation rate are briefly reviewed. The concept of the *dynamic earth system*, ocean - solid earth - atmosphere, is introduced and is used to provide a global perspective of the role the dynamic oceans play not only in modifying the earth's climate, but also in unison with the earth's variable rotation rate. The oceanic data sources to be used in this research, which include classical oceanographic in-situ measurements and satellite altimetry observations, are pointed out. The present thesis research objectives are highlighted and the research contributions are listed.

The early chapters in the dissertation are devoted to background knowledge required to tackle the problem of the earth's variable length-of-day in the context of dynamic changes in the oceanic circulation.

Chapter 2 presents the basic earth rotation concepts. The general theoretical formulation of the problem of excitation of length-of-day variations is reviewed. The mathematical formulation has been kept brief, since it is more than adequately covered in the subject's literature. Here, only the essential elements of the mathematical formulation of the LOD excitation equations are given, in order to facilitate the developments in later chapters. The current status of the LOD research, in particular the non-tidal geophysical excitation sources, is the most important aspect considered, because the principal aim of this research is to point out the connection between the variable ocean circulation and the LOD fluctuations. The present day results regarding

the LOD variations, in the time frame of several days up to 2 years, and their present day interpretations are summarized from the available recent literature. The previous work on the subject of oceanic excitation of  $\Delta LOD$  is, finally, critically reviewed.

Since the main objective of this research work is the study of the influence of the space-time variations of the oceanic circulation on the LOD, Chapter 3 reviews the basic concepts, definitions, and mathematical modelling of the general ocean circulation. Basic material from the general oceanographic literature is drawn and used to describe the problem of ocean dynamics. The developments in this chapter follow the classical dynamic oceanography approach towards the description of ocean dynamics, namely the use of dynamic topography fields and the geostrophic equations to quantify the oceanic flow fields. The concepts of *steady-state* and *time-variable* oceanic circulation are elaborated and the space-time scales of both components of the circulation are discussed. The practical techniques of recovering the steady-state (quasi-permanent) ocean circulation are treated towards the end of the chapter.

Chapter 4 offers the unique opportunity to introduce the oceanography of the modern era. Oceanography from space is introduced and the role of satellite altimetry in quantifying surface ocean dynamics, both in space and time, is elaborated. The case of satellite altimetry as the undisputed candidate for the determination of quasi-synoptic oceanic variability is argued in favour of our  $\Delta LOD$  related investigations. The particular aspects of satellite altimetry involved in the recovery of ocean dynamics information, are examined. A survey of the existing techniques for studying the temporal variations of the sea surface topography is included. The most recent development in the techniques used for extracting global oceanic mesoscale variability from satellite

altimetry is presented, since conceptually it is very much like the technique that was independently developed in this thesis research.

Chapters 5, 6, 7, and 8 report on the major developments made in this research and the results obtained.

Chapter 5 presents the ocean dynamics results obtained from the analyses of in-situ specific volume mean seasonal fields using the classical oceanographic formulations. Long-term mean seasonal ocean dynamic topography fields are presented, discussed, and subsequently analysed to produce mean seasonal ocean current velocity fields for the top 2 km of the ocean water column. These ocean current velocity fields are used to describe the mean seasonal changes of the steady-state (quasi-permanent) general ocean circulation.

Chapter 6 is really the “heart” of the analyses on oceanic variability performed in this research work. Innovative ideas regarding the exploitation of the quasi-synoptic ocean surface monitoring offered by satellite altimetry are put to work. Ocean surface dynamics are obtained from 2 years (Nov'86-Nov'88) of GEOSAT/ERM altimetry. A general overview of the GEOSAT/ERM is given and the GEOSAT GDR is briefly discussed. The GEOSAT/ERM data base used in this thesis research is briefly described. The data pre-processing and data editing criteria used with the GEOSAT data base are presented in some detail. Most importantly, a new philosophy of how to obtain ocean current variability directly from satellite altimetry is extensively and critically argued. The new technique is used to directly produce space-time ocean current variability. A time series, just over 2 years long, of zonally averaged ocean current vari-

ability fields was constructed and the results reveal intriguing oceanic processes. This time series, the first of its kind, will subsequently be used to study the oceanic excitation of  $\Delta LOD$ .

Chapter 7 brings us back to the subject of discussing the earth's variable rotation rate. The ocean current variability in space and time, is converted into a global integral quantity, the axial relative oceanic angular momentum (ROAM), which is the required quantity for the evaluation of the influence of the varying ocean circulation on the variable LOD.  $\Delta ROAM$  estimates from both the quasi-permanent ocean circulation (Chapter 5) and the time-variable ocean circulation (Chapter 6), are reported, discussed, and critically evaluated.

Chapter 8 is the culmination of the research work reported in this dissertation. At the final stages of the research, the connection between the observed  $\Delta LOD$ , the  $\Delta LOD$  inferred from global atmospheric wind data and the  $\Delta LOD$  inferred from ocean currents, is examined using three (3) concurrent time series. Spectral analyses of the three time series are presented and intercomparison studies are carried out.

The last chapter, Chapter 9, summarizes the research findings. Proposals for future research are put forward and new questions are asked.



## **Chapter 2: Earth Rotation -- Length-of-Day**

### **Concepts**

The transfer of angular momentum between the atmosphere, solid earth and oceans is rapidly emerging as a problem of great scientific importance. Numerous studies have by now demonstrated that the angular momentum transfer between the atmosphere and the solid earth makes a major contribution to short-term variations in the length of the day. Meanwhile, there is more emphasis than before put on candidate excitation sources other than the atmosphere. For a long time, it has been recognized that the oceans have not been treated as extensively and adequately as the atmosphere for their contribution to the Earth System's overall angular momentum budget. But before we depart into this direction of earth rotation research, it is appropriate to present the underlying concepts of Earth Rotation and Length-of-Day.

The highlights of this chapter include a break down of the earth's motion in space; the governing equations of motion of a deformable earth and the law of conservation of angular momentum of the closed Earth System; the need for precise LOD observations

and the modern geodetic techniques that provide them. Finally, an account of the current state of affairs in this extremely active, multidisciplinary field of science is given.

## 2.1. Preamble

The earth participates in a number of motions simultaneously. In order to generally describe them, we can conveniently split them into three separate categories: translational motions of its centre of mass, rotational motions about its centre of mass and any variations of shape that may be taking place at any instant of time. In this thesis work only one aspect of the second kind of motion is of direct interest to us, i.e., the earth's diurnal rotation around its polar axis.

In describing the earth's diurnal rotation, we no longer treat the earth as a “point-mass”, but as a dimensional body. In the first approximation the dynamic earth can be treated as a rigid body. Hence, in conformity with the basic theorem of rigid body dynamics, its motion is decomposable into rigid body translation and rigid body rotation about its centre of mass. We are only concerned here with the dynamics of rotation. In this regard, the centre of mass of the earth is taken as the fixed point of rotation. For this purpose two coordinate systems, an inertial coordinate system and a body-fixed coordinate system, both with origin at the earth's centre of mass, are the working coordinate systems with respect to which motions are reckoned. Generally speaking, the inertial system has no rotation with respect to the distant quasars; the body system is fixed with respect to the body (nominally, the mantle).

The position of the earth's spin axis in the inertial coordinate system describes a composite conical motion, which is generally labelled *precession* and *nutation*. These gyroscopic motions result from the external gravitational torques exerted on the spinning earth by the sun and the moon. Since the luni-solar torque is a function of the positions of the moon and the sun, it changes continuously with time, thus, giving rise to a whole gamut of nutation periods ranging from 5.64 days to 18.6 years (e.g., see *Yoder et al.* [1981]). Of course, the position and orientation of the earth in space at any time is the result of the superposition of all the aforementioned motions.

The motion of the earth's instantaneous axis of rotation with respect to the body-fixed coordinate system (polar motion) attracts immediate attention. However, our principal scope of research is the period of the earth's diurnal motion, the *day*. The assumption that the rotational speed of the earth is essentially constant leads to the conclusion that the length of the day (LOD) is a naturally useful measure of the passage of time. Thus, until recent times the rotation rate of the earth has served as the basis for time-keeping.

## **2.2. Basic Concepts and Relationships**

The purpose of this section is to introduce some relevant elements of Earth Rotation as a basis of discussion on further developments and is by no means intended to be an exhaustive presentation on this subject.

### 2.2.1. Rotational Motion of a Deformable Earth - Fundamental Relations

There is an extensive body of literature covering the subject of the earth's rotational dynamics. Mainly because of historical reasons, the developed theories on earth rotational dynamics can be classified under two broad titles: rigid-earth theories (from *Euler* to *Kinoshita*), and theories of a deformable earth (elastic earth with a liquid core). Such a working partitioning has recently appeared in the textbook of *Moritz & Mueller* [1987]. Approaching the subject from the geophysical aspect, the two classic monographs on earth rotation *Munk & MacDonald* [1960] and *Lambeck* [1980] are indispensable.

In this subsection we present the fundamental relationships that are necessary in this thesis work to provide the geophysical setting of our computations.

The fundamental equation governing the rotation of any body (rigid or deformable) in the absence of any external forces and written in an inertial reference frame, is

$$\frac{D \mathbf{H}}{D t} = \mathbf{0} \quad (2.1)$$

where;

- $\mathbf{H}$  - is the angular momentum vector of the body, and
- $D/Dt$  - denotes the time derivative with respect to the inertial frame.

Sometimes equation (2.1) is also referred to as the Euler's dynamic equation and it expresses the principle of conservation of global angular momentum of any rotating body. When external torques,  $\mathbf{L}$ , are considered, Euler's equation is written as

$$\frac{D\mathbf{H}}{D t} = \mathbf{L} \quad (2.2)$$

Alternatively, we may write Euler's dynamical equation in a rotating body-fixed reference frame. Its form is then given by

$$\frac{d\mathbf{H}}{dt} + \underline{\underline{\Omega}} \times \mathbf{H} = \mathbf{L} \quad (2.3)$$

where,

- $\underline{\underline{\Omega}}$  - is rotation vector of the body with respect to the inertial frame, and
- $d/dt$  - denotes the time derivative in a system rotating with  $\underline{\underline{\Omega}}$  with respect to the inertial frame.

It should be clarified that we are only concerned with the conservation of spin angular momentum of the body thus we exclude the aspect of the body's orbital angular momentum.

In the absence of external torques,

$$\mathbf{L} = \mathbf{0} \quad (2.4)$$

and equation (2.3) becomes

$$\frac{d\mathbf{H}}{dt} + \underline{\Omega} \times \mathbf{H} = \mathbf{0} \quad (2.5)$$

We may write  $\mathbf{H}$  as

$$\mathbf{H}(t) = \mathbf{I}(t) \underline{\Omega}(t) + \mathbf{h}(t) \quad (2.6)$$

where,

- $\mathbf{I}(t)$  - is the earth's time-dependent inertia tensor, and
- $\mathbf{h}(t)$  - is the relative angular momentum, representing the net contribution to  $\mathbf{H}(t)$  of the relative motion of the mass elements of the body with respect to the body-fixed coordinate system, and has the form

$$\mathbf{h}(t) = \int_V \rho (\mathbf{r} \times \mathbf{v}) dV \quad (2.7)$$

where,

- $\rho$  - is the density of the mass element,
- $\mathbf{r}$  - is the position vector of the mass element, and
- $\mathbf{v}$  - is the velocity of the mass element with respect to the body-fixed coordinate system.

Introducing equation (2.6) into equation (2.5) we obtain

$$\frac{d}{dt} [\mathbf{I}(t) \underline{\Omega}(t) + \mathbf{h}(t)] + \underline{\Omega}(t) \times [\mathbf{I}(t) \underline{\Omega}(t) + \mathbf{h}(t)] = \mathbf{0} \quad (2.8)$$

which is the homogeneous Liouville equation of motion valid for any deformable body.

Let us now remove the arbitrariness of the earth-fixed coordinate system (and consequently that of  $\underline{\Omega}$ ) by defining it as the time-dependent mean mantle coordinate system (and consequently  $\underline{\Omega}$  is the time-dependent mean rotation vector of the mantle, which is the quantity detected by the observations). For this particular choice of  $\underline{\Omega}$

$$\mathbf{h}(t)^{mantle} = \mathbf{0}$$

i.e., there is no contribution to the relative angular momentum from motion in the mantle, but there are contributions from the atmospheric and oceanic circulations and from the liquid core,

$$\mathbf{h} = \mathbf{h}^{atmo} + \mathbf{h}^{ocean} + \mathbf{h}^{core} \quad (2.9)$$

Since equation (2.8) describes the time perturbations of the Earth System from the state of an equilibrium rigid earth, it is convenient to express both the time-dependent inertia tensor  $\mathbf{I}$  and the time-dependent rotation vector  $\underline{\Omega}$  in terms of small departures from the equilibrium state.

Therefore,

$$\mathbf{I}(t) = \mathbf{I}_0 + \mathbf{c}(t) \quad (2.10)$$

and,

$$\underline{\Omega}(t) = \underline{\Omega}_0 + \delta\underline{\Omega}(t) \quad (2.11)$$

with

$$\mathbf{I}_0 = \begin{bmatrix} A & 0 & 0 \\ 0 & A & 0 \\ 0 & 0 & C \end{bmatrix} \quad (2.12)$$

$$\mathbf{c}(t) = \begin{bmatrix} c_{11} & c_{12} & c_{13} \\ c_{21} & c_{22} & c_{23} \\ c_{31} & c_{32} & c_{33} \end{bmatrix} \quad (2.13)$$

$$\underline{\Omega}_0 = \begin{bmatrix} 0 \\ 0 \\ \Omega_0 \end{bmatrix} \quad (2.14)$$

$$\delta\underline{\Omega}(t) = \begin{bmatrix} m_1 \\ m_2 \\ m_3 \end{bmatrix} \Omega_0 \quad (2.15)$$

where;

- $\mathbf{I}_0$  - is the inertia tensor of the undeformed earth, whose principal axes of inertia coincide with the coordinate axes, acknowledging that the earth possesses rotational symmetry ( $A = B$ );
- $A, C$  - are the principal moments of inertia (equatorial and polar, respectively), which are constant in time;
- $\mathbf{c}(t)$  - describes the temporal variability of the ES's mass geometry caused by mass redistribution due to geophysical processes;
- $\Omega_0$  - corresponds to the uniform speed of rotation of the ES about the z-axis;
- $m_1(t), m_2(t)$  - express the deviations of the actual rotation axis from the adopted z-axis of the mean mantle coordinate system (polar motion components);
- $m_3(t)$  - expresses the variations of the rotational speed of the earth, which are related to changes in the LOD.

Both  $\mathbf{c}(t)$  and  $\delta\underline{\Omega}(t)$ , are considered small perturbations, whose squares, products and higher powers can be neglected (i.e., linear perturbations). Substituting equations (2.10), (2.11), (2.12), (2.13), (2.14) and (2.15) into equation (2.8) and performing subsequent algebraic manipulations, retaining only terms of the first order in the perturbations, we arrive at the system of linear perturbation equations,



$$A \Omega_0 \frac{dm_1}{dt} + [C - A] \Omega_0^2 m_2 + \Omega_0 \frac{dc_{13}}{dt} - \Omega_0^2 c_{23} + \frac{dh_1}{dt} - \Omega_0 h_2 = 0 \quad (2.16a)$$

$$A \Omega_0 \frac{dm_2}{dt} - [C - A] \Omega_0^2 m_1 + \Omega_0 \frac{dc_{23}}{dt} + \Omega_0^2 c_{13} + \frac{dh_2}{dt} + \Omega_0 h_1 = 0 \quad (2.16b)$$

$$C \Omega_0 \frac{dm_3}{dt} + \Omega_0 \frac{dc_{33}}{dt} + \frac{dh_3}{dt} = 0 \quad (2.16c)$$

In principle, the system of equations (2.16) allows us to solve for  $m_3$  and  $(m_1, m_2)$  once we know  $h_i$  and  $c_{ij}$  for a given excitation process.

Rearranging equations (2.16) we obtain a more useful form of the differential equations of motion

$$\frac{A}{\Omega_0 [C - A]} \frac{dm_1}{dt} + m_2 = \psi_1 \quad (2.17a)$$

$$\frac{A}{\Omega_0 [C - A]} \frac{dm_2}{dt} - m_1 = \psi_2 \quad (2.17b)$$

$$\frac{1}{\Omega_0} \frac{dm_3}{dt} = \frac{d\psi_3}{dt} \quad (2.17c)$$

where,

$$\psi_1 = \left[ -\Omega_0 \frac{dc_{13}}{dt} + \Omega_0^2 c_{23} - \frac{dh_1}{dt} + \Omega_0 h_2 \right] / (\Omega_0^2 [C - A]) \quad (2.18a)$$

$$\psi_2 = \left[ -\Omega_0 \frac{dc_{23}}{dt} - \Omega_0^2 c_{13} - \frac{dh_2}{dt} - \Omega_0 h_1 \right] / (\Omega_0^2 [C - A]) \quad (2.18b)$$

$$\psi_3 = \left[ -h_3 - \Omega_0 c_{33} \right] / (\Omega_0^2 C) \quad (2.18c)$$

The functions  $\psi_i$  ( $i=1,2,3$ ) are the forcing functions. In earth rotation studies they are customarily called the *geophysical excitation functions*. Thus, the set of equations

(2.17) allows an apparent separation <sup>1</sup> between geophysically measurable quantities ( $\psi_i$ ) and astronomically measurable quantities ( $m_i$ ).

In this dissertation we expressly deal with the time variations of the rotational speed of the Earth System. Thereafter, we concentrate on equation (2.17c). Its solution is given by

$$m_3 = \psi_3 + \text{constant} \quad (2.19)$$

or,

$$\Omega_0 C [ 1 + m_3 ] + \Omega_0 c_{33} + h_3 = \text{constant}' \quad (2.20)$$

which expresses the conservation of the axial angular momentum of the composite Earth System about the mean rotation axis of the mantle. It follows that the excitation equation of LOD is (apart from a constant)

$$m_3 = - \frac{1}{C\Omega_0} [ h_3 + \Omega_0 c_{33} ] \quad (2.21)$$

or, written in a more compact form

$$m_3 = m_3^{\text{motion}} + m_3^{\text{matter}} \quad (2.22)$$

the “motion” term relating to the relative axial angular momentum and the “matter” term to the mass redistribution within the Earth System.

Since (see *Barnes et al.* [1983])

---

<sup>1</sup> The situation, however, is more complicated because  $h_i$  and  $c_{ij}$  are dependent on the  $m_i$  as well (the incremental centrifugal force caused by a change in the rotation also deforms the earth). Thus, the second order perturbation equations will be inherently more complicated. However, the effects of the  $m$ -dependent terms turn out to be negligible. For more details see, for example, *Wahr*, [1986; 1988].

$$m_3 = \frac{\Omega_3 - \Omega_0}{\Omega_0} \quad (2.23)$$

$$T = \frac{2\pi}{\Omega_3} \quad \text{and} \quad T_0 = \frac{2\pi}{\Omega_0} \quad (2.24)$$

it follows that [Barnes *et al.*, 1983]

$$m_3 = - \frac{\Delta LOD}{LOD} \quad (2.25)$$

where  $\Delta LOD$  is the excess length-of-day from the nominal value of  $T_0 = 2\pi/\Omega_0 = 86400$  sec. Equation (2.25) represents the proportional change in the length of the day.

The decor for our investigations has been set. Equation (2.21) is the starting point. The relative axial angular momentum  $h_3$  is the excitation component of LOD that we will deal with from now on. We write the  $h_3$  for the composite Earth System (recalling that the choice of the mean mantle coordinate system has forced  $h_3^{\text{mantle}} = 0$ ) as,

$$h_3 = h_3^{\text{atmo}} + h_3^{\text{ocean}} + h_3^{\text{core}} \quad (2.26)$$

The  $h_3^{\text{ocean}}$  component associated with the variable oceanic circulation is the quantity to which we shall devote our efforts in the rest of this thesis work. This component has been inadequately treated in previous earth rotation studies because of sheer lack of direct global oceanic data time series. It is the component that has been hitherto considered as having a negligible influence on the total axial angular momentum budget. Based mostly on indirect modelling of the global oceanic velocity field  $\mathbf{v}$  (recall definition of  $\mathbf{h}$ , i.e., equation 2.7), or on order-of-magnitude calculations, its esti-

mated contribution amounts to approximately 10% of the total RAAM budget of the ES [Lambeck, 1980; Wahr, 1983].

The need for a thorough and as far as possible conclusive study of  $h_3^{ocean}$  has today become an important issue for three reasons. First,  $\Delta LOD$  observations enjoy increased accuracies, thus the decreased level of observational noise allows better resolution of the excitation functions. Second, there are observational techniques that can provide direct, global, nearly synoptic ocean monitoring such as satellite altimetry. Satellite altimetric missions have today been recognized as one of the tools necessary to probe the exceedingly changing ocean. Third, an affirmative answer regarding the contribution of  $h_3^{ocean}$  is important because it will allow LOD investigations to concentrate more decisively on other hypotheses about excitation sources and their proper treatment (e.g., global groundwater fluctuations).

To conclude this sub-section, we present the explicit form of  $h_3^{ocean}$  that will be used in estimating the Relative Oceanic Angular Momentum (ROAM) budget from ocean current velocity fields (it can be derived from equation 2.7):

$$h_3^{ocean}(t) = \int_0^r \int_{-\frac{\pi}{2}}^{\frac{\pi}{2}} \int_0^{2\pi} r^3 \rho_w u(\phi, \lambda, r, t) \cos^2 \phi \, d\phi \, d\lambda \, dr \quad (2.27)$$

where,

- $r$  - is the radial coordinate;
- $\rho_w$  - is the material density of sea water,

- $\phi, \lambda, r$  - are spherical coordinates (latitude, longitude and ocean depth, respectively), and
- $u(\phi, \lambda, r, t)$  - is the east-west component of the time variable ocean current velocity field (positive east).

From this point on, the major theme in this dissertation will be the determination of  $u(\phi, \lambda, r, t)$  by combining knowledge and observations from oceanography and satellite altimetry.

### 2.3. Requirements for Precision LOD

Non-tidal time variations in LOD are manifestations of the complex nature of interactions between the components of the Earth System. Their observation is essential in revealing the excitation sources and transfer mechanisms of these changes. Therefore, our interest in the earth's rotation rate (equivalently, LOD) and its time variations ( $\Delta LOD$ ), both irregular and periodic, stems from a fundamental single source: greater understanding of the properties and the behaviour of the Earth System.

Variations in ER are of further interest as they contribute to the level of uncertainty in precision geodesy and geodynamics. A major application of ER theory and results is the establishment of precise inertial and terrestrial reference systems suitable for global applications of geodetic positioning techniques. At the same time extra-terrestrial geodetic positioning techniques are the providers of highly accurate, rapid observations of ERPs.

Increasing the accuracy of ERP observations is, of course, part of the requirement to better understand the geophysical processes taking place within the ES. Removal of more accurate LOD excitation estimates from LOD observations allows us to study the residual variations which may reveal additional information regarding other excitation mechanisms. Moreover, observed short-term LOD fluctuations bear the signature of atmospheric variations. The understanding of weather and climate will be greatly benefited from LOD observations, if these observations can serve as monitoring indices and predictors of world weather and climate. The implications of such an advancement will be tremendous in every facet of human activity.

Irregular changes in LOD on time scales of the order of decades are attributed to mantle/liquid-core coupling. Improved accuracy of long-term LOD observations may in the future provide some clues to the nature of the coupling mechanism and subsequently to the nature of the geomagnetic field.

To summarize the statements made above, any discordance between geophysical LOD excitation estimates and observed non-tidal LOD values is open for investigation and interpretation, at the level that current observational accuracies allow and global geophysical data bases exist.

In anticipation of future advances in space geodesy and availability of global atmospheric and oceanic ancillary data and intensive observational campaigns, the NASA Workshop on Geodynamics and Geology in July of 1989 [Dickey *et al.*, 1989] has formulated plans for an ambitious program which includes:

- determination of the earth's rotation vector and its variations with the highest possible accuracy and with a temporal frequency of at least 4 cycles per day;
- improvement of analysis and modelling capabilities to match the improved spatial and temporal resolution of the data sources; and
- availability of geophysical, atmospheric and oceanic data sets in such multiplicity and variation that will allow enhanced interpretation of the interaction processes.

## 2.4. Current Status of LOD Research

The first complete book-length review on the subject of the LOD and its variations appeared in *Munk & MacDonald* [1960]. *Lambeck* [1980] reviewed and reported advances in this interdisciplinary field during the following 20 years (1960 till 1980). The 1980's have seen a flurry of publications on LOD observational results, developments in terms of evaluation and interpretation of LOD geophysical excitation functions and progress in terms of theoretical advancements.

*Hide* [1985] reviewed the short term variations in the LOD and *Wahr* [1985] stressed the geophysical implications of earth rotation measurements. A detailed review covering a broad spectrum of LOD variations was also given by *Dickey & Eubanks* [1986]. Most recently, two special volumes have appeared on the subject of ER that need to be mentioned: “*Earth Rotation : Solved and Unsolved Problems*” [*Cazenave*, ed., 1986] and “*Space Geodesy and Geodynamics*” [*Anderson & Cazenave*, eds., 1986]. *Moritz*

& *Mueller* [1987] have contributed a much needed textbook on earth rotation principles and several conference proceedings have been published.

However, it is rather difficult to cite a single publication at the end of this decade that can be regarded as a “monograph” publication on the subject. A regrouping of information resources and achievements in LOD research is required in the 1990's, because there is a great deal of research activity planned during this new decade. A consolidation of the current status of research is a must. No attempt will be made in this section to fill such a demand; it is beyond the scope of this work. Instead, some of the highlights in the current LOD research will be referenced in support of the investigations carried out in our research.

Essentially, two summaries will be given: one for the current status of LOD observational results, the second being devoted to the short term (less than 5 years) LOD geophysical excitations of non-tidal origin, their numerical evaluations and present day interpretations of the currently available results.

#### **2.4.1. Contemporary LOD Observational Techniques**

Crude records of LOD going back as far as the middle of the sixteenth century have been constructed from astrometric data, in which the motion of planets and the earth's moon serve as accurate clocks. The adoption of atomic clocks in 1955 eliminated clock errors as a serious error source. Until 1988, BIH regularly collected data from approximately 50 to 80 astrometric observatories scattered around the world, which determined the time of the meridian passage of stars. The uncertainty of these



measurements is no better than few milliseconds, and these data do contain systematic errors.

However, the scene has changed during the last 15 years because of the high-quality LOD time series generated by the modern space geodetic techniques of LLR, SLR and VLBI. These new techniques signify the progress made in geodetic extra-terrestrial positioning over the last two decades.

The rapid development of space geodesy has led to a number of national and international programs that promoted the collection and analysis of LOD observations from the above mentioned three techniques. MERIT (Monitoring Earth Rotation and Inter-comparison of the Techniques of observation and analysis) [Wilkins, 1980], was an international effort to evaluate the geodetic techniques, sponsored by the IUGG/IAG. Project MERIT, during its main campaign (Sept. 1983 - Oct. 1984), yielded the most accurate ER data series obtained until that time.

The LLR, SLR and VLBI techniques are today providing routine LOD determinations at the sub-millisecond level (0.05 to 0.1 ms for UT1 determination over 3 to 5 day averaging periods [Carter & Robertson, 1986]), representing an almost ten-fold improvement in accuracy relative to the traditional techniques based on optical astrometry [Dickey *et al.*, 1989]. By comparison, the classical techniques are probably accurate only to about 0.5 to 1.0 ms for values of UT1 averaged over 5 days and more accurate for longer averaging times [Paquet, 1986].

Another, equally important, asset of the LLR, SLR, and VLBI techniques is the high temporal resolution of LOD determinations they can provide, ranging from a few hours to a few days [*Eanes et al.*, 1984; *Robertson et al.*, 1985; *Carter & Robertson*, 1986].

Although all of these modern techniques provide excellent results for ERP determinations, the multi-station VLBI technique currently provides the lowest formal errors [*Dickey et al.*, 1989]. However, the existing observations from the classical astrometric techniques remain invaluable at the present time when investigating LOD variations at decadal and longer periods, because the new techniques simply have not been in existence long enough.

The combination of the variety of geodetic LOD determinations into a unique time series is, of course, complicated by irregular data spacing and the accuracies of the disparate time series. Researchers at JPL (see, for example, *Morabito et al.* [1986; 1988]) addressed the existing problems in processing ERP determinations from a variety of spaced-based geodetic techniques and noted that:

- no deterministic models are available to describe the rapid fluctuations in ER and thus, tackle the irregular data spacing problem;
- the data from the different measurement techniques are of irregular quality and have a wide range of formal errors.

To overcome those two basic problems, they have combined Kalman filtering and auto-regressive (AR) time series analysis techniques with the various raw observations

of ERPs from the three techniques [Morabito *et al.*, 1988] and have been able to produce both predictions and smoothings of the ERP time series.

To summarize, a concise status report of the current LLR, SLR and VLBI observation programs for ER has been given in Dickey *et al.* [1989]. One major conclusion regarding the use of the contemporary observing techniques can be clearly stated: these techniques have enabled detection of not only much smaller variations in LOD (and polar motion), but at even higher frequencies than was previously possible. Work still needs to be done to identify any possible systematic errors in the observational techniques. Although it does not seem that they are important, there still remain differences between the various LOD determinations of the order of few tenths of milliseconds (e.g., see IERS annual report 1989, pp. II-25).

Since January 1, 1988 the International Earth Rotation Service (IERS) has replaced the International Polar Motion Service (IPMS) and the earth rotation section of BIH, and has been delegated the responsibility for: (a) the international coordination of all contemporary ER observation programs; (b) the responsibility for defining and maintaining conventional celestial and terrestrial reference systems; and, (c) collecting, archiving and disseminating observation and data analysis results to the various scientific users.

The IERS bulletins contain VLBI, SLR and LLR results reported from a world-wide network of observatories. Regular VLBI submissions to the IERS include polar motion, universal time, precession and nutation values at 5-day and quasi-regular 1-day intervals. SLR observations of the LAGEOS satellite (from a primary network of about

25 stations) are currently the most frequent regular source of ER data available to IERS (3-day intervals). The primary role of the LLR data in IERS (3 stations observing on a regular basis), is for investigating the long-term variations in the rotation rate of the earth.

#### **2.4.2. Short-Term Geophysical LOD Excitation Sources: Current Status**

In the previous sub-section we briefly referenced the advancements made in the LOD observational techniques during the last 15 years. Those advancements were complemented by equally crucial advancements in global atmospheric data acquisition and analysis.

In this sub-section we will concentrate our discussion on the geophysical sources of LOD excitation, especially on time scales from several days to a few years since this is the time frame that our oceanic analyses will report on. Changes in the LOD at these time scales associated with tidal perturbations are due to changes in the inertia tensor of the solid earth. The tidal perturbations are much easier to model accurately than any other variable excitation source. We will not devote any more space to them in this summary. The interested reader can refer to *Yoder et al.* [1981, 1983] and *Luo et al.* [1987] for recent reviews of the tidal influences on the variable LOD.

The most recent summary (at the time of writing) of the current status of research regarding the atmospheric excitation of the LOD variations can be found in *Dickey* [1989].

Briefly, the results from the RAAM analyses have shown that:

- changes in the axial RAAM contain a large amplitude seasonal cycle, dominated by annual and semi-annual harmonics (of approximately 0.5 and 0.3 milliseconds amplitudes, respectively);
- the annual RAAM cycles in the two hemispheres are 180° out of phase and the northern hemisphere (NH) has a larger annual amplitude (compare this finding with the land-mass distribution between the two hemispheres);
- superimposed on the seasonal cycles is the irregular “50-day” oscillation [*Langley et al.*, 1981] (with approximately 0.2 ms amplitude), with the band between 40 and 60 days reflecting a very complex structure.
- most of the non-seasonal changes occur in regions from 10° to 25° South and 20° to 35° North;
- a number of studies have indicated that significant, relatively small, imbalances exist between the observed and inferred non-tidal axial angular momentum budgets at the annual and semi-annual periods, with the semi-annual discrepancy being larger [*Eubanks et al.*, 1984; 1985; *Morgan et al.*, 1985].

Thus, one of the major conclusions consolidated during the last 10 years of research activity is that, fluctuations in the LOD over the time-scale of the 2 years or less, apart from the tidal influences, are dominated by atmospheric processes, with the wind field

playing the master role [Lambeck & Hopgood, 1982; Rosen & Salstein, 1983; Barnes et al., 1983; Eubanks et al., 1985; Rosen & Salstein, 1985; Dickey & Eubanks, 1986].

There is a statistically significant correlation observed between interannual LOD changes and a widely used meteorological index for the Southern Oscillation (SOI) during the period 1962-1985 [Chao, 1988]. A number of authors have linked interannual LOD changes to the Quasi-Biennial Oscillation (QBO) of the stratosphere (see, e.g., Ottmans & London [1982]) and strong El Nino events [Eubanks et al., 1986; Chao, 1989].

Perfect correlation between the LOD and the SOI should not be expected since the SOI is derived from local measurements, while the RAAM and  $\Delta LOD$  are global quantities.

It is interesting to note here that these recent interpretation studies have started to look at the latitude dependence of the axial RAAM variations, thus looking deeper and deeper in the causality mechanisms of the excitations.

The potential future role of axial RAAM results as a real-time *proxy* index of  $\Delta LOD$  has started to be advocated more and more often (e.g., see Dickey [1989]).

Improvements in the global atmospheric data bases, in numerical modelling of the atmospheric circulation and further theoretical work (e.g., Barnes et al. [1983]), sparked an almost exclusive interest in the exchange of the angular momentum between the atmosphere and the solid earth (mantle and crust). This has become very evident from the proliferation of scientific articles on the subject of common fluctuations be-

tween LOD and axial RAAM, especially in the higher frequency part of the spectrum (e.g., *Rosen & Salstein* [1983; 1985]).

The national meteorological services of Japan (JMA), United States (NMC) and United Kingdom (UKMO) and the European Centre for Medium-range Weather Forecasting (ECMWF) maintain global atmospheric forecasting models which, among other things, produce operational RAAM time series at 12-hour and 24-hour intervals by combining measurements of atmospheric variables such as pressure and wind speed with their model forecast values in some statistically optimal fashion.

Calculations of AAM are carried out using the formulation of *Barnes et al.* [1983], i.e., computing the effective AAM functions (EAMF), a three-dimensional vector which includes Love number corrections for rotational and surface loading deformation of the earth. The EAMFs can be directly evaluated from meteorological data.

Error bars associated with global values of axial RAAM are not easily assessed through conventional analysis techniques, even though the sources of errors can be largely attributed to inadequacies in data coverage and forecast models.

The assessment of the level of uncertainty in current calculations of axial RAAM is done by comparisons between time series produced by different operational weather centres. The different operational time series generally agree quite well, although certain differences are evident [*Rosen*, 1986; *Gross et al.*, 1989]. For example, the overall standard deviation of the difference between the 1981-1983 RAAM time series derived from NMC and ECMWF analyses amounts to  $0.407 \times 10^{25} \text{ kg m}^2 \text{ s}^{-1}$  [*Rosen*, 1986].

For example, during 1980-1981 the difference in the global values of AAM between the two centres amounted to as much as 10% at the annual period [Rosen, 1986].

The effect of including upper stratospheric winds in the production of the axial RAAM series has been shown to have ramifications on the seasonal time scales [Rosen & Salstein, 1985]. The inclusion of stratospheric data in the axial RAAM estimation has considerably reduced the discrepancies at the semi-annual period, however, there still exist discrepancies in the annual period. In any case, it is clear that future attempts at studying the causes for seasonal fluctuations in LOD should take into account winds in the upper stratosphere.

The discussion in the preceding paragraphs on the RAAM results focused on the contribution of the atmospheric winds towards the observed LOD variations, i.e., on the  $h_3^{atmo}$  term in eq. (2.26) and the  $m_3^{motion}$  in eq. (2.22). The angular momentum variations of the atmosphere due to the re-distribution of the air masses are related to the surface pressure (the  $m_3^{matter}$  term in eq. (2.22)). Barnes *et al.* [1983], Morgan *et al.* [1985], Eubanks *et al.* [1985] and Rosen *et al.* [1989] have reported that the changes in the pressure term associated with the atmosphere are typically much smaller than the motion term associated with the variable winds, the expected variation being about 10% of that due to the winds at the seasonal periods. Most of the calculations of axial AAM for LOD studies ignore the contribution of the pressure term because no reliable estimates of the wet component of the atmospheric pressure are yet available (see, for example, Morgan *et al.* [1985]).



The recently restructured earth rotation service, namely IERS, maintains a sub-bureau at the NMC/NOAA to provide RAAM data to those who are involved in the investigation of the relationship between the atmospheric circulation and the rotation of the earth.

There is very little to report from the literature about other candidate short-term LOD excitation sources. Global ground water changes and snow cover variations primarily affect the LOD by changing the earth's polar moment of inertia. However, detailed data to reveal seasonal variations in LOD due to these agents are not yet available. The review of the literature on the oceanic excitation of LOD variations is reported in the next sub-section.

#### **2.4.3. Oceanic Excitation of Short-term LOD Variations: Status Report**

In the previous sub-section we saw that most of the short-term, non-tidal, variations in LOD have been found to “mirror” the angular momentum content of the atmosphere. The “difference” margins are of the order of 10% of the atmospheric variations and it has been *speculated* for a long time that the influence of the oceans is of the same order [Eubanks *et al.*, 1986; Gonella, 1986; Eubanks *et al.*, 1985; 1984; Wahr, 1983; Lambeck, 1980; Munk & MacDonald, 1960].

The question of how changes in the ocean circulation influence the rotation rate of the earth still remains unanswered to a very large degree. Thus, it is today more and more emphatically recognized that the role of the oceans in LOD fluctuations needs to be carefully investigated [Christou, 1984; Dickey *et al.*, 1989] and properly eval-

uated. The residual time series, i.e., the  $\Delta LOD$  budget of the earth system after the removal of the tidal and atmospheric contributions, are known well enough to allow the investigation of the contributions from the variable oceanic circulation. However, because of lack of direct, global oceanic data (either in the form of global synoptic sea level changes or global synoptic ocean current velocity fields) very few studies have attempted to address this problem, with inconclusive results as yet.

Changes in the ocean circulation are associated with changes in the ocean current velocity fields, both in space and time. It is, therefore, natural to relate those changes to variations of relative oceanic angular momentum (ROAM). While estimates of RAAM are directly available from atmospheric numerical models used in weather forecasting, similar oceanic estimates are not yet available. Nevertheless, it is well known [*Munk & MacDonald*, 1960; *Lambeck*, 1980] that one order of magnitude exists between axial RAAM and axial ROAM budgets. Order of magnitude calculations (e.g., *Gonella* [1986]) have been the classical approach to quantifying the oceanic contributions to LOD fluctuations. *Gonella* [1986] acknowledges that ocean current data are not yet available on a global scale and ROAM cannot yet be computed as adequately as the RAAM estimates.

Particular attention has only been given to axial ROAM studies related to the ACC since it is the only zonal oceanic flow unimpeded by the continents. A brief survey of literature regarding studies of the ACC variations follows.

*Lambeck* [1980] summarized the available information about the average water volume transport through the Drake's Passage (the body of water between South America and

Antarctica) up until the late 1970's, by pointing to the works of *Kort*, [1962]; *Van Loon*, [1971]; *Lamb*, [1972]; and *Baker et al.*, [1977]. Based on the transport estimates deduced from the work of *Baker et al.* [1977], *Lambeck* [1980] calculated the total angular momentum of uncompensated flow associated with the ACC to be approximately  $0.7 \times 10^{25} \text{ kg m}^2 \text{ s}^{-1}$ .

The study of the ACC and its space and time fluctuations has attracted extensive oceanographic research during the past 10-15 years and the relationship between wind stress and transport through Drake's Passage has been examined by several authors, e.g., *Bryden & Pillsbury* [1977], *Nowlin et al.* [1977], *The Polar Group* [1980], *Georgi & Toole* [1982], *Nowlin & Clifford* [1982], *Baker* [1982], *Whitworth* [1983], *Fu & Chelton* [1984], *Whitworth & Peterson* [1985], *Nowlin & Klinck* [1986], *Peterson* [1988], to name only a few.

An informative summary on the volume transport through Drake's Passage can be found in a very recent article by *Johnson* [1989], where the relationship between the structure of the wind stress curl and volume transport is addressed.

*Brosche & Sundermann* [1985] have looked into the problem of oceanic contributions to  $\Delta LOD$  by isolating the ACC as the sole serious candidate of axial ROAM and have estimated its influence on LOD variations considering the mass transport variations through the Drake Passage. They claim that the marginal discrepancy in the angular momentum balance of the solid earth plus atmosphere at the semi-annual frequency could be explained in amplitude and phase by the ACC ROAM budget fluctuations (about 0.05 ms in amplitude).

*Johns et al.* [1987] investigated again the role of the ACC in the earth's angular momentum budget using three years of data (1977 - 1980) of oceanic flow through the Drake Passage. Direct comparisons were made between the ACC and residual LOD -RLOD- (i.e., LOD minus RAAM). Their basic conclusion was that at the annual, semi-annual and shorter periods, fluctuations in the ACC appear too weak to account for the observed fluctuations in the RLOD.

*Eubanks et al.* [1984; 1985] state that changes in the oceanic circulation may contribute as much as 0.2 to 0.3 ms to the unexplained seasonal changes in LOD, while *Rosen & Salstein* [1985] have claimed that there is no need to invoke other excitation mechanisms, because at least the semi-annual discrepancies between LOD and the axial RAAM are almost completely accounted for by the inclusion of stratospheric wind data (between 100 and 1 mbar) in the RAAM calculations.

*Wahr* [1983] has investigated the role of the oceanic circulation towards LOD variations by using a simple, one layer wind-driven ocean numerical model truncated at 36°S latitude. Global surface pressure data was used to obtain the curl of the wind stress which was used to drive the numerical ocean model, and thus determine the 3-dimensional structure of the ocean current velocity field. The results of his study did not provide any new information and basically the conclusions stated in *Lambeck & Hopgood* [1982] and *Lambeck* [1980] were, once more, reiterated. In one phrase, these conclusions are: ...“about 10% of the total excitations come from hydrological and oceanographic phenomena for which little more than order of magnitude estimates are possible at present”... [*Lambeck & Hopgood*, 1982; *Wahr*, 1983].

A preliminary analysis of the work reported in Chapter 5 of this dissertation was presented by *Christou & Langley* [1988]. It is the first comprehensive treatment of direct global ocean current data fields for the evaluation of axial ROAM mean seasonal budgets.

In summary, the role of the world oceans in LOD fluctuations was difficult to investigate in the past due to limitations regarding the availability of global oceanic data bases. However, satellite altimetry advancements over the past 5 years have changed the scene. Today, there exists the first significant global, nearly synoptic oceanic data base generated by the GEOSAT Exact Repeat Mission. The planned TOPEX/POSEIDON altimetric mission in the early 1990's [*Stewart et al.*, 1986] in conjunction with the planned ERS-1 and NROSS satellite missions and the concurrent WOCE programme [*Chelton*, 1988] are the next generation means of obtaining a better, more complete and more accurate oceanic data base suitable for  $\Delta LOD$  studies.

In subsequent chapters of this dissertation we shall report on the use of the GEOSAT generated oceanic data base as the means of providing axial ROAM time series, and in doing so, discuss tantalizing questions regarding the oceans' effect on the earth's variable rotation rate.

## **Chapter 3: Ocean Dynamics - Oceanic**

### **Variability**

#### **3.1. Preliminaries**

Ocean dynamics is concerned with the ocean circulation and the physical state of the ocean. It is also intimately related to the world climate. The dynamic movements of the oceans are of interest and importance not only to all those who use the ocean or its borders for recreation or livelihood, but for all earth sciences.

A clarification statement is immediately necessary. The ocean dynamics and oceanic variability examined in this thesis research do not include motions of tidal origin.

The oceans' general circulation may be conceptualized as the 3-dimensional velocity field through an appropriately small fixed volume in space, averaged over sufficiently long time.

The forces that affect the ocean in a state of rest are the forces of gravitation and of external and internal pressure. The effect of wind friction (wind stress) at the air/sea

interface represents another external force. If the oceans were filled with completely motionless homogeneous water under only the influence of gravitational and centrifugal forces, then they would assume the shape of an ideal surface which would be a level surface (i.e., a surface on which the gravity potential is constant), the *geoid*.

A stratified ocean is an ocean in which the density of water changes in space. The field of internal pressure in a stratified ocean is partly determined by the field of mass. This part of the internal field is called the relative field of pressure. Thus, the total field of pressure in the ocean is composed of the relative field and the fields caused by the non-gravitational external forces such as the atmospheric pressure and the wind stress [Neumann & Pierson, 1966]. It is obvious that these external forces will cause the sea surface to slope. The mean (general) circulation of the oceans is a result of the total pressure field, i.e., the external force-field and the internal relative force-field, both of which are dependent on the distribution of solar energy over the earth [Duxbury, 1971]. The interaction of the external forces with the oceanic motions and their variation with time are among the fundamental problems yet to be fully solved in oceanography.

Knowledge of the mass distribution in the sea is required for all computations of the relative field of pressure. The field of mass can be represented by either the distribution of density, or its reciprocal value, called the *specific volume*. Surfaces of equal density are called *isopycnic surfaces* and surfaces of equal specific volume are labelled *isosteric surfaces*. In vertical or horizontal sections across the oceanic space, the lines of equal density are called isopycnals and the lines of equal specific volume are labelled isosterals.

The ocean exhibits a wide variety of phenomena, both surface and sub-surface, on a broad spectrum of space and time scales that differ greatly in their manner and degree of dependence on each of the following factors:

- the oceans' initial state at time  $t_0$ ;
- the astronomical, atmospheric and geophysical forcing;
- flow through any open boundary segments of a region;
- bottom topography and coastline geometry; and,
- the physical and dynamical properties of the ocean fluid.

The characteristics of oceanic variability in the space domain are generally represented by basin scale (larger than 1000 km), intermediate scale (300-1000 km) and small scale (50-300 km) variations. The temporal characteristics of oceanic variability incorporate short period (less than 1 day), intermediate period (1 to 100 days), long period (100 days to 2 years) and “stationary” phenomena.

### **3.2. General Ocean Circulation**

Generally speaking, the *zero-th* approximation of the ocean surface is a figure defined by the equilibrium between the gravitational forces acting upon all the masses of the earth and the centrifugal forces set up by the earth's spin. This surface is nothing else but a special equipotential surface of the earth's gravity field, the *geoid* as mentioned in section 3.1. However, the oceanic part of the geoid has superimposed on it *height anomalies* generated by the action of systematic winds on the sea surface, the internal field of mass, as well as the effect of systematic differences in atmospheric pressure and the moisture evaporated from and precipitated onto the various areas of the sea, and periodic anomalies such as the ocean tides.



A multiyear average of those ocean surface height anomalies (the major tidal constituents obviously do not contribute to the multiyear average figure) produces an oceanic picture which we can term the global (or general) ocean circulation. This quasi-stationary part of the ocean height anomalies will be called the quasi-permanent sea surface topography (Q-P SST). In this case, the ocean surface is a figure in the *first* approximation, that describes the long-term average departures of the ocean surface from that of the geoid, i.e., the quasi-permanent SST. The Q-P SST manifests itself in the ocean as the global system of principal ocean currents with relatively slowly varying geographic distribution and intensity. Thus, a more formal definition of the general ocean circulation would be: the distribution of and physics governing currents and related water properties on basin-wide spatial scales, with temporal scales in the range from several years to several tens of years. In this event, the mean flow field will have a smooth spatial variation.

To understand the general ocean circulation and the distribution of properties in the ocean, it is necessary to study both the mean state and the low frequency variations. Therefore, one major objective of oceanography is to obtain world-wide maps of mean flow at low frequencies at several ocean depth levels. However, this necessitates long periods of continuous measurements to quantify the mean flow field, since there are highly variable mesoscale fields which obscure the mean flow. By mesoscale fields we refer here to small- and intermediate-scale and intermediate- and long-period variable phenomena.

The wavenumber spectrum of the general ocean circulation is not yet very well known (the one derived from the POLYMODE oceanographic experiment is, of course, the

best presently available - see *Wunsch* [1983]). Figure 3.1 (adapted from *Maul et al.* [1980]) is a useful summary of the frequency-wavelength regions of some of the most important dynamic processes in the ocean.

The general ocean circulation, qualitatively, can be divided into two parts, the thermohaline and wind-driven components, or in other words, it is in part due to changes in the density field caused by weather and climatic changes and in part due to the wind stress at the air/sea interface.

In summary, one may state that a characteristic of the thermohaline circulation of the oceans is that it originates as a vertical flow, sinking to mid-depth or even to the ocean bottom, followed by horizontal flow. The wind-driven circulation is principally confined in the upper few hundreds of metres of the water column and therefore is primarily a horizontal circulation in contrast to the thermohaline one. Ocean currents are then a result of the combined effects of the thermohaline and wind-driven motions. Furthermore, since ocean currents are really displacements of water masses, the distribution of mass in the sea becomes of particular importance in all hydrodynamic investigations.

## frequency-wavelength regions of some important dynamic processes

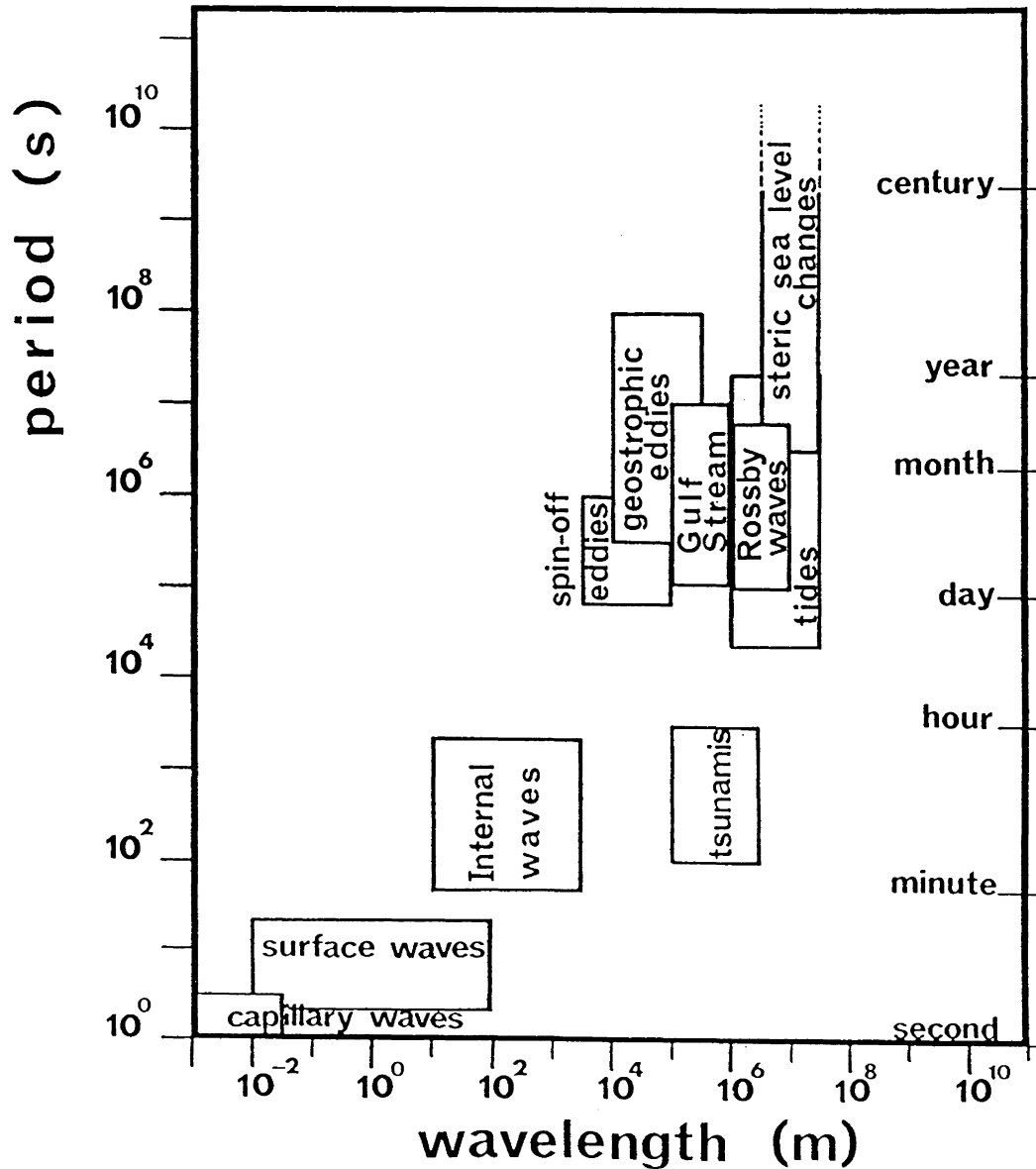


Fig. 3.1. Graphical summary of the frequency - wavelength regions of some important dynamic processes in the ocean (adapted from *Maul et al.*, [1980]). The frequency - wavelength regions of interest to this thesis research fall between:  $10^5$  to  $10^8$  seconds and  $10^5$  to  $10^8$  metres, respectively.

**Wind-Driven Circulation:** The oceans acquire momentum and kinetic energy directly from the atmosphere because of the friction of the wind against its surface; this momentum is imparted both to pure drift currents and waves [Monin *et al.*, 1977]. The waves, in turn, appear capable of transferring momentum to currents.

The surface wind field, characterized by the horizontal distribution of the curl of the frictional stress, is responsible for the generation of horizontal pressure gradients which give rise to wind-driven (gradient) currents. As a result, then, the pattern of the currents in the upper ocean reflects to a great degree the averaged wind field in the surface air layer. However, it should be emphasized here that the resultant direction of motion in the open ocean is not the same as that of the wind. The rotation of the earth gives rise to the Coriolis force (in an earth-bound coordinate system) which causes the wind-driven currents in the upper layer of the ocean to move in a direction to the right of the wind direction in the NH (to the left in the SH). Also, it should be appreciated that while the wind primarily causes horizontal motion, there exist consequent vertical motions manifested in terms of upwelling or downwelling of waters (divergence and convergence zones in the oceans, respectively).

**Thermohaline Circulation:** Another important source that drives the quasi-stationary circulation in the ocean is heating and cooling of the ocean waters, thereby changing their density, which is not only dependent on pressure but also on temperature and salinity. Hence, the circulation generated by factors that directly affect the temperature and salinity is called the thermohaline circulation. Generally speaking, salinity variations make a smaller contribution to the thermohaline circulation than thermal processes.

Increases (decreases) in the density of the surface waters due to cooling (heating) and salinization (desalinization), generate buoyancy forces that cause the water to sink (rise), thereby creating the prime driver of thermohaline circulation. The deeper ocean circulation (deeper than, say, 500 metres) is predominantly the result of the thermohaline circulation, since the wind-driven circulation seldom penetrates deeper than the top 500-metre layer of the ocean.

**The Overall Circulation:** Ocean currents are then the result of the combined effects of the thermohaline motions and the wind-driven ones. The prominent characteristic surface flow patterns make up the general circulation. The most ubiquitous features of the surface flow patterns are the very large “subtropical gyres” that span the entire east-west dimension of each ocean basin in both the northern and southern hemispheres. Almost every ocean, except the Arctic Ocean, has such a basin-wide gyre, although there are important modifications in the flow patterns brought about by geography and wind systems in the Indian Ocean and in the ACC regions. It is apparent from any general circulation map of the oceans that eastward oceanic flow occurs where the winds are westerlies (meteorological conventions followed for the wind fields) and westward oceanic flow where the winds are easterlies. It is also apparent from these schematic maps of the general ocean circulation that the subtropical gyres are anticyclonic in both hemispheres (clockwise in the NH, counter-clockwise in the SH). From their latitudinal positions, it is evident that they are closely linked to the curl of the wind stress, with Coriolis effects and continental boundaries playing a role as well.

The ACC lies roughly between 40°S to 60°S, in the zone of the southern hemisphere westerlies, and is the only oceanic zonal flow unimpeded by continental barriers. This current is the oceanic analogue of the jet stream in the atmospheric circulation.

The schematic general surface circulation of the ocean includes, in addition to the sub-tropical gyres and the ACC, the equatorial current systems. Both the North Equatorial and the South Equatorial systems are mainly westward flows above and below the equator, separated by an Equatorial Counter Current and a near-surface Equatorial Undercurrent, both flowing east.

Branching from and merging with these major components of the general ocean circulation are scores of secondary flow systems, complementing the principal currents. These secondary oceanic surface and sub-surface circulation features are usually given geographically related names (e.g., the Greenland Current, the Labrador Current, etc.).

As a final note, it happens that the continents provide impervious north-south barriers to the motion of ocean water. The existence of those barriers is one of the outstanding differences between the oceanic and atmospheric circulations.

### **3.3. Geostrophic Flow and Ocean Dynamic Topography**

It has already been stated that a fundamental goal of physical oceanography is to determine the 3-dimensional circulation of the oceans as a function of space and time. Unfortunately, direct measurements of the complete current velocity field over a long enough time interval has been impossible to accomplish. In consequence, direct measurements of currents had to be restricted to key-localities of limited area and for

purposes such as testing theories, thus providing only a small portion of our observed knowledge of the ocean circulation.

To counter balance the insufficiency of direct measurements, indirect methods have been developed and successfully used. The chief indirect method has been to observe the distributions of several water properties (tracers), which can be performed more expeditiously, and to deduce flow from these distributions. In the majority of cases, this indirect method provides us with only the direction of flow and not its magnitude. An alternative indirect procedure is to use the so-called *dynamic method*, whereby the distribution of the water density field (as another property) can provide information on both the flow direction and its magnitude. The calculation of the vector current field, thus, is obtained using the so-called *geostrophic approximation*.

The geostrophic approximation method is based on a simplified view of ocean dynamics in which friction is neglected and boundaries are assumed to be far away. Qualitatively speaking, this results in a balance between the force due to a horizontal pressure gradient and an apparent force, the Coriolis force, resulting from the fact that the oceans are a rotating fluid. The pressure field manifests itself as a slope of the constant density surfaces (isopycnics) in the ocean relative to level (gravity equipotential) surfaces, the free ocean surface itself being a special case of an isopycnic surface. Just as winds in the atmosphere circulate around highs and lows, the ocean water movement tends to be along, rather than down, the pressure contours (isobars). Most of the available information on subsurface currents has been obtained by the use of the geostrophic method. Hence, the large-scale motion in the ocean has been termed the geostrophic flow or, more correctly, the quasi-geostrophic flow, simply meaning

that the motion is not perfectly geostrophic. The quasi-permanent SST is then required for practically determining the quasi-geostrophic surface flow.

Mathematically speaking now, to quantify ocean circulation, the non-tidal hydrodynamic equations (the so-called Navier-Stokes equations) for a rotating homogeneous fluid can be written in vector notation as (see *Coleman* [1981, pp. 64]):

$$\frac{\partial \dot{\mathbf{x}}}{\partial t} + \dot{\mathbf{x}} \cdot \nabla \dot{\mathbf{x}} + 2 \underline{\Omega} \times \dot{\mathbf{x}} = - \frac{\nabla p}{\rho_w} + \mathbf{g} + \mu \nabla^2 \dot{\mathbf{x}} \quad (3.1)$$

and referenced to a local cartesian coordinate system defined such that the (x,y) plane defines the local horizon at a point  $P(\phi, \lambda, h)$ , the x-axis being oriented east, the y-axis north, and the z-axis coincides with the outward vertical at point P. The notation in eq. (3.1) is as follows:

- $\dot{\mathbf{x}}$  - is the total velocity vector having components  $(\dot{x}, \dot{y}, \dot{z})$ ;
- $\underline{\Omega}$  - is the rotation vector of the earth having components  $(0, \Omega \cos \phi, \Omega \sin \phi)$ ;
- $\mathbf{g}$  - is the gravitational acceleration;
- $p$  - is the pressure field defined in terms of surface stresses;
- $\rho_w$  - is the sea water density;
- $\mu$  - is the kinematic viscosity;
- $\nabla^2$  - is the Laplacian operator;
- $\nabla$  - is the gradient operator; and
- $P(\phi, \lambda, h)$  - is any point in the ocean, and  $\phi, \lambda$  denote, to the order of flattening, latitude and longitude on a spherical coordinate system and  $h$  the elevation of point P above the reference surface.

Rewriting eq. (3.1) in cartesian component form we have (see *Coleman* [1981, pp. 65]):

$$\ddot{x} + 2 \Omega (z \cos \phi - y \sin \phi) = - \frac{1}{\rho_w} \frac{\partial p}{\partial x} + F_1 \quad (3.2a)$$



$$\ddot{y} + 2 \Omega (\dot{x} \sin \phi) = -\frac{1}{\rho_w} \frac{\partial p}{\partial y} + F_2 \quad (3.2b)$$

$$\ddot{z} - 2 \Omega (\dot{x} \cos \phi) = -\frac{1}{\rho_w} \frac{\partial p}{\partial z} + F_3 - g \quad (3.2c)$$

- $\ddot{x}, \ddot{y}, \ddot{z}$  - are acceleration components, and
- $F_i$  - are the components of the frictional forces.

Equations (3.2) are applicable at any depth in the ocean. The effect of the winds at the air/sea interface, apart from the implicit appearance in the form of horizontal pressure gradients, is explicitly included in the force terms  $F_i$  when applying eqs. (3.2) at the surface.

In the case of the large-scale ocean flow, the expected magnitudes of  $\dot{x}$  and  $\dot{y}$  are of the order of  $3 \text{ m s}^{-1}$ ,  $\dot{z}$  being about four orders of magnitude smaller. Also, in the context of the large-scale flow, the acceleration terms can be safely considered negligible, i.e., in the context of other than short-period wave motions. With these assumptions further simplifications can be introduced in eqs. (3.2). Specifically, eq. (3.2c) reduces to the basic hydrostatic relation for steady, uniform flow, if  $F_3 = 0$ ,

$$0 = -\frac{\partial p}{\partial z} - g \rho_w \quad (3.3)$$

and eqs. (3.2a) and (3.2b) reduce to

$$\ddot{x} - 2 \Omega \sin \phi \dot{y} = -\frac{1}{\rho_w} \frac{\partial p}{\partial x} + F_1 \quad (3.4a)$$

$$\ddot{y} + 2 \Omega \sin \phi \dot{x} = -\frac{1}{\rho_w} \frac{\partial p}{\partial y} + F_2 \quad (3.4b)$$

Defining the Coriolis parameter as

$$f = 2 \Omega \sin \phi \quad (3.5)$$

we rewrite eqs. (3.4) as

$$\ddot{x} - f\dot{y} = - \frac{1}{\rho_w} \frac{\partial p}{\partial x} + F_1 \quad (3.6a)$$

$$\ddot{y} + f\dot{x} = - \frac{1}{\rho_w} \frac{\partial p}{\partial y} + F_2 \quad (3.6b)$$

Under the assumptions of a non-accelerated system ( $\ddot{x} = \ddot{y} = 0$ ) and the absence of frictional forces ( $F_1 = F_2 = 0$ ) the system of governing equations becomes:

$$- f\dot{y} = - \frac{1}{\rho_w} \frac{\partial p}{\partial x} \quad (3.7a)$$

$$+ f\dot{x} = - \frac{1}{\rho_w} \frac{\partial p}{\partial y} \quad (3.7b)$$

$$0 = - \frac{\partial p}{\partial z} - g \rho_w \quad (3.7c)$$

To unify the notation in this section with the notation we will use in the rest of this thesis let us define

$$\dot{x} = u \quad \text{and} \quad \dot{y} = v \quad (3.8)$$

where  $u$  is the east-west velocity component (positive east) and  $v$  the north-south one (positive north). Therefore,

$$fu = - \frac{1}{\rho_w} \frac{\partial p}{\partial y} \quad (3.9a)$$

$$fv = + \frac{1}{\rho_w} \frac{\partial p}{\partial x} \quad (3.9b)$$

$$- g \rho_w = + \frac{\partial p}{\partial z} \quad (3.9c)$$

The first two equations represent the geostrophic equilibrium conditions and the third the hydrostatic equilibrium condition. The implication of the geostrophic equilibrium equations is that a north-south horizontal pressure gradient gives rise to an east-west current velocity component, whilst an east-west horizontal pressure gradient component gives rise to a north-south current velocity component. In other words, flow direction is along pressure contours (i.e., along isobars) rather than down the pressure contours.

Since the pressure field in the ocean is directly related to the distribution of density, the horizontal slopes of the isopycnic surfaces with respect to level surfaces can provide the geostrophic flow at any point in the body of the ocean. Combining equation (3.9c) with equations (3.9a) and (3.9b) we obtain (and accounting for a change of sign in (3.9c) because in the ocean positive  $z$  is in the direction of depth),

$$f \frac{\partial}{\partial z} (\rho_w u) = - \frac{\partial}{\partial y} \left( \frac{\partial p}{\partial z} \right) \quad (3.10a)$$

$$f \frac{\partial}{\partial z} (\rho_w v) = \frac{\partial}{\partial x} \left( \frac{\partial p}{\partial z} \right) \quad (3.10b)$$

which integrated with respect to depth between  $z_0$  and  $z$  yield the velocity components

$$u(y,z) = - \frac{g}{\rho_0 f} \int_{z_0}^z \frac{\partial \rho_w}{\partial y} dz + u_s(x) \quad (3.11a)$$

$$v(x,z) = + \frac{g}{\rho_0 f} \int_{z_0}^z \frac{\partial \rho_w}{\partial x} dz + v_s(y) \quad (3.11b)$$

where,

- $z_0$  - is an arbitrary point along the vertical direction from which we can start the integration (called the *reference level*),
- $\rho_0$  - is a nominal value of density of the sea water (i.e., a global average value of the density of sea water), and
- $u_s(x), v_s(y)$  - are integration constants, or *reference velocities*, dependent upon the arbitrary reference level  $z_0$ .

The integral terms in eqs. (3.11) are often called the *relative velocity* or *thermal wind term* (the term has been coined from atmospheric work on wind fields). The constants of integration are normally unknown. A measurement of  $u$  and  $v$  at any depth  $z$  for a given  $x$  and  $y$  fixes the  $u_s$  and  $v_s$ . For example, if the surface velocities  $u_0(x, z=0)$  and  $v_0(y, z=0)$  were known, the reference level  $z_0$  could be chosen to be the surface of the ocean. Theoretically, the reference velocities  $u_s$  and  $v_s$  can be determined by measuring the slope of the sea surface with respect to the level surface, the geoid:

$$u_s = - \frac{g}{f} \frac{\partial \zeta}{\partial y} \quad (3.12a)$$

$$v_s = + \frac{g}{f} \frac{\partial \zeta}{\partial x} \quad (3.12b)$$

The quantity  $\zeta$  is the sea surface topography (SST), i.e., the departure of the ocean surface from the equipotential surface, the geoid. This slope is so small, typically of the order of  $10^{-3} \text{ m/km}$  (or,  $10^{-6}$ ), that its measurement is not a trivial matter.

Fixing  $u_s$  and  $v_s$ , of course, permits the determination of the absolute ocean current velocity field everywhere in the water column. Historically, the usual assumption has been to choose a reference level so that the velocity is zero there. Phrased differently, the essential assumption is that nothing much happens deep in the ocean and that the reference velocity is zero (*level of no-motion*) at a standard depth, e.g., 1000 dbars or,

1500 dbars or, 2000 dbars, etc.. However, recent research (see *Stommel & Schott*[1977], *Wunsch* [1978], *Wunsch & Gaposchkin* [1980]) has shown that this so-called *level of no-motion* is a generally poor assumption; the depth of the contours of zero velocity in the real ocean can vary greatly and the contours can even intersect the surface and the bottom of the ocean many times. In these studies alternatives to the concept of level of no-motion also have been proposed.

Two features of the geostrophic flow are noteworthy:

- (a) the slopes associated with the surface flow are very small; and,
- (b) the flow cannot be in strict geostrophic balance, because if it were, the flow could not evolve, implying that there would be neither sources nor sinks of energy and momentum. Nevertheless, the deviations from geostrophic balance tend to be small, and oceanic flows are usually treated as quasi-geostrophic.

In practice, the derivatives  $\partial\rho/\partial y$ ,  $\partial\rho/\partial x$  in eqs. (3.11) are not directly computed, but an auxiliary variable is normally introduced, the *dynamic height*. In principle, the dynamic height describes the geopotential distance between two isobaric surfaces, but in practice is usually perceived as the geometrical distance between the isobaric surfaces. As we shall see in the following sections, it also allows the estimation of the relative geostrophic velocity field for the whole ocean, if the temperature and salinity distributions are known.

In most cases, dynamic topography maps (i.e., 2-dimensional compilations of dynamic heights) for ocean-basin size areas, have been prepared from data collected by various oceanographic expeditions and ships of opportunity, in different parts of the oceans and over many years. Most of our information on subsurface large-scale currents has been obtained from these data compilations and by the use of the geostrophic method. The fact that well-defined features of the large-scale ocean circulation appear on such maps, or are repeated when there are sufficient data to prepare maps of the same area for several seasons or several individual years, indicates that these prominent features on the ocean dynamic topography maps must also be prominent features of the oceans' general circulation.

### 3.4. Classical Oceanographic Description of Oceanic Circulation

As we have already mentioned in the previous section, the reason that the geostrophic equations are used to determine the ocean current velocity field is because direct measurements of ocean currents in sufficient quantity to be useful is both impractical and unaffordably expensive. Instead, the density structure along the vertical direction is computed from measurements of the profile of temperature and salinity.

Recalling eqs. (3.11), let us focus temporarily on the integral quantity

$$\int_{z_0}^z \frac{\partial \rho_w}{\partial x} dz \quad (3.13)$$

This integral can be transformed by using the auxiliary variable *dynamic height*,  $D$ , such as [Fomin, 1964, page 142]

$$\int_{z_0}^z \frac{\partial \rho_w}{\partial x} dz = \frac{\rho_0}{g} \frac{\partial D}{\partial x} \quad (3.14)$$

where,

- $z_0$  - is the depth of the level of no motion,
- $\rho_0$  - is a nominal value for density of the sea water, and
- $D$  - is the dynamic height of an isobaric surface  $p$  (at depth  $z$ ) above the “zero” surface  $p_0$  (at depth  $z_0$ ), such that

$$D = D_0 + \Delta D \quad (3.15)$$

where,

- $D_0$  - is the dynamic height of the isobaric surface  $p$  above the “zero” surface of a *standard ocean* that has uniform values of salinity and temperature, i.e., 35‰ and 0°C respectively;
- $\Delta D$  - is the excess dynamic height (or, *dynamic height anomaly*) of the isobaric surface  $p$  from that of the “standard” ocean.

The dynamic height  $D$  of an isobaric surface  $p_1$  relative to an isobaric surface  $p_2$  (with  $p_1 > p_2$ ) is given by [Fomin, 1964, page 1] as:

$$D = \int_{p_2}^{p_1} \alpha dp \quad (3.16)$$

where,

- $\alpha$  - is the specific volume of sea water, defined as the inverse of density  $\rho$  ( $\alpha = 1/\rho$ ), and
- $p$  - is pressure.

Then, the definition in eq. (3.15) yields

$$\Delta D = \int_{p_2}^{p_1} \alpha dp - \int_{p_2}^{p_1} \alpha_0 dp \quad (3.17)$$

or,

$$\Delta D = \int_{p_2}^{p_1} [ \alpha(S,T,p) - \alpha_0(35^0/_{00}, 0^{\circ}C, p) ] dp \quad (3.18)$$

where,

- $S$  - is the salinity in parts per thousand of the sea water at pressure  $p$  (equivalently at depth  $z$ ),
- $T$  - is the temperature in  $^{\circ}C$  of the sea water at pressure  $p$  (equivalently at depth  $z$ ), and
- $35^0/_{00}, 0^{\circ}C$  - are uniform values of salinity and temperature of a “standard” ocean, with  $\alpha_0$  being only a function of pressure (depth)

The term appearing in the square brackets of the integral expression in eq. (3.18) is commonly called the *anomaly of specific volume* ( $\delta$ ):

$$\delta = [ \alpha(S,T,p) - \alpha_0(35^0/_{00}, 0^{\circ}C, p) ] \quad (3.19)$$

and eq. (3.18) can be compactly written as

$$\Delta D = \int_{p_2}^{p_1} \delta dp \quad (3.20)$$

Using eq. (3.15) we find that

$$\frac{\partial}{\partial x} (D) = \frac{\partial}{\partial x} (\Delta D) \quad (3.21)$$

and the geostrophic ocean current velocity components (given in eqs. 3.11) with the help of eq. (3.14) and eq. (3.21), obtain the following form:

$$\hat{u}(y,z) = -\frac{1}{f} \frac{\partial \Delta D}{\partial y} \quad (3.22a)$$



$$\hat{v}(x,z) = \frac{1}{f} \frac{\partial \Delta D}{\partial x} \quad (3.22b)$$

where  $\hat{u}$  and  $\hat{v}$  indicate velocity estimates, and also remembering that the assumption of the level of no-motion has rendered  $u_e$  and  $v_e$  equal to zero.

The dynamic height anomaly  $\Delta D$  is used in oceanography to construct dynamic topography maps of the oceans, thus providing the classical description of relative oceanic circulation. The north-south and east-west gradients of these maps provide the geostrophic east-west and north-south ocean current velocity components, respectively, relative to a pre-selected reference pressure level. Recalling the definition of the Coriolis parameter  $f$  (eq. 3.5), we see that the geostrophic ocean current velocities cannot be computed at the equator, because the geostrophic equations degenerate at latitude  $\phi = 0$ .

One last note concerning the units of the dynamic height anomaly  $\Delta D$  is appropriate. The SI units of  $\Delta D$  are  $m^2 s^{-2}$ , in other words units of potential. Therefore, the formal definition of dynamic height anomaly is *geopotential thickness anomaly*, which is defined as the excess of actual geopotential difference between two isobaric surfaces, over the geopotential difference in a homogeneous water column of salinity 35‰ and temperature 0°C.

Geopotential thickness anomaly maps for the world oceans have been constructed in the past through painstaking efforts of data collection, data quality evaluation, data analysis and display. The geopotential thickness anomaly maps presented in the

*Climatological Atlas of the World Ocean* [Levitus, 1982] are the most complete set of global maps produced to date.

### 3.5. Oceanic Variability in Space and Time

The classical descriptive picture of the ocean circulation emerged essentially from a geographically sparse data set, compositing years of discrete measurements, widely spaced in the horizontal and vertical dimension. Thus, time-dependent circulation features were aliased in space and time and the conceptualization of currents and mean circulation was based upon smeared fields derived from incomplete and in many cases inadequate data sets. Vast areas of the oceans still remain unexplored, e.g., the southern Pacific.

From the past few decades of oceanographic research, it is known that over great areas of the oceans there exists a variety of time-dependent processes. These time-dependent fluctuations can have energy levels one or more orders of magnitude larger than those of the mean flow [Stewart, 1981; Holland *et al.*, 1983], and also contribute dynamically to the large-scale mean flow.

All types of variable flow are commonly referred to, by physical oceanographers, by the generic term *eddies*. In analogy to atmospheric sciences, the general ocean circulation can be thought of as the “climate” of the oceans, while the eddy variability can be thought of as the “internal weather” of the oceans. The generic term *eddies* encompasses a large class of space and time variations. The spatial scales of variability can range from tens to hundreds and thousands of kilometres. The time scales can range

from weeks to months and years. The large-scale ocean current variations are usually considered to be in approximate geostrophic balance [Robinson, 1983b]. The term *mesoscale eddies* has been coined simply to indicate motions of less than the oceanic gyre scale; a typical mid-ocean spatial scale is 100 km with a life-time of the order of several weeks. These mid-ocean mesoscale eddies have swirl speeds of the order of  $10\text{cm s}^{-1}$ , which are usually considerably greater than the long-term average flow [Robinson, 1983]. A detailed account on the subject of eddies and their influence in the oceanic circulation can be found in Robinson [1983a].

In this dissertation, we will use as a working definition of oceanic variability, the temporal characteristics of the ocean occurring in the time frame from one month up to two years. Within this time frame, the spatial scales we will be concerned with cover the range from 100 km to ocean basin widths.

A number of time-dependent processes manifest themselves within this selected time frame:

- mesoscale oceanic eddies (including current meanders, ring vortices, mid-ocean eddies, etc.);
- seasonal and higher frequency variations in the dynamic state of the ocean, mainly reflecting the seasonal and higher frequency variations in the atmospheric forcing of the upper oceanic layers, through temperature, surface salinity and wind-stress fluctuations; and,

- interannual variations such as the Southern Oscillation in the tropical oceans and the *El Niño* phenomenon.

There are several observables that can be used to quantify these space/time variations of the oceans. Among such observables are:

- surface and subsurface directly measured current velocities;
- sea level heights;
- sea level slopes;
- thermodynamic properties reflecting the state of the sea water such as temperature and salinity;
- concentrations of suspended organic and mineral elements, concentrations of dissolved gases, etc.

Other data types already used for studying oceanic variability include velocity measurements obtained from neutrally buoyant floats. Satellite-tracked drifters can yield eddy kinetic energy at different depths. Potential energy variations are available from XBTs (expendable bathythermographs). Most of these observational techniques, however, suffer from temporal and spatial sampling limitations.

It is obvious that the different kinds of measurements of the variation of a given oceanographic quantity are best made in the space-time scale of the particular variation.

Thus, the study of the different time-dependent phenomena necessitates different observing and sampling strategies, making the whole process even more complex for instrumentation, logistics, data discretization and analysis. The amount of effort and money required to study the oceanic variability across the whole ocean are unrealistically large. Optimal subsets of observations have been conducted in the past by means of national and international cooperation programmes, e.g., North-East Atlantic Dynamic Study (NEADS), Mid-Ocean Dynamics Experiment (MODE) and POLYMODE, Local Dynamics Experiment (LDE), Synoptic Dynamical Experiment (SDE), International Decade of Ocean Exploration (IDOE), etc.

Further advancements in the knowledge of the ocean circulation will come from the international programmes scheduled in the early 1990's such as the World Climate Research Program (WCRP) which has two oceanographic components: the World Ocean Circulation Experiment (WOCE) and the Tropical Ocean and Global Atmosphere (TOGA). WOCE [McWilliams, 1984] will study the global ocean circulation, its variability and the ocean's interaction with the atmosphere. TOGA [Webster & Fieux, 1984] will study the interannual variability of the tropical ocean and global atmosphere, including the *El Niño* phenomenon, as well as the mechanisms which determine those variations and their predictability.

The central elements of the WOCE programme include the determination of such physical quantities as [McWilliams, 1984] (the principal observing techniques are listed in parentheses):

- ocean surface geopotential (*satellite altimetry, tide gauges*);
- wind-forcing (*scatterometers, sea level pressure, meteorological models*);

- mid-depth velocities (*ocean deep-drifters*);
- surface layer thermodynamics and circulation (*satellite altimetry, ships, surface drifters, meteorological models, XBTs, ocean acoustic tomography*);
- variability of dynamic height and chemical tracers (*shipboard surveys, ocean acoustic tomography, deep drifters, satellite altimetry*).

The central elements of the TOGA programme include the determination of such physical quantities as [Webster & Fieux, 1984]:

- ocean surface temperature;
- surface salinity;
- sea level;
- surface currents;
- wind speed and wind stress;
- surface flux measurements of radiation, moisture, and heat;
- precipitation.

Space-based sensors are indispensable for the success of both projects. Special working groups have been set up to study the fulfillment of the temporal and spatial resolution and accuracy requirements when satellite sensors are employed. Of particular interest to us is the forthcoming TOPEX/POSEIDON altimetric mission [Stewart *et al.*, 1986; Chelton, 1988], that is scheduled to provide unprecedented geodetic / oceanographic information on ocean topography and surface dynamics. Both projects (WOCE and TOGA) have already started evaluating information on oceanic variables provided by the GEOSAT altimetric mission (1985-1989). As we have stated earlier in the dissertation, the GEOSAT/ERM altimetry data are also the main source of information exploited in the present research for the purpose of estimating the space -

time variations of sea surface topography (SST) gradients, which are linked to the variable oceanic circulation.

Unlike other oceanographic observables obtained from space-based platforms, sea surface topography is an oceanic variable that is dynamically related to the three dimensional ocean circulation. The ocean surface elevation (above the equipotential surface) represents a direct boundary condition on the interior quasi-geostrophic flow fields of the oceans (recall eqs. 3.12). Moreover, the slopes of the SST along the descending and ascending altimetry tracks are directly determinable, which makes satellite altimetry even more attractive for ocean circulation studies, as we shall see in subsequent chapters. This is not so for surface temperature, sea surface roughness, dielectric constant for sea water, etc., all of which are determinable from space, but whose relationship to the flow field over the water column is obscure, at the least.

To focus a little deeper our discussion on the variability aspect, one is faced with many important physical constraints in seeking critical observables for understanding the oceanic variability on a global scale. The size of the oceans means that the observable must be measured globally. Whatever one chooses to use as an observable, it must have some directly computable relationship to oceanic flow. The time resolution of the observations is critical for the time scale of the variability to be investigated. Therefore, the global scope necessarily requires satellite techniques; sea surface topography, or sea surface topography gradients, are directly linked to surface flow magnitude and direction and the space/time resolution can be optimized by tuning the satellite orbital characteristics. Hence, satellite altimetry derived SST, or SST gradients most preferably, emerges as a unique useful observable in the context of monitoring the space/time

oceanic variability. The most obvious flaw of satellite altimetry for variability studies, is that it only provides the surface expression of the 3-dimensional ocean time dependent processes. Subsurface oceanographic in-situ information is still required for the complete 3-dimensional ocean dynamics. However, the most realistic alternative in deriving the subsurface information is the numerical modelling of the dynamic processes, and is briefly presented in the next section.

### **3.6. Ocean Dynamics Modelling Techniques**

The fact that the ocean waters are nothing else but a geophysical fluid, lend themselves to descriptive as well as theoretical studies of their dynamic regimes. Thus, a complex system like the world's oceans requires, as we saw earlier, difficult and sometimes unattainable in-situ observations before its study can progress further as a deductive body of knowledge. On the other hand, fluid dynamics theory and mathematical models offer this deductive knowledge without the need to make observations in stormy weather in the open sea. These mathematical models (analytical or numerical) are abstractions of the circulation characteristics of the oceans. Simple and highly idealized conceptual models, with incomplete physics built-in, have captured some of the aspects of oceanic circulation and have made possible major advances in understanding the general circulation of the oceans. Often these models have been built on the basis of homogeneous density oceans with smoothly and steadily flowing currents driven by steady winds. Because of practical limitations and the non-availability of the required computational power in the past, these models, often called general circulation models (GCM), can simulate a limited number of possible competing dynamic pro-



cesses from the gamut of real oceanic processes. Nevertheless, they have provided us with comprehensive descriptions of global and regional ocean dynamics.

At present, there are two kinds of ocean numerical models: general circulation models (GCM) and eddy-resolving general circulation models (EGCM). The first kind is designed to study the global structure of the ocean circulation (major oceanic gyres) and the 3-dimensional ocean density structure. The second kind includes mesoscale eddy phenomena in simulating the actual ocean dynamics, i.e., perturbations of the steady flow characteristics with specific space and time scales. An excellent description of the state-of-affairs in computer modelling in physical oceanography (i.e., on numerical ocean circulation models) has been presented by *Holland & McWilliams* [1987].

A third class of ocean GCMs has emerged during the past few years. These are oceanic data assimilation models, which incorporate procedures to include observed kinematic or dynamic constraints between the variables of the model, which are either directly observable or inferred from statistical relationships. In this case, the initial boundary conditions are updated on a regular basis by feeding the model real data.

Inherent in all model building is the question of how well, or how close the linear and non-linear dynamical regimes of the investigated system are represented in the model, without the model becoming monstrous and unsolvable.

The role of satellite altimetry in providing observations of such oceanic variables that are useful as constraints in data assimilation models is today critically examined. Investigation of satellite altimetry data assimilation techniques is also one of the key

objectives of the WOCE programme (see, for example, Chelton [1988], Stewart et al. [1986]). Hulburt [1984] gives an excellent summary on the subject of ocean forecasting and the role satellite altimetry data will play in this respect.

We believe that there is one additional observable that can contribute valuable constraints to general circulation models and should be incorporated in the data assimilation techniques. This is the sea level height changes recorded by tide gauges spread all over the coastal and islandic regions of the world. A near real-time sea level change network is already in place for most of the south Pacific Ocean yielding a wealth of information [Wyrki, 1985].

**Elaboration on ocean circulation models:** In order to study the large-scale ocean circulation and be able to calculate ocean currents, a system of governing equations and appropriate boundary conditions are necessary. To investigate the large-scale currents in a baroclinic ocean (i.e., an ocean with variable vertical density structure) we can use the so-called Boussinesq approximation of the hydrodynamic equations of motion [Marchuk & Sarkisyan, 1989], the hydrostatic equation, the equation of continuity of incompressible fluids, the equation of transfer of heat and salt, and finally the equation of state, i.e., a system of seven equations with seven unknown parameters (see equations 1.1 through 1.7 in *Marchuk and Sarkisyan [1989]*). The seven unknown quantities are the three velocity components of the fluid (which are usually defined in global scale problems along the east-west, north-south, and local vertical directions), pressure, density, temperature and salinity. In general terms, the problem can be identified as an initial value boundary problem. Boundary conditions will be, generally

speaking again, supplied on the ocean surface, at the ocean bottom, and at the sides of the ocean basins (lateral boundaries).

The system of equations and boundary conditions represent the main equations for any problem in ocean dynamics. However, we have to deal with a complicated system of non-linear equations and most of the time we opt for alternatives which simplify these equations, so that they can be solved to a satisfactory degree of approximation without a perceptible loss of accuracy. The first simplification to adopt concerns the equations and the boundary conditions for large-scale flows. Thus, certain non-linear terms can be excluded from the formulation, leading to what may be called the quasi-geostrophic linear model. In that way, it is possible to construct a simpler, more economical scheme for the calculation of the world ocean currents. The quasi-geostrophic model is not applicable at the equator belt due to the presence of the Coriolis parameter in the equations. Usually a narrow equatorial belt with a width of few degrees on each side of the equator is left out of the computations.

The initial data play a crucial role in forecasting ocean currents. The simplest scale analysis has shown that for forecasting the ocean current velocity field, one needs a fine resolution grid, with grid spacing of 100 km or less, for the initial data [*Marchuk & Sarkisyan, 1989*]. But the number of hydrological stations is so small that direct in-situ measurements cannot provide the information on the oceanic fields needed for the proper initialization of the models. This is where the contribution of satellite altimetry comes into play. Direct observations of the SST gradient field on a synoptic time-scale (defined here as a few to several days) for the whole ocean is more than welcome. In fact, satellite altimetry is the only technique that can possibly provide both

the spatial and temporal resolution. Nevertheless, the data from coastal and islandic tide gauges is definitely an asset and it should not be ignored.

### 3.7. Summary

To summarize this chapter:

- as recently as 25 years ago, it was assumed that oceanic parameters varied smoothly with depth. Newly developed instruments and recent observations, however, have shown that the vertical distributions of oceanic properties are often far from varying smoothly.
- major ocean current systems circulate continuously, but with fluctuating velocity and position;
- the oceans cannot any more be treated as a steady-state system of large-scale wind-driven currents with a weaker thermohaline deep circulation;
- detailed studies in recent years have revealed a hitherto unexpected wealth of detail in the form of eddy fields, a collective term used under the general rubric of space-time variability;
- to advance our knowledge of the oceans, we need more data in two forms: global synoptic data and time series observations over periods of at least a few years, preferably 3-5 years long. The term synoptic

data here denotes data for an area collected as quickly as possible so as to alleviate the effect of time variations.

- it is quite clear that there are never going to be enough oceanographic expeditions to satisfy the data requirements, and the only possible way in which this extra information is going to be obtained is by using satellites to observe as many as possible of the surface characteristics together with realistic in-situ oceanographic instrumentation for mainly subsurface characteristics;
- to use numerical modelling techniques for both large-scale and intermediate-scale motion studies, one needs the best available information on sea surface slopes, on the density distribution and on air/sea exchange processes in order to be able to initialize the numerical studies as well as to test their results. *Satellite altimetry is the only technique capable of fulfilling the role of the provider of sea surface slopes at regular intervals and with global coverage*

## Chapter 4: Satellite Altimetry

### 4.1. Preliminary Considerations

For almost a century, the modern era of oceanographic research has depended on ocean measurements made by sea-faring ships as part of either dedicated expeditions or ships of opportunity. Until 20 years ago, these earth-bound platforms had made possible all the knowledge we had about the oceans. The space age, however, changed irrevocably the concept of *surveying the earth and its environment*.

Space-based platforms carrying a multitude of sensors today provide continuous, all-weather, day or night, global observations (direct or indirect) of a large number of physical parameters describing the earth system. Satellite oceanography is just one of the many disciplines that emerged during the past two decades and which already enjoys the benefits of the space age. Simply put, satellite-based oceanographic platforms differ from shipboard oceanographic platforms only in being more convenient, more expeditious, unmanned, passive or active global data collectors.

To date, it has been shown that oceanography dedicated sensors aboard satellites are capable of measuring sea level height, surface winds, ocean wave regimes, sea water

temperature and salinity, ocean currents, phytoplankton, fish schools, sea ice, and even bathymetry. From a different stand point, *space platforms are environmental vigilantes, not only for naturally occurring phenomena, but also for man-induced environmental hazards.*

A valuable general reference on satellite oceanography is the book by *Stewart* [1985]. A number of books on remote sensing contain chapters or sections on the subject of oceanography from space. Most notable are books that contain collections of papers published on the subject, such as those by *Gower*, [1981] and at an earlier date by *Ewing* [1965]. Several scientific journals have published special issues and special volumes on applications, theory and instrumentation, such as the *Journal of Geophysical Research (JGR)*, Vol. 84 (B8), 1979 on the scientific results of the GEOS-3 mission, *JGR*, Vol. 87 (C5), 1982 on the SEASAT mission geophysical evaluation, *JGR*, Vol. 88 (C3), 1983 on the scientific results of the SEASAT mission, the *IEEE Journal of Oceanic Engineering (OE)* , Vol. 2 (1), 1977 on Radio Oceanography, *IEEE OE*, Vol. 5 (2), 1980 on SEASAT sensors, *Marine Geodesy*, Vol. 8 No. 1-4, 1984 on satellite altimetry, just to name a few.

All space-based sensors operate using the properties of electromagnetic wave propagation. Their operational principles depend on the way electromagnetic energy interacts with matter. Remote sensing of the oceans is based on the response of a given sensor to the ocean surface. It is rather convenient to divide this response into two types:

- (a) geometric; and
- (b) physical.

Under the first category, we classify changes in the ocean surface relief resulting from a number of generating forces, such as tidal, geostrophic and wind action. Under the second category, we classify changes in the physical characteristics of the ocean waters, such as temperature, salinity, ocean colour, sea-state, refractivity, reflectivity, etc.

Satellite imagery in the visual and infrared portion of the spectrum has proved useful for studies of ice conditions and monitoring large-scale sea-ice coverage and movements. Both visible and infrared systems are severely limited by cloud cover, darkness being a serious limiting factor for sensors operating in the visible part of the spectrum.

Satellite microwave techniques, however, offer all-weather, day and night observations. They employ either passive or active sensors. Passive systems (microwave radiometers-scanners) on one hand, measure the electromagnetic energy (EM) emitted by matter. Active measurements on the other hand, are made by a variety of special radars. Two types are particularly useful in discerning oceanic parameters: *scatterometers* and *altimeters*. Scatterometers “illuminate” the sea surface at non-vertical angles and then measure the intensity of the returned signal, which is directly related to the roughness of the sea surface. Measurements of intensity are used to calculate surface wind velocity. Altimeters “illuminate” the sea surface at the nadir using a short pulse of EM radiation, and then measure the travel time, intensity and structure of the reflected pulse. The intensity and structure of the returned pulse are used to derive wind speed and wave height, respectively. The two-way travel time of the pulse is related to the height (altitude) of the spacecraft above the ocean surface.



The main point we wish to make in this section is that the proposals of the late 1960s and early 1970s regarding geodetic/oceanographic satellite remote sensing applications have for the most part been tested and validated during the late 1970s and early 1980s. The result has been the foundation of the next crucial step, that is, putting in place satellite systems for delivering sensor data of global oceanic parameters on a long term, consistent and easily accessible basis, e.g., the European ERS-1 and the Franco-American joint TOPEX/POSEIDON missions scheduled for the early 1990s.

The radar altimeter sensor will be analysed in some more detail in the next section, because in this dissertation only data from this sensor are used to extract ocean dynamics information.

## 4.2. Radar Altimetry

The feasibility of determining ocean related parameters from active, nadir looking microwave radars has been discussed and demonstrated by a number of authors including *Greenwood et al.* [1969], *Miller & Hammond* [1972], *McGoogan* [1975], *Walsh* [1974; 1979], *Parsons* [1979], *Fedor et al.* [1979], *Brown* [1977; 1979] etc.

A satellite radar altimeter consists of, for simplicity:

- a transmitter,
- a sensitive receiver, and
- an accurate clock.

In principle, the radar altimeter sends out short pulses of EM energy toward the ocean surface, which are bounced back and captured by the altimeter antenna. An informa-

tive and simple enough exposure of the operational principles of pulse-limited radar altimeters is given in *Stewart* [1985; Ch. 14]. The most recent summary on altimeter sensor algorithms is given in *Chelton* [1988].

The interaction of the altimeter transmitted EM radiation (in the form of high repetition sharp pulses) with the instantaneous ocean surface provides the basic measurements the altimeter is capable of performing:

- (a) the time delay between the transmission and reception time of the radar pulse;
- (b) the shape (broadening-stretching) of the leading edge of the returned signal; and,
- (c) the amplitude of the returned signal.

In reality, the returned signal is not a pure pulse but an average returned waveform. There are four parameters that need to be resolved in order to determine the leading edge of the average returned waveform: the mean time of returned signal arrival, the rise time of the leading edge, the plateau amplitude of the waveform and finally, the average noise level (altimeter jitter).

Troughs of waves tend to reflect altimeter pulses better than do wave crests. Thus, the centroid of the distribution of returned signal power is shifted away from the mean sea surface level illuminated by the transmitted signal towards the troughs of the waves. This shift is referred to as the *electromagnetic bias* (EM-bias) and it causes the

altimeter to overestimate the mean height of the illuminated instantaneous ocean area (labelled from now on as the altimeter's *footprint*). The altimeter, therefore, determines the altitude of the spacecraft above the instantaneous electromagnetic sea surface (IEMSS), by measuring the interval between transmission and reception of the pulse, making also allowance for the transmitter/receiver internal time delays. The IEMSS can be related to the instantaneous mean sea surface (IMSS) if the average wave height over the altimeter's footprint is known.

The stretching of the leading edge of the sea echo signal is a direct measure of the r.m.s wave height at nadir. The higher the waves, the longer the rise time of the leading edge of the returned signal.

Under certain assumptions, it is also possible to infer the along track surface wind speed using the amplitude of the returned signal. The power of the returned signal is expressed as the normalized radar cross section  $\sigma_0$ , which is proportional to the ratio of received to transmitted power, normalized by the area illuminated by the radar pulse [Chelton, 1988]. The wind speed is estimated from measurements of  $\sigma_0$ , using either theoretical or empirical model functions that relate sea surface roughness (represented by  $\sigma_0$ ) to near-surface winds.

The primary quantity of interest to us here is the altitude of the spacecraft above the IMSS. This quantity, along with satellite orbital information, can be used to deduce the mean height of the IMSS above a reference surface, that is, the reference surface used for the orbital height determination. Thus, the IMSS measurement is also intimately

related to the earth's non-uniform gravity field. We shall see more details on this subject in subsequent sections.

#### 4.2.1. Satellite Altimetry Errors

Accurate altimeter measurements are difficult to make, and several sources of error must be considered. Three broad classes of errors influence altimeter measurements:

- (a) sensor (instrumental) errors;
- (b) signal propagation errors; and,
- (c) spacecraft position errors.

Under instrumental errors we can distinguish altimeter timing errors, altimeter calibration errors, altimeter pointing errors, altimeter tracking errors, and altimeter noise. Some of these errors are evaluated on the ground before launch, and some during the initial mission evaluation period. Fortunately, most of these errors can be controlled or eliminated from the observations to a very large extent. A brief account of these type of errors can be found in *Stewart* [1985, pp. 273-274] and *Chelton* [1988].

Under signal propagation errors we can distinguish ionospheric and tropospheric refraction errors, which affect the travel time of the emitted EM radiation. Furthermore, the tropospheric refraction errors can be broken down into dry and wet tropospheric delays.

The ionospheric delay errors can be either estimated by operating the altimeter at two widely spaced frequencies, or using ground based measurements to observe the total electron content of the ionosphere, or by using empirical ionospheric models. In the

first case (dual frequency altimeters) the ionospheric delay errors are almost totally eliminated. In the case of ground based measurements of the state of the ionosphere, the propagation delays can be only partially compensated, because of the limited way of mapping accurately the total electron content along each satellite transmission path at all times. The ionospheric empirical models offer the last resort, since they can only depict an average picture of the ionosphere's state at any location and time. "Quiet sun" periods (i.e., low ionospheric activity) can be effectively exploited by scheduling altimeter missions carrying single frequency altimeters at such times and thus, minimizing the influence of unmodelled ionospheric delays on the measurements.

The dry tropospheric delay, although larger in magnitude than the wet one, is nearly constant in the zenith direction and thus much easier to account for than the wet one. Atmospheric surface pressure data can be used to estimate the dry component. However, the water vapour content of the troposphere is difficult to handle observationally. It is usually compensated for by employing empirical models. An expensive alternative is to include in the spacecraft's payload a microwave radiometer, which is capable of directly mapping the water vapour content along the altimeter signal travel path to provide on-line wet delay corrections.

Under spacecraft position errors we can distinguish orbital errors and coordinate system errors. The satellite's orbit is the "reference frame" from which the altimeter measurements are made. Since the radar sensor operates in a nadir looking mode, an error in the radial component of the satellite's position vector, directly produces an error in the determination of the height of the sea surface.

In theory, the ephemerides of a satellite (i.e., tabulated values of the position and velocity of the satellite as a function of time) can be calculated from Newton's equations of motion, by knowing the forces acting upon the satellite. In practice, the acting forces are not known with sufficient accuracy to permit accurate calculations of the ephemerides between infrequent observations of the satellite's position vector by ground-based tracking stations. Thus, an accurate ephemeris, in addition to accurate ground-tracking, requires accurate estimates of the forces acting on the satellite and numerical integration of the equations of motion. The accuracy of the numerical integration, of course, depends critically on the knowledge of the applied forces. Those forces, in relative order of importance (for typical altimetric satellites), are:

- (a) the spatially varying components of the earth's gravity field;
- (b) atmospheric drag;
- (c) solar radiation pressure;
- (d) ocean tides; earth tides;
- (e) third body gravitational effects (moon, sun); and,
- (f) outgassing from the satellite.

Uncertainties in the knowledge of the earth's gravity field directly propagate into radial orbital errors. In addition, these uncertainties introduce geographical correlations into the radial orbital errors. The best ephemerides of altimetric satellites still have errors of a few to several decimetres, thus dominating the altimeter measurements.

Closely allied with the orbital errors are the errors associated with the coordinate system of the network of ground-based stations used to track the satellite's positions. The satellite coordinate system (the orbital coordinate system) is also related to a geocentric coordinate system through such parameters as polar motion and length-of-day. In addi-

tion, station coordinates are influenced by earth tides, ocean loading and tectonic movements.

A comprehensive error budget delineating individual error sources can be found, for example, in *Stewart* [1981, Table 2, pp. xi], *Stewart* [1985, Table 14.3, pp. 267], *Stewart et al.* [1986, Table 2, pp. 7]. However, what is important to stress here is that each error manifests itself in a more or less unique way according to wavelength and its time-varying behaviour. This wavenumber / frequency split of error sources becomes very helpful in designing analytical and numerical techniques that remove certain influences from the altimetry measurements.

A detailed expose of the nature, modelling and reduction techniques of the radial orbit errors for ocean dynamics applications of satellite altimetry can be found in studies by *Wunsch & Gaposchkin* [1980], *Colombo* [1984], *Wagner* [1985], *Tapley & Rosborough* [1985], *Rosborough* [1986], *Pisacane* [1986], *Mazzega* [1986], *Tai & Fu* [1986], *Engelis* [1987], etc.

In summary, instrumental errors, propagation errors, and sea surface state taken together, can amount to an inaccuracy of 10-30 cm in altimeter height under typically favourable conditions and, fortunately, can be reduced to acceptable levels for ocean dynamics applications as we shall see later on. Only uncertainties in the knowledge of the earth's gravity field (being critical for defining both the geoid and the satellite's ephemerides) remain as important and partially solved problems today. Using present day gravity field knowledge and tracking techniques, orbits can be calculated with an uncertainty of +/- 40 to 100 cm in the radial direction. Expected improvements in the

knowledge of the earth's gravity field, and new methods of continuously tracking satellites using radio signals from the Global Positioning System (GPS), should make possible calculations of the radial component of satellite position vectors with an accuracy of +/- 5 to 15 cm for the next generation altimetry missions such as TOPEX/POSEIDON [Stewart *et al.*, 1986].

### 4.3. Satellite Altimetry Geometrical Considerations

Some of the fundamental geometric relations involved in satellite altimetry measurements are schematically presented in Figure 4.1.

The basic altimeter measurement is the geometric distance between the altimeter's antenna electrical centre and the IEMSS over the altimeter's footprint. If the distance between the center of mass of the satellite and the antenna electrical centre is known, then the geometrical quantity "measured" is the altitude  $a$  in Fig. 4.1 of the spacecraft above the IEMSS. Knowledge of the distance "center of mass to electrical centre" is not required for studies of temporal variations of oceanic parameters, since it can be treated as a constant bias.

The basic altimeter *derived* quantity is the geometric distance between the instantaneous mean sea surface (IMSS) and the reference ellipsoid, above which the geodetic height  $h$  of the satellite's centre of mass is reckoned. We will label the quantity  $\zeta$  in Fig. 4.1 as the instantaneous sea surface height (ISSH).



# SCHEMATIC SATELLITE ALTIMETRY GEOMETRY

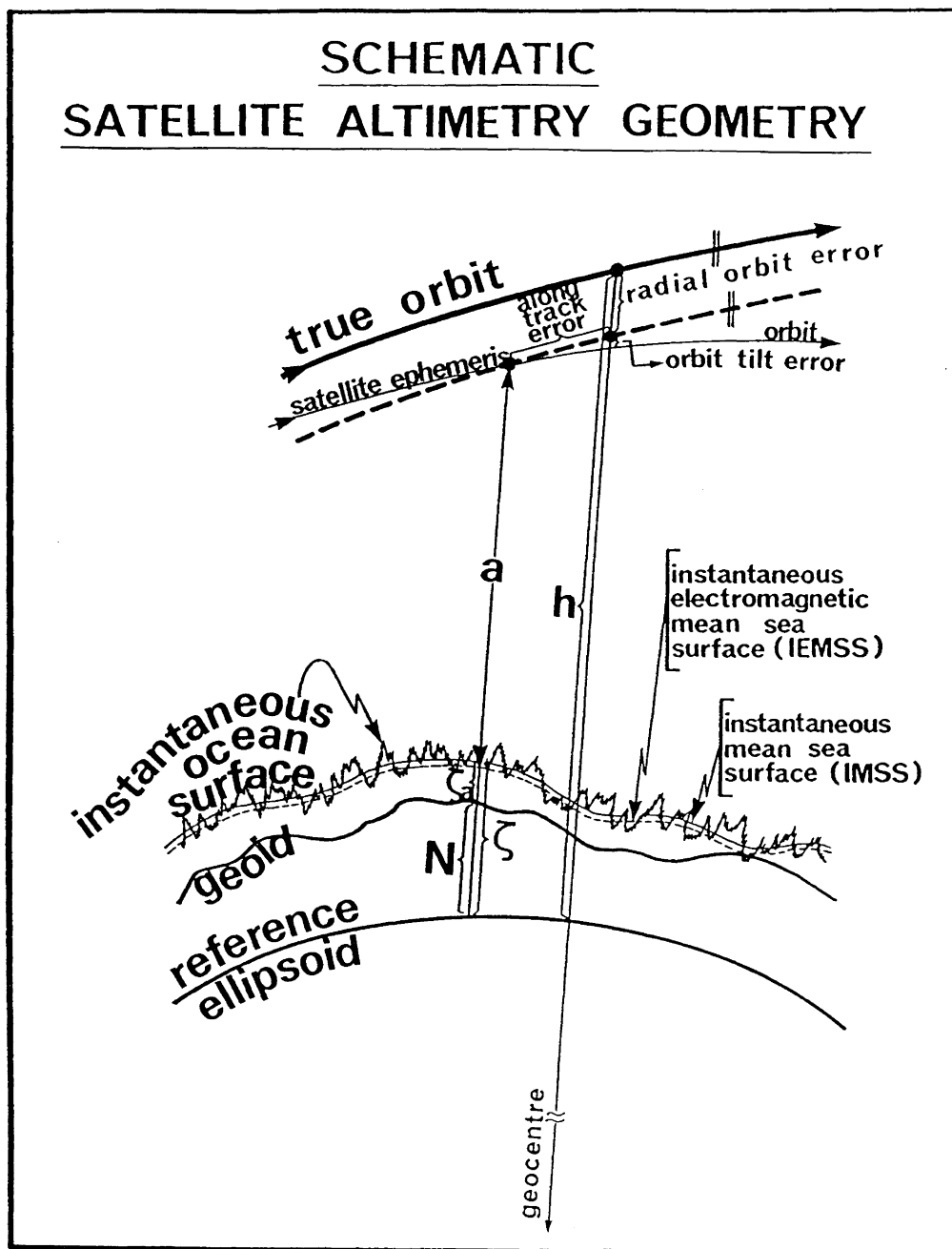


Fig. 4.1. Schematic illustration of fundamental geometric relations involved in satellite altimetry measurements.

The geometrical distance between the reference ellipsoid and the equipotential level surface, the geoid, is the geoidal height  $N$ . The departure of the IMSS from the geoid is the instantaneous sea surface topography (ISST) and it will be labelled here as  $(\zeta_a)$ . The quantity  $\zeta_a$ , all non-oceanographic effects removed, is the ultimate quantity to be studied for oceanic space/time variability.

For quantitative ocean dynamics studies, there is a potentially large number of contributions towards the basic altimeter derived quantity  $\zeta$ , which can be either viewed as errors or as corrections. We select here to treat them as corrections. They involve either the measurements  $a$  and/or the determination of the satellite's geodetic height  $h$ . Ideally, if both  $a$  and  $h$  were free of errors then we could write,

$$\zeta \equiv h - a \quad (\text{ideally}) \quad (4.1)$$

Let us briefly see what corrections should be applied to both  $a$  and  $h$  to be able to extract the corrected ISSH. For convenience, we will group these corrections into three categories:

- (i) instrument and air/sea interface corrections;
- (ii) atmospheric propagation corrections; and
- (iii) external physical and geophysical corrections.

A number of instrumental corrections and air/sea interface corrections must be applied to obtain accurate range estimates  $a$ . The most important are [*Chelton*, 1988]: the bias in onboard tracker timing estimates, calibration biases, antenna mispointing and antenna gain pattern and attenuation, as far as instrumental corrections are concerned; electromagnetic bias and skewness bias, for air/sea interface corrections. Usually, most

of these corrections are applied either during ground based processing before the altimeter data are released for scientific use or evaluated during pre-launch and post-launch mission validation stages. However, earlier experience with satellite altimetry data has shown that certain corrections may still be required to be applied to the released data records, e.g., time-tagging bias in the SEASAT records.

The EM-bias (see section 4.2) is purely due to the interaction between EM radiation and the sea surface and depends on a variety of surface wave characteristics. However, the only wave characteristic that is measured by the altimeter is the significant wave height (SWH). Since the EM-bias tends to increase with wave height, it is generally expressed as a percentage of the SWH. The order of magnitude of this correction is derived empirically from in-orbit measurements and usually ranges from 1% to 5% of the SWH. It has to be always subtracted from the measurement of the range  $a$ . Since SWH tends to vary latitudinally (see, for example, *Chelton et al.* [1981]), any systematic errors in the EM-bias would introduce latitudinal biases in the range measurements, which would result in erroneous mean zonal geostrophic currents estimated from altimetry data.

The skewness bias is related to the distribution of sea surface height within the altimeter footprint. If the distribution is not symmetric (see *Chelton* [1988, pp.26-27]) then, the IEMSS is further shifted towards the wave troughs [*Hayne & Hancock*, 1982]. At the present time, estimates of the magnitude of the skewness bias in altimetric data records are very uncertain [*Chelton*, 1988].

Atmospheric propagation corrections (ionospheric and tropospheric delays) must be applied to the range measurements  $a$ . Details about obtaining these corrections have already been presented in section 4.2.1.

The altimeter range measurement also contains the signature of the total tide, i.e., ocean tide plus earth tide plus ocean tide loading effects, as the oceans and the sea floor respond to tidal forces. It is common practice to account for the ocean tidal height by using global empirical models (e.g., *Schwiderski* [1980]) in the open ocean areas, where the validity of the models is assessed to be about 10 cm or better. Earth (body) tide is corrected for by using analytical expressions of the tide generating potential. The effect of ocean tide loading can be corrected for by using an approximate relationship between ocean tidal height and elastic yielding of the sea-floor. In the past, this secondary effect has not been considered, because it was below the level of the altimeter measurement precision.

An additional correction to the altimeter range that is necessary, is due to atmospheric pressure effects over the entire ocean surface. Changes of atmospheric pressure about the mean pressure over the whole ocean give rise to changes in the sea level height. This is commonly referred to as the “inverted barometer response” of the ocean. As a rule of thumb, an increase (decrease) of 1 mbar in atmospheric pressure over the mean pressure, results in a decrease (increase) of 1 cm of the ocean surface elevation. The correction can be evaluated from the hydrostatic equation if the actual sea level atmospheric pressure is known.

The tidal corrections and the inverse barometer effect are collectively here labelled “external geophysical corrections”.

The most serious limiting factor, however, in accurately determining the instantaneous sea surface height (ISSH) is the knowledge of the precise geodetic height of the satellite.

#### **4.4. Satellite Altimetry and Orbits**

Precise orbit determination (POD) is required to determine the satellite's state vector at all times. This is accomplished by a combination of ground based observations of the spacecraft's range and range rate, and dynamical orbit modelling used to reconstruct the spacecraft's trajectory whenever the satellite is not in the field of view of the tracking stations. Currently, the major source of POD error is the radial orbit error.

The reason that the radial orbital error is the most important one is because it directly degrades the information on the ISSH. The along-track orbital error component is of second order in significance, while the cross-track orbital error component, is practically of no significance, since the satellite's footprint has large enough dimensions (larger usually than 1.5 km in diameter) to make any cross-track positional uncertainty inconsequential to the altimeter measured range.

The radial orbital error can reach magnitudes of several metres. The bulk of this error is due to insufficient knowledge of the geopotential (potential coefficient errors) and due to initial satellite state vector errors used in orbit integration. An extensive inves-

tigation of the nature and structure of orbital errors as they pertain to satellite altimetry can be found in *Engelis* [1987].

In a conceptual way, the radial orbital error,  $\Delta r$ , can be expressed as the sum of two principal components:

$$\Delta r = \Delta r^G + \Delta r^I \quad (4.2)$$

where  $\Delta r^G$  represents the radial errors of direct gravitational origin and  $\Delta r^I$  the radial errors due to initial satellite state vector errors. Furthermore, following *Engelis* [1987], we can partition the errors of direct gravitational origin into first order ( $\Delta r_1^G$ ), resonant ( $\Delta r_r^G$ ), and second order components ( $\Delta r_2^G$ ):

$$\Delta r^G = \Delta r_1^G + \Delta r_r^G + \Delta r_2^G \quad (4.3)$$

A similar partition of the radial orbit error due to initial state vector uncertainty is:

$$\Delta r^I = \Delta r_1^I + \Delta r_2^I \quad (4.4)$$

Then equation (4.2) can be written in an expanded form:

$$\Delta r = \Delta r_1^G + \Delta r_r^G + \Delta r_2^G + \Delta r_1^I + \Delta r_2^I \quad (4.5)$$

Without going into any more details, what is important to realize is that the radial orbit error components in equation (4.5) predominantly manifest themselves as *1 cycle / revolution* signatures. This result is extremely useful when developing analysis techniques for the recovery of oceanic parameters from satellite altimetry. The *1 cycle /*

*revolution* radial orbital error is, therefore, a long wavelength error compared with the wavelengths of the time-varying SST features. Of course, there are additional frequencies of the radial orbital error at *2 cycles / revolution* and *3 cycles / revolution* etc., however, their amplitude is much smaller than the *1 cycle / revolution* one.

Since the predominant radial orbit error is of long wavelength nature, the usual way to deal with it when processing ISSH observations has been to model it either as an algebraic polynomial in time or as a trigonometric polynomial in time. Depending on the satellite arc-length over which the algebraic polynomial is applied, it can be represented as a radial shift only for arcs shorter approximately than 1000 km, a shift and a slope for arcs shorter approximately than 10,000 km, or as a quadratic polynomial for arcs up to half an orbit revolution. The trigonometric polynomials are usually employed to model one complete orbit revolution.

One last note regarding radial orbit determination: atmospheric propagation effects enter indirectly into the determination of the satellite's geodetic height through the ground station tracking measurements, as do the tidal influences on the satellite's orbit and the positions of the tracking stations.

#### **4.5. Ocean Dynamics Information from Satellite Altimetry**

Oceanography from space has successfully demonstrated its “unlimited” capabilities in the past two decades through such satellite missions as *Skylab* (1973), *GEOS-3* (1975-1978), and *SEASAT* (1978).

The first dedicated oceanographic satellite altimetry mission was the SEASAT mission. Unfortunately the satellite ceased to function in October of 1978, 3 months after its launch. The 3-month long data sets from the SEASAT mission provided the scientific community with almost a full decade of multi-disciplinary research. Most importantly, the SEASAT mission demonstrated among other things, that a short-pulse altimeter is capable of resolving +/-10 cm ocean-surface elevation changes.

The long-lived GEOSAT satellite (1985-1990) promises a tremendous wealth of information to be extracted from the global ocean data base it generated. It is expected that oceanographic applications will culminate with the currently operational *GEOSAT* mission (1985-1989) and the enroute missions of *ERS-1* (1991) and *TOPEX/POSEIDON* (1992).

In section 4.3 we briefly presented the fundamental geometric relations involved in satellite altimetry measurements. In Figure 4.1 we illustrated the conceptual relationship between the altimeter's geodetic height  $h$ , the altimeter measured range  $a$ , the geoidal height  $N$ , the height of the instantaneous mean sea surface  $\zeta$  above the reference ellipsoid, and the instantaneous sea surface topography (ISST)  $\zeta_a$ .

The ISST can be determined, in concept, quite simply from satellite altimeter measurements using an expression that relates the above cited last three quantities:

$$\zeta_a = \zeta - N = [ h - a ] - N \quad (4.6)$$



The expected magnitude of SST is of the order of  $\pm 1$  to 2 metres and its time variations (apart from tidal, wind setup and wave effects) are expected to be of the order of 1m. The heights  $\zeta$  contain errors from a number of sources as we have seen in earlier sections. These errors must be held below 10 cm if these data are to be used in determining the quantity  $\zeta_a$ . Although these accuracies are stringent, they are possible. Also, as we have seen earlier, the horizontal gradients of  $\zeta_a$  can be related to the ocean surface circulation through the geostrophic equations presented in Chapter 3, equations (3.12). A gradient with magnitude of  $2 \times 10^{-6}$ , corresponds to a sea surface slope of 20 cm / 100 km.

It is therefore evident from equation (4.6), that the accuracy of the ISST determination for ocean dynamics studies depends upon:

- (i) the geodetic height of the satellite being defined to +/- 10 cm;
- (ii) the geoid, being defined with equivalent precision; and
- (iii) the radar altimeter range, being at the sub-decimetre level.

The imprint of the gravity field on the ocean surface is quite stable, meaning that within time scales of few to several years, the geoid time variations are for all practical purposes negligible. This statement leaves us only to be concerned with the spatial variations of the geoid signal over the oceans. In contrast, ocean dynamics phenomena -as the name suggests- display relief signatures that change with time. Thus, it is possible in practice to separate geoidal from oceanographic effects in altimetry data, something that has been done successfully in the past decade of altimetry applications. None the

less, the altimetry data, namely  $\zeta$ , cannot be utilized fully without independent and accurate models of the marine geoid, if expressions such as (4.3) are used to obtain the oceanographic signal  $\zeta_a$ .

We return to equation (4.6) which is now written as:

$$\zeta_a(\phi, \lambda, t) = \zeta(\phi, \lambda, t) - N(\phi, \lambda, t) \quad (4.7)$$

Since the time variations of the geoid over a few years are generally believed to be well below the currently available altimetry accuracies, we can write

$$N(\phi, \lambda, t) = \overline{N(\phi, \lambda)} \quad (4.8)$$

and, hence

$$\zeta_a(\phi, \lambda, t) = \zeta(\phi, \lambda, t) - \overline{N(\phi, \lambda)} \quad (4.9)$$

where the overbar denotes the time-averaging operation.

Spatial variations in  $\zeta_a$  can then be computed from

$$\frac{\partial \zeta_a}{\partial x} = \frac{\partial \zeta}{\partial x} - \frac{\partial \overline{N}}{\partial x} \quad (4.10)$$

where  $x$  is the spatial coordinate. The implications of eq. (4.10) are immediate. It gives the horizontal gradient of ISST, which is the quantity directly related to surface ocean dynamics as we saw in Chapter 3. There are several serious complications hidden behind these last three simple equations, which relate to the measurement and the

modelling processes that provide  $\zeta$  and  $N$ . These complications arise from the accuracy with which these quantities can be derived as well as from the fact that the errors associated with  $\zeta$  and  $\bar{N}$  occur at different space and time scales. Generally speaking, a useful estimate of  $\partial\zeta/\partial x$  can be obtained by using various smoothing, filtering, or other statistical techniques.

Given that the time variable circulation is discernible from the altimeter measurements, since the marine geoid can safely be assumed time-invariant within the working time scales of a few days to a few years, the problem becomes one of ocean sampling strategy.

The satellite orbital parameters, specifically orbit inclination and altitude, set the spatial and temporal sampling scales the particular altimetry mission can provide us with. Therefore, there is an interplay between time and space resolution of oceanic phenomena and orbit configuration. This interrelationship dictates the satellite based oceanic space/time scales recoverable, and the objective of the mission becomes an optimization problem with specific goals in mind. The orbital inclination defines the maximum latitudinal (poleward) coverage, while the satellite's ascending node precession rate dictates the size of the "grid" generated by the satellite's groundtrack at the equator.

An orbit suitable for ocean dynamics studies is, of course, an orbit that will allow revisiting of the same oceanic location at regular time intervals. Shorter time intervals of revisiting one location results in coarser groundtrack spacing at the equator, thus effectively limiting the spatial resolution, while a denser grid of groundtracks will re-

sult in less frequent observations at the same location. Thus, a trade-off must be achieved between those two sampling strategies that will allow meaningful recovery of ocean dynamics information. Figure 4.2 (adapted from *Born et al.* [1984]) shows the inverse relationship between spatial and temporal resolution which prevents adequate sampling of oceanic phenomena in both space and time simultaneously.

From Figure 4.2 it is also clear that there will not be any significant information for oceanic parameters below a critical wavelength for a given optimal orbit.

In view of all of the above discussion, the methods of analyses required for ocean dynamics studies are also dependent upon the wavenumber / frequency characteristics recoverable from a particular satellite altimetric mission. Moreover, certain error sources associated with the altimetric observations may play havoc with the recovery of the desired wavenumber / frequency oceanic characteristic scales.

Procedures for circumventing these sort of problems have been developed and successfully used in the past 10 years. For example, since the geoid can be considered time-invariant at time scales less than few years, it is possible to measure the time variable component of SST and thus the time variable component of oceanic flow by using only the measured altimeter range and orbit information. This becomes obvious from eq. (4.9) if we write it for two different time-epochs for the same oceanic location. The epoch-to-epoch difference ensures that the time variable SST (i.e.,  $\Delta\zeta_a$ ) becomes independent of the geoid knowledge.

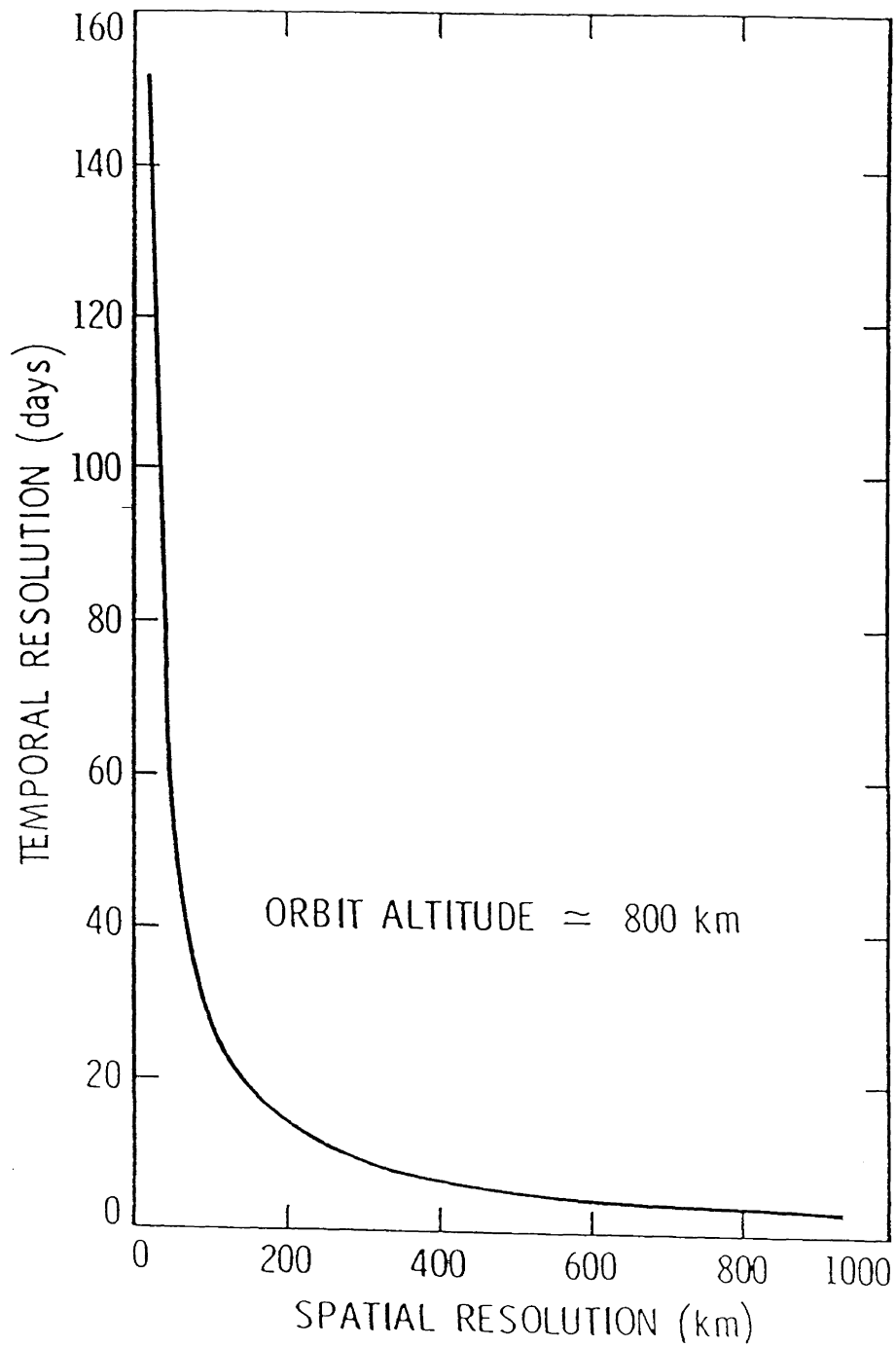


Fig. 4.2. Graphical illustration of the inverse relationship between spatial and temporal resolution of satellite altimetry measurements (adapted from *Born et al.* [1984]). This inverse relationship prevents adequate resolution of ocean dynamics phenomena in both space and time *simultaneously*. Temporal resolution refers to the time between repeated tracks, while spatial resolution is related to cross-track spacing at the equator.

These “geoid-independent” analysis techniques for studying the temporal variations of the SST fall into two basic categories:

- (a) collinear tracks (overlapping passes) analyses; and
- (b) mean sea surface models.

There is, however, a third technique that under certain circumstances can also be used to determine the time variable SST, and is essentially a by-product of the *cross-over adjustment technique* used to correct for orbital errors. In essence, this is also a geoid-independent technique, since at a cross-over point the geoidal height  $N$  is by definition the same. More information about these techniques will be presented in the next section.

At this point it is desirable to summarize the information made available in this chapter so far. A satellite measures the instantaneous sea surface topography (ISST) averaged over the satellite's footprint. Once all the pertinent corrections are applied to the measured ISST, the space-time SST field (i.e.,  $\zeta_a(\phi, \lambda, t)$ ) can be determined. The spatial variation of SST provides information on the oceanic flow field. Time variations of SST at one location provide information on the time variable oceanic flow. Time variations of SST are independent of the geoid signal, assuming time scales of up to few years. It is immaterial for surface ocean dynamics studies, whether we deal with the determination of the SST or its spatial derivatives directly.

## 4.6. Techniques for Studying Temporal Variations of SST

Since the theme of this thesis work is the investigation of the ocean current variability and its influence on the LOD, the time varying component of the SST is the signal we are interested in. The horizontal gradients of the SST as a function of position and time are the primary parameters needed to quantify the variable ocean surface circulation.

It is convenient to treat the SST as the sum of mean and fluctuation quantities:

$$\zeta_a(\phi, \lambda, t) = \overline{\zeta_a(\phi, \lambda)} + \zeta_a^*(\phi, \lambda, t) \quad (4.11)$$

where an overbar indicates a time-averaged mean and an asterisk indicates the fluctuating part. This facilitates the treatment of the surface oceanic circulation as a smooth, steady circulation with a superimposed time varying flow component. The time varying constituents of the SST are expected to have frequencies ranging from a few days for transient phenomena, to a year for seasonal variations, with amplitudes varying from 1 to 2 cm to about 1 m. Of course, only those time varying constituents of the SST that fit the temporal and spatial sampling characteristics of the altimetric mission can be successfully determined.

Most oceanographic applications of satellite altimetry to date have been confined to the study of the time varying component of the SST. There are three methods frequently used in this kind of study as we have already said: the overlapping pass method (also known as repeat-track or collinear pass method) in which the differences between altimetric measurements taken along nearly repeating tracks are used; the mean sea

surface model method in which the differences between altimetric measurements and an altimetrically constructed mean sea surface model are used; and the cross-over differences method, in which the differences between altimetric measurements taken at the intersections of ascending and descending tracks are used.

Common to all these techniques is that a tilt and a bias are usually removed (in one or another way) over a distance of several thousand kilometres along each track so as to minimize the long wavelength orbital and tidal errors. However, this modelling procedure always results in removing the long wavelength oceanic variability too. This makes the results applicable only for studying the mesoscale oceanic variability.

The first attempt at using altimetric data for oceanic mesoscale variability studies was made by *Huang et al.* [1978], utilizing GEOS-3 data in the Gulf Stream region. Follow-up studies in the same area or other oceanic regions of immediate oceanographic interest were conducted by a score of investigators using GEOS-3 and/or SEASAT collected data. Using data from collinear tracks during the last 24 days of the SEASAT mission, *Cheney et al.* [1983] made the first global map of oceanic mesoscale variability based on satellite altimetry. For a comprehensive review of the subject of mesoscale variability, the article by *Fu* [1983] is an illuminating source. All of the previous global studies of the time varying SST have produced so-called *rms mesoscale variability* maps. A by-product of these maps is the so-called *eddy kinetic energy* (EKE) maps, which quantify the energetics of the different oceanic regions.

A brief review of the existing techniques used for the recovery of the fluctuating part of the SST from satellite altimetry follows.



### 4.6.1. Overlapping Pass Analysis

This technique is based on the condition that every certain number of revolutions of the satellite around the earth, the satellite will have a repeating ground track (the condition for a repeating ground track is determined by the relationship between the angular rotation rate of the earth and the instantaneous rate of precession of the orbital node of the satellite).

Considering the situation of two overlapping passes, labelled pass-1 and pass-2, the  $j^{\text{th}}$  observation of pass-1 and the  $k^{\text{th}}$  observation of pass-2 have identical latitudes and longitudes. Then, the following equation can be used to obtain information on the time varying component of the SST:

$$\begin{aligned} \zeta_{a,2}(\phi, \lambda, t + \Delta t) - \zeta_{a,1}(\phi, \lambda, t) &= [\zeta_{2k}(\phi, \lambda, t + \Delta t) - \overline{N(\phi, \lambda)}] - \\ & \quad [\zeta_{1j}(\phi, \lambda, t) - \overline{N(\phi, \lambda)}] \quad (4.12) \\ &= \zeta_{2k}(\phi, \lambda, t + \Delta t) - \zeta_{1j}(\phi, \lambda, t) \end{aligned}$$

where  $\zeta_{2k}$  and  $\zeta_{1j}$  are the observed SSHs on pass-2 and pass-1, respectively. It is tacitly assumed that all relevant corrections have already been incorporated into the measured SSHs. It is also obvious that the positions of each altimeter measurement  $\zeta_{1j}$ ,  $\zeta_{2k}$  along each repeat pass will not match exactly, so by using one pass as a reference, any other pass can be fitted to the reference pass by some sort of along track interpolation (usually a linear interpolation is employed). This technique has limitations when a large number of overlapping passes are to be compared (because of variable pass-

lengths) and if the reference pass chosen exhibits high noise levels in the individual measurements.

A variation of this technique partially overcomes such limitations if each repeating ground track is compared to the mean of all the overlapping passes considered in a set. Still an interpolation is necessary to bring together all the observations to be compared. Simply stated, pass-2 in eq. (4.12) is replaced by the mean profile constructed from all the passes.

It is obvious that an exact match of repeating tracks cannot be achieved. Each repeating ground track is displaced in longitude (sometimes by as much as  $\pm 1$  km), which results in the  $j$ -th observation (pass-1) and  $k$ -th observation (pass-2) not having the same geoidal height. It depends therefore on the spatial gradients of the geoid to be able to identify oceanic variability as accurately as possible.

In brief, this analysis technique follows 4 steps:

- (a) errors in the altimeter range introduced by the error sources identified in earlier sections, are corrected;
- (b) using precision orbit determination data (either included in the altimeter record or computed separately), SSH relative to the reference ellipsoid is calculated;
- (c) each track is fitted to have zero bias and no tilt along the arc segment. This last step removes most of the long wavelength error involved in

the orbit determination as well as any long wavelength contributions from other error sources or SST itself. Finally,

- (d) the average height for all repeat tracks is removed from each of the repeat track segments.

By taking successive first differences of  $\Delta\text{SSH}$  along each repeat satellite track, the cross-track variable surface geostrophic current speed  $v^*$  is obtained from the expression:

$$\left| v^* \right| = \frac{g}{f} \left| \frac{\partial \zeta_a^*}{\partial x} \right| \quad (4.13)$$

where  $\zeta_a^*$  is the fluctuation of SST,  $f$  is the Coriolis parameter and  $x$  is in the distance reckoned in the along track direction. There is of course an indeterminacy problem regarding the direction of the current when calculated in this fashion. The magnitude is well determined but the direction of the variable current velocity is ambiguous. This makes the determination of a global 2-dimensional ocean current velocity field difficult to construct. A partial solution to this direct approach is to involve an intermediate step. The 2-dimensional height variability field ( $\zeta_a^*$ ) can be constructed first, using some optimal interpolation technique in both space and time simultaneously. This field can subsequently be used to determine the variable surface current velocity field. To our knowledge such an approach has not been fully tried yet.

As a final note, a disadvantage of using collinear pass analysis techniques for global surface ocean dynamics is the lack of a unique datum for intercomparisons between

overlapping sets of tracks. Also this type of analysis is restricted in both the space and time coverage obtained, thus forcing us to elaborate interpolation procedures. The technique, however, has performed well for regional studies of ocean dynamics, (see for example, *Thompson et al.* [1983]).

#### **4.6.2. Mean Sea Surface Models**

This technique consists of first minimizing the radial orbital errors by performing a least squares adjustment of each pass at cross-over points through a bias and a tilt parameter within the study area. The cross-over differences in the study area are minimized, the altimetric observations are corrected using the improved orbital heights, and mean sea surface maps are constructed representative of the data span analysed. Comparisons of sequential mean sea surface maps reveal information on the SSH variability. A variation of the technique includes the construction of a time-averaged mean sea surface map and subsequent differencing of this time-averaged map from the individual mean sea surface maps. Thus, this procedure eventually leads to a time series of sea surface topography maps.

A disadvantage of this method is that significant geoid errors are introduced into the time series variability maps as a result of the much sparser data coverage for the mean sea surface maps than for the time-averaged mean map with which the differencing is made.

### 4.6.3. Cross-over Differences Method

Maps of oceanic mesoscale variability can be obtained from cross-over differences as well. After the cross-over adjustment is performed to minimize the long wavelength orbital errors, the magnitude of the residual cross-over differences (i.e., the post-fit cross-over differences) is a measure of the oceanic mesoscale variability (see for example, *Cheney & Marsh [1981]*). Time series of residual cross-over differences are then used to produce *rms* variability maps useful for identifying the high and low kinetic energy oceanic areas in the world. Of course, there have been several variations of the cross-over differences method developed.

### 4.6.4. New Developments

Very recently, a new technique for extracting global oceanic mesoscale variability was presented by *Sandwell & Zhang [1989]*. This technique is conceptually very much like the technique that was independently developed in this thesis work to extract the time varying ocean current velocity field. The technique is based on the fact that long wavelength radial orbit error, as well as other long wavelength errors (e.g., unmodelled tides, atmospheric propagation delays and electromagnetic bias in the altimetry measurements) are suppressed by taking the derivative (slope) of each altimeter profile. Therefore, instead of working with the sea surface height  $\zeta$  as a signal, this technique works with the sea surface slope. Of course, variations in sea surface slope are proportional to changes in current velocities. The advocates of this technique obtain the time varying sea surface slope field by differencing a time-averaged slope profile from the individual slope profiles. Since this technique is used with a two-point stride along

the altimetry profiles, it also uses a low-pass filter to suppress the short wavelength altimeter noise (effectively suppressing wavelengths less than 100 km). The time-averaged slope profile is then constructed from the filtered slope profiles. A global *rms slope variability map* has been constructed using approximately 1 year of satellite altimetry data collected by the GEOSAT/ERM between November 1986 and November 1987.

The advantages, quoted by the authors of this technique, are:

- it is a simpler technique compared to the techniques that were used in the past and conceptually described in the previous subsections;
- no orbit adjustment techniques are necessary;
- it does not introduce edge effects as other filtering methods developed in the past did, thus allowing the inclusion and analysis of even very short profiles; and
- it by-passes the initial step of estimating the SST itself, and examines the gradient of the sea surface that in this case can be measured directly.

#### **4.7. Summary**

Time variations of SST although small compared to the permanent undulations created by the geopotential, are large compared with the precision supplied by a modern satellite altimeter radar.

For oceanographic applications of satellite altimetry data, long wavelength systematic errors in the geodetic height of the satellite create difficulties.

The dominant radial orbital error has a frequency of 1 cycle per revolution with a wavelength of approximately 40,000 km.

Sea height variability can be observed independently of the geoid topography either at cross-overs of the satellite's ground track or, along repeating (collinear) tracks. Both measures of variability have been used successfully, but the latter is preferred because more consistent and uniform time series of observations are realized. Newly developed techniques such as SST slope analysis are promising new interesting results for oceanic space/time variability.

The parameters of interest in quantifying the variable ocean surface circulation are the gradients (slopes) of the time varying component of the SST.

## **Chapter 5: Oceanic Variability Results from Classical Oceanographic Descriptions**

In this chapter, the practical application of the oceanographic principles that we dealt with in Chapter 3 is materialized. In-situ oceanographic measurements of specific volume are analysed to produce dynamic topography fields of the global ocean for four seasons and three selected pressure levels. The mean seasonal 3-dimensional structure of ocean dynamic topography will subsequently help us to derive the 3-dimensional structure of mean ocean current velocity fields. These mean seasonal ocean current velocity fields are used to provide information on the long-term, large-scale oceanic variability. Therefore, the purpose of Chapter 5 is to outline the data sources and computational procedures that were employed in this thesis research in order to obtain the space-time fluctuations of the general ocean circulation. The final goal, of course, is to use these space-time fluctuations to produce mean ROAM estimates (discussed in Chapter 7).

Observations made years apart and separated by thousands of kilometres must be combined to depict large-scale and long-term oceanic processes. Consequently, we



know much about climatic long-term average conditions, but little or nothing about the day-to-day or month-to-month changes in the ocean.

In the “open ocean”, far from the edges of the continental margins, oceanic processes are dominated by the incoming solar energy and by the winds. Since temperature and salinity control the behaviour of the oceans, they are the most frequently sampled variables by the oceanographers at sea. Temperature and salinity data are analysed to obtain estimates of density, ocean dynamic topography and ocean currents.

Ocean dynamic topography is ideally computed relative to a level surface, i.e., a surface of constant gravitational potential. A convenient measure of the geopotential anomaly of a surface is the dynamic height anomaly of the surface relative to some reference level surface. More formally, this quantity is labelled *geopotential thickness anomaly* (see Chapter 3) and is given in units of potential ( $m^2s^{-2}$ ). In practice, the computation of ocean dynamic topography or, dynamic height anomaly, is based on determining the distribution of isopycnal surfaces or, the reciprocal of the density field, the specific volume (isosteric) surfaces within the ocean. The so-obtained estimates of ocean dynamic topography (and ocean currents) are only relative to a surface which may or may not be an equipotential surface.

The computation of ocean currents, once the ocean dynamic topography is known, is simply a matter of applying the geostrophic equations and using as input data the horizontal gradients of the ocean dynamic topography. Since the horizontal pressure gradient and thus, the geostrophic speed (see Chapter 3) are identically zero when the pressure surface is parallel to an equipotential surface, it has been customary in

oceanography to select a reference level at which currents are assumed small or, practically zero, i.e., a *level of no-motion*. In the analysis of the oceanographic data carried out in this research work, we have followed this oceanographic practice too. Although it is generally recognized that the level of no-motion is a poor assumption, it is beyond the scope of the present work to evaluate critically this practice. It has been done elsewhere, e.g., *Stommel & Schott* [1977], *Wunsch* [1978], *Wunsch & Gaposchkin* [1980].

The purpose of the discussion in the sections that follow is to outline the data sources used and the computational procedures involved in this research for the determination of the long-term ocean current variability from classical oceanographic observations.

### **5.1. Description of Specific Volume Data Sets**

The data used for our computations of the mean seasonal ocean current fields are based on global specific volume fields obtained from the National Oceanographic Data Center (NODC), Washington, D.C.

In August 1985, the NODC announced the availability of data tapes containing seasonal statistics of observed ocean data by five-degree squares at 30 standard levels [NOAA, 1985]. The data tapes were prepared by Sydney Levitus in relation to the “Climatological Atlas of the World Ocean” [Levitus, 1982]. These data tapes are based on a synthesis of all ocean temperature, salinity, and oxygen data available from all NODC data files [NOAA, 1985].

The NODC data sets considered here consist of four files (one for every season) of five-degree squares of specific volume statistics computed through procedures outlined in *Levitus* [1982]. Each file covers 30 standard oceanographic depth levels, as indicated in Table 5.1. Level 29 is not a NODC standard level. The data for this level are interpolations from observed level values above and below this level.

Standard Level	Depth (m)	Standard Level	Depth (m)	Standard Level	Depth (m)
1	0	11	250	21	1200
2	10	12	300	22	1300
3	20	13	400	23	1400
4	30	14	500	24	1500
5	50	15	600	25	1750
6	75	16	700	26	2000
7	100	17	800	27	2500
8	125	18	900	28	3000
9	150	19	1000	29	3500
10	200	20	1100	30	4000

**Table 5.1. Standard Depth Levels:** (Reproduced from NODC Data Announcement Bulletin). Level 29 is not a NODC standard level.

In the NODC files the seasons are defined for the Northern Hemisphere and they correspond to: *Winter* (February - March - April); *Spring* (May - June - July); *Summer* (August - September - October); and *Fall* (November - December - January).

Each of the four original NODC data files contains information on latitude, longitude, and depth codes for each oceanic grid cell of 5-degree square of mean specific volume value, its standard deviation and the number of observations contributing to the mean.

Since grid cells on land and oceanic data-void areas were not included in the original NODC data files, we have assigned default values (e. g., -999.9) to all empty grid cells during the process of unpacking the specific volume data. Thus, we have produced a stack of 30 fully “observed” matrices of 36 rows (in latitude) by 72 columns (in longitude) of specific volume data for each season. The reason for creating full matrices is rather obvious: it allows quicker data processing in the analysis steps to follow. Graphics procedures were also developed which allow selective plotting of specific volume data coverage in terms of individual season and ocean depth level. Sample plots of specific volume data-void grid cells are shown in Figures 5.1a, 5.1b, and 5.1c for three selected standard levels and all four seasons, namely level 14, 19, and 26 of Table 5.1.

## **5.2. Data Processing and Analysis**

In this section we outline the computational formulae and steps required to calculate the *mean seasonal dynamic topography fields*.

### **5.2.1. Computation of Specific Volume Anomaly**

One of the important properties of sea water is density and its variation with temperature ( $T$ ), pressure ( $p$ ) and salinity ( $S$ ). Density changes due to the compressibility of sea water are much larger than density changes due to either thermal expansion or to saline expansion, over the range of temperature and salinity values observed in the world ocean.

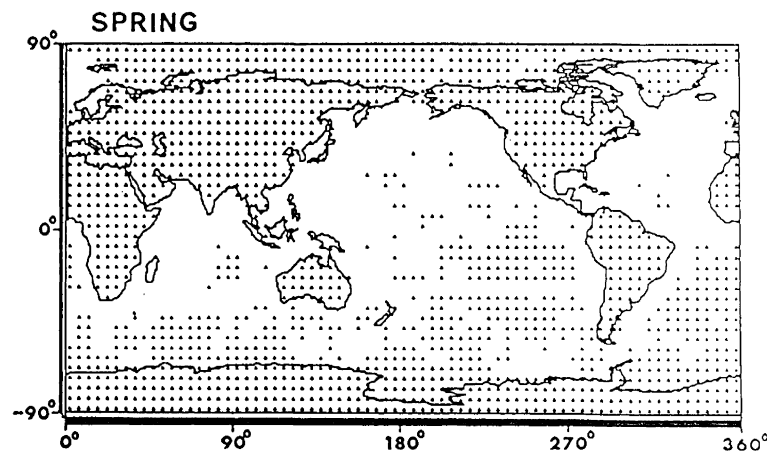
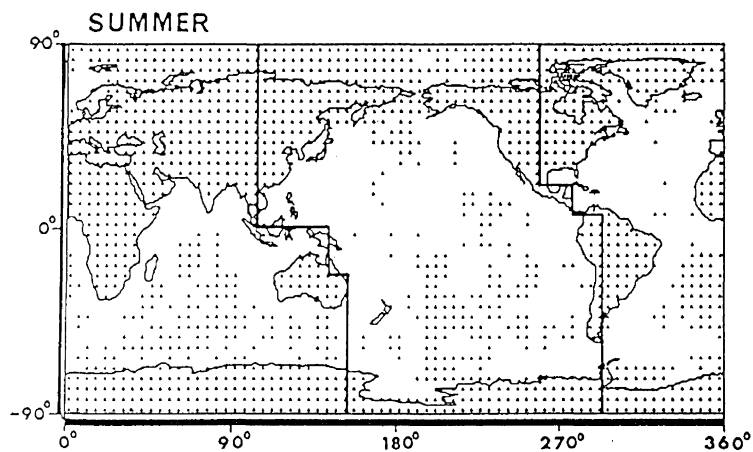
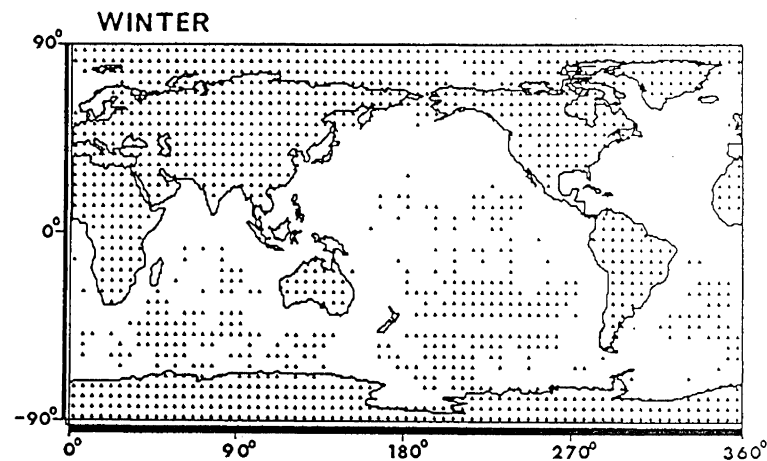
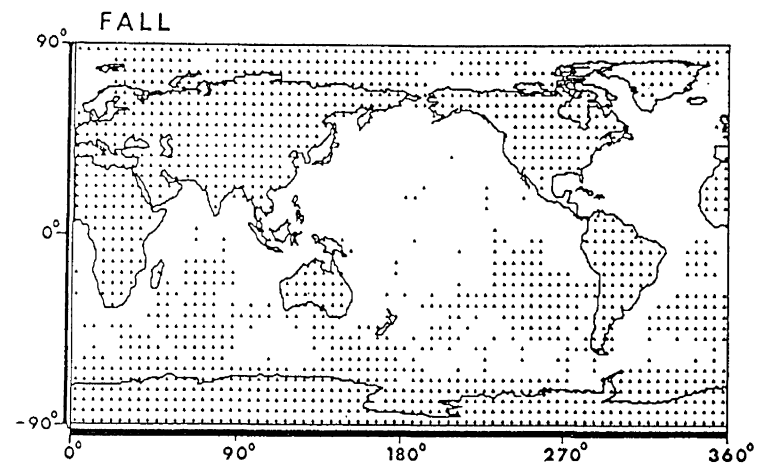


Fig. 5.1a. Specific volume data-void grid cells at 500 dbar (level 14 of Table 5.1) for all four seasons. The dots indicate missing values of 5° by 5° squares in latitude and longitude. Seasons are defined in the text. The lines superposed on the Summer season represent a sample boxing procedure of oceanic regions that was used in subsequent interpolation techniques.

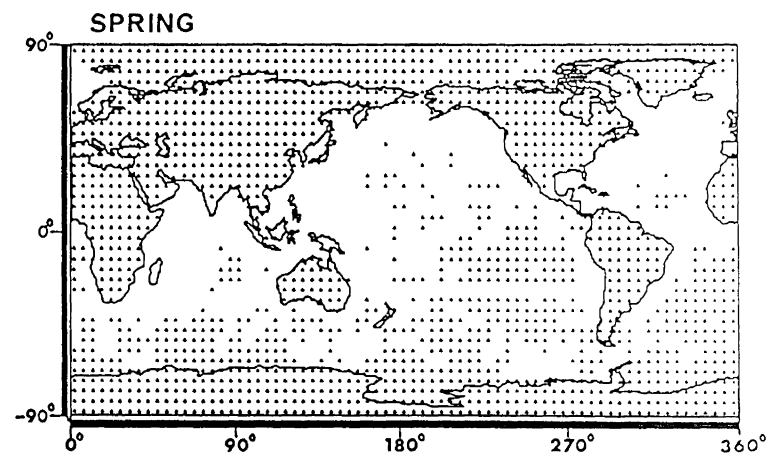
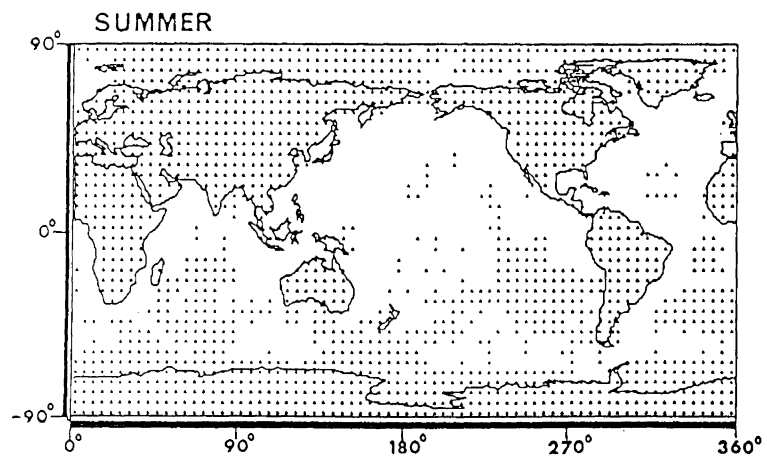
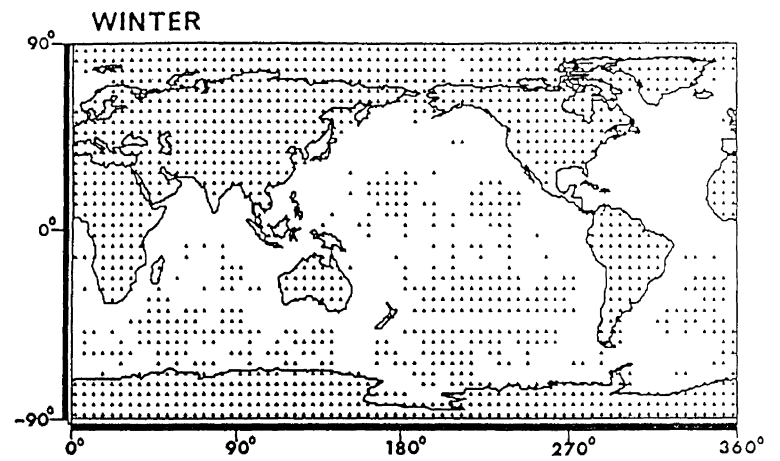
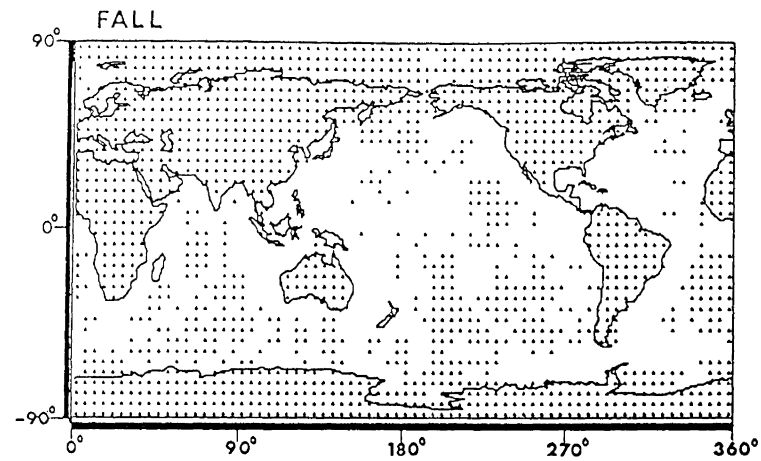


Fig. 5.1b. Same as Figure 5.1a, but for the 1000 dbar pressure surface (level 19 of Table 5.1).

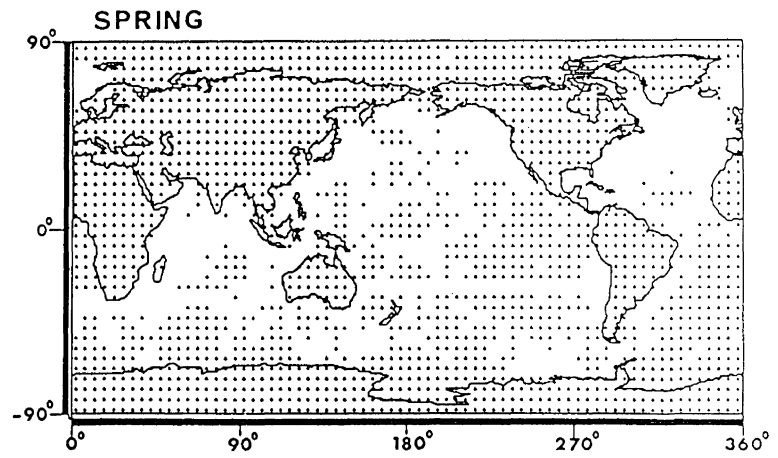
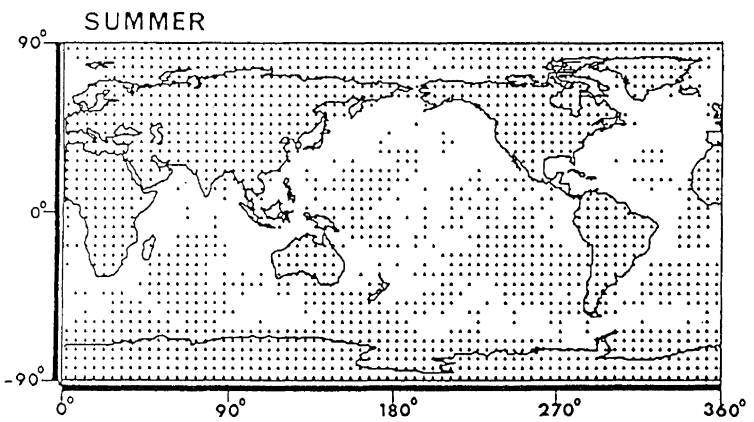
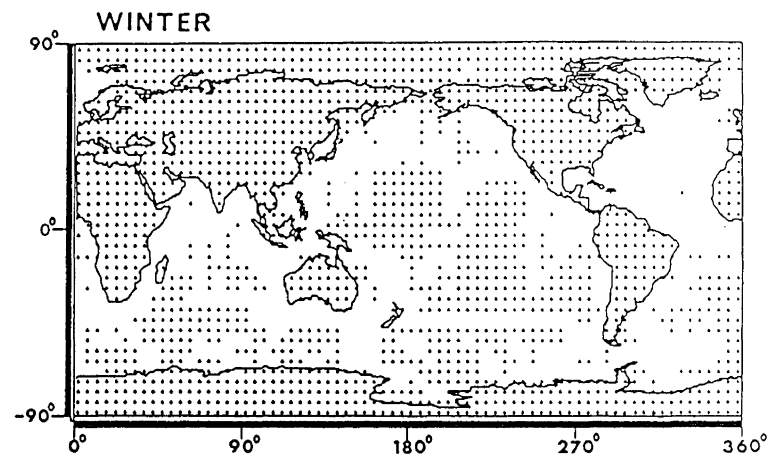
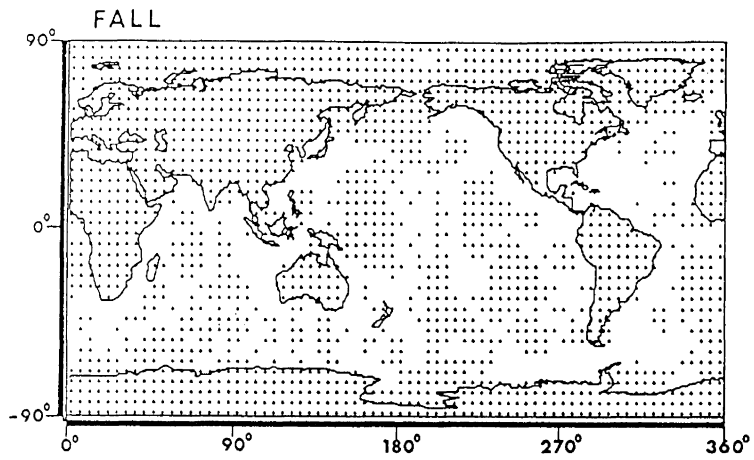


Fig. 5.1c. Same as Figure 5.1a, but for the 2000 dbar pressure surface (level 26 of Table 5.1).

From the early measurements of the variation of density with temperature, pressure, and salinity, it was found that the most convenient way to express the results is in terms of *specific volume* (reciprocal density) as follows [Pond & Pickard, 1983]:

$$\alpha(S,T,p) = \alpha(35^{\circ}/_{00}, 0^{\circ}C, p) + \delta_S + \delta_T + \delta_{S,T} + \delta_{S,p} + \delta_{T,p} + \delta_{S,T,p} \quad (5.1)$$

or, as the *anomaly of specific volume*

$$\delta_{\alpha} = \alpha(S,T,p) - \alpha(35^{\circ}/_{00}, 0^{\circ}C, p) = \Delta_{S,T} + \delta_{S,p} + \delta_{T,p} + \delta_{S,T,p} \quad (5.2)$$

where;

- $\alpha(S,T,p)$  - is the specific volume of a sample of sea water of salinity S (expressed in parts per thousand), temperature T (expressed in degrees Celsius), and pressure p (expressed in millibars). These are the observed data in the NODC files;
- $\alpha(35^{\circ}/_{00}, 0^{\circ}C, p)$  - is the specific volume of an arbitrary “standard” sea water sample of salinity 35‰, temperature 0°C, and pressure p at the depth of the sample. This term expresses the effect of pressure on specific volume.
- $\delta_{\alpha}$  - is the *specific volume anomaly* and represents the sum of the six anomaly terms in eq. (5.1);
- $\Delta_{S,T}$  - is called *thermosteric anomaly* and accounts for most of the effect of salinity and temperature, disregarding pressure ( $\Delta_{S,T} = \delta_S + \delta_T + \delta_{S,T}$ );
- $\delta_{S,p}$  - accounts for most of the combined effects of salinity and pressure;



- $\delta_{T,p}$  - accounts for most of the combined effects of temperature and pressure; and finally,
- $\delta_{S,T,p}$  - is usually so small that is always neglected with the present day accuracy of measurements (or determination) of the parameters S, T, and p.

In water depths less than 1000 m, the thermosteric anomaly  $\Delta_{S,T}$  is the major component of  $\delta_\alpha$ .

From a slightly different point of view, we can say that the actual specific volume  $\alpha(S,T,p)$  can be considered as composed of two fields, that is, the invariant field  $\alpha(35^\circ/\text{oo}, 0^\circ\text{C}, p)$  and the variant field  $\delta_\alpha$ , the anomaly of specific volume. The  $\delta_\alpha$  field then, describes the field of mass in the ocean.

In section 3.4, we have already presented the significance of the specific volume anomaly in calculating the quantity we termed *dynamic height anomaly* (see equations 3.18 and 3.20). We reiterate here its definition:

*Geopotential thickness anomaly or, dynamic height anomaly or, ocean dynamic topography is defined between two isobaric surfaces  $p_1$  and  $p_2$  in the ocean, as the integral of the difference between the actual specific volume and the specific volume of a standard ocean, over the pressure difference.*

The specific volume data contained in the NODC data tapes have been computed based on the old *equation of state* of sea water, the so-called Knudsen-Ekman equations [Fofonoff, 1962]. We present these equations below for completeness and clarification of the calculations.

The equation for the computation of density of a parcel of sea water given the in-situ measurements of salinity, temperature and pressure is [Fofonoff, 1962]:

$$\rho(S,T,p) = \frac{1 + 10^{-3} \sigma_t}{1 - \mu p} \quad (5.3)$$

where;

- $\sigma_t$  - is the anomaly of specific gravity of the sea water parcel or, *sigma-t*;
- $p$  - is pressure; and
- $\mu$  - is the mean compressibility of sea water.

The quantity *sigma-t* is defined as:

$$\sigma_t = [ \rho(S,T,0) - 1 ] \times 10^3 \quad (5.4)$$

and the expression for the computation of *sigma-t* is [Fofonoff, 1962]:

$$\sigma_t = \Sigma_t + (\sigma_0 - \Sigma_0) [1 - A_t + B_t (\sigma_0 + \Sigma_0) ] \quad (5.5)$$

in which;

- $\Sigma_t$  - is the anomaly of specific gravity of pure water at temperature T;
- $\Sigma_0$  - is the anomaly of specific gravity of pure water (at temperature  $0^\circ C$  [ $\Sigma_0 = -0.1324$  ] );

- $A_i$  and  $B_i$  - are polynomials in temperature (their explicit expressions are given in *ibid.*);
- $\sigma_0$  - is the “density” of a parcel of sea water with salinity  $S$  at a temperature of  $0^\circ$  Celsius and pressure equal to zero. (It is the oceanographic convention to assume that pressure at the sea surface is equal to zero. Thus, the sea surface is the upper-most isobaric surface in the ocean.)

The quantity *sigma-0* is defined as:

$$\sigma_0 = [ \rho(S,0,0) - 1 ] \times 10^3 \quad (5.6)$$

and the equation for the computation of *sigma-0* is [*Neumann & Pierson, 1966*]:

$$\sigma_0 = -0.093 + 0.8149 S - 0.000482 S^2 + 0.0000068 S^3 \quad (5.7)$$

The mean compressibility  $\mu$  of sea water is given as a function of salinity, temperature and pressure [*Fofonoff, 1962*]:

$$\begin{aligned} 10^9 \mu = & [ 4886 / (1 + 1.83 \times 10^{-5} p) ] - \\ & [ 227 + 28.33 T - 0.551 T^2 + 0.004 T^3 ] + \\ & 10^4 p \times [ 105.5 + 9.50 T - 0.158 T^2 ] - \\ & 1.5 \times 10^{-8} T p^2 - \\ & [ ( \sigma_0 - 28 ) / 10 ] \times \\ & \{ [147.3 - 2.72 T + 0.04 T^2] - 10^{-4} p [32.4 - 0.87 T + 0.02 T^2] \} + \\ & [ ( \sigma_0 - 28 ) / 10 ]^2 \times [4.5 - 0.1 T - 10^{-4} p (1.8 - 0.06 T) ] \end{aligned} \quad (5.8)$$

In the above equation pressure is expressed in units of decibars and temperature in degrees Celsius.

The above set of equations corresponds to the *Knudsen-Ekman* equation of state for sea water. There is a new equation of state for sea water, called the *International Equation of State* for sea water of 1980 (IES'80), based on the new definition of practical salinity (the Practical Salinity Scale of 1978 or, PSS'78) and new sets of observations and analyses. The set of equations for computing in-situ density using the IES'80 is described in the UNESCO Technical Paper in Marine Science, No. 36 [UNESCO, 1981] and in *Fofonoff & Millard* [1983].

Since the available NODC data of in-situ specific volume (recall that  $\alpha = 1/\rho$ ) were computed based on the Knudsen-Ekman equations, the computations of the anomaly of specific volume  $\delta_\alpha$  in this thesis work were carried out using the old equation of state instead of the improved IES'80 one.

It is not difficult to transform the specific volume values from the old equation of state to the new IES'80 one (for details see *Pond & Pickard* [1983]). *Levitus & Koblinsky* [1989] state that the differences between density values produced by these two sets of equations of state for sea water are relatively small. For more details about the inaccuracies in the Knudsen-Ekman equation of state also see *Mamayev* [1975]. However, in our opinion there would be no real gain using the IES'80 and PSS'78 formulae, since the quality of the salinity, temperature and pressure data collected in the past is, very likely, not matching the improvements offered by the new formulae. Furthermore, for the purpose of this research, i. e., determination of the long-term large-scale ocean

current variability, the numerical differences between the two equations of state will not affect our results, especially in view of all the approximations that are used to compute the ocean dynamic topography fields.

For the computation of  $\alpha(35\text{‰}, 0^\circ\text{C}, p)$  we start with equation (5.3) which we rewrite for  $T = 0^\circ$  Celsius as:

$$\rho(S, 0, p) = \frac{1 + 10^{-3} \sigma_0}{1 - \mu_0 p} \quad (5.9)$$

where  $\sigma_0$  is given by eq. (5.7) if we substitute the value  $35\text{‰}$  for the salinity (S), and  $\mu_0$  is calculated from eq. (5.8) if we set all the terms containing the variable (T) to zero.

The sigma-0 for  $35\text{‰}$  is:

$$\sigma_0(35\text{‰}) = 28.12960 \quad (5.10)$$

Using the computational formulae of the specific volume of a standard ocean as presented above, the next two computational steps were followed in the analysis of the specific volume data.

A vector of 30 elements was computed for the specific volume of the standard ocean, since  $\alpha(35\text{‰}, 0^\circ\text{C}, p)$  is a function of pressure only. Specific volume anomaly fields were subsequently computed (see equation 5.2) and four new seasonal stack files (each one consisting of 30 levels of 36 rows by 72 columns) of specific volume anomaly were created and permanently stored. These files were then used to compute the mean seasonal ocean dynamic topography fields as explained in the next subsection.

### 5.2.2. Dynamic Topography Computations

In Chapter 3, we have presented eq. (3.20). This is the computational formula we will use to obtain the geopotential thickness anomaly,  $\Delta D$ , between two isobaric surfaces  $p_1$  and  $p_2$ .

As it is explained, for example, in *Levitus* [1982] or *Fomin* [1964], in the actual computations of dynamic topography, the pressure  $p$  (in units of decibars) is replaced by depth  $z$  (in units of metres) and the pressure differential  $dp$  is replaced by the quantity:

$$dp = \rho_0 g dz \quad (5.11)$$

where,  $\rho_0$  is a nominal, mean value of sea water density,  $g$  is a mean value of the acceleration of gravity, and  $dz$  represents the difference in depth between two surfaces of constant depth. The approximation involved in replacing pressure by depth in eq. (3.20) results in a maximum 10% error in the estimation of  $\Delta D$  [*Fomin*, 1964]. The numerical evaluation of the integral in eq. (3.20) is a trivial matter.

From the specific volume anomaly files we computed dynamic topography seasonal stack files. The integration was carried out from the top to the bottom depth level, and at every level the partial sum of the computed dynamic topography was stored for every grid cell for each of the four seasons. Thus, 4 seasonal files of 29 levels each, containing 36 rows by 72 columns, were created. Each record of the 36 by 72 matrix contains latitude-, longitude-, and reference level depth-code, and the computed dynamic height anomaly value. Of course, there are grid cells with default values that

represent three different situations: (a) the cell is on land; (b) the ocean depth at the particular cell location is less than the lower integration limit; and/or (c) it is an oceanic data-void cell. Plotting procedures for each season and depth level were developed for selective plotting of empty (full) cell coverage of dynamic topography and for dynamic topography contouring. These procedures also incorporated automatic overlays of other specially created data files such as world coastlines or masking files for land masses and shallow waters.

### **5.3. Mean Seasonal Dynamic Topography Fields for the Global Ocean**

For each season, 29 mean seasonal dynamic topography files were computed. Due to the spatial incompleteness of the  $5^{\circ}$  by  $5^{\circ}$  (in latitude and longitude) digital maps, especially with regard to the lower depth levels, and due to sparse coverage in the southern hemisphere, interpolation procedures were necessary to produce better coverage maps. However, because of the extremely large computational burden required to interpolate all 29 computed files for each one of the four seasons, we decided to limit our investigations by selecting only 3 reference depths with respect to which full coverage maps of dynamic topography would be computed.

We selected the 500 m, 1000 m and 2000 m ocean depths since the in between layers are the most representative layers of ocean current dynamics regimes (surface layer, mid-depth and deep layer circulation). We should also keep in mind that data coverage below 2000 m is severely limited in the analysed data sets. Another criterion for selecting the 2000 m depth as the lower depth, is that for most of the oceans not much activity takes place at lower depths, thus allowing us later on to impose the (poor but

useful) assumption that this depth can be representative of the level of no-motion (see also, *Montgomery* [1969]). An additional incentive for selecting these 3 reference depths, was that we could directly compare the result of the interpolated mean seasonal dynamic topography at these levels with other published results on either global mean annual maps or regional mean seasonal maps. This comparison will also add confidence for the subsequent computations of mean seasonal ocean current velocity fields.

A spline surface representation of the dynamic topography field was chosen as opposed to more classical surface representations (e.g. least squares two-dimensional polynomials), because unusual local features do not affect the behaviour of the function at distant points. Moreover, undesirable oscillations such as those produced by two-dimensional polynomials can be avoided. The spline function chosen here is a bivariate spline [*Harder and Desmarais*, 1972; *Meinguet*, 1979]. This choice results in an order N algorithm being used, where N is the number of input data points. The surface generated can be thought of as one that would be formed if a stiff, thin metal plate were forced through the given data points.

We have also experimented with local two-dimensional polynomial fits, but the results obtained showed in several occasions erroneous dynamic topography features. A slight modification of the algorithm described by *Akima* [1978] was used for this experimentation. The local two-dimensional polynomial fit method would have worked well for a fairly smooth function and with given data points uniformly distributed over the whole area.



The surface spline functions that were used provided an interpolated surface which preserved the existing structure of the dynamic topography field and densified the “observed” network of grid points, thus producing a smooth, almost “continuous”  $5^{\circ}$  by  $5^{\circ}$  distribution of dynamic heights over the whole ocean. It should be mentioned, however, that we had to pay a price for the use of the surface splines. The computer processing time required by the spline functions exceeded by far the one required by any of the polynomial fits we tried.

To further improve the computational speed of the surface spline interpolating function and reduce the extreme memory requirements, we devised a boxing procedure which also accommodates the fact that each ocean is more or less an entity by itself. Special consideration in the boxing procedure was needed for the Atlantic Ocean, since its area is artificially divided by the zero meridian into two parts in the input data sets. Cut-and-paste procedures were employed to enable the use of an “Atlantic Ocean box”. A sample boxing-procedure was shown in Figure 5.1a for the summer season.

It is obvious from the above discussion that the interpolated surfaces cannot yield a realistic and acceptable structure of dynamic topography on a scale smaller than that of the “observed” grid, i.e., five degrees. It is also obvious that any grid point interpolated value below approximately  $65^{\circ}$  S latitude is less realistic and representative of the dynamic topography field. However, in the worst of cases, we have at least succeeded in coming up with the smoothest possible surfaces. To conclude, the chosen interpolation scheme has provided with a more complete areal coverage than the original data alone could provide.

After the complete 5° by 5° grid was obtained we produced 1° by 1° full matrices of seasonal dynamic topographies, for all three selected levels, using linear interpolation in latitude and longitude directions. Two reasons can be given for doing this: firstly, a 1° by 1° file resolution allowed us to use a more realistic masking procedure for land and shallow-depth oceanic areas. Thus, crude outlines of data coverage would not appear and smoother contours would be produced. Secondly, it would allow a more direct visual (and digital if desired) comparison of our computed annual mean surfaces with the mean annual dynamic topographies published by *Levitus* [1982].

To summarize the analysis procedures, it should be stated that the reliability of the interpolated grid points is generally limited by the density and distribution of the “observed” network of points. It is our guess that the so-produced dynamic topography contours over large-size data-void areas can be in error by +/- 10 dyn. cm maximum. Although the NODC data files did contain error estimates for the mean seasonal values of specific volume, we have not used them to properly assess the accuracy of the computed dynamic topography fields because of: (a) all the approximations involved in carrying out the computation of dynamic topography; and (b) the inability to formally compute error estimates from the available computer algorithm of the surface spline interpolation.

A few remarks regarding the display of the interpolated dynamic topography maps are worthwhile. Three different masking files were prepared to eliminate points on land and shallow oceanic areas in the spline interpolated surfaces. Masking files of different grid resolutions for land areas and shallow waters were constructed from the original DBDB5 and ETOPO5 digital terrain bathymetry and land digital terrain models

(DTMs), of 5 by 5 minute resolution in both in latitude and longitude. These original data sets were kindly made available to us by J. Woodside of the Atlantic Geoscience Centre at the Bedford Institute of Oceanography [J. Woodside, personal communication, 1987]. Grid generalization procedures were developed as part of this thesis work to provide 5° by 5° as well as 1° by 1° resolution global DTMs for both land masking and shallow seas masking depending on the ocean depth. These files have also been used as overlays in our computer graphics procedures used to display the maps shown here.

All of the computed series of mean seasonal dynamic topography maps were fully computer generated and are displayed in Figures 5.2a, 5.2b, and 5.2c for the four seasons and the different depth levels.

As was mentioned earlier, we have also computed mean annual dynamic topography maps from the mean seasonal ones for comparison purposes. The annual values were computed as a straight arithmetic average value of the four seasonal values. The mean annual dynamic topography maps are displayed in Figures 5.3a, 5.3b, and 5.3c for each of the three selected reference levels. Figures 5.3d and 5.3e display the sub-surface layers' annual dynamic topography at 500 dbar relative to 1000 dbar and at 1000 dbar relative to 2000 dbar, respectively.

The general patterns of the isobars (dynamic topography isolines) on our annual maps are in good agreement with those shown by *Levitus* [1982, Figures 56 and 67]. The same conclusion applies when we compare our mean annual maps with those prepared by *Wyrki* [1974; 1975] for the Pacific Ocean.

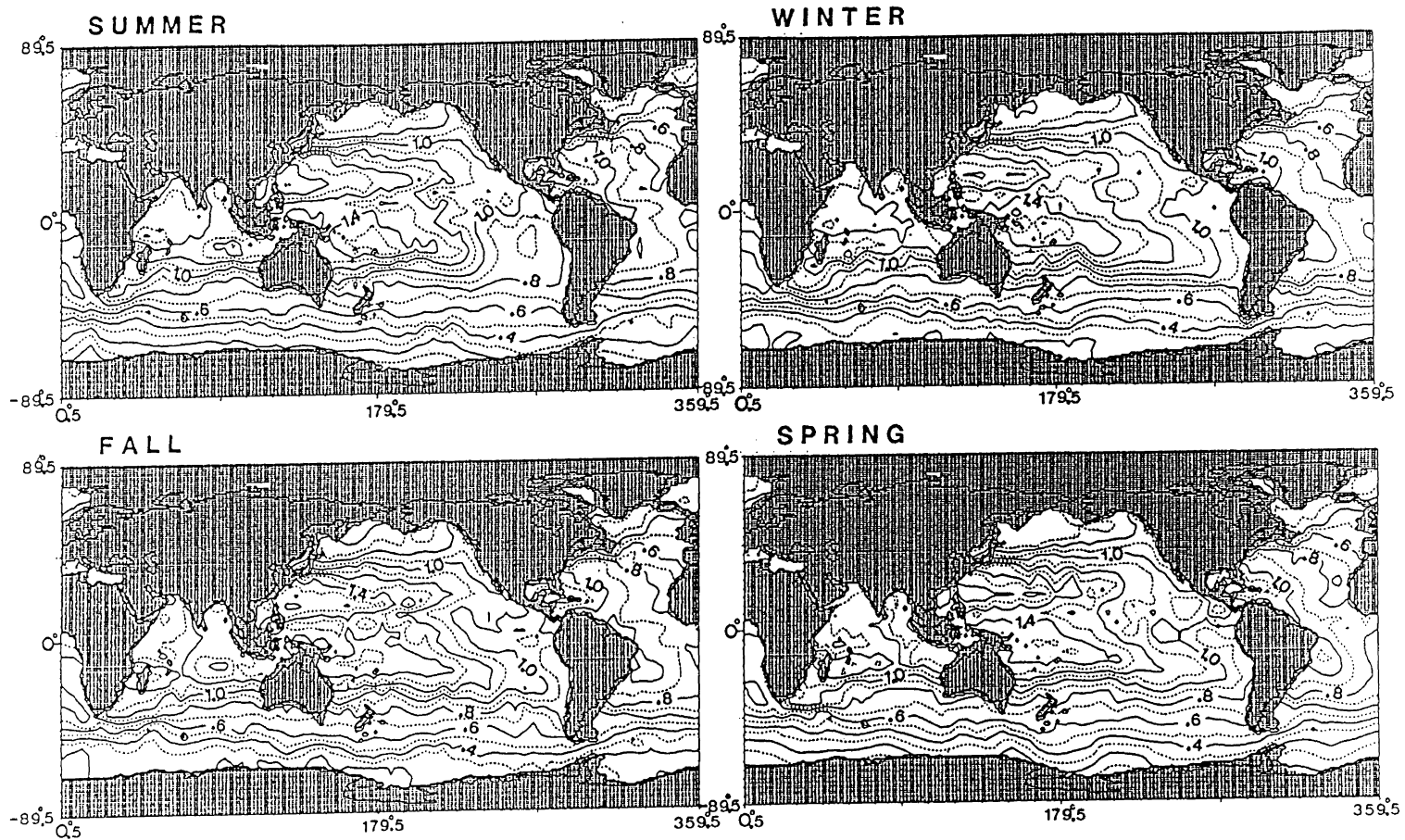


Fig. 5.2a. Global Mean Seasonal Dynamic Topography Maps relative to 500 dbar (in units of dynamic metres). The contour interval is 10 dynamic centimetres.

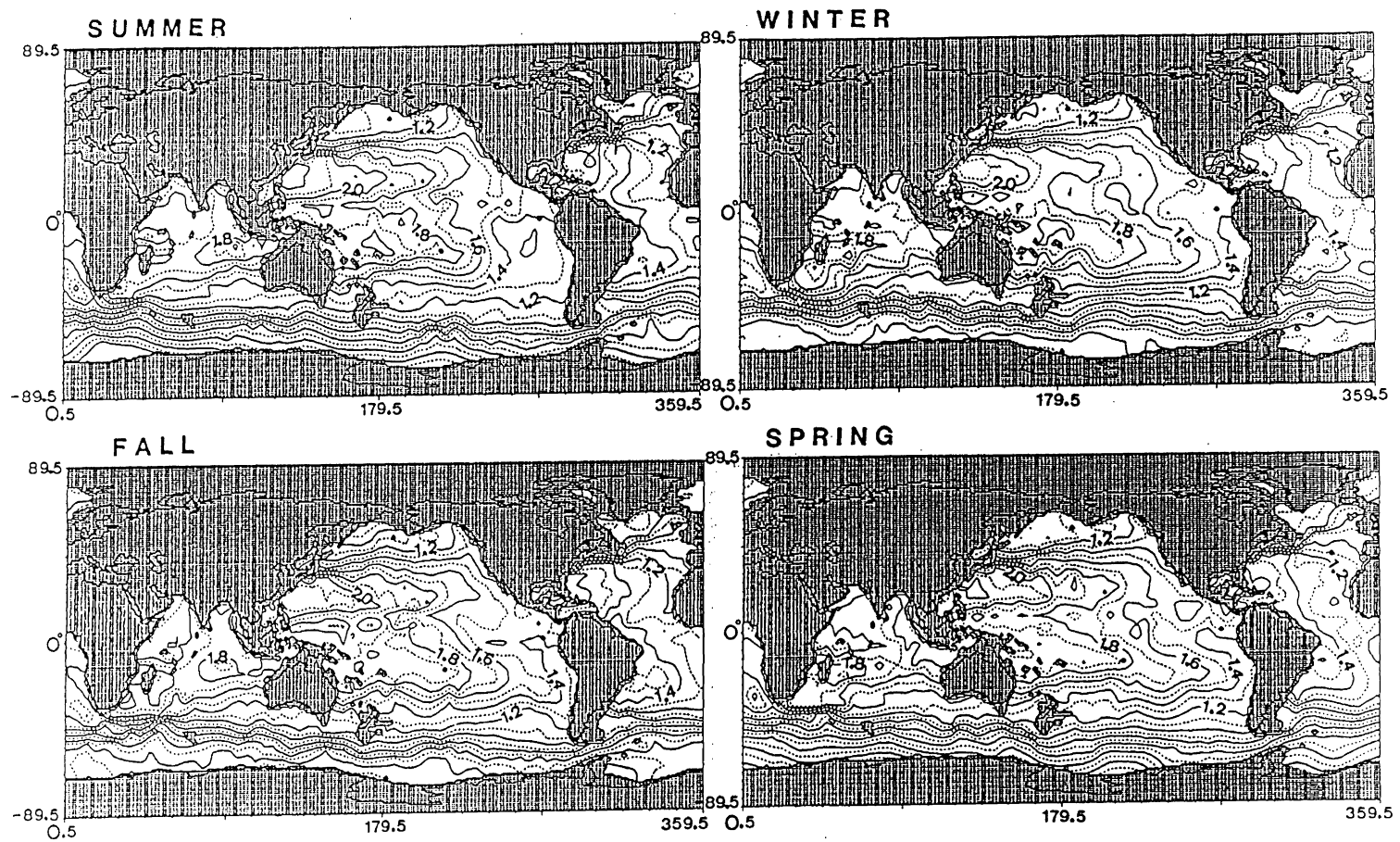


Fig. 5.2b. Same as Figure 5.2a, but relative to 1000 dbar pressure surface.

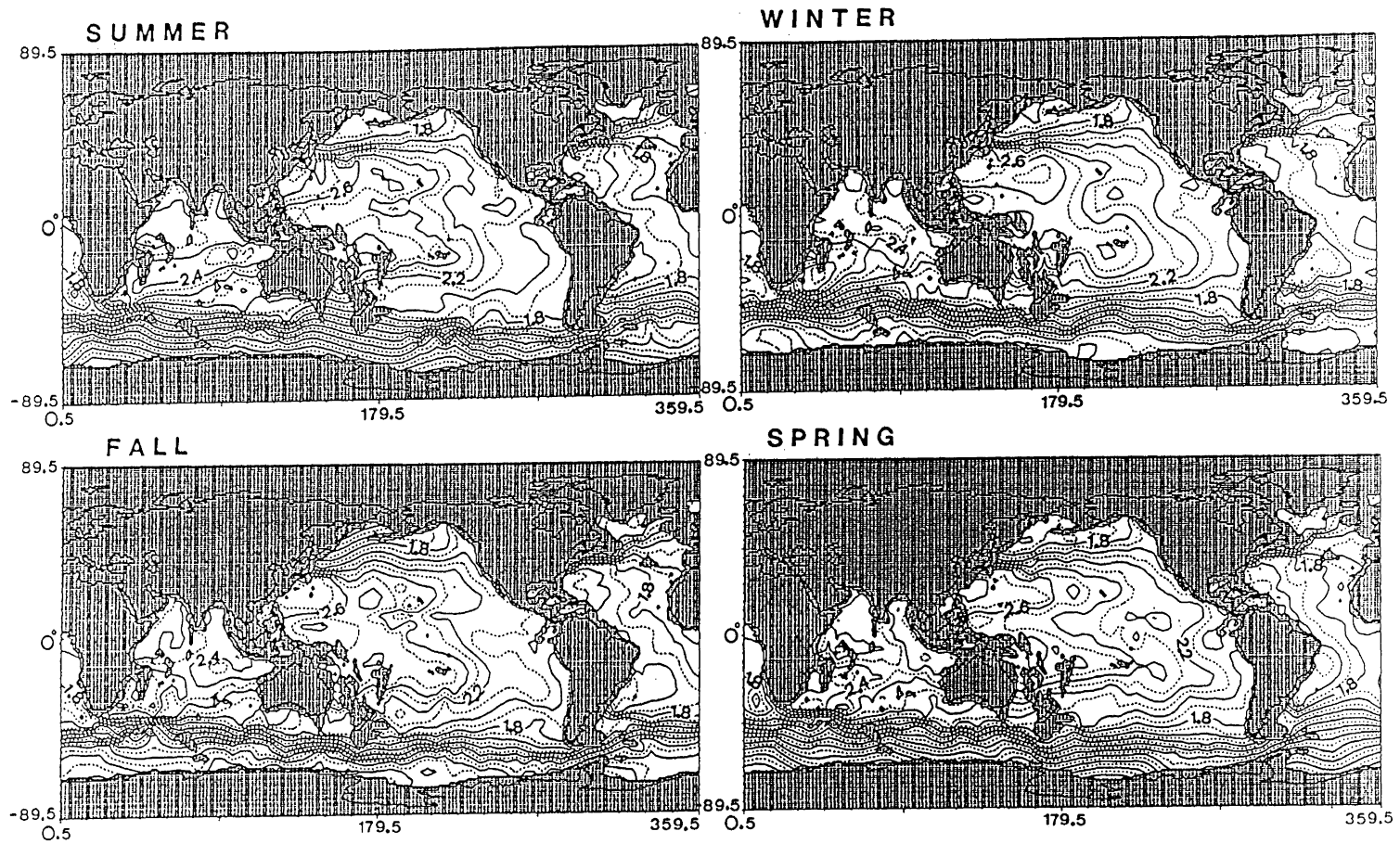


Fig. 5.2c. Same as Figure 5.2a, but relative to 2000 dbar pressure surface.

Dynamic Topography relative to 500 db

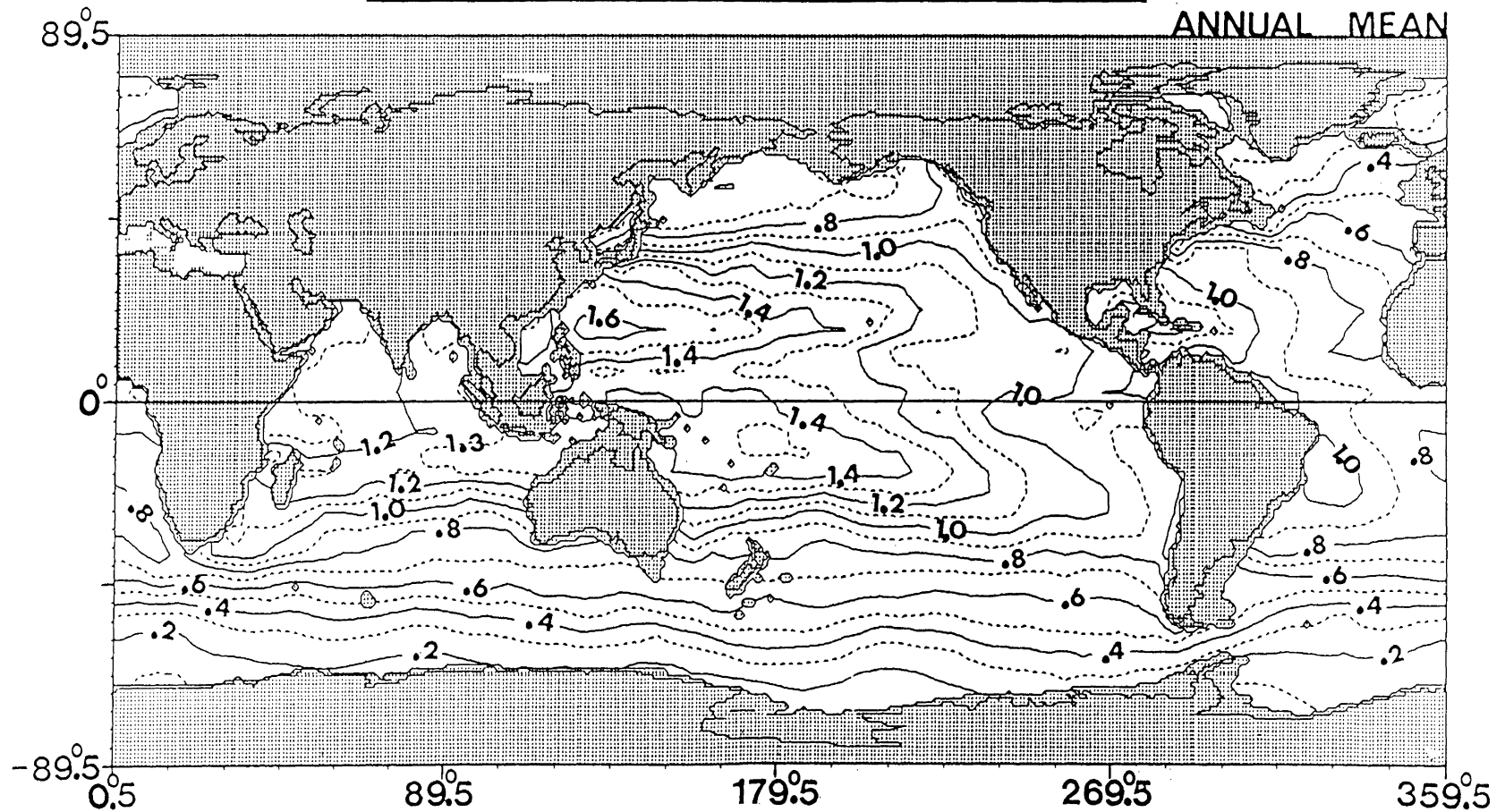


Fig. 5.3a. Global Mean Annual Dynamic Topography Maps relative to 500 dbar computed from the mean seasonal maps (Figures 5.2) as the arithmetic average of the four seasons (in units of dynamic metres). The contour interval is 10 dynamic centimetres.

Dynamic Topography relative to 1000 db

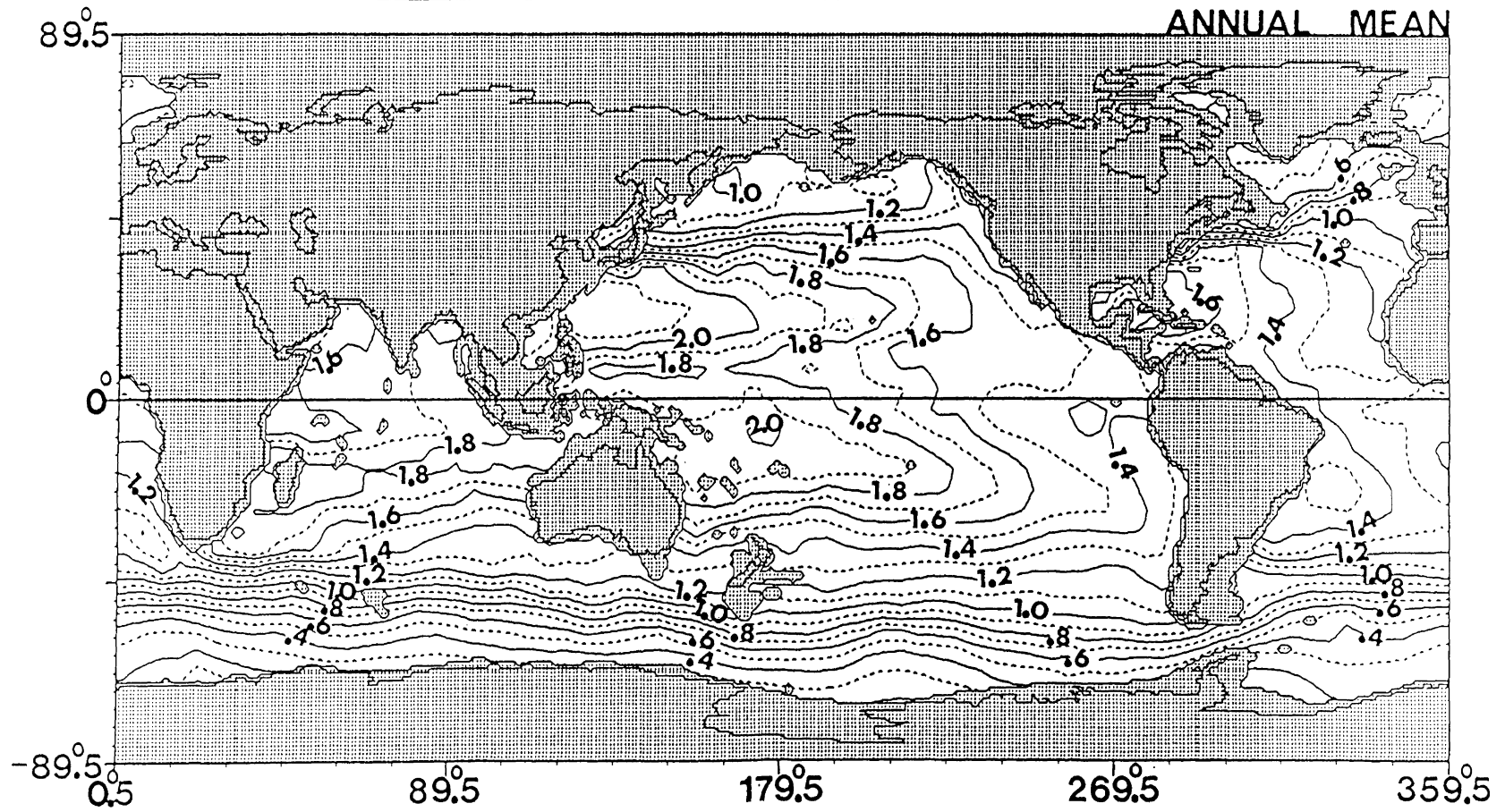


Fig. 5.3b. Same as Figure 5.3a, but relative to 1000 dbar pressure surface.





Annual Mean Dynamic Topography at 500 db relative to 1000 db

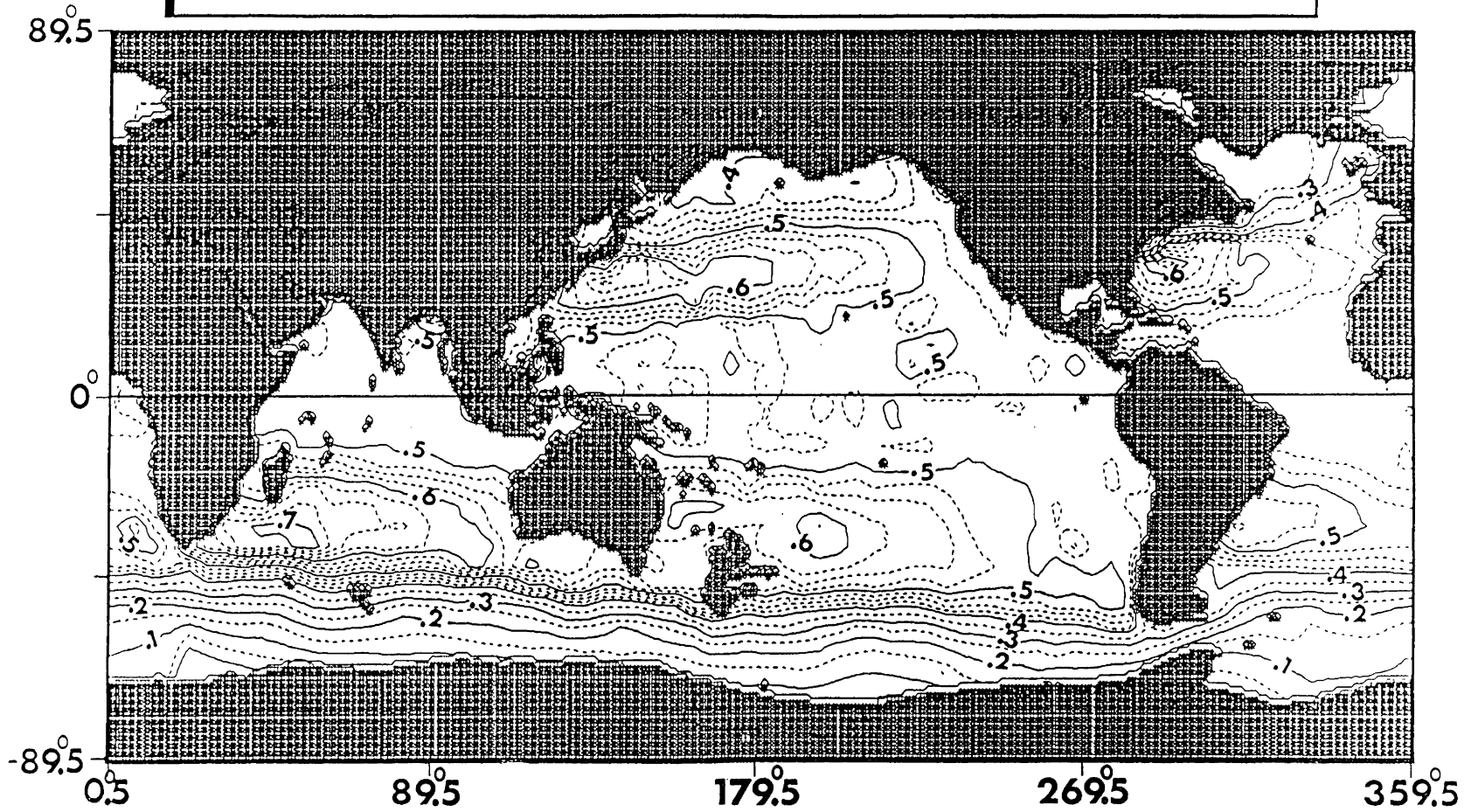


Fig. 5.3d

Annual Mean Dynamic Topography at 1000 db relative to 2000 db

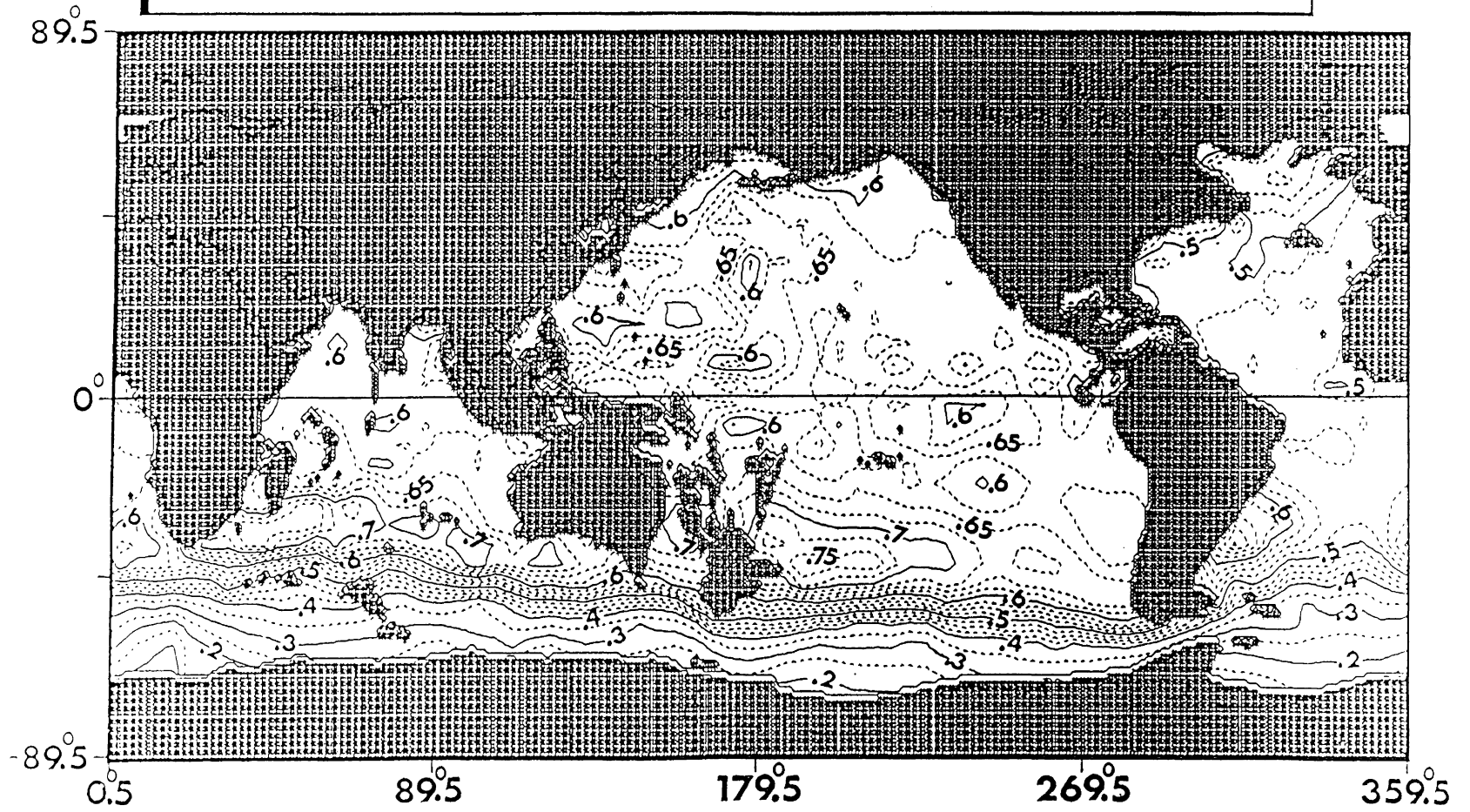


Fig. 5.3e

The good agreement of our annual maps with other, independently computed ones, indicates that the spline interpolated mean seasonal maps did not produce erroneous dynamic topography features in most data-void areas. However, there are some differences between our annual maps and the ones mentioned above, notably below approximately 65°S latitude. The magnitude and distribution of these differences suggest that they originate from the interpolated values. Examination of empty cell plots not only shows relatively less data in those areas, but also that there are not enough “peripheral control” data points as compared to other data-void areas. Thus non-representative dynamic height values below approximately 65°S latitude are to be expected. In addition, digital comparisons between our annual maps and those prepared by *Levitus* [1982] may serve as a general error estimate of our interpolated global representations, since the *Levitus* mean annual 1° by 1° fields were obtained using an objective analysis (space and time interpolation) scheme very different from the one we used here. These comparisons could then lead to general basin-wide *rms* error estimates for our seasonal analysis.

We will not give any interpretation regarding the features that appear in the annual mean maps. This has been done rather exhaustively in several regional or global studies of dynamic topography, for example: *Wyrki* [1974; 1975] for the Pacific Ocean, *Levitus* [1982] for the world ocean, *Reid* [1986] for the Southern Ocean, just to name a few.

It should be reiterated that although we present our results on a 1° by 1° global grid, this was only a practical solution to the problem of applying a refined masking

procedure, and excluding shallow-depth ocean areas. There is no more spatial information content than what is contained in the original 5° by 5° resolution grid.

Global representations of ocean dynamic topography fields, such as those presented, are based on sporadic measurements both in space and time. It should be recognized therefore, that these quasi-stationary dynamic topography maps contain only a fraction of the actual spectrum of the sea surface topography. However, these maps can still be a useful guide in the design of techniques to recover the sea surface dynamic topography from satellite altimetry. Further improvements can be expected if such seasonal fields as the ones described here are used as initial guess fields in satellite altimetry applications. It has already been demonstrated that satellite altimeter cross-over discrepancies improve if some a-priori knowledge of the quasi-stationary ocean circulation is used (see for example: *Marsh et al.* [1988], *Tapley et al.* [1988], *Engelis and Knudsen* [1989]). However, to our knowledge, the only a-priori quasi-permanent sea surface topography information that has been incorporated in this line of studies has been the Levitus annual mean dynamic topography referenced to 2000 dbar and expressed in terms of a low-degree spherical harmonic expansion.

In summary, one of our initial objectives was accomplished in this chapter. We analysed the most recently compiled “observed” specific volume statistics to arrive at a “continuous” global representation of dynamic topography fields for a number of pressure levels. The standard oceanographic practice of displaying the ocean dynamic topography using isobaric surfaces as reference surfaces was followed, thus yielding only relative dynamic heights. Previous analyses describing the seasonal fluctuations of dynamic topography are relatively limited and usually encompass the presentation

of monthly or seasonal dynamic topography fields for limited parts of ocean basins, or as in a few cases, entire ocean basins. For example, *Wyrski* [1974; 1975] has produced monthly and seasonal maps of dynamic topography for the Indian and Pacific Oceans and *Levitus* [1982], seasonal distributions for the world ocean from the surface down to 250 m depth. To our knowledge, the analyses presented here are the first attempt to produce global ocean mean seasonal dynamic topography fields and their mean seasonal variation.

One of the most important problems in physical oceanography that still remains unsolved is the definition of the absolute sea surface topography. Means of solving this problem have been briefly described in Chapter 3 and to great length by *Wunsch & Gaposchkin* [1980].

As a closing statement for this section, we reiterate that the dynamic topographies presented here were referenced to the 500 dbar, 1000 dbar, and 2000 dbar pressure surfaces. The question remains as to the adequacy of the 2000 dbar surface to serve as a level surface, or in terms of geostrophic currents, as a level of no-motion.

#### **5.4. Space-Time Variability of the Quasi-Permanent Ocean Dynamic Topography**

In this section, we present the results of the mean seasonal variations of dynamic topography. This series of maps represents the space-time variability of the Q-P ocean dynamic topography. The variability maps have been constructed by taking the difference between the mean seasonal maps and mean annual maps and are displayed

in Figures 5.4a, 5.4b, and 5.4c for each of the three reference pressure surfaces. The stippled areas on these maps represent negative differences (i. e., values below the annual mean) and the white areas positive differences (i. e., values above the annual mean). We shall refer to these maps, from now on, as the *difference-maps*.

This series of long-term variability maps can be used to discuss the large-scale flow patterns and how they change in time, location and depth. Generally speaking, dynamic height relative to a pressure reference surface, varies according to changes in the oceans' 3-dimensional density structure. There are several reasons for these changes to occur. Following *Wyrki* [1974], the most important are:

- (a) the annual variation of the temperature and salinity structure of the oceans;
- (b) the seasonal shift of the mean flow axes of the ocean currents; and
- (c) the meandering of ocean currents.

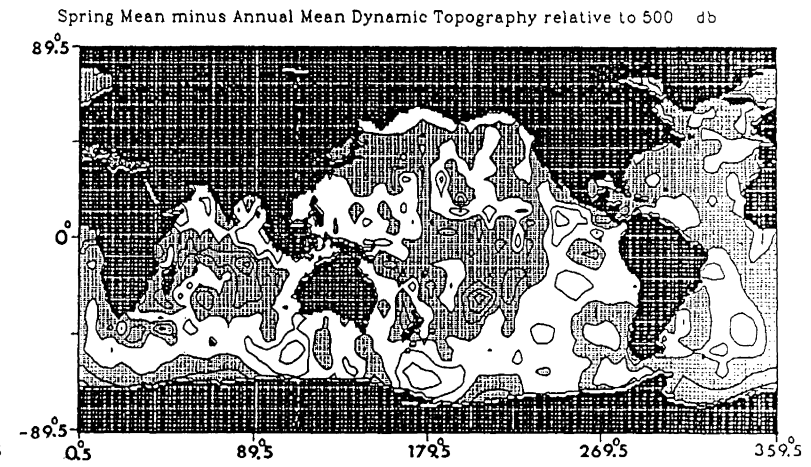
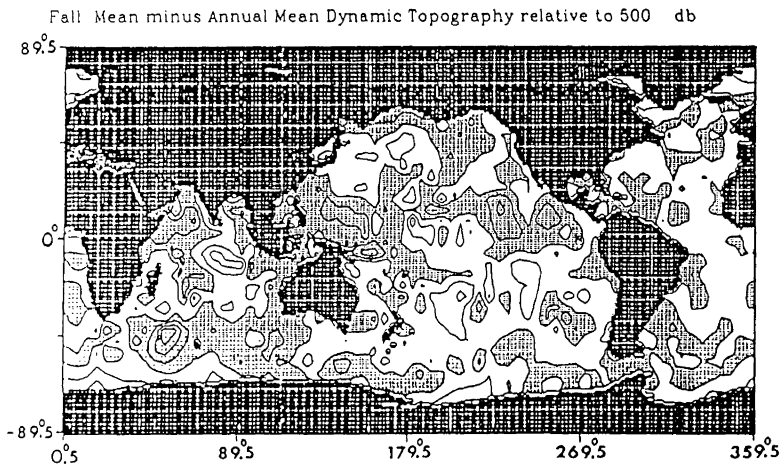
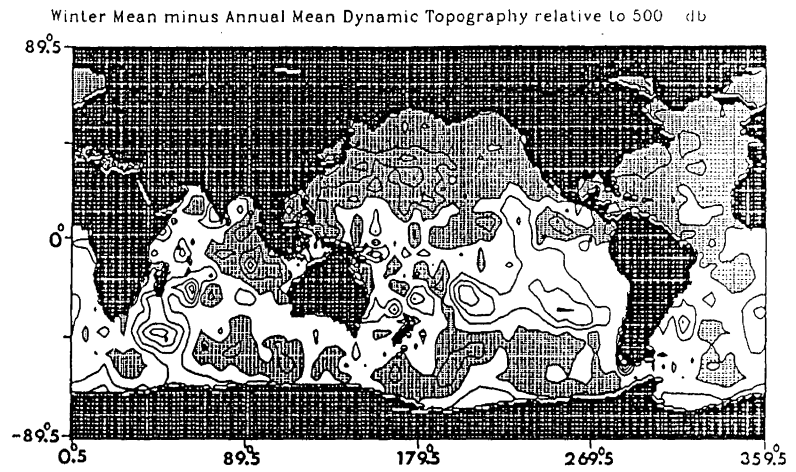
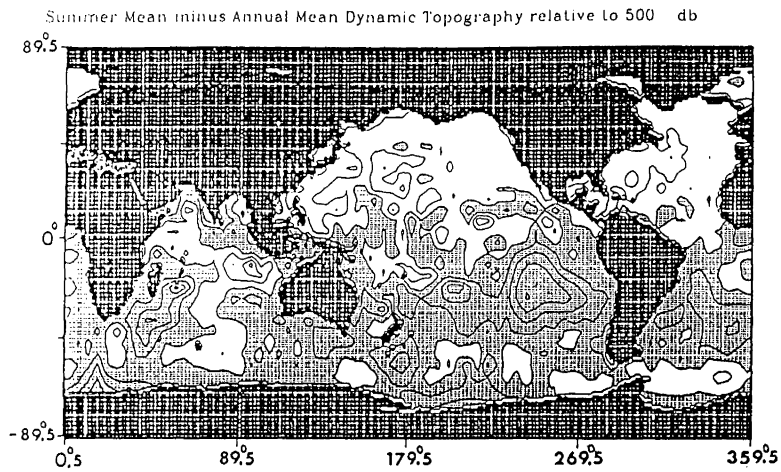


Fig. 5.4a. Mean Seasonal Difference-Maps of Dynamic Topography for the global ocean relative to 500 dbar. The differences are computed as seasonal mean minus annual mean value of dynamic topography. The contour interval is 5 dynamic centimetres. Negative areas are stippled. Positive areas are white.



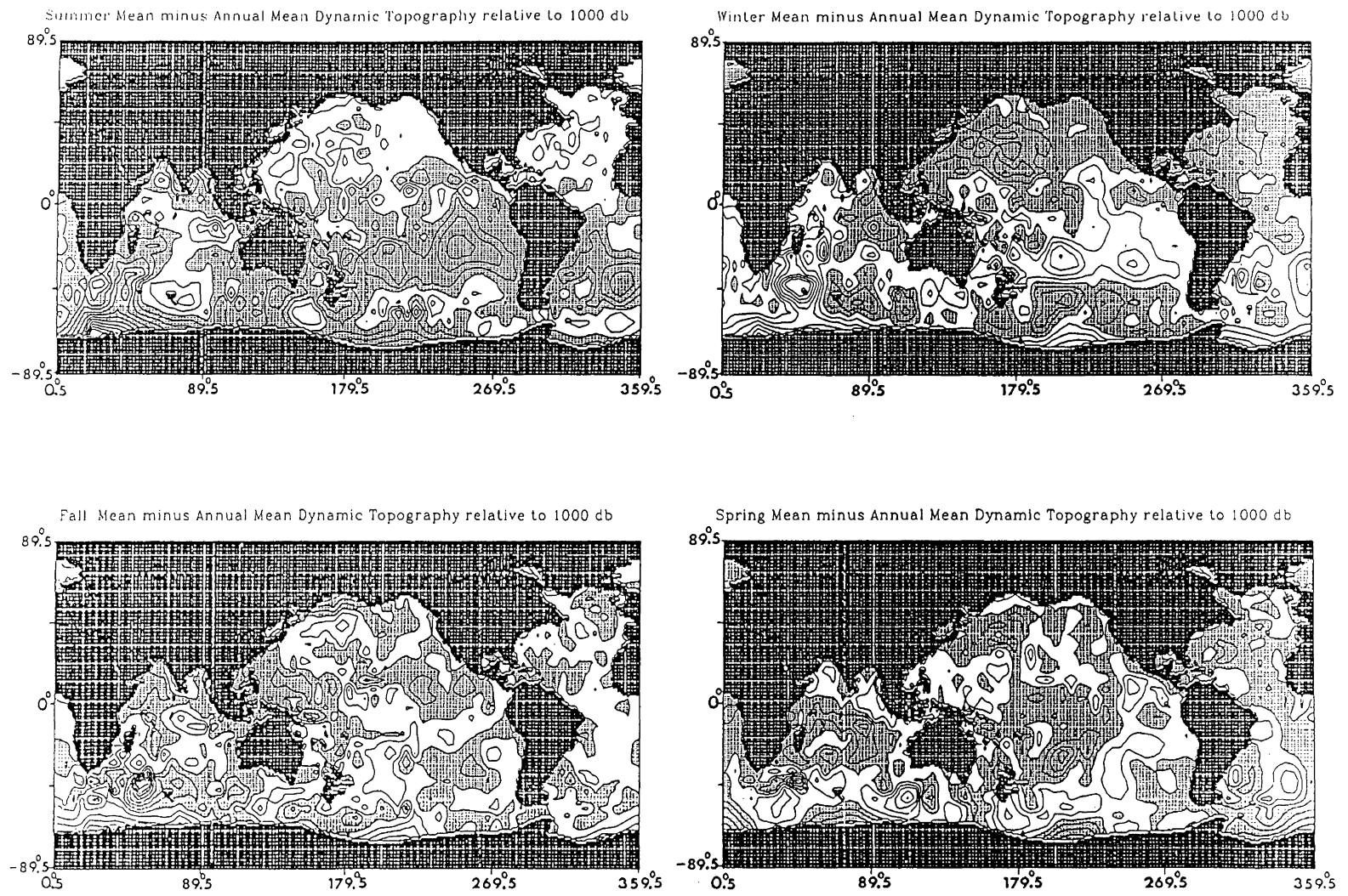


Fig. 5.4b. Same as Figure 5.4a, but relative to 1000 dbar pressure surface.

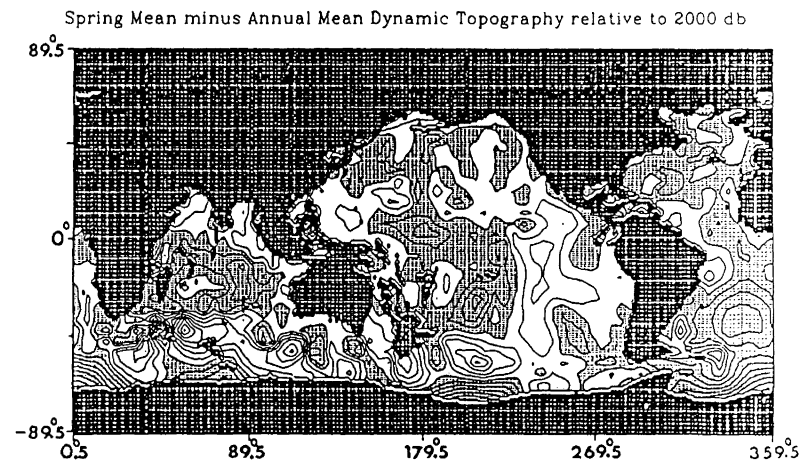
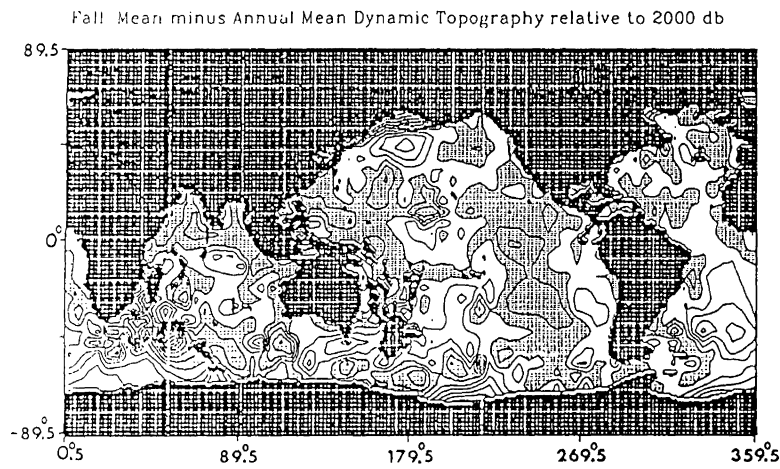
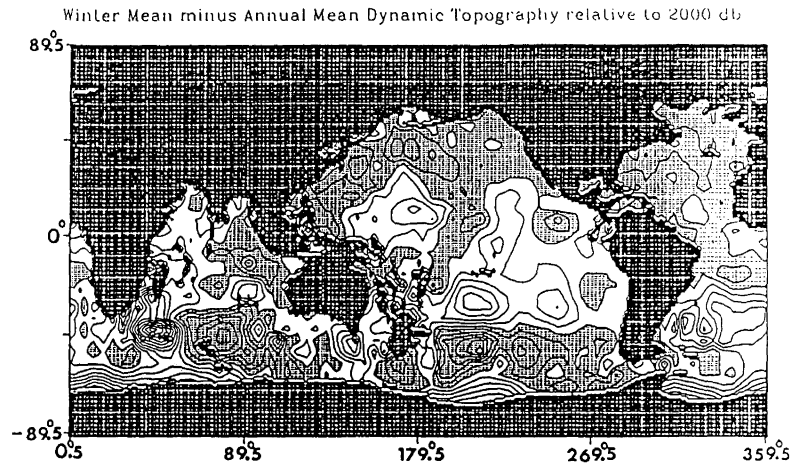
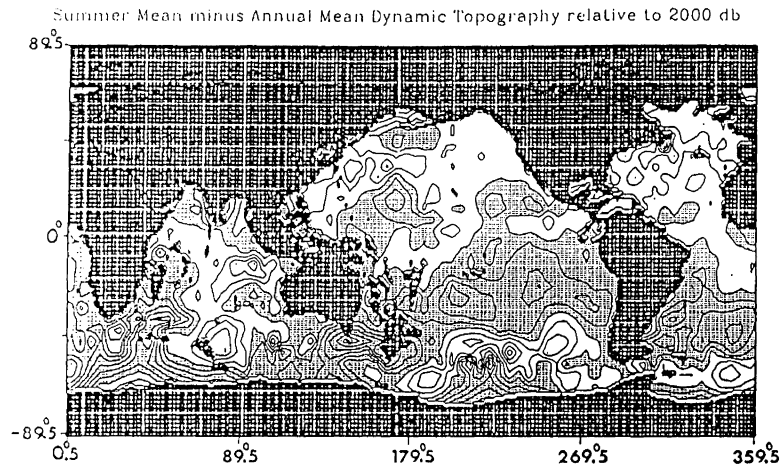


Fig. 5.4c. Same as Figure 5.4a, but relative to 2000 dbar pressure surface.

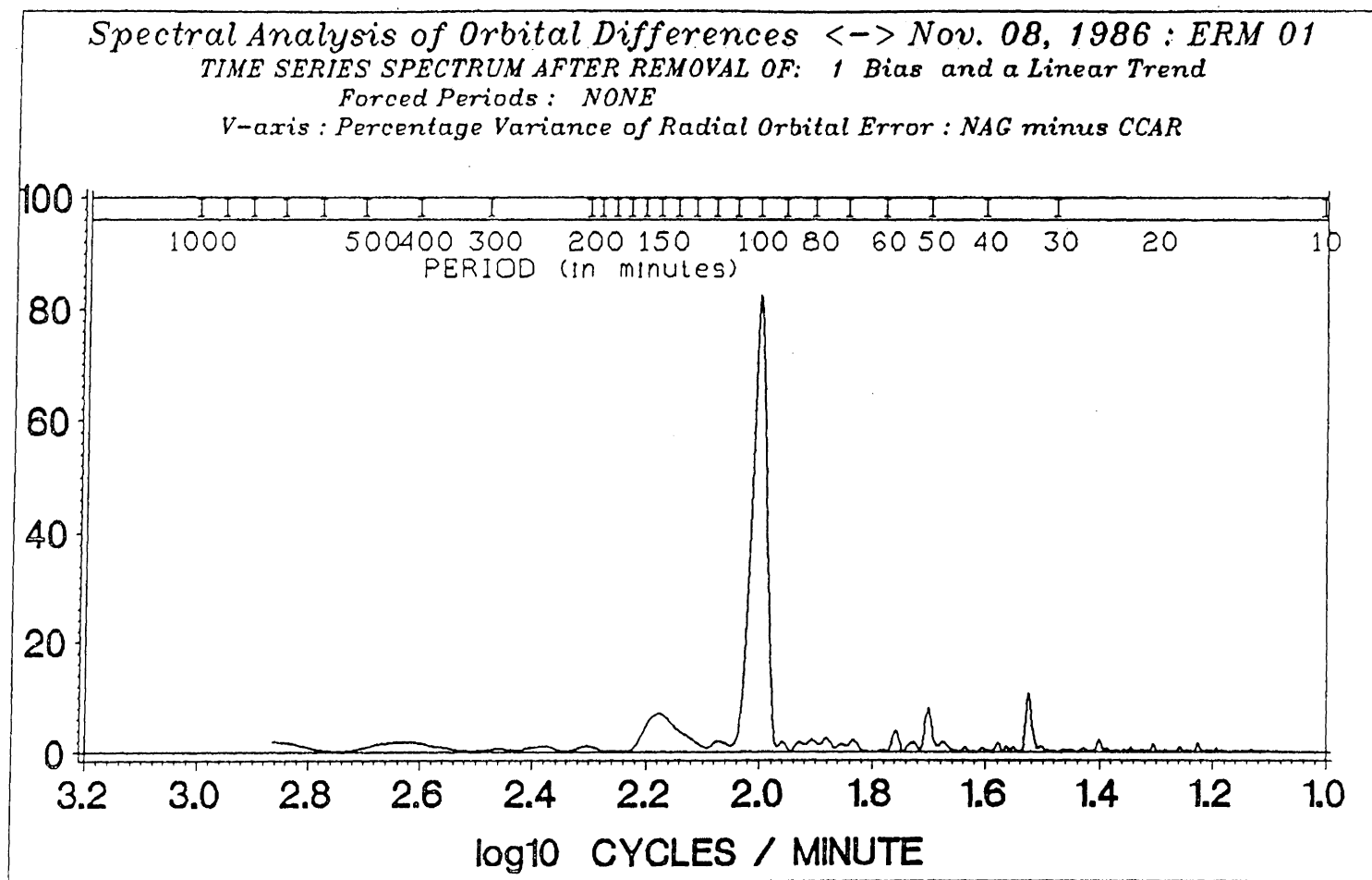


Fig. 6.4b. The least squares spectrum of the NAG minus GSFC/CCAR radial orbital differences. The 1 cycle per revolution frequency dominates the spectrum. Other frequencies at 2 and 3 cycles per revolution are also present, but their amplitude is very small compared to the estimated 7.15 m amplitude of the once per revolution radial orbital error for the 1-day data span analysed here.

It is noted that all subsequent processing has been carried out using the RISSH fields corrected for the inverse barometer response of the ocean. It should also be remembered that the RISSH field is, in the zero-th approximation, a representation of the instantaneous SST.

The first main processing step involves the computation of along-track average SST slopes. In section 6.4 we have explained the reasons for doing this. Here, we briefly explain the mechanics of carrying out this operation. The processing of the RISSH files is sequential in nature, since each edited data record carries an arc index. Thus, an ascending (or descending) arc is loaded into memory each time and the total number of data points in the arc is estimated. The number of data points in each  $1^\circ$  latitude belt of the overlaid grid mesh is computed (in reality pointers are used in this task). Two screening procedures are invoked which ensure that in each latitude belt there are at least 5 altimetry profile points with a minimum time separation between the first and the last one (recall pixel-segment definition in section 6.4) of 8 seconds. The points belonging to a pixel-segment are then fitted by a least squares line. The estimated slope of the line fit is the desired SST average gradient. The attribute “average” is used here and throughout this chapter in the context of spatial averaging. Associated standard deviations are also produced for the polynomial coefficients. The estimated SST gradients are routinely compared to an upper-bound slope of  $2 \times 10^{-5}$  radians, and they are rejected if they exceed this value.

A local Cartesian coordinate system with origin at the centre of the host grid-cell containing the pixel-segment and with the x-axis pointing east, the y-axis pointing north, is used throughout these calculations.

The final product of this processing step is a GDR gradient-file containing the mean time, mean latitude and longitude of the pixel-segment used in the gradient estimation, the SST estimated gradient and its associated standard deviation, the x- and y-axis length components of the pixel-segment, the host-cell latitude and longitude indices, the arc index (ascending or descending), and the revolution and ERM indices.

Once all the GDR files from one ERM have been processed, a composite gradient image time-frame is created from all the GDR gradient files. It is obvious that in a gradient image time-frame, there are going to be pixels with along-track SST average gradients from both, ascending and descending arcs, pixels with along-track average gradients from ascending arcs only, pixels with along-track average gradients from descending arcs only, and pixels without any gradient information (excluding pixels on land).

Since along-track average gradients from both ascending and descending arcs are needed to estimate the average gradients in two orthogonal directions (east-west and north-south), then a considerable amount of otherwise useful gradient information from only ascending or only descending tracks in an area will be lost. This situation is a result of the individual ERM data coverage and there is nothing that can be done, other than to resort to some kind of interpolation procedure. However, interpolating in space and time, even within one ERM, is not a trivial matter at all.

Many scenarios of how to deal with partially available gradient information were investigated and numerous lengthy computations were performed. The approach finally adopted relies on the fact that the global ocean circulation has, primarily, zonal

characteristics, i.e., most of the circulation features have an east-west orientation. If this is translated into gradient information then, the zonal average of both ascending and descending arc gradients should represent the zonally averaged ocean circulation.

Generally, the term “zonal average” is used to denote integration (summation) of a property or quantity, around a latitude belt. In practice, we computed  $1^{\circ}$  zonal average gradients from ascending and descending arcs separately, and for each ocean basin alone. If a pixel in the gradient image time-frame was lacking gradient information from one and/or the other arc, the pixel value was filled-in by the basin-wide computed “zonal average” of the required gradient(s). Thus, the partially available observed gradient field in a pixel was rendered useful by exploiting the zonal characteristics of the ocean circulation. We have called this interpolation scheme a *primitive objective analysis technique*, because it uses spatial characteristics of the quantity under investigation to produce more complete data coverage. Standard deviations associated with the “zonal averages” were also computed. Two comments regarding the computed zonal average gradients are necessary. Firstly, the “zonal averages” can be considered as smooth versions of the gradients that could be observed. At the same time, it is also recognized that any uncertainty in the observed gradients is smeared into the basin-wide zonal average gradients. However, less accurate information is better than no information at all. A rigorous objective analysis technique is a step being seriously considered in our future plans of refining the analysis procedures presently employed.

Secondly, we have tested the effect of the basin-wide “zonal averages” fill-in process. In brief, the tests that were carried out are as follows. We selected an ERM with relatively substantial amount of pixels containing information about only one of the

along-track gradients. The selected ERM was ERM37. We created a file of “empty pixels”, i.e., no gradient information at all. This file was used as a mask file to eliminate gradient information from the pixel coverage of ERM17. The pixel coverage of ERM17 is “full” compared with the one of ERM37. Thus, a test-ERM was created and the basin-wide interpolation scheme was applied to it.

The interpolated test-ERM was then compared with the non-interpolated test-ERM and the original ERM17. The comparisons were carried out in terms of zonally averaged zonal current velocities by 1° latitude belts. These comparisons showed the following:

- (a) the test-ERM retains the same general structure of zonally averaged zonal currents compared to the original ERM17 structure; but shows considerably reduced magnitude of zonally averaged zonal velocities (by as much as 40% to 50%);
- (b) the interpolated test-ERM has the same structure of zonally averaged zonal currents as the one generated by the original ERM17;
- (c) the magnitude of the zonal averages computed from the interpolated test-ERM is by 10% to 15% lower than the corresponding magnitude of the original ERM17 ones;
- (d) an incomplete gradient-image time-frame can easily lead to an underestimation (in absolute value) of zonal averages.

The last point above was also investigated for ERM23 and ERM39 because these two ERMs lack considerable gradient pixel information. During ERM23, 6 days of coverage were lost due to malfunction. The non-interpolated ERM23 lacks about 30% of observations. The interpolated ERM23 did not produce any dramatic features or changes in terms of zonally averaged zonal velocities and the same applies for ERM39. Finally, it should be mentioned that the interpolation procedure is a computational step in the software that was run for each ERM, thus it has been routinely applied for all 44 ERMs analysed in here and not just selectively for a few ERMs. One last comment about the interpolation procedure. Certainly it is not the best procedure that someone can ever use. In future research more or even better alternatives will be explored.

Some additional comments are necessary at this point. One comment is with regard to inaccurate knowledge of the applied tidal corrections in the original data records. Significant long wavelength errors in the tidal model used to reduce the altimetry data are expected to contribute very little, if at all, to the estimated SST gradients. One possible estimation of the error introduced by tidal mismodelling can be given by a comparison of different tidal models: the differences between tidal models are expected to be less than 5 cm in the open ocean, especially after averaging in space and/or in time. Examining closely the situation, descending and ascending passes are not at the same phase of the tidal signal. We believe that tidal mismodelling errors are considerably reduced by any kind of averaging. This might not be the case for shallow seas and shelf areas. However, since the final goal of our investigation is the computation of global quantities, such as estimation of global relative OAM time series, the influence of tidal inaccuracies over such areas will be minimal in an integral sense.



Another comment is relevant regarding the use of a geoid model as a reference surface. In order to eliminate from our estimated gradients any geoid contamination, time variations of SST slopes should only be estimated from averages involving the same number of descending and ascending SST gradients, estimated at the same locations. Respecting this condition, the variability signal is devoid of geoid contamination. Unfortunately, this is too difficult a restriction to impose when one deals with real data acquisition and processing. On top of this, the interpolation scheme we chose to fill in the gradient data gaps will have an additional adverse influence. On the other hand, this interpolation processing step was judged necessary because the spatial ERM coverage throughout the first 44 GEOSAT repeat cycles invariably leaves large oceanic areas covered by only ascending or only descending arcs. An incomplete gradient image time-frame would lead to a biased result (overestimation or underestimation) of the global ROAM budget due to lack of zonal contributions.

The last processing step in this series of computations involves the calculation of ocean current velocity fields from the along-track SST gradients. To illustrate the concepts involved, Figure 6.5 represents an idealized situation over a pixel in the gradient image. The pixel-segments along the ascending and descending arcs are used to obtain the along-track gradients, as we have already discussed.

The general equation of a plane in a Cartesian coordinate system is written as:

$$z(x,y) = A x + B y + C \quad (6.4)$$

Requiring that the four points  $A_1(x_1^\alpha, y_1^\alpha, z_1^\alpha)$  ,  $A_2(x_2^\alpha, y_2^\alpha, z_2^\alpha)$  ,  $D_1(x_1^\delta, y_1^\delta, z_1^\delta)$  and  $D_2(x_2^\delta, y_2^\delta, z_2^\delta)$  belong to a plane, we have the following system of equations:

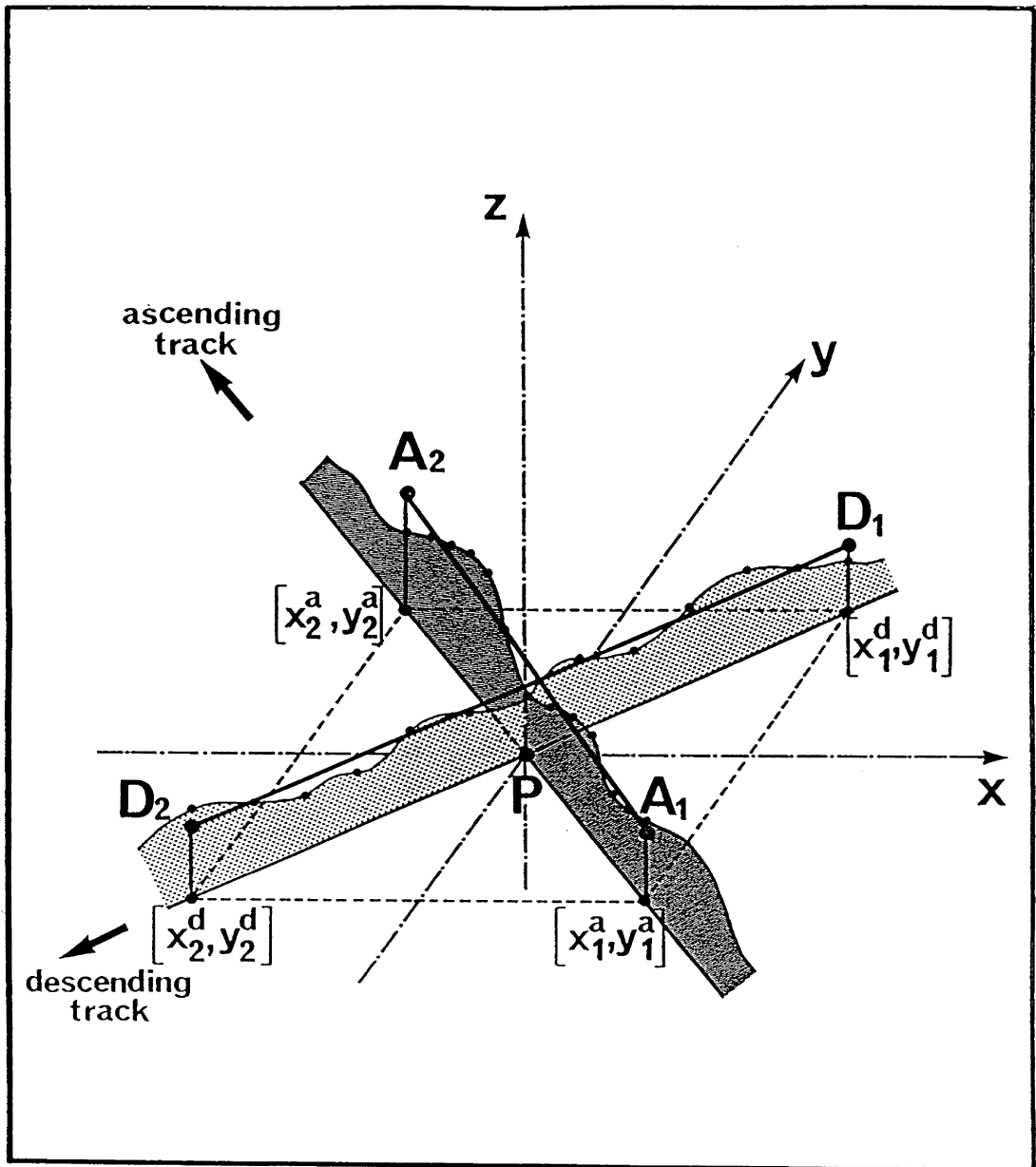


Fig. 6.5. Idealized situation over an  $1^\circ$  by  $1^\circ$  pixel in the gradient image. The pixel segments  $A_1 A_2$  and  $D_1 D_2$  along the ascending and descending arcs are used to obtain the the along-track gradients of the SST.

$$z_1^a(x_1^a, y_1^a) = A x_1^a + B y_1^a + C \quad (6.5a)$$

$$z_2^a(x_2^a, y_2^a) = A x_2^a + B y_2^a + C \quad (6.5b)$$

$$z_1^d(x_1^d, y_1^d) = A x_1^d + B y_1^d + C \quad (6.5c)$$

$$z_2^d(x_2^d, y_2^d) = A x_2^d + B y_2^d + C \quad (6.5d)$$

Differencing the top two equations we have:

$$z_2^a - z_1^a = A [x_2^a - x_1^a] + B [y_2^a - y_1^a] \quad (6.6)$$

or,

$$\Delta z^a = A \Delta x^a + B \Delta y^a \quad (6.7)$$

and by dividing both sides by  $\sqrt{(\Delta x^a)^2 + (\Delta y^a)^2} = \Delta r^a$  we obtain

$$A \frac{\Delta x^a}{\Delta r^a} + B \frac{\Delta y^a}{\Delta r^a} = \frac{\Delta z^a}{\Delta r^a} \quad (6.8a)$$

Similarly for the descending track we have

$$A \frac{\Delta x^d}{\Delta r^d} + B \frac{\Delta y^d}{\Delta r^d} = \frac{\Delta z^d}{\Delta r^d} \quad (6.8b)$$

We can immediately recognize that the right hand sides of the above two equations are the along-track average gradients we have already estimated through the least squares line fits, while the coefficients  $A$  and  $B$  are the local gradients of the plane in the x- (east-west) and y- (north-south) directions, respectively. The  $A$  and  $B$  slopes of the local surface (image pixel) are directly related to the ocean current velocity local-average vector. Hence, from the gradient image time-frame we directly estimate the average velocity vector field if both the ascending and descending along-track gradients are available. The velocity vector is given by

$$\text{magnitude} = \sqrt{A^2 + B^2} \quad (6.9)$$

$$\text{azimuth} = \arctan \frac{A}{B} \quad (6.10)$$

It should be mentioned that the associated standard deviations of the observed RISSHs were used in the determination of the along-track average gradients and their respective error estimates during the least squares line fit. The along-track average gradient error estimates, in turn, were taken into account in the estimation of the  $A$  and  $B$  plane-parameters and their associated standard deviations. Thus, the ocean current velocity local-average vector components have properly assessed error estimates too.

To summarize, the gradient image time-frame final processing step involves the estimation of the  $A$  and  $B$  plane-parameters for each individual image pixel. The slopes  $A$  and  $B$  were related through the geostrophic equations to the north-south and east-west ocean current velocity components, respectively. This was the common goal of all the data processing steps. From now on, only ocean current velocity time-frames will be considered. Finally, for each ocean current velocity time-frame there is also an image of standard deviations associated with it.

## **6.8. Ocean Current Variability from the GEOSAT/ERM Data Set**

In the previous section we saw how the ocean current velocity time-frame is estimated. The technique was applied to the first 44 repeat cycles of the GEOSAT civilian mission. Therefore, there is a stack of 44 snapshots of the global ocean current velocity field, one every 17 days.

One way to represent time variations from a stack of images is to take successive differences between time-frames. In this thesis work, we chose to represent spatial/temporal variability in a different way, for two reasons. First, the reference geoid is still imbedded in the individual time-frames. Second, we want to examine ocean current variability from satellite altimetry and relate it to the long-term mean oceanographic compilations (see Chapter 5), in order to obtain a more or less 3-dimensional picture of the time varying ocean and thus help our investigations towards LOD fluctuations.

Space/time ocean surface current variability is computed here with respect to the 2-year mean surface ocean current velocity field. The average ocean current velocity time-frame from all 44 ERMs was computed and subsequently subtracted from each individual velocity time-frame. This operation accomplishes two results: it renders a geoid-free ocean current velocity time-frame and at the same time it provides the space/time fluctuations with respect to a 2-year long mean. The time averaged velocity frame was computed pixel by pixel, by taking the average when more than 40 repeat-cycle pixel values were available.

Because it is difficult to display 4-dimensional information using conventional graphical representations, and because for LOD studies the east-west component of the ocean current velocity field is the relevant quantity, we have contracted one dimension, in particular, the longitudinal one. In other words, we have estimated the zonal average of the current velocity fluctuations for every  $1^\circ$  latitude belt between  $65^\circ S$  and  $65^\circ N$ . The results can be displayed in three fashions: (a) as a 3-dimensional plot (x-axis representing 1 degree latitude belts, y-axis representing time, and z-axis representing the

magnitude of the zonal current variability) as in Figures 6.6a and 6.6b; (b) as a contour plot (Figure 6.7); and, (c) as a collection of 2-dimensional individual plots (*Appendix I*). Each display offers different advantages.

A general comment that can be drawn from either set of maps is that most of the velocity variability is confined in the north and south tropical zones (between  $23^{\circ}S$  and  $23^{\circ}N$ ). However, there are significant changes observed in the south subtropical zones and the higher southern latitudes between  $50^{\circ}S$  and  $60^{\circ}S$ . The latter are very likely associated with the Antarctic Circumpolar Current (ACC). A reminder is due at this point. The zonal velocities displayed, express excursions from the 2-year long zonal mean.

A very striking change appears to happen after the 33<sup>rd</sup> time-frame (i.e., from ERM34 on). The 34<sup>th</sup> frame represents the period May 22, 1988 to June 07, 1988. There is a sudden influx of negative zonal velocity anomalies (westward velocity anomalies) on each side of the Tropic of Capricorn with respect to the 2-year mean. It continues through ERM35 together with a small build-up of westward velocities in the northern extra-tropics and the picture changes during June 25, 1988 - July 11, 1988 (ERM36). The westward velocities retreat to a minimum at the latitudes bounding the Tropic of Capricorn as well as in the northern extra-tropics, while there is an eastward intensification in the southern extra-tropics accompanied by a similar one in the northern tropical zone. The situation changes even more radically during the next repeat cycle (ERM37- July 12 to July 28, 1988). There are large changes happening in all latitude bands. The generally quite southern higher latitudes experience many-fold magnitude changes in westward velocities, while both tropical zones experience very







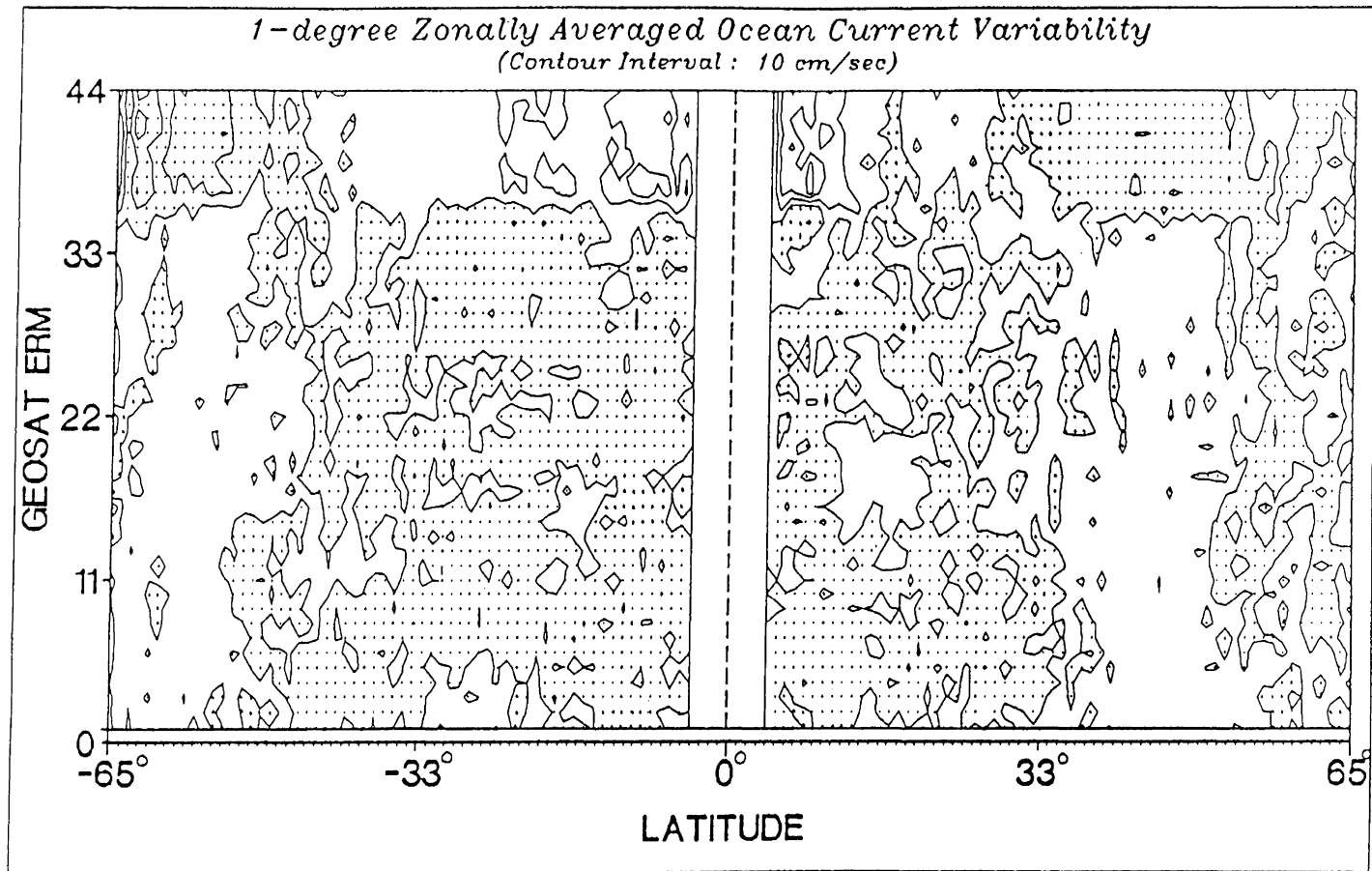


Fig. 6.7. Contour plot of the 2-year long 1-degree zonally averaged variability of ocean currents. Negative values indicate westward zonal average velocity variations. Areas of westward zonal velocities are stippled. White areas denote eastward zonal average velocity variations, except for a latitude band of 4 degrees on each side of the equator where no ocean current computations were performed. The contour interval is 10 cm/s.

large eastward velocity changes. This picture, though very slowly subsiding, continues throughout the second half of 1988. This is a very peculiar phenomenon indeed.

We have tried to examine the reasons for such dramatic changes in the zonal current velocity anomalies. The first cause we tried to rule out as a possible candidate involves data or software problems. Regarding software problems, the same software code was used with each run for each one of the 44 ERMs. The designed package contains 7 processing steps in two batch files. The only changes that are made for the runs for each ERM are the names of the input and output files. We consider the possibility of software causes as rather unlikely because no software changes were made during the processing of all 44 ERMs. Regarding data problems, in general, the GEOSAT coverage becomes sparser from ERM37 on. This can be deduced from the number of data records available on the original ERM tapes. However, we have examples of more serious data coverage reduction for ERM23 and no drastic changes are seen in the results from this ERM. The tests performed for the lack of adequate average - gradient information in the incomplete gradient-image time frame (reported in the previous section) did not show any trend of that kind. From the information we have received with the original ERM data tapes there is no reason or indication to suspect that there have been orbital changes from ERM37 on. Based on the above statements, we concluded that data or software problems are not very likely the reasons for the "abnormal" changes. Therefore, we accept the changes with reservations, especially with regard to their magnitude. At the same time we would like to examine these changes in the light of possible phenomena that could, at least partially, be responsible for an unusual behaviour.

The first investigation undertaken involves the south tropical zones. For that purpose, we acquired information on the Southern Oscillation Index (SOI) for the period January 1986 to December 1988. The SOI is the normalized sea-level pressure difference between the island of Tahiti and Darwin Australia. This information was made available to us by L. Miller, of NOAA [*personal communication*, 1989], and is contained in the *Climate Diagnostics Bulletin*. From the tabular monthly values of the Tahiti-Darwin SOI, we produced the SOI-plot displayed in Figure 6.8. The Tahiti-Darwin SOI is a description of the sea-level pressure differential, in other words, it is a round-about description of sea level height anomalies across half of the south equatorial Pacific basin. We note that there is a reversal in the sign of the Tahiti-Darwin SOI occurring at approximately the same time we start observing the unusual changes in the zonal velocity fields, i.e., May-June, 1988. A general agreement is note worthy. However, it does not constitute a definitive explanation of what we see in the GEOSAT data analyses of the variable ocean current velocity fields. The best way to assimilate the SOI changes with our results is to acknowledge that there is an indication for a potential relationship that demands further research, both qualitatively and quantitatively.

An interesting discussion on the unusual behaviour of the tropical Pacific Ocean during this period is contained in an article that appeared in “Research News” in the August 26, 1988 issue of the journal *Science* [Kerr, 1988]. In this article, it is stated that a precipitous drop in the temperatures of the tropical Pacific waters by about 2°C below normal, occurred by June 1988. This chilling of the tropical Pacific had always been seen as a part of the *El Nino* cycle. The name *La Nina* has been coined for these cold events. Generally, *La Nina* has the opposite effect of *El Nino* in a given area.

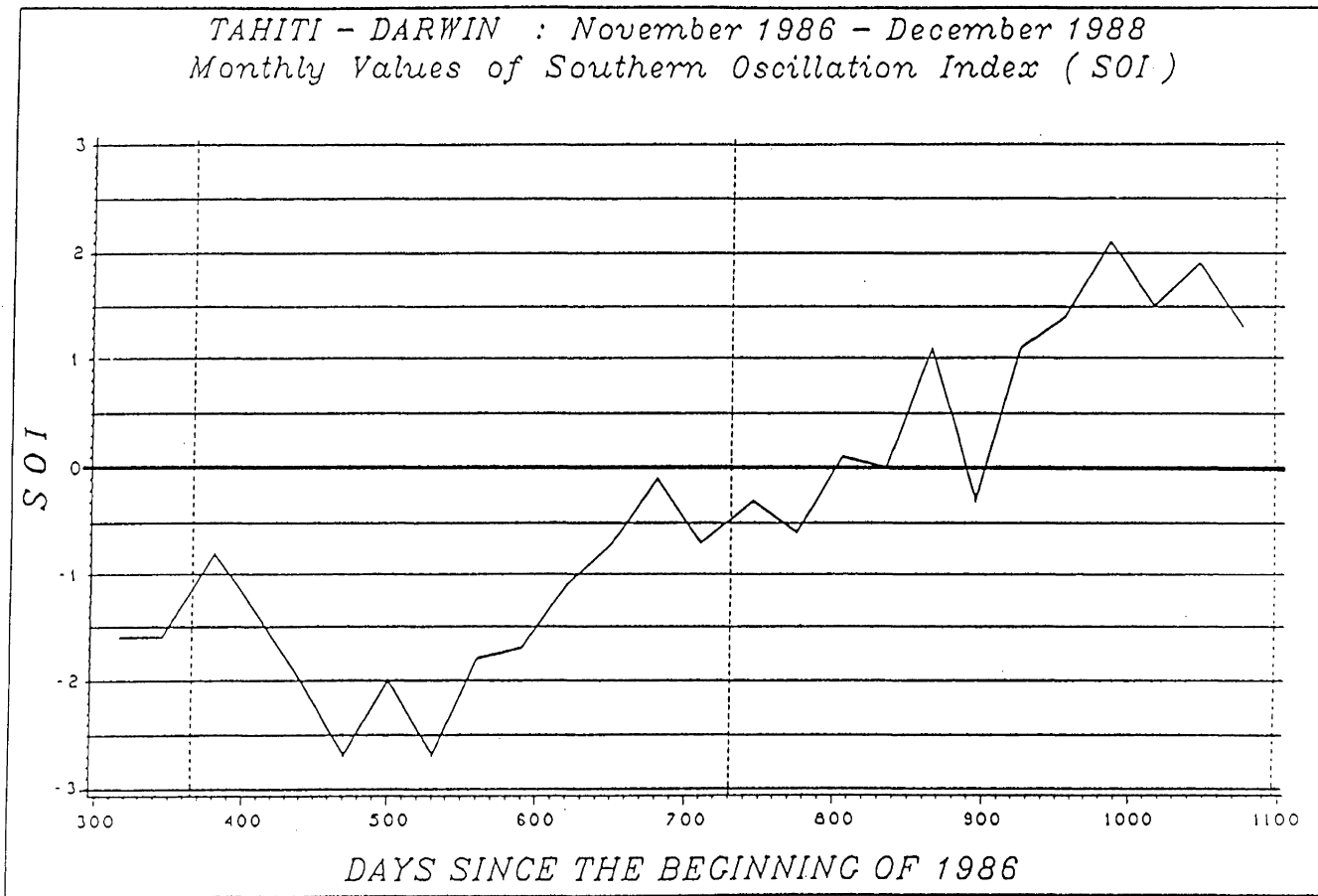


Fig. 6.8. Monthly mean values of the Tahiti - Darwin SOI for the period November 1986 - December 1988. The plot was generated from the tabular values listed in the *Climate Diagnostics Bulletin*.

*El Nino* is expressed as a negative SOI (warm events), while *La Nina* as a positive SOI (cold events). *Kerr* [1988] finally states that this *La Nina* is likely to continue during the rest of 1988 and into the spring of 1989. It may be said that this observation supports the trend we see in our zonal ocean current variability maps.

Regarding now the tropical Pacific waters, *El Nino* is associated with episodes of enhanced warm-water upwelling, while *La Nina* with episodes of enhanced cold-water upwelling. It is natural to expect that this phenomenon should be reflected in the ocean circulation patterns of the tropical Pacific ocean. *Bradley et al.* [1987] state that both *El Nino* and *La Nina* events do have an impact on large scale atmospheric circulation patterns. A strong correlation between equatorial Pacific sea surface temperature (SSt) and tropical tropospheric mean temperature (TTt) has been reported, with the SSt leading the TTt by about 6 months [*Bradley et al.*, 1987]. Furthermore, *Bradley et al.* [1987] have demonstrated that ENSO events have a powerful influence on large scale temperature and precipitation patterns in the northern hemisphere tropical latitudes.

Anomalous behaviour of dynamic heights has been observed in the western equatorial Pacific during the late spring and summer of 1988 [*McPhaden et al.* 1990] and anomalous sea surface elevations occurred in the late summer of the same year in the northern equatorial Atlantic [*Carton & Katz*, 1990]. However, both studies are confined in relatively small regions and no generalizations should be made. Sea level height variations showing interesting trends in 1988 compared with the ones in 1987 are shown in the sea level height maps from the eastern Pacific GOES Stations (see Climate Diagnostics Bulletin, November 1989). The point we want to draw attention to is that there are general evidences for unusual behaviour in the tropical latitudes both

northern and southern ones. On the other hand, we have found no literature reports on unusual behaviour in other latitude bands to provide some external general support for our results.

In conclusion, it is too early to be certain that the behaviour of the zonal ocean current variability such as the one we have computed from the GEOSAT altimetry is a manifestation of the *El Nino - La Nina* cycle. Definitely, there are enough intriguing questions generated by the observations we have pointed out. Moreover, we see in our zonal ocean current variability maps that the unusual behaviour does not only involve the tropical zones, but also the southern higher latitudes and northern mid-latitudes. Is there a teleconnection, and if yes, from where is it coming? Has such a behaviour been observed in other data sets? What is the coupling of the oceans with the atmosphere and what is the impact on earth rotational dynamics? These are some of the questions that we would like to examine thoroughly in future investigations, in conjunction with improvements in our analysis and processing techniques.

## 6.9. Summary

The altitude of the satellite above the sea surface can be determined to a precision of the order of 5 cm using radar altimeters such as the one aboard GEOSAT. Accurate determination of the satellite's orbit along with the precise measurement of its altitude above the sea surface yields the instantaneous mean sea surface height, which, combined with knowledge of the geoid can provide the absolute sea surface topography field. The sea surface topography gradients yield in turn the kinetic energy of

geostrophic flow, i.e., from SST slopes one can obtain the surface ocean current velocity field.

A satellite altimeter in an exactly repeating orbit, such as the GEOSAT/ERM, can be used to study the temporal variations along repeated segments of subsatellite tracks and to determine the time-varying component of surface velocity. This quantity gives the fluctuating component of the ocean surface circulation, but leaves the mean value completely undetermined in the absence of the geoid. The fluctuations in the oceanic circulation are generally of the same order as the time-averaged circulation.

The fluctuating part of the oceanic circulation combined with some reasonable quantitative knowledge of the subsurface flow characteristics (see, for example, Chapter 5), eventually determine the general 3-dimensional, time-varying circulation of the oceans. This has been the major theme in this thesis work, with the ultimate goal of associating the time-varying ocean circulation with the fluctuations in the LOD (see Chapter 2).

In practice, the first 44 repeat cycles of the GEOSAT/ERM altimetry data, covering the period Nov. 8, 1986 to Nov. 24, 1988, were used to obtain the time-varying global ocean current velocity field. Each “point on the chart” represents the average temporal/spatial behaviour of the ocean over a 17-day period. In essence, we have constructed the first global time series of surface ocean current velocity variability fields useful for LOD variability analyses, using direct oceanic observables. A new way of looking at satellite altimetry data was developed for that purpose.

The underlying philosophy of the technique developed was based on directly estimating the gradient ocean surface, thus allowing the direct estimation of the velocity field without the need of the sea surface height field as an intermediary, and without the need of orbit adjustments. The gradient analysis technique not only allowed the transformation of observation space, but also resulted in a high-pass filtering operation. Most of the long wavelength orbital errors were thus removed. Slope profiles were constructed that allowed the systematic study of slope differences over the time span of 2 years. The long wavelength component, i.e., the time-averaged component of the surface oceanic circulation had to be removed. The bottom line is that the technique developed here is a simple, computationally efficient, and conceptually elegant one.

The results of the ocean current variability analyses (displayed in Figures 6.6, 6.7 and Appendix I) may have opened the oceans' Pandora's box regarding medium- to large-scale ocean / atmosphere coupled dynamic processes such as the *El Nino - La Nina* cycle and the Southern Oscillation. The implications of such interactions will be extremely important regarding the transfer of global properties between the earth system components such as energy, mass, and angular momentum. Nevertheless, these kind of results, if they are actually that striking, they still have to be independently confirmed.



## **Chapter 7: The Estimation of Relative Oceanic Angular Momentum**

At the very beginning of this dissertation (Chapter 1) we stated the objectives of this research work. The first two objectives, namely:

- (1) exploitation of satellite based geodetic observations and techniques useful for monitoring ocean surface dynamics both in space and time on a routine basis (as long as satellite altimetry data are available); and
- (2) exploitation of in-situ oceanographic observations to provide information on the 3-dimensional structure of ocean dynamics as a reference frame for the synoptic ocean monitoring,

have been fulfilled. In Chapter 5, we have seen how the specific volume ocean information in space and time, was translated into mean seasonal ocean current velocity fields for the top 2 km of the ocean water column. In Chapter 6, we gave the summary of how to extract surface ocean current variability from the space geodetic technique of satellite altimetry.

In essence, we have generated time series of a virtual 3-dimensional ocean circulation. It is time to capitalize on the information and move towards the third objective of this research, namely:

- (3) the determination of axial relative oceanic angular momentum (ROAM) in the form of time series, necessary for studying the effect of the variable oceanic circulation on the length-of-day (LOD) fluctuations.

It is useful to note at this point that the ocean current velocity fields computed (see Chapter 5 and 6) contain both the east-west  $u$  and north-south  $v$  components of the velocity vector. However, for the purpose of evaluating the effect of the ocean current variability on the LOD, we only need the east-west component of the velocity vector (or what we will call the  $u$ -field). In the following section we show how the oceanic  $u$ -field is transformed into axial relative oceanic angular momentum (ROAM).

## 7.1. Basic Relationships

The explicit form of the axial ROAM was given in eq. (2.27) and is repeated here:

$$h_3^{ocean} = \int_0^r \int_{-\frac{\pi}{2}}^{\frac{\pi}{2}} \int_0^{2\pi} r^3 \rho_w u(\phi, \lambda, r, t) \cos^2 \phi \, d\phi \, d\lambda \, dr \quad (7.1)$$

where:

- $r$  - is the radial coordinate;

- $\rho_w$  - is the material density of sea water;
- $\phi, \lambda, r$  - are spherical coordinates (latitude, longitude and ocean depth, respectively); and
- $u(\phi, \lambda, r, t)$  - is the east-west component of the ocean current velocity field.

The space/time variations of the oceanic u-field directly produce temporal variations in the axial ROAM which, consequently, are partly responsible for the observed fluctuations in the LOD. The idealized situation for carrying out routine computations of the axial ROAM budget would be to have the oceanic u-field available on a regular 3-dimensional grid covering the global ocean at regular, short time intervals. Then, calculating values of the ROAM about the polar axis relative to an earth-fixed frame (more precisely, relative to a mantle-fixed frame) from analyses of u-fields becomes a straight-forward application of the integral in eq. (7.1).

However, the real situation is far from ideal. The availability of data and numerical techniques regarding axial ROAM calculations lag far behind their counterparts of operational calculations of axial relative atmospheric angular momentum (RAAM). Nevertheless, we have attempted here to produce time series of the oceanic u-field from all the possible available information to date, i.e., from in-situ oceanographic descriptions and from satellite altimetry derived ocean surface descriptions. The u-field time series derived from purely oceanographic observations of specific volume are inherently 3-dimensional, but are limited in terms of time resolution. They can only be used to infer an average seasonal description of the temporal variations of  $h_3^{ocean}$ ,

while at the same time are dependent on the assumption of the level of no-motion. On the other hand, the time resolution of the satellite altimetry derived u-fields represents a drastic improvement over the “specific-volume” derived u-fields; however, we only have a description of the space/time behaviour of the surface u-fields.

We have chosen to represent the ocean circulation as the sum of two components, i.e., the sum of the mean and the fluctuating component. Since the east-west component of the ocean current velocity field is the quantity of interest in the present investigations, we have the following working partition:

$$u(\phi, \lambda, r, t) = \overline{u(\phi, \lambda, r)} + u^*(\phi, \lambda, r, t) \quad (7.2)$$

where:

- $\overline{u(\phi, \lambda, r)}$  - represents the time-averaged east-west ocean current velocity field;
- and
- $u^*(\phi, \lambda, r, t)$  - represents the fluctuating east-west ocean current velocity field.

The time-averaged ocean current velocity field has been computed from the in-situ oceanographic data (the seasonal  $\bar{u}$ - fields discussed earlier in Chapter 5 do represent well the general ocean circulation patterns). The  $\bar{u}$ -field was estimated at the sea surface, at 500m relative to 2000m, and at 1000m relative to 2000m. The assumption of the level of no-motion used in Chapter 5 has rendered the  $\bar{u}$ -field to be zero at 2000m, thus the current velocities at all other surfaces are relative to the 2000m reference level.

The fluctuating ocean current velocity field  $u^*$  has been computed during the period Nov. 86 to Nov. 88 from the GEOSAT altimetry observations (discussed in Chapter 6). The important characteristic of the altimetry derived  $u^*$ -field, however, is that it is only known at the sea surface. This fact will add complications in utilizing the  $u^*$ -field in ROAM estimation, since it is not known at all depths in the ocean. We shall see in the next section how we have at the present time moved around these added complications.

Let us now return back to eq. (7.1) of axial relative angular momentum. For practical calculations of  $h_3^{ocean}$  time series, we have assumed that the density  $\rho_w$  of sea water is constant, that is,

$$\rho_w(\phi, \lambda, r, t) = \rho_0 = \text{constant} \quad (7.3)$$

and also that the ocean is a fluid envelop of constant thickness  $\Delta r$  such that

$$\bar{R} \leq r \leq \bar{R} + \Delta r \quad (7.4)$$

where  $\bar{R}$  is the mean radius of the earth. Under these assumptions and approximations, eq. (7.1) becomes

$$h_3^{ocean} = \bar{R}^3 \rho_0 \int_{\bar{R}}^{\bar{R} + \Delta r} \int_{-\frac{\pi}{2}}^{\frac{\pi}{2}} \int_0^{2\pi} u(\phi, \lambda, r, t) \cos^2 \phi \, d\phi \, d\lambda \, dr \quad (7.5)$$

We define the quantity  $[u]$  to be the zonal average current using the spatial averaging operator

$$[A] = \frac{1}{2\pi} \int_0^{2\pi} A d\lambda \quad (7.6)$$

thus,

$$[u]_{\phi, r, t} = \frac{1}{2\pi} \int_0^{2\pi} u(\phi, \lambda, r, t) d\lambda \quad (7.7)$$

or,

$$2\pi [u]_{\phi, r, t} = \int_0^{2\pi} u(\phi, \lambda, r, t) d\lambda \quad (7.8)$$

and upon substitution into equation (7.5) we obtain

$$h_3^{ocean} = 2\pi \bar{R}^3 \rho_0 \int_{\bar{R}}^{\bar{R}+\Delta r} \int_{-\frac{\pi}{2}}^{\frac{\pi}{2}} [u]_{\phi, r, t} \cos^2\phi d\phi dr \quad (7.9)$$

and upon substitution of integration by summation

$$h_3^{ocean}(t) = 2\pi \bar{R}^3 \rho_0 \sum_{i=1}^n \Delta r_i \sum_{j=1}^m [u_j]_{r_i, t} \cos^2\phi_j \Delta\phi \quad (7.10)$$

where

$$\Delta r = \sum_{i=1}^n \Delta r_i$$

we obtain the discrete form of the axial ROAM time series suitable for evaluation using computer algorithms. Therefore, if the zonal average [u]-field can be estimated for discrete oceanic layers  $\Delta r_i$  at discrete times  $t_k$ , then a time series of length  $k$  of axial ROAM can be readily evaluated. It should be made clear that in the discrete formulation the estimated [u]-field was appropriately weighted by the fraction of each latitude band occupied by ocean areas as opposed to land areas.

On the assumption that a change  $\Delta h_3^{ocean}$  in the axial ROAM is accompanied by an equal, but opposite, change in the angular momentum of the solid earth - atmosphere

subsystem (see equations 2.18c, 2.20, 2.21, 2.25), it is possible to obtain a linear relationship between  $\Delta h_3^{ocean}$  and the  $\Delta LOD$  associated with it, i.e., following the same formulation as the one presented in *Rosen et al.* [1989], *Rosen & Salstein* [1983], *Langley et al.* [1981], etc:

$$\Delta LOD = 1.68 \times 10^{-29} \Delta h_3^{ocean} \quad (7.11)$$

where  $\Delta LOD$  is in units of seconds, and  $\Delta h_3^{ocean}$  is in units of  $kg\ m^2\ s^{-1}$ . Additional assumptions involved in deriving the relation presented in eq. (7.11) are [*Rosen et al.*, 1989]: only the earth's crust and mantle and not its core are involved in LOD changes within the time frame spanned by the time series, and that the moment of inertia of the earth's crust and mantle is constant in time.

Equation (7.10) will be used in the next sections to arrive at ROAM estimates from the quasi-permanent ocean circulation (section 7.2) and  $\Delta ROAM$  estimates from the satellite altimetry derived mesoscale ocean variability (sections 7.3 and 7.4). Equation (7.11) will be used later on in Chapter 8.

## 7.2. ROAM Estimates from the Quasi-Permanent Ocean Circulation

As we have already discussed in Chapter 5, long-term mean seasonal relative ocean current velocity fields have been computed for three different layers of the ocean, namely for the 0-500 m, 500-1000 m, and 1000-2000 m layers. The underlying assumption is that the ocean current velocity at 2000 m is constrained to be zero. Mean annual relative ocean current velocity fields have been subsequently computed, i.e., the quasi-permanent seasonal and annual  $[\bar{u}]$  -fields, and have been integrated between

70°S and 70°N latitude, to produce a long-term mean axial ROAM time series, using the formulae cited in the previous section. Owing to the smallness of the Coriolis parameter, exaggerated values of current velocities are expected at low latitudes (i.e., between 5° S and 5° N). Therefore, we have not computed any contribution to the ROAM budgets from these latitude belts. It is difficult to provide an order of magnitude estimate for this missing contribution. The currents in the equatorial zone form a complicated system of currents flowing mainly in the zonal direction. The North and South Equatorial Currents are westward directed, while the Equatorial Counter Current and the Equatorial Undercurrent are eastward directed. It is not possible at the moment with the information available to us to estimate what the net effect of the equatorial current systems on ROAM could be.

In brief, the computed order of magnitude of long-term mean axial ROAM conforms with what the oceanic budget is generally believed to be *vis a vis* the budget of the axial RAAM, i.e., about 10% of the RAAM budget, which is approximately  $1.3 \times 10^{26} \text{ kg m}^2 \text{ s}^{-1}$  [Oort & Peixoto, 1986]. Figure 7.1 shows the long-term mean axial ROAM seasonal and annual budgets computed here (in units of  $10^{25} \text{ kg m}^2 \text{ s}^{-1}$ ) and associated with:

- (a) the “Global Ocean”;
- (b) the Northern Hemisphere - NH;
- (c) the Southern Hemisphere - SH;
- (d) the Antarctic Circumpolar Current - ACC.



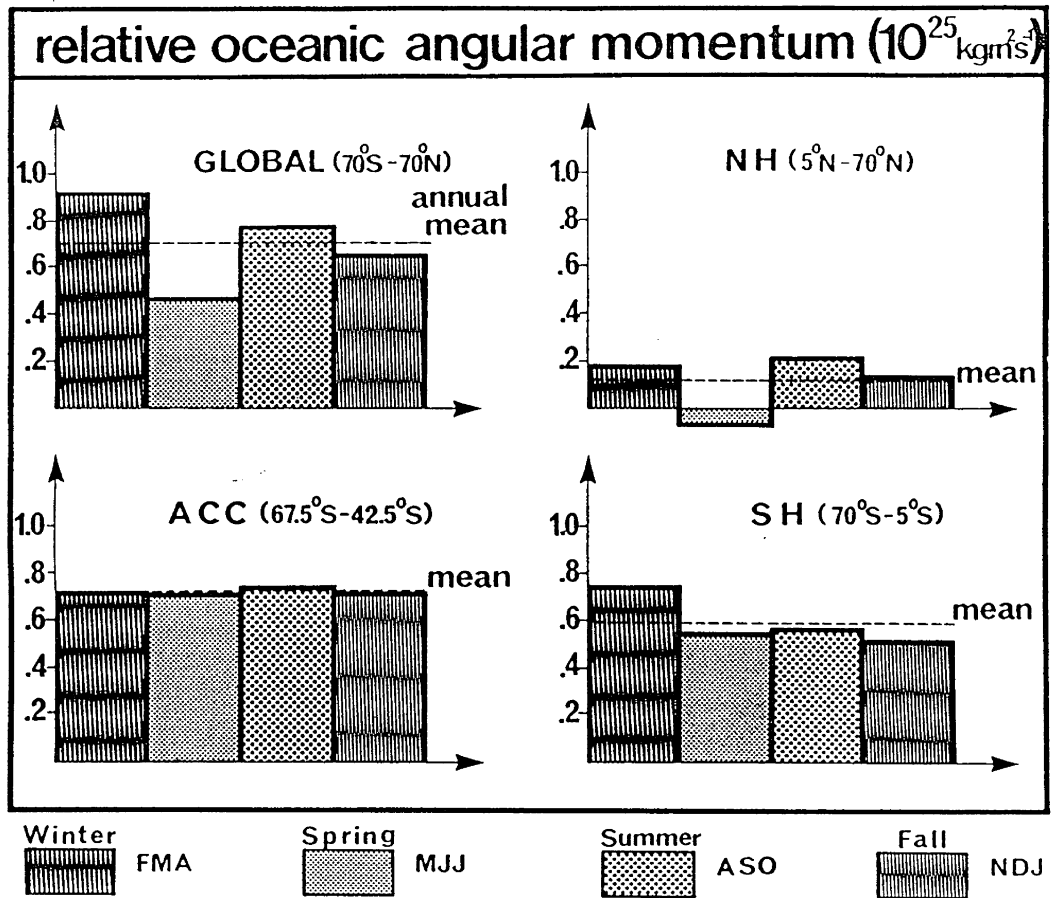


Fig. 7.1. Relative oceanic angular momentum (axial ROAM) budget computed for different integration limits for all seasons and the annual mean, in units of  $10^{25} \text{ kg m}^2 \text{ s}^{-1}$ . The ocean current seasonal fields have been computed from the mean seasonal dynamic topography fields using the geostrophic approximation and the concept of the level of no-motion for the pressure surface at 2000 dbar. The definition of the seasons is also shown at the bottom of the figure, with respect to the northern hemisphere.

The results for the individual latitude distributions (NH, SH, ACC) are easily obtained by varying the latitudinal domain of the integration in eq. (7.9) or, the contributing latitude belts in eq. (7.10) in the discrete case. The integration limits for the individual estimates are also shown on Figure 7.1. We have adopted as the mean ACC axis the latitude of 55°S. The long-term mean axial ROAM annual budget is indicated by a dashed line. Table 7.1 presents in a numerical fashion the axial ROAM estimates obtained from the quasi-permanent ocean circulation.

units $10^{25} \text{ kg m}^2 \text{ s}^{-1}$	GLOBAL	N H	S H	ACC
ANNUAL	0.70	0.11	0.59	0.72
WINTER (FMA)	0.92	0.18	0.74	0.72
SPRING (MJJ)	0.46	-0.08	0.54	0.71
SUMMER (ASO)	0.78	0.21	0.57	0.73
FALL (NDJ)	0.65	0.13	0.51	0.71

**Table 7.1** Axial Relative Oceanic Angular Momentum (ROAM) Results: Long-term mean annual and mean seasonal estimates of axial ROAM determined from the analysis of global relative ocean current velocity fields referenced to the 2000 m depth as the level of no-motion.

The ACC's important role in the overall axial ROAM budget is qualitatively and quantitatively demonstrated in this figure. (compare the Global ROAM budget with the ACC associated one). The ACC is the only “true” zonal oceanic circulation, unimpeded by continental barriers, apart from the narrow constriction at Drake's Passage. The ACC's axial ROAM annual budget estimated in this thesis work, agrees very well with the order of magnitude of ACC associated angular momentum value of  $0.7 \times 10^{25} \text{ kg m}^2 \text{ s}^{-1}$  reported in *Lambeck* [1980, pp. 165] and obtained from order of

magnitude volume transport estimates. Caution, however, is required; the integration of the ocean current u-fields we have computed, has been carried out over the whole ACC latitude band while the estimates reported by Lambeck were obtained from volume transport estimates from Drake's Passage.

It can be easily deduced from Figure 7.1 that the ACC's ROAM budget varies very little between seasons. A detailed discussion about previous work on the ACC's role in LOD variations was presented in Chapter 2, section 2.4.3. Let us put our findings from the in-situ oceanographic data analysis into perspective. The computed ACC long-term mean seasonal ROAM variations are very small and it may even be argued that they are not significant. However, a speculation on the obtained results might be helpful to gain further insight. From Table 7.1 it can be seen that the ACC's maximum ROAM value occurs during the southern hemisphere winter season.

Comparing the findings from the present analyses (Table 7.1) with the findings of the work of *Brosche & Sundermann* [1985], there is a qualitative agreement regarding their statement that extreme westerlies occur in February-March and September -October. These periods correspond well with the NH-definition of the seasons of our ROAM estimates. Larger ROAM values occur in winter (February - March - April) and summer (August - September - October), with the summer estimate being higher than the winter one (see Table 7.1). Therefore, there is some ground to speculate that there is a semi-annual variability, at least in a qualitative way, associated with the ACC's axial ROAM. However, our analysis does not support the numerical results produced by *Brosche & Sundermann* [1985]. Furthermore, a distinction must be made. Most of the ACC associated ROAM estimates from previous studies that have been reported in the

literature (see, for example, *Brosche & Sundermann* [1985]) are based on volume transport estimates derived primarily from oceanographic measurements confined to the relatively narrow Drake Passage. It is in our opinion, somewhat of an oversimplification to assume that from oceanographic measurements at one location (Drake Passage), general inferences about the ACC's behaviour in space and time and its relation to  $\Delta LOD$  can be drawn. Indeed, this is recognized by *Brosche & Sundermann* [1985] in their conclusions too.

A more recent study of the role of the ACC in the earth's angular momentum budget was conducted by *Johns et al.* [1987] using three years of data describing the oceanic flow through the Drake Passage again. They found that the seasonal fluctuations in the angular momentum associated with the ACC are generally too weak. Although their conclusions support the findings of our study, we still maintain that the ACC is a zonal current with substantial latitudinal extent and spatial variation and localized or even regional measurements are not suitable to evaluate the actual ACC's angular momentum budget. It is rather unfortunate that in-situ specific volume data do not exist in abundance for this part of the world ocean, to firmly establish the ACC associated angular momentum seasonal variations.

A few more comments can be made about the results displayed in Figure 7.1. The ROAM budget associated with the SH by far exceeds the ROAM budget of the NH. This is a rather expected fact, since the SH is dominated by oceans and is home to the ACC. The variations in ROAM, however, are more pronounced in the NH budget than in the SH one.

Quantitatively speaking now, a change in axial ROAM of the order of  $0.1 \times 10^{25} \text{ kg m}^2 \text{ s}^{-1}$  produces a  $\Delta LOD$  of the order of 0.02 milliseconds, using equation (7.11). Thus, a seasonal change in the global axial ROAM of the order of  $0.25 \times 10^{25} \text{ kg m}^2 \text{ s}^{-1}$  (for example, winter long-term mean with respect to the long-term annual mean) will produce a  $\Delta LOD$  of the order of 0.05 milliseconds, which is about the expected order of magnitude of the oceanic contribution towards  $\Delta LOD$  (see, for example, *Eubanks et al.* [1985]). Of course, this pre-supposes that there is a direct transfer of oceanic angular momentum to and from the solid earth and atmosphere and that we accept the conservation of angular momentum within the closed ocean - solid earth - atmosphere system.

To summarize, the axial ROAM estimates obtained from the quasi-permanent ocean circulation have been produced from velocity fields referenced to the 2000 m reference level with the assumption that motion “ceases” to exist at this depth. This choice of the 2000 m level, apart from being an arbitrary datum to which to reference velocities, was also a matter of convenience as far as data availability and data processing were concerned. Indeed, the main general ocean circulation patterns are well represented. However, it is also recognized that there exist strong currents in the deep ocean, penetrating deeper than 2000 m. The ACC constitutes a very good example of a deep flow (see, for example, Figure 65 in *Levitus* [1982]). Therefore, the axial ROAM budget may well increase if data and analysis techniques permit better representations of the global ocean current fields.

In conclusion, although the quasi-permanent ocean circulation associated ROAM estimates provided a comprehensive set of numerical values regarding the effect of the

oceans on LOD variations, the fact that the quasi-permanent circulation could only be computed for the four seasons, makes these time series marginally useful.

### 7.3. ROAM Estimates from the Time-Variable Ocean Circulation

In Chapter 6 we saw that the reference geoid model slopes had been combined with the observed sea surface slopes to produce the geoid-dependent sea surface topography slopes. The separation of the ocean current velocity field into mean and fluctuating parts allows the separation of the geoid model slopes from the observed sea surface slopes. As we have already explained in the previous chapter, the 2-year long time-averaged image frame was computed from the 44 image time-frames using repeated ocean current velocity estimates over at least 40 time-frames. Differences between individual image time-frames and the time-averaged image over the 44 repeat cycles that we have analysed express then the time dependent behaviour of the ocean circulation with respect to the mean for the two year period from Nov. 86 to Nov. 88. Hence, we have generated a stack of 44 images of the  $u^*$ -field from the GEOSAT altimetry, where time is the dimension along which the images have been stacked. From those  $u^*$ -fields we have generated a series of  $[u^*]$ -fields which were displayed in Figures 6.6, 6.7 and Appendix I.

These computed  $[u^*]$ -fields have been integrated using the same formulation presented in section 7.1. It is clear that by integrating the altimetry generated  $[u^*]$ -fields, we are directly computing the fluctuations of the axial relative oceanic angular momentum, namely the axial  $\Delta ROAM$ . Hence, we have a direct estimate of the time variations of

ROAM with respect to the 2-year mean, which in turn can be directly related to  $\Delta LOD$  through eq. (7.11).

Some important computational details should be mentioned at this point. The latitudinal integration domain was between  $65^{\circ}S$  and  $65^{\circ}N$  latitude. The reason for this stems from the early stages of the GEOSAT altimetry data pre-processing. During the data editing stages of the GEOSAT records, altimetry observations of SSH were eliminated right at the beginning if they were beyond latitude 65 degrees north or south. This “quality control” procedure potentially removed all the data records obtained over sea ice conditions found in higher latitudes.

The most important computational detail relates to the integration carried out along the radial coordinate, i.e., the thickness of the oceanic layer. The results of  $\Delta ROAM$  were computed using an one-sided integration. To explain: from satellite altimetry, we have computed the surface expression of the time variable ocean circulation. In order to compute ROAM values from ocean current fields we need to know not only the surface flow but a depth integrated flow. Under these circumstances, a numerical ocean model is needed to transfer dynamically the satellite altimetry derived surface flow into sub-surface current information. Although such an analysis tool can be said that is visible in the horizon today (in the form of global, eddy-resolving ocean models) it is not yet readily available for routine practical computations such as those needed in the present study. Therefore, we must add an assumption about how the zonal current flow changes with depth to render useful the computations we have carried out so far for the next step of ROAM estimation.

The time variations of the sea surface slopes we have computed from the GEOSAT altimetry should reflect to a large extent changes in circulation occurring in the whole ocean water column. Since it is customary in physical oceanography to subdivide the water masses that constitute the vertical structure of the ocean into:

- surface waters (depths from 0 to an average of 250 m);
- intermediate waters (with a lower depth boundary at depths between 1000 and 2000 m);
- deep waters (with a lower boundary at about 4000 m);
- bottom waters,

and since seasonal temperature variations are usually detected from the surface down to 200 to 300 m depths (i. e., seasonal thermocline), we believe that it is a reasonable subjective assumption to associate the observed surface ocean current variability with an oceanic layer of approximate thickness of 250 m. Hence, a global oceanic layer of uniform thickness of 250 m is chosen as the layer for which there is an one-to-one correspondence between the variations in surface zonal geostrophic flow and depth integrated zonal flow (i.e., zonal transport equals thickness of layer times surface zonal geostrophic velocity).

The impact of making this assumption is that the ROAM estimates will mirror the space and time changes of the computed zonal ocean current variability, but the absolute values will admittedly be uncertain to within an unknown scale factor. We believe that this assumption likely does not overestimate  $\Delta ROAM$  simply because any zonal transport below the surface layer (from 250 m to the bottom of the ocean) is totally ignored. Hence, the  $\Delta ROAM$  function was computed by choosing  $i=1$  in equation (7.10) and  $\Delta r_1 = 250m$  .



Nevertheless, as we said before, the proper way to transfer surface information into subsurface one is through the assimilation of observed data into numerical circulation models (briefly discussed in Chapter 3). Until such techniques become readily available for global analyses, the difficulty to relate synoptic surface variability to subsurface ocean dynamics and therefore properly scaled  $\Delta ROAM$  values will still be present.

#### 7.4. The ROAM Time Series

The  $\Delta ROAM$  time series consists of 44 points along the time axis, each point representing a 17-day average value of the  $\Delta ROAM$  function. The  $\Delta ROAM$  values computed here are essentially the integral over latitude of the  $[u^*]$ -fields scaled by the oceanic layer thickness  $\Delta r$ . Therefore, the discussion pertaining to the  $[u^*]$ -field time series is relevant for the  $\Delta ROAM$  time series. However, there are several issues to discuss from a different perspective by inspecting the  $\Delta ROAM$  time series plots.

Figure 7.2a displays the *global*  $\Delta ROAM$  time series. The equatorial zone between  $4^{\circ}S$  and  $4^{\circ}N$  latitude has been excluded from the computations (recall that the geostrophic relation breaks down at the equator and that geostrophic currents attain unreasonably large values very near the equator). Figures 7.2c and 7.2d display the  $\Delta ROAM$  time series associated with the Northern Hemisphere ( $4^{\circ}N$  to  $65^{\circ}N$ ) and Southern Hemisphere ( $4^{\circ}S$  to  $65^{\circ}S$ ), respectively. Figures 7.2e and 7.2f display the  $\Delta ROAM$  time series associated with the northern and southern hemisphere tropical belts ( $4^{\circ}S$  to  $23^{\circ}S$  and  $4^{\circ}N$  to  $23^{\circ}N$ ), respectively). Figure 7.2g displays the  $\Delta ROAM$  time series associated with the ACC ( $45^{\circ}S$  to  $65^{\circ}S$  latitude belt).

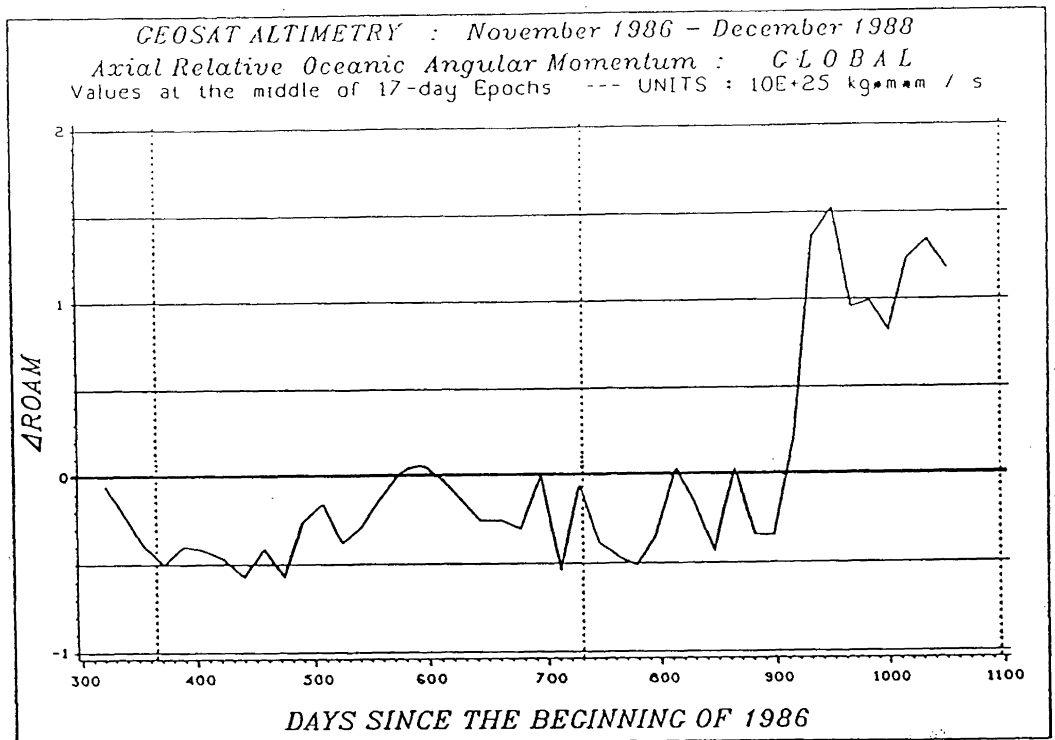


Fig. 7.2a.

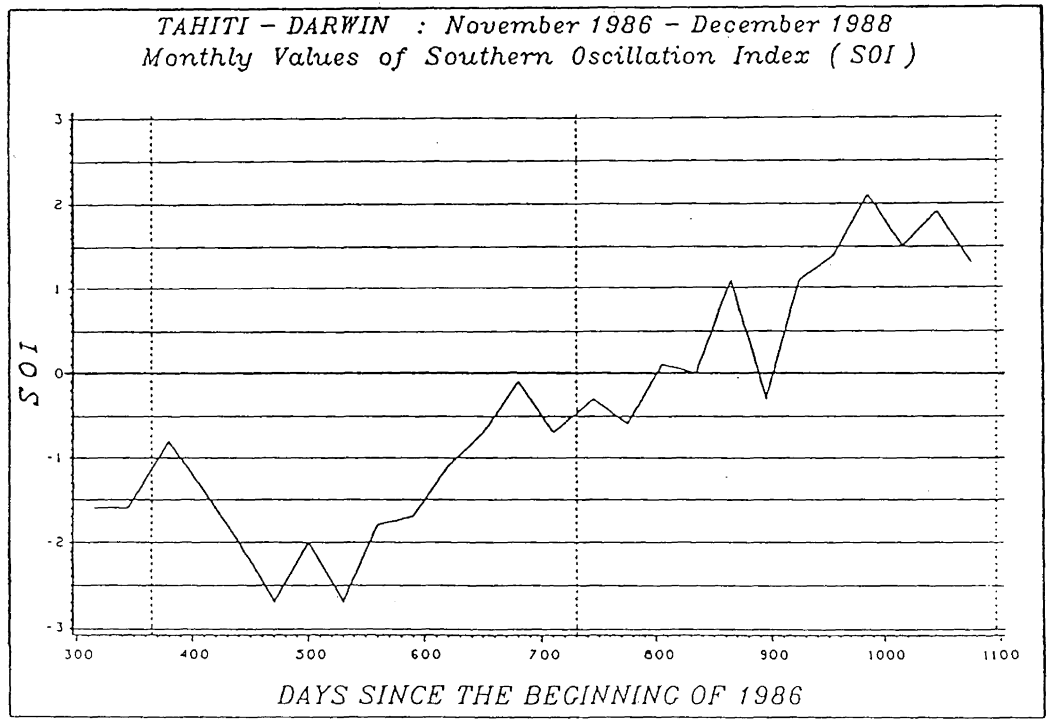


Fig. 7.2b

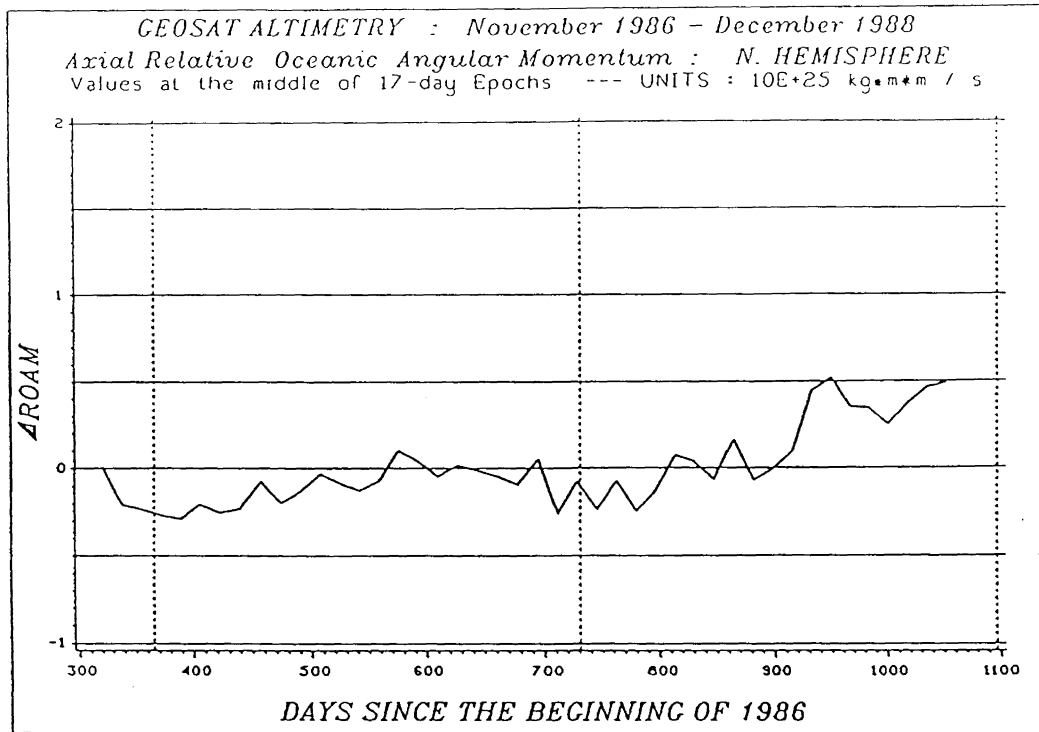


Fig. 7.2c.

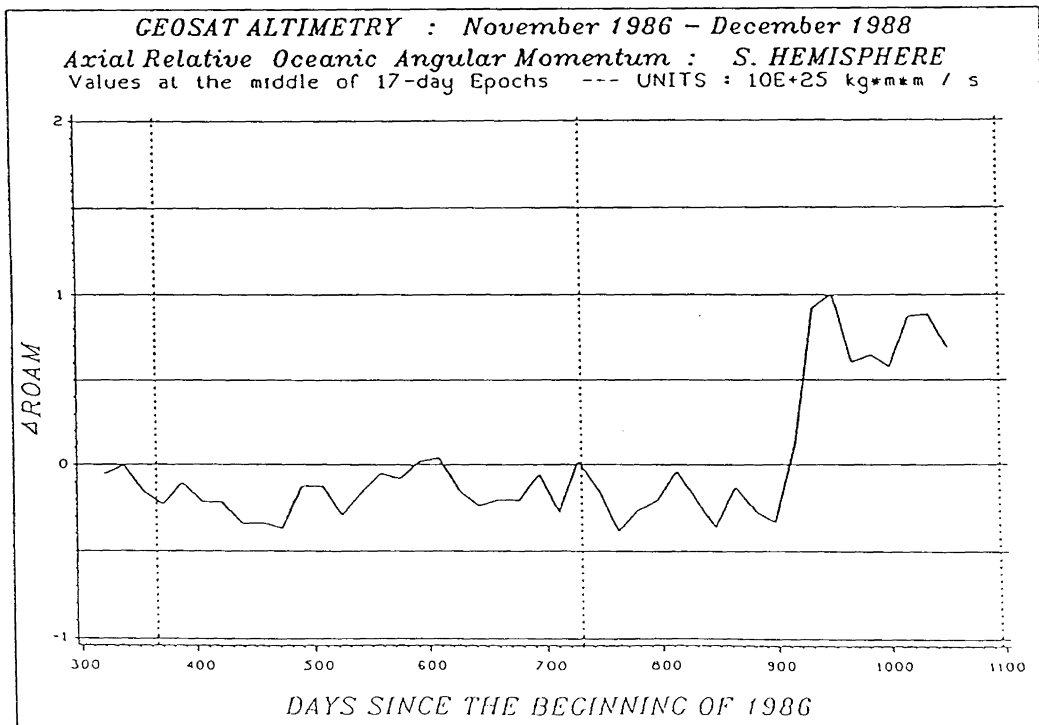


Fig. 7.2d

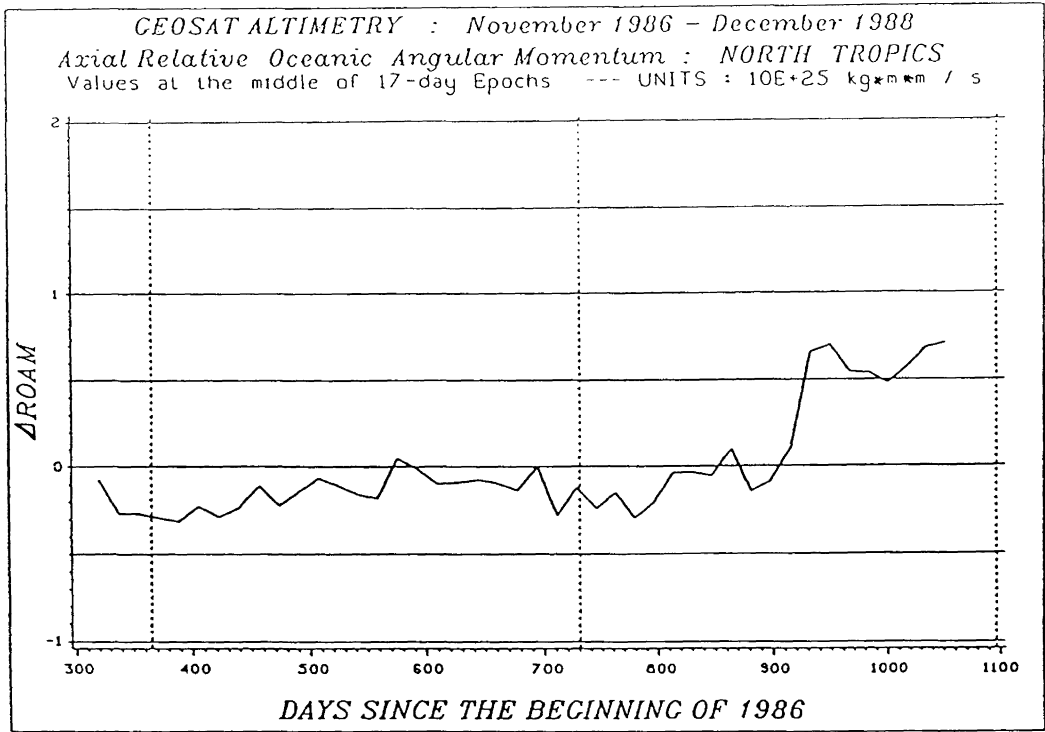


Fig. 7.2e.

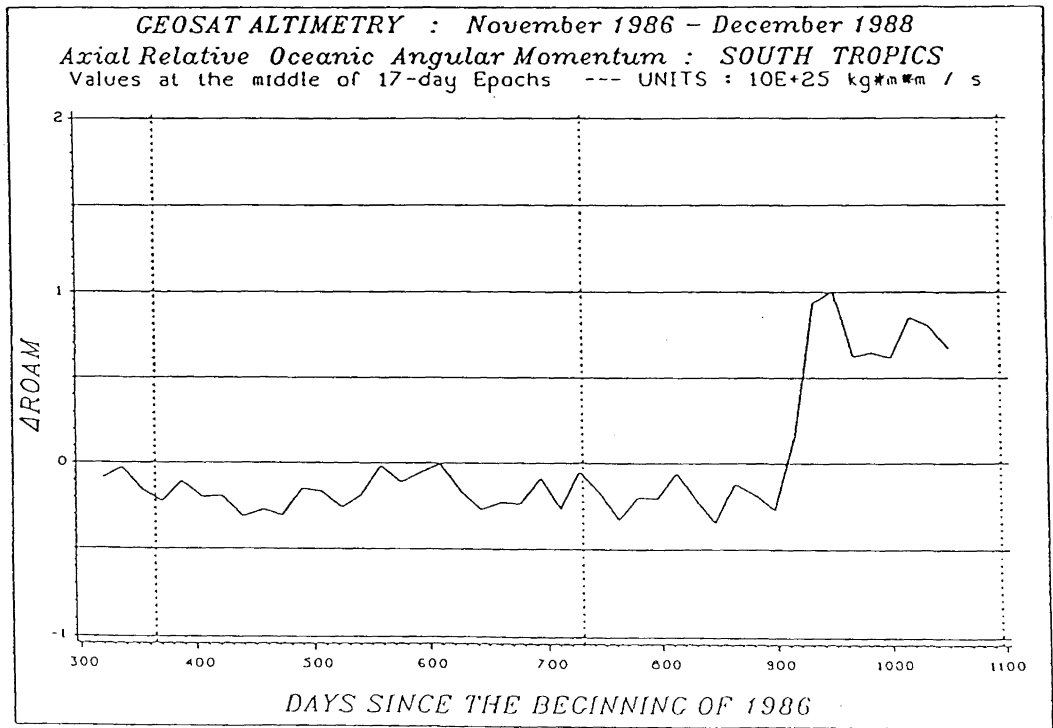


Fig. 7.2f

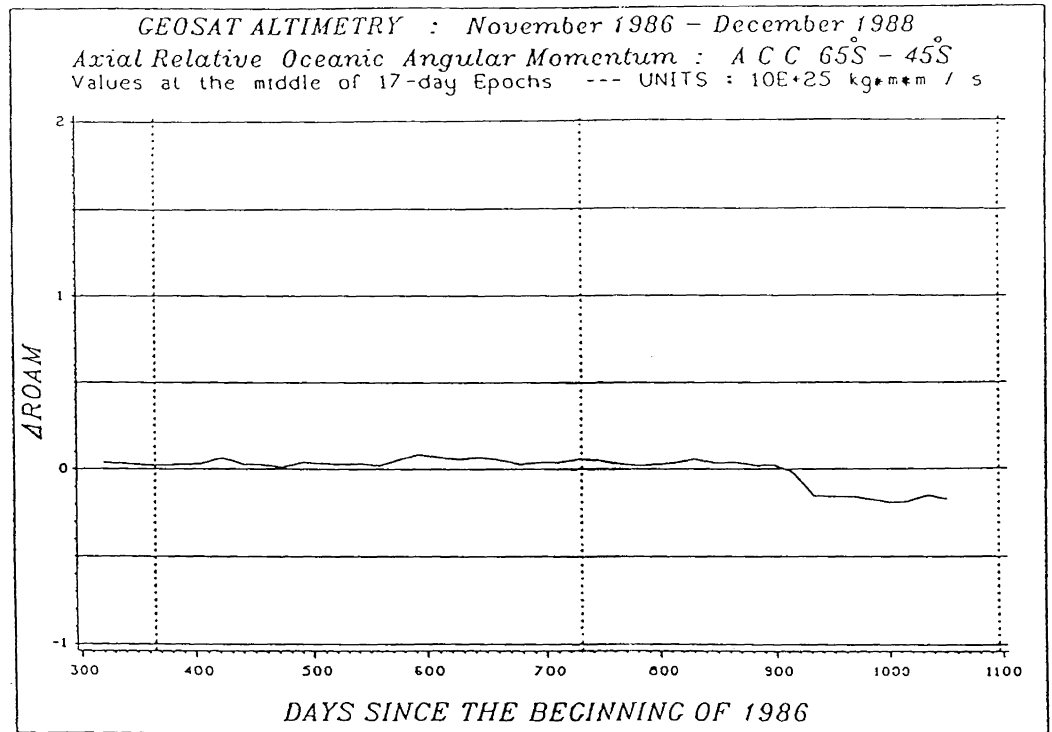


Fig. 7.2g.

We will examine first the global  $\Delta ROAM$  time series. The first observation to be made is that the range of the  $\Delta ROAM$  values is of the order of  $0.5 \times 10^{25} \text{ kg m}^2 \text{ s}^{-1}$ , except for the period after day-915 (see Figure 7.2a and remember that day-0 is January 1, 1986). A radical increase in ROAM occurred suddenly around day-915 (corresponding to the 17-day period from June 25 to July 11, 1988), and persists thereafter. We have already seen this change in the behaviour of the  $[u^*]$ -fields examined in Chapter 6. It is a rather puzzling behaviour. Close examination of the  $\Delta ROAM$  time series by latitude belts (Figures 7.2c, 7.2d, 7.2e, and 7.2f) reveals that this sudden influx in eastward ROAM is predominantly associated with the southern latitudes, and more particularly with the southern tropics, which dominate the change in magnitude. While the low latitude regions show an increase (eastward flux of ROAM), the southern high latitude regions associated with the ACC show a decrease (loss of ROAM), but less pronounced. The net effect is still a large increase in ROAM relative to the 2-year mean.

In Chapter 6 we have compared the unusual  $[u^*]$ -field behaviour with the Tahiti - Darwin SOI, in an attempt to link this behaviour with other oceanic parameters. In this section we will try to discuss the  $\Delta ROAM$  behaviour in the context of these SOI observations. Figure 7.2b displays the monthly SOI time series for the same time span the  $\Delta ROAM$  has been computed. The SOI time series show that there is transition from negative values to positive values during the spring of 1988, followed by a rapid increase of positive values about the beginning of July of 1988. Closer inspection of the latitude belt break-down of the  $\Delta ROAM$  time series reveals that the global ROAM budget during that period is dominated by the SH contribution, i.e., a much stronger change occurs in the SH than in the NH. Further latitude break-down shows that the extreme changes both hemispheres originate from the tropical latitude belts, the

southern tropics dominating not only the SH estimates but also exceeding the northern tropics estimates by almost 50%. This visual inspection suggests that the computed ocean current variability may not be totally unrelated to the behaviour displayed by the SOI values. Formal correlation studies are planned in future work. The question is, are the ROAM fluctuations reflecting a realistic event-like month-long strong burst or should they be dismissed immediately? We believe it is too early to accept or dismiss any hypothesis. Confirmation should come from other data and additional evidence must be collected before any affirmative answer is given. However, it is an extremely interesting and puzzling event, worth pursuing further in future research.

As we have discussed in section 7.2, a change in the ROAM of  $0.1 \times 10^{25} \text{ kg m}^2 \text{ s}^{-1}$  is equivalent to a change of approximately 0.02 milliseconds in the length-of-day. From Figure 7.2a it is obvious that apart from the event-like fluctuations around days 915-932 there are fluctuations in ROAM of the order of  $0.5 \times 10^{25} \text{ kg m}^2 \text{ s}^{-1}$  occurring over time intervals ranging from 17 days to 2-3 months. These ROAM variations are capable of producing LOD changes of the order of 0.1 milliseconds over these time intervals and they are simply too large to ignore. It is thus shown numerically for the first time that the ocean current contributions to  $\Delta LOD$  are not small and are certainly above the threshold of observability with today's LOD observational capabilities. The fact that the atmospheric excitation of LOD variations is by far the most dominant source (apart from the tidal influences), does not imply that the oceanic contributions should be neglected. As ocean circulation related information increases day by day we believe that more detailed investigation of the role of the oceans towards the angular momentum balance of the whole earth system is warranted. Moreover, the ocean/atmosphere coupling is being studied more deeply today and the "solid earth -

atmosphere” closed system must be replaced by the “ocean - solid earth - atmosphere” one.

In conclusion, we have produced the first realistic  $\Delta ROAM$  time series using direct observations of ocean current variability. However, the  $\Delta ROAM$  time series we have just presented are not the ultimate ones. We consider them as test series for proof-of-concept analyses. They can be considerably improved as we shall see in a later chapter. The point remains: there is enough oceanic signal to be analysed for  $\Delta LOD$  studies. This is exactly the subject of the next chapter, where we investigate the computed  $\Delta ROAM$  time series in the context of associated changes in the length-of-day.



## Chapter 8: The ROAM, RAAM, and LOD Time Series

So far the major effort in this research has been the generation of axial relative oceanic angular momentum (ROAM) time series. We have succeeded in generating a 2-year long  $\Delta ROAM$  time series from the GEOSAT/ERM altimetric data.

Once such a time series is obtained, the natural progression is to try to put it in the context of LOD associated variations. For this reason, we have obtained observed  $\Delta LOD$  time series and axial relative atmospheric angular momentum (RAAM) time series, generated by the variable wind. Both of these time series overlap with the November 1986 - November 1988 time period for which we have  $\Delta ROAM$  estimates. This is the first time, to our knowledge, that a concurrent set of observed time series from all three earth system components (ocean - solid earth - atmosphere) has been established and investigated. Thus, in this chapter, we will try to establish some initial relations between the solid earth's LOD fluctuations as observed by geodetic extra-terrestrial techniques (VLBI), the  $\Delta RAAM$  as estimated from operational weather forecasting wind analyses (NMC), and the  $\Delta ROAM$  as calculated in this thesis work. Of course, the ocean - solid earth - atmosphere will be considered as a closed system, i.e.,

changes in axial angular momentum, say in the solid earth component, must be balanced by opposite changes of the atmospheric and/or oceanic component. In simpler words, intercomparison studies will be carried out between the three time series data sets with the goal of establishing a connection between all three earth system components.

There is a reserved tone in the statement made above. As we have already stressed, the altimetry generated  $\Delta ROAM$  time series is not the ultimate time series one can get. It is only a beginning, an exploratory step, in creating directly observed ocean current variability and ROAM estimates. There is plenty of room for improvements, both with regard to the altimetry data processing and the conversion of the surface ocean current variability into subsurface information. Although this is going to be the subject of future research, the estimated  $\Delta ROAM_{86-88}$  time series, as it stands, serves the purpose of a test-bed time series.

## 8.1. The LOD Time Series

We have obtained  $\Delta LOD$  data in the form of daily values at 0:00 UT, spanning the period April 2, 1985 through December 31, 1988, from Atmospheric and Environmental Research, Inc., Cambridge, MA, [Rosen & Salstein, *personal communication*, 1989]. The  $\Delta LOD$  values represent the excess length-of-day from 86400 seconds. This  $\Delta LOD$  data set is based on daily intensive VLBI observations published by the IRIS [Robertson *et al.*, 1985] subcommission of the CSTG. The data set is described in detail by Rosen *et al.*, [1989]. All solid body tidal terms with periods up through 18.6 years

have been removed from the received time series according to the *Yoder et al.* [1981] model.

The data from the period between November 1986 and December 1988 was extracted from the received data series for use in the analyses performed in this thesis research. This subset time series is displayed in Figures 8.1. Figure 8.1a represents the original  $\Delta LOD$  time series while Figure 8.1b represents the same time series after the removal of the 2-year long mean value of 1.488322 milliseconds. The range of the LOD variations seen in Figure 8.1b, is of the order of  $\pm 1ms$ . The variations demonstrate the complex character of the solid earth's rotation rate. By just looking at Figures 8.1a and 8.1b we can clearly see that there are annual, semi-annual and higher frequency signals in the data series. Frequency analysis of these time series will be reported in a subsequent section.

## 8.2. The RAAM-Wind Time Series

We have also obtained two data sets representing estimates of the axial component of the atmosphere's relative angular momentum, computed from the time varying wind fields, again from Atmospheric Environmental Research, Inc., Cambridge, MA, [Rosen & Salstein, *personal communication*, 1989]. The two RAAM-wind data sets refer to the 100 mbar and 50 mbar atmospheric height. We will designate them from now on by RAAMW100 and RAAMW050, respectively. The RAAM values are nominally available up to twice daily, at 0:00 and 12:00 UT, and they span the period between December 30, 1985 through December 31, 1988. We have selected to work here with only the 0:00 UT values. A clarification is also useful at this point.

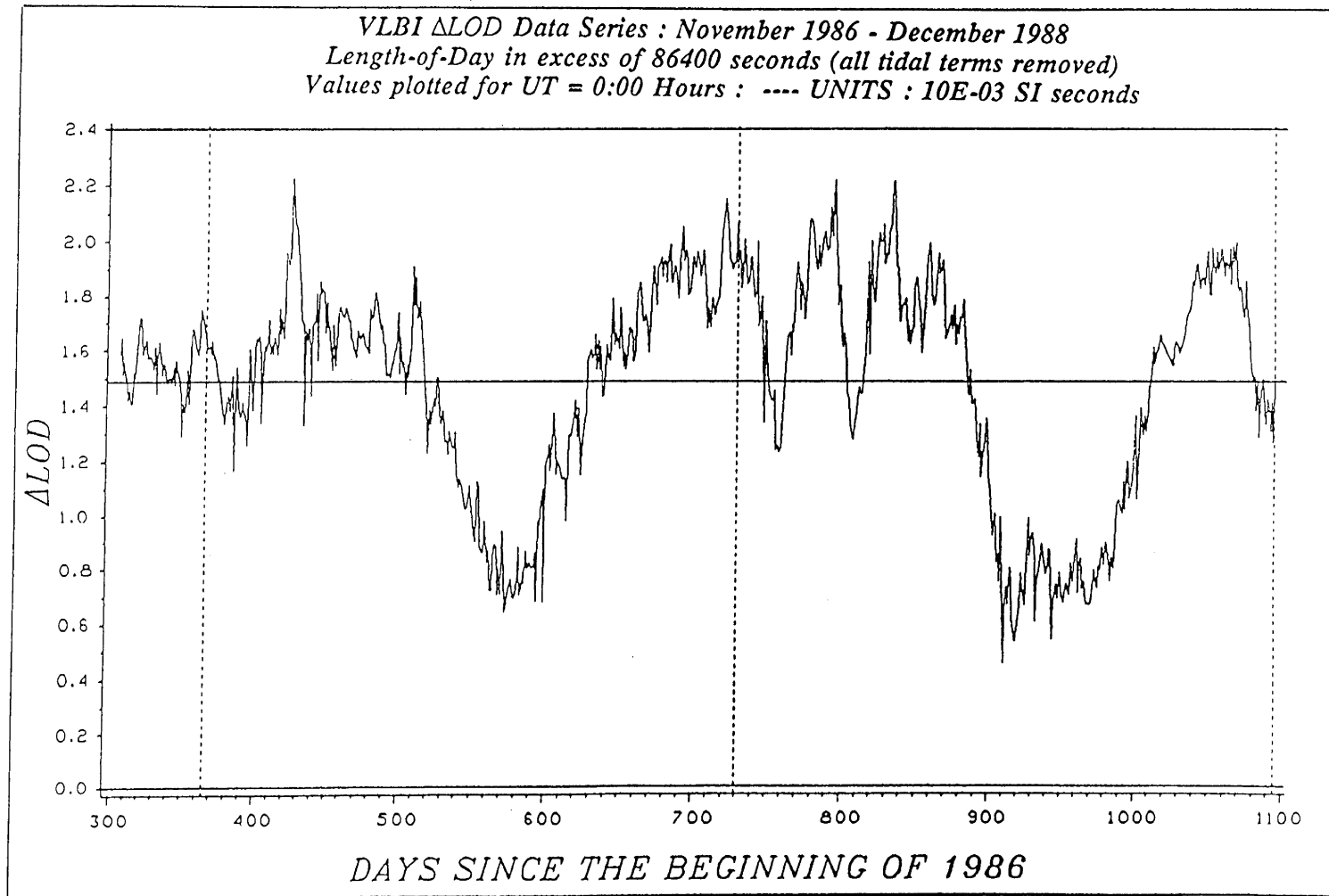


Fig. 8.1a

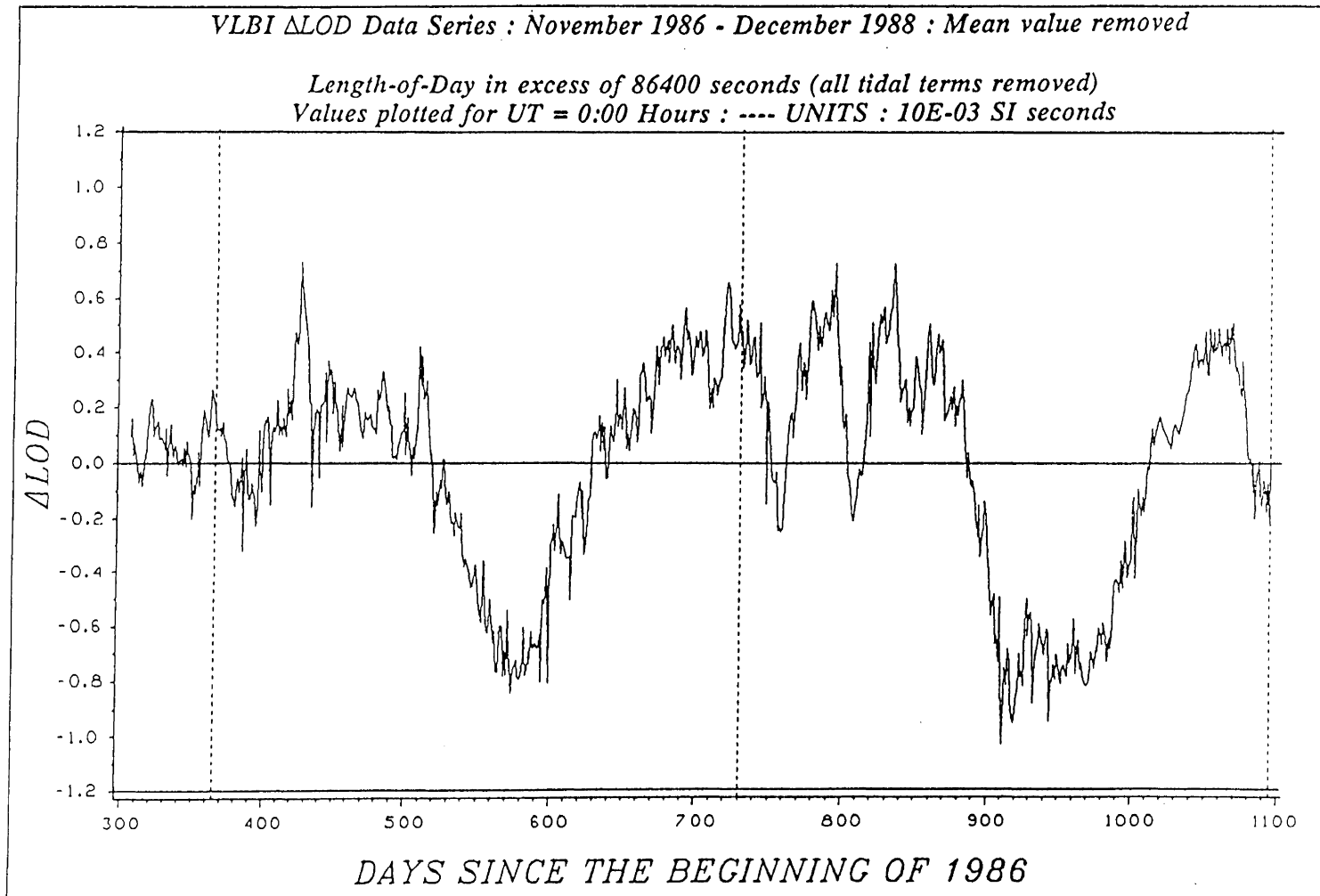


Fig. 8.1b

The AAM series we received pertain only to the wind term (i. e., to the  $m_3^{\text{motion}}$  term in equation 2.22). The pressure term related data series (i. e., the  $m_3^{\text{matter}}$  term in equation 2.22) were not available to us at that time.

The RAAM values have been computed by integrating the zonal wind fields from 1000 mbar to 100 mbar, and from 1000 mbar to 50 mbar, respectively. The received data records contain RAAM values for the NH, SH, and global integrals. It is worthwhile pointing out that these RAAM values are based on the reduction and analysis of meteorological data for weather forecasting performed at the U.S. National Meteorological Center (NMC). A variety of atmospheric variables, including the local wind vector, are estimated at each grid point of a 3-dimensional numerical forecast model. The grid point data values are updated several times daily by using a so-called forecast/assimilation technique, i.e., a sort of weighted average of the forecast field from the previous model update, and any new (observed) meteorological data. The axial RAAM is one component of the total relative angular momentum vector, estimated at 12 -hour (and/or 24-hour) intervals from the appropriate integral of the grid point wind velocity estimates of the current model update.

Data from the period between November 1986 and December 1988 has been extracted from the received NMC operational RAAM data series to be used in this thesis work. The subset axial RAAM data series are displayed in Figures 8.2. The global axial RAAMW100, together with the individual hemispheric (NH, SH) contributions are displayed in Figure 8.2a, while the RAAMW050 global, NH, and SH series are displayed in Figure 8.2b. The inclusion of the lower stratospheric winds (100 mbar to 50 mbar atmospheric height) apparently causes only an increase in the magnitude of the

RAAM budget. It does not seem that it produces any new signatures in the RAAM series. This is shown in Figure 8.2c where we have plotted the differences between the RAAMW050 and RAAMW100 global, NH, and SH values.

It is immediately obvious from Figures 8.2a and 8.2b, that major changes in the two hemispheres are 180 degrees out of phase with each other, i.e., maxima in the NH are associated with minima in the SH and vice versa. The same comment applies for the lower stratospheric RAAM contributions (see Figure 8.2c). It is also noted that the SH experiences half the range of the NH variations. There is immediate visual correlation between the  $\Delta LOD$  time series and the global RAAM time series, as has been repeatedly discussed in the literature. Strong annual and semi-annual periodicities are clearly seen in all three RAAM time series plots (Figures 8.2a, 8.2b, and 8.2c). Especially noticeable is the strong semi-annual signal in the lower stratosphere RAAM data series (Figure 8.2c). Of course, all three time series display characteristics of higher frequency signals. The 2-year long mean was also removed from the RAAM time series and the resulting series have been labelled the  $\Delta RAAM$  series (i. e., the variations in the RAAM with respect to the 2-year long data span).

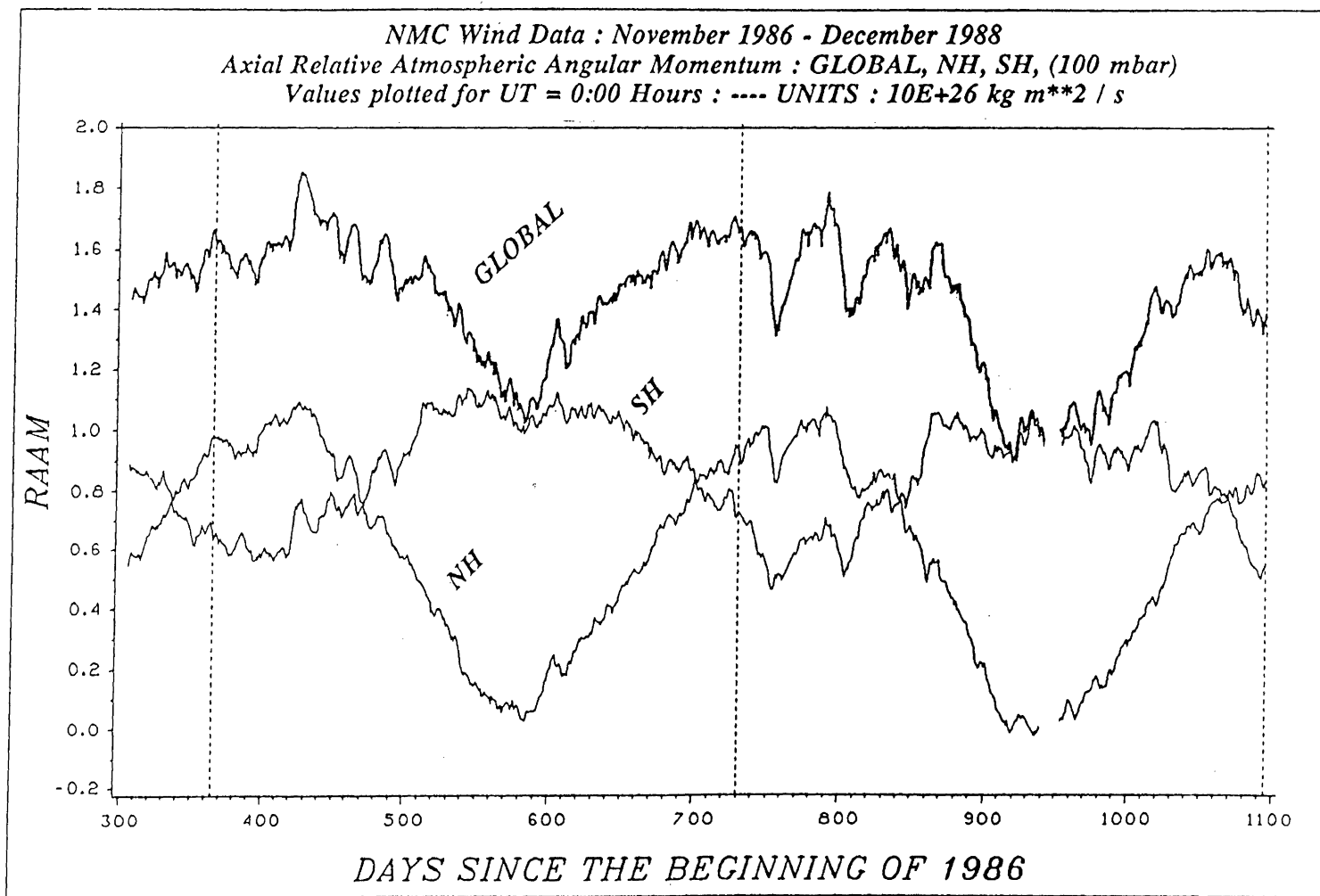


Fig. 8.2a



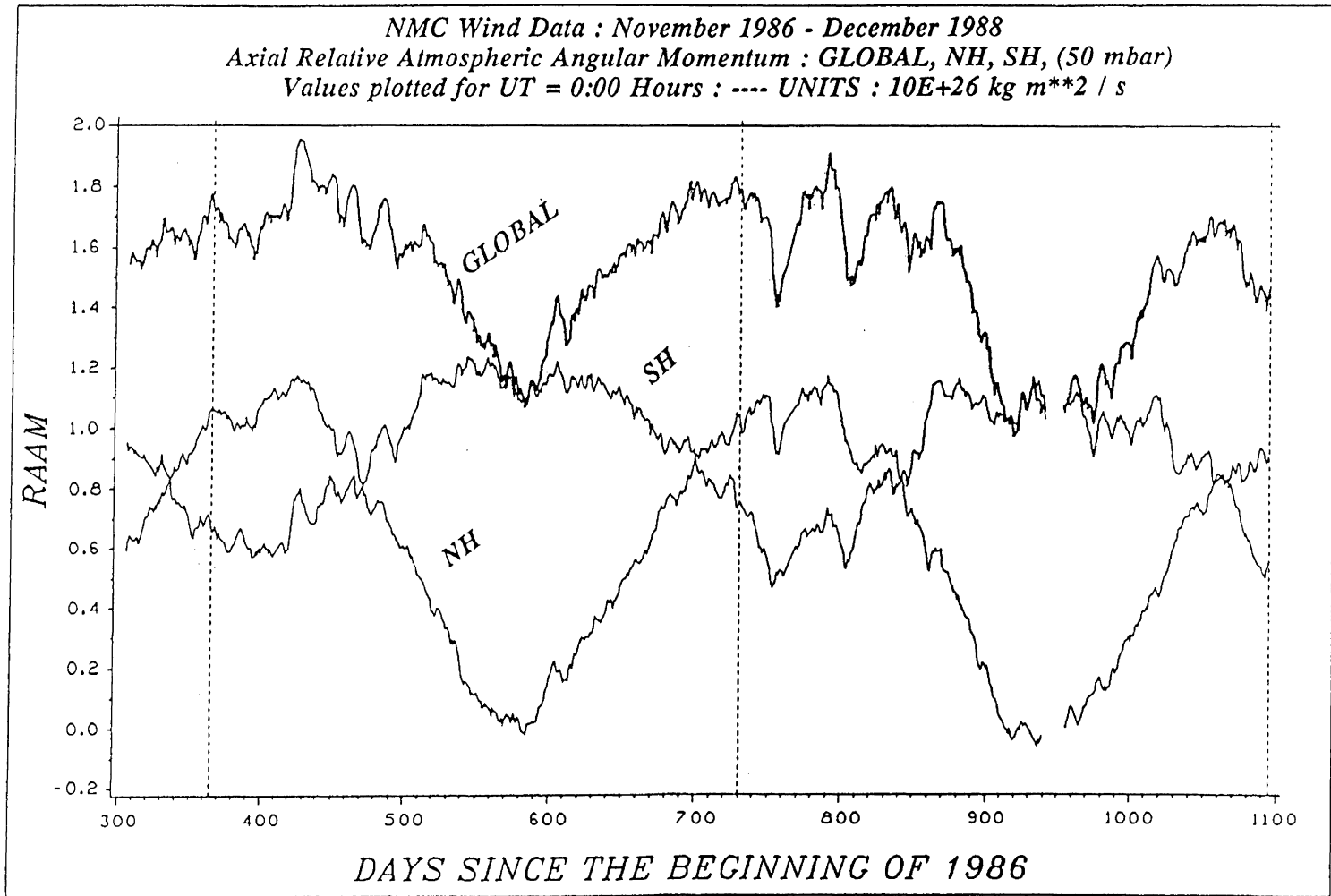


Fig. 8.2b

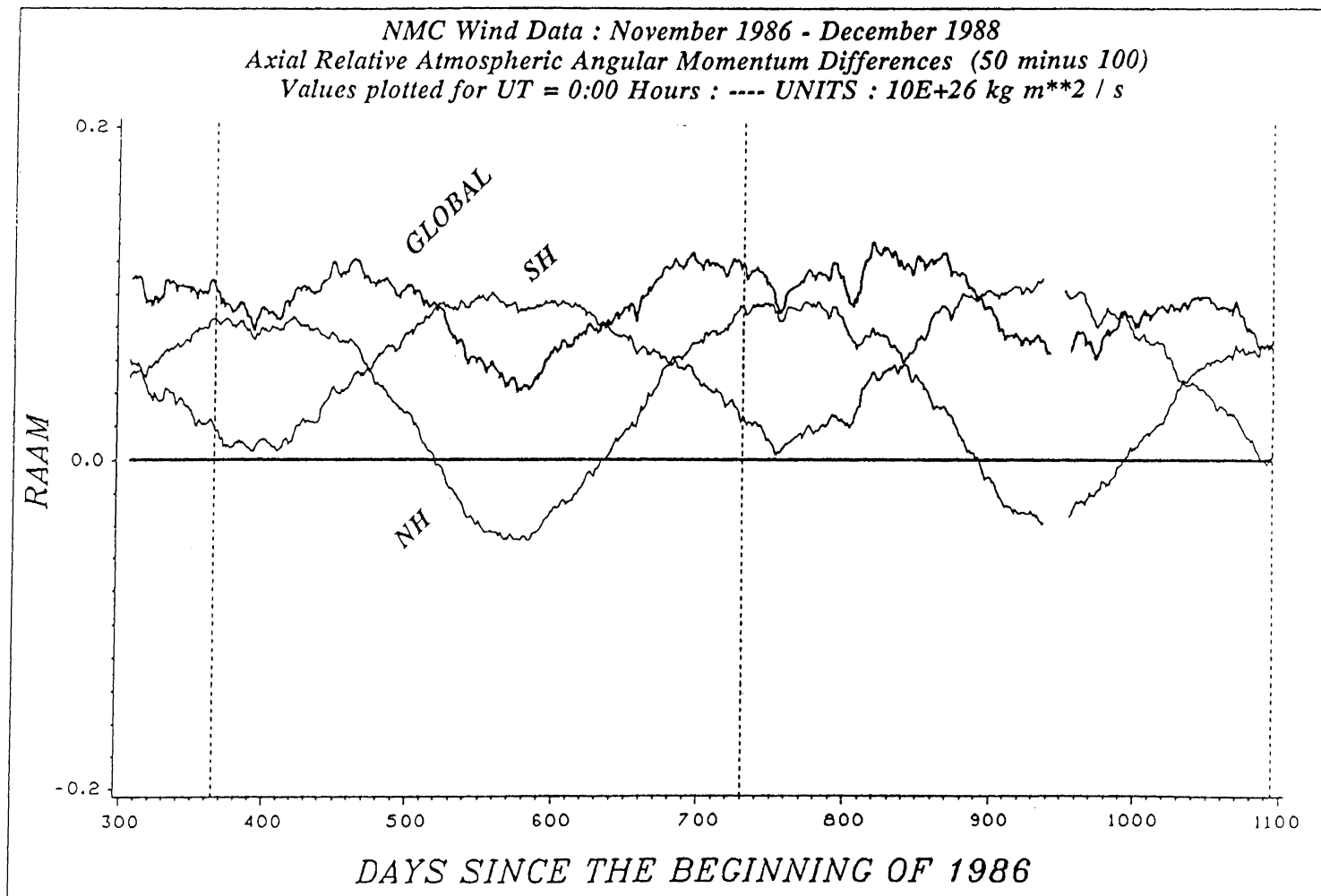


Fig. 8.2c

### 8.3. Comparison Between Observed LOD Fluctuations and Inferred Ones from the RAAM and ROAM Time Series

We have carried out a series of comparative studies between the observed  $\Delta LOD$ , the axial  $\Delta RAAM$  data set and the axial  $\Delta ROAM$  data series constructed from satellite altimetry. As we said earlier only the 0:00 UT values of the atmospheric series were used here. The comparisons between the data series reported here have been carried out in the frequency domain and are presented in the subsequent subsection. For the comparisons performed, we have computed for both the  $\Delta RAAM$  and  $\Delta ROAM$  time series, the equivalent  $\Delta LOD$  data series using the formulation of eq. (7.11) under the assumptions that the ocean - solid earth - atmosphere is a closed system, and that only the earth's crust and mantle are involved in LOD changes. We have labelled these time series RAAM-inferred and ROAM-inferred  $\Delta LOD$ . Figures 8.3a, 8.3b, and 8.3c display the equivalent  $\Delta LOD$  from  $\Delta RAAMW050$ ,  $\Delta RAAMW100$ , and  $\Delta ROAM$ , respectively. It is noted here that both the length-of-day and atmospheric time series consist of daily values at 0:00 UT, while the oceanic time series consist of 17-day average values. Figure 8.3d displays the equivalent  $\Delta LOD$  of the difference,  $\Delta RAAMW050$  minus  $\Delta RAAMW100$ , while Figure 8.3e is a blow-up of Figure 8.3d. Figures 8.3a, 8.3b, 8.3c, and 8.3d are all plotted with the same scale for quick reference of relative magnitudes. Figure 8.3f is a superposition plot of the ROAM-inferred  $\Delta LOD$  and the contribution of the lower stratosphere between 100 and 50 mbar. Finally, Figures 8.3g and 8.3h display the residual  $\Delta LOD$  between the observed and the atmospheric-inferred  $\Delta LOD$  for the two atmospheric data series available. Superimposed are the ROAM-inferred  $\Delta LOD$  and the 17-day running mean of the residual  $\Delta LOD$ .

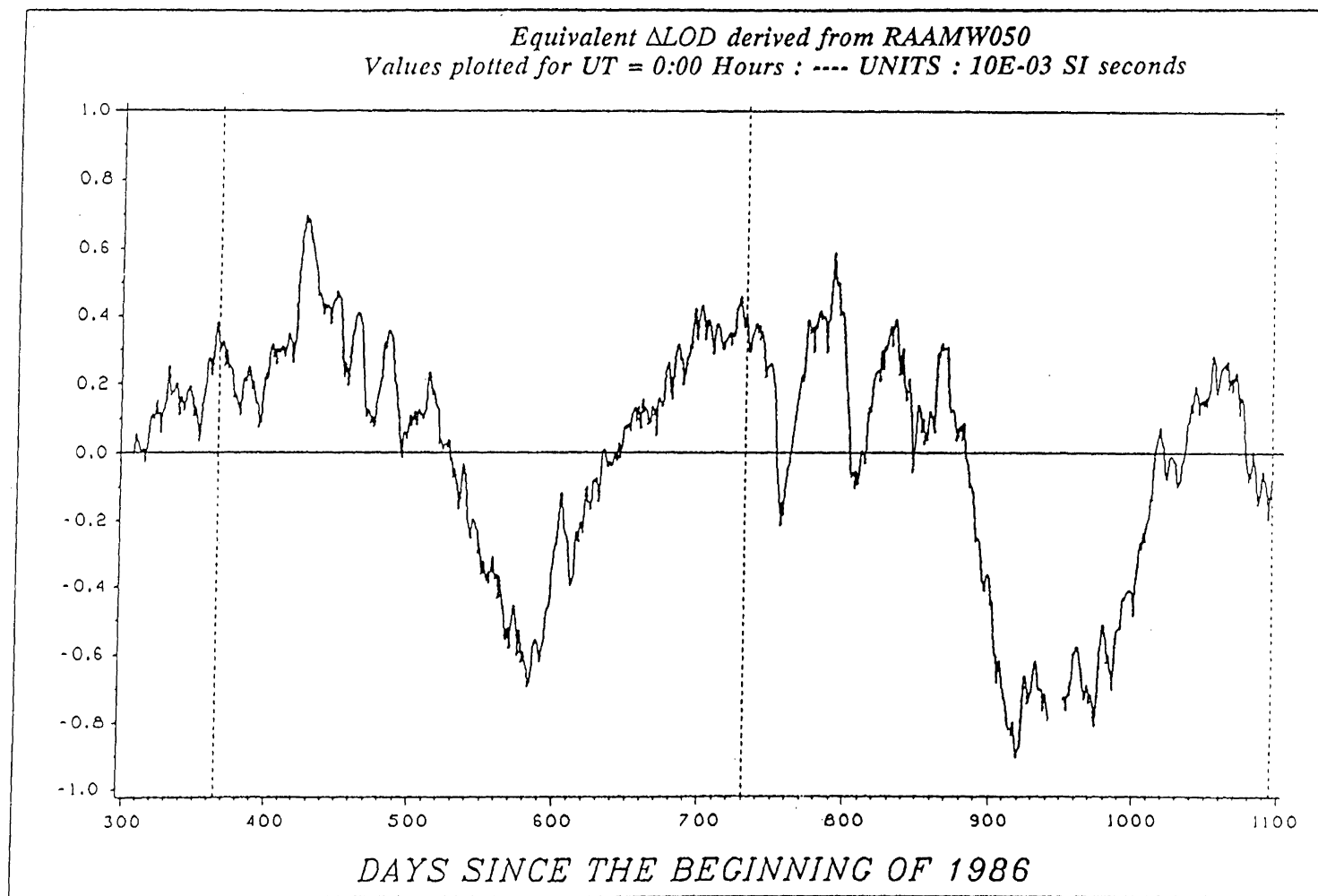


Fig. 8.3a

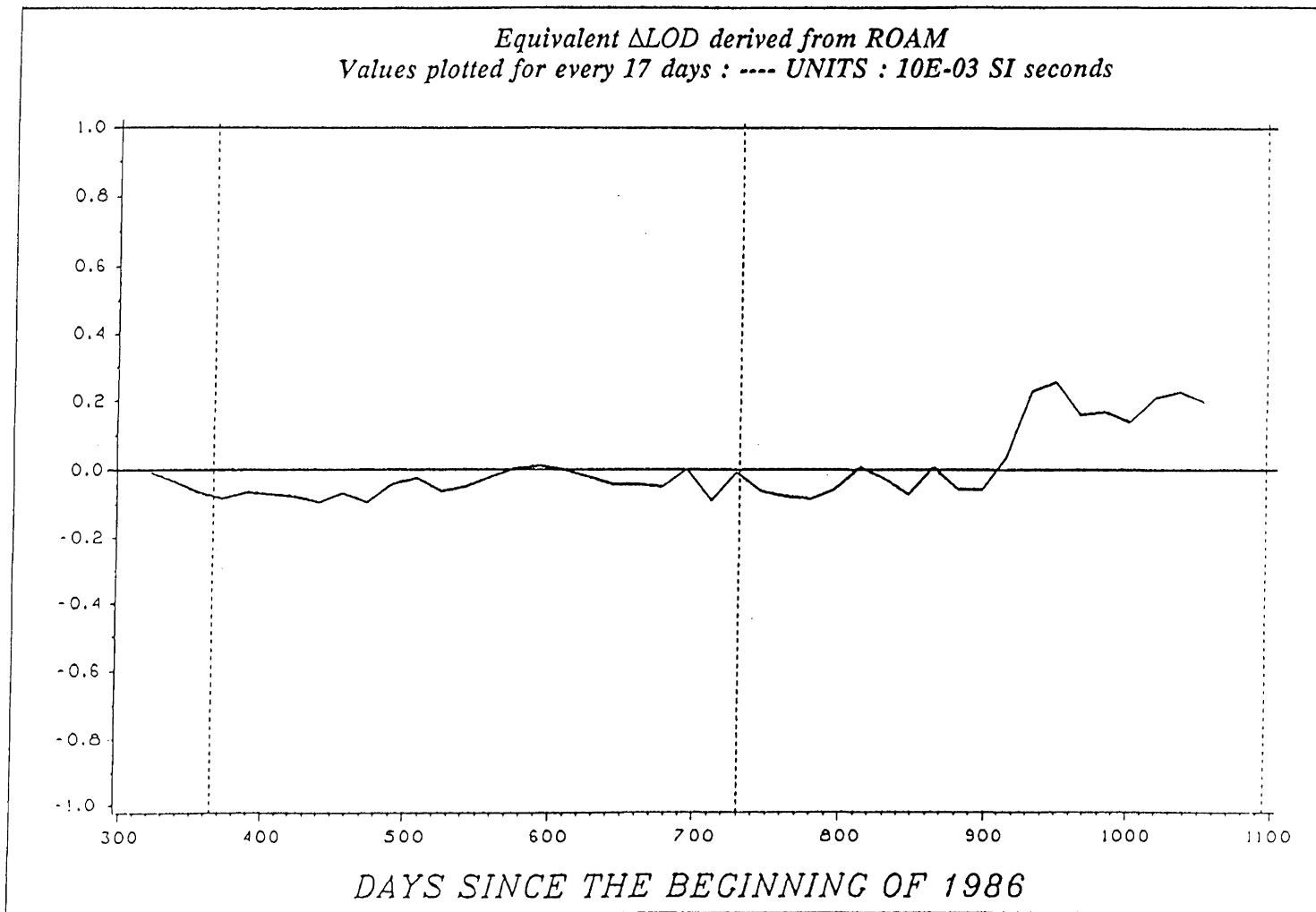


Fig. 8.3c

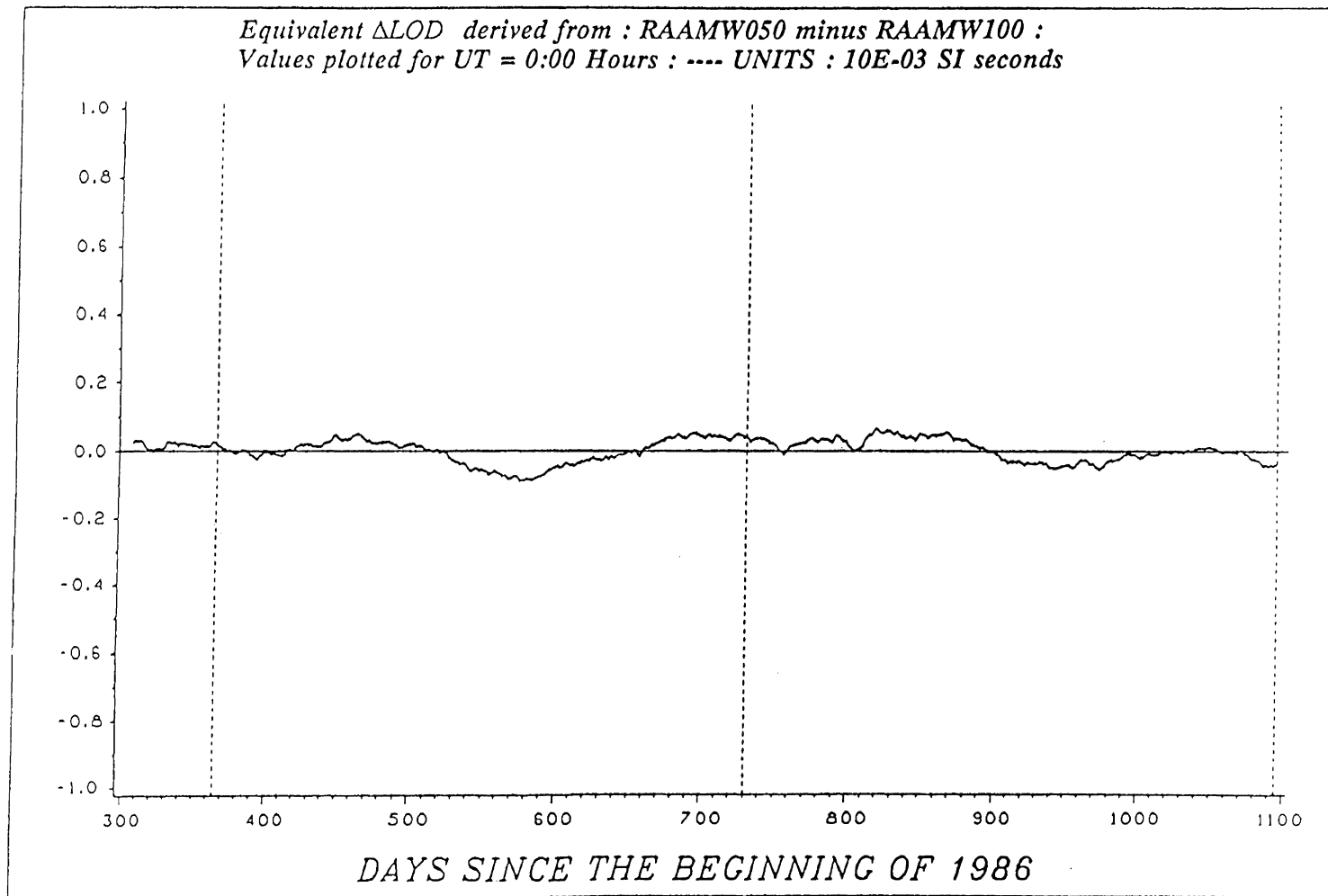


Fig. 8.3d

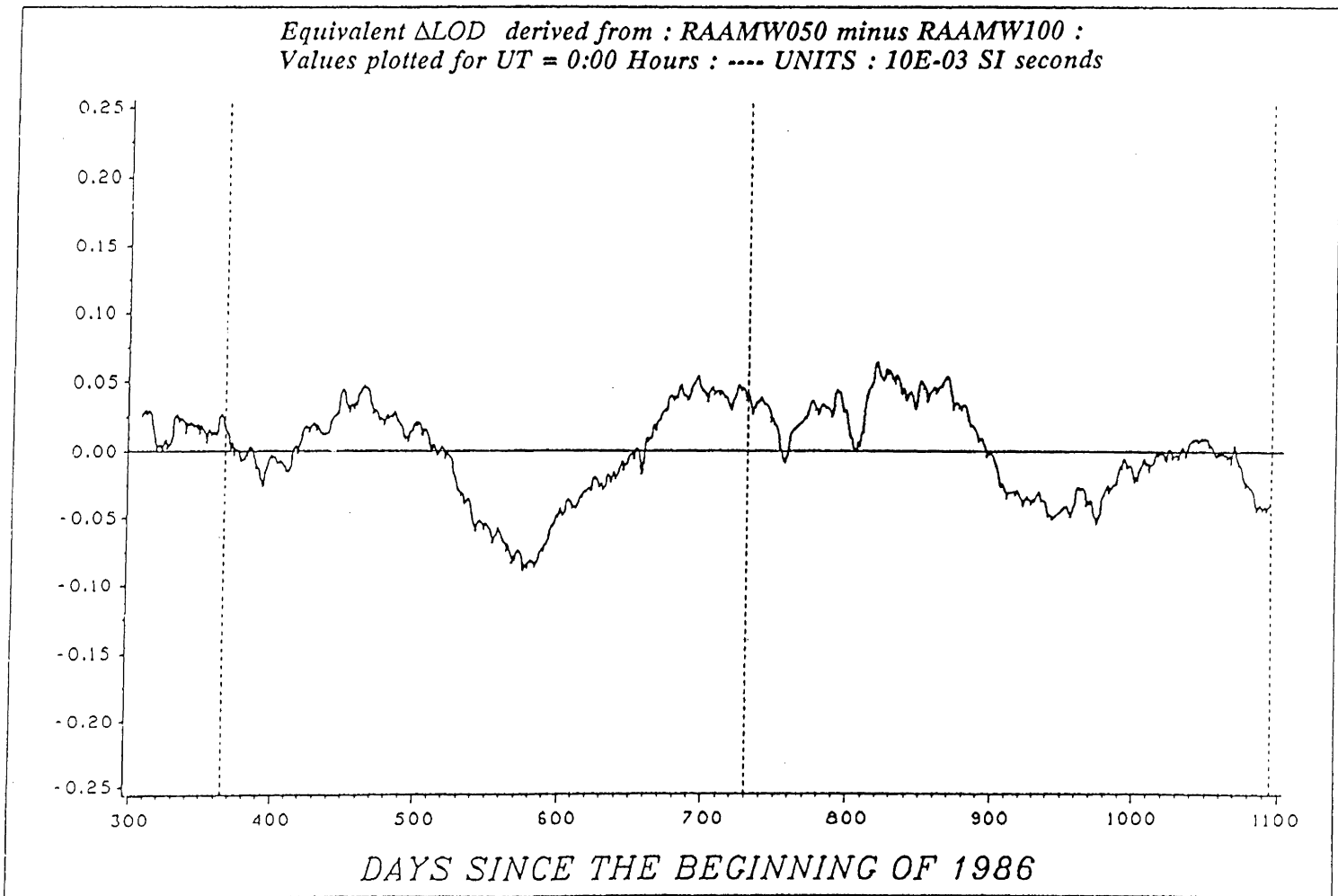


Fig. 8.3e

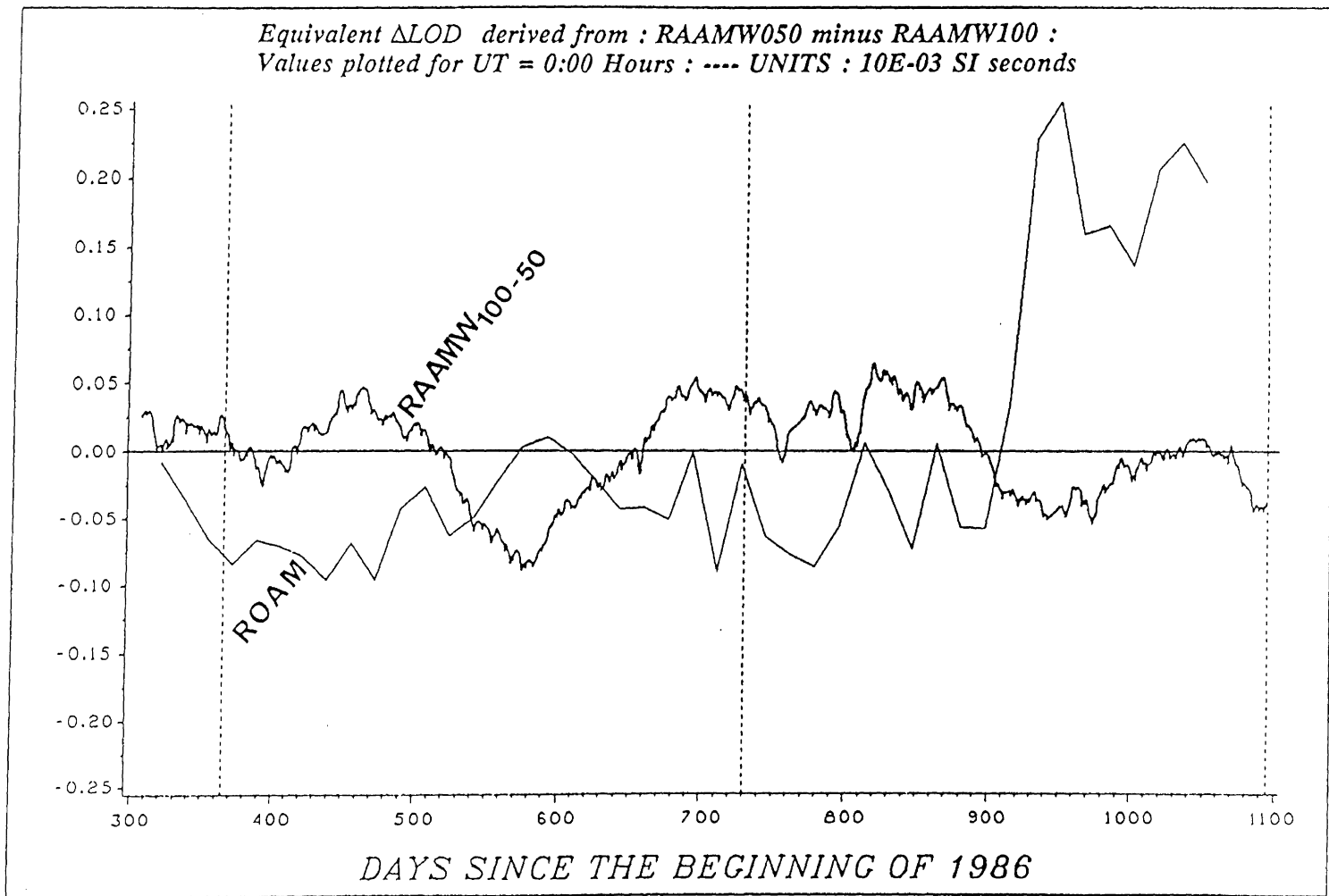


Fig. 8.3f



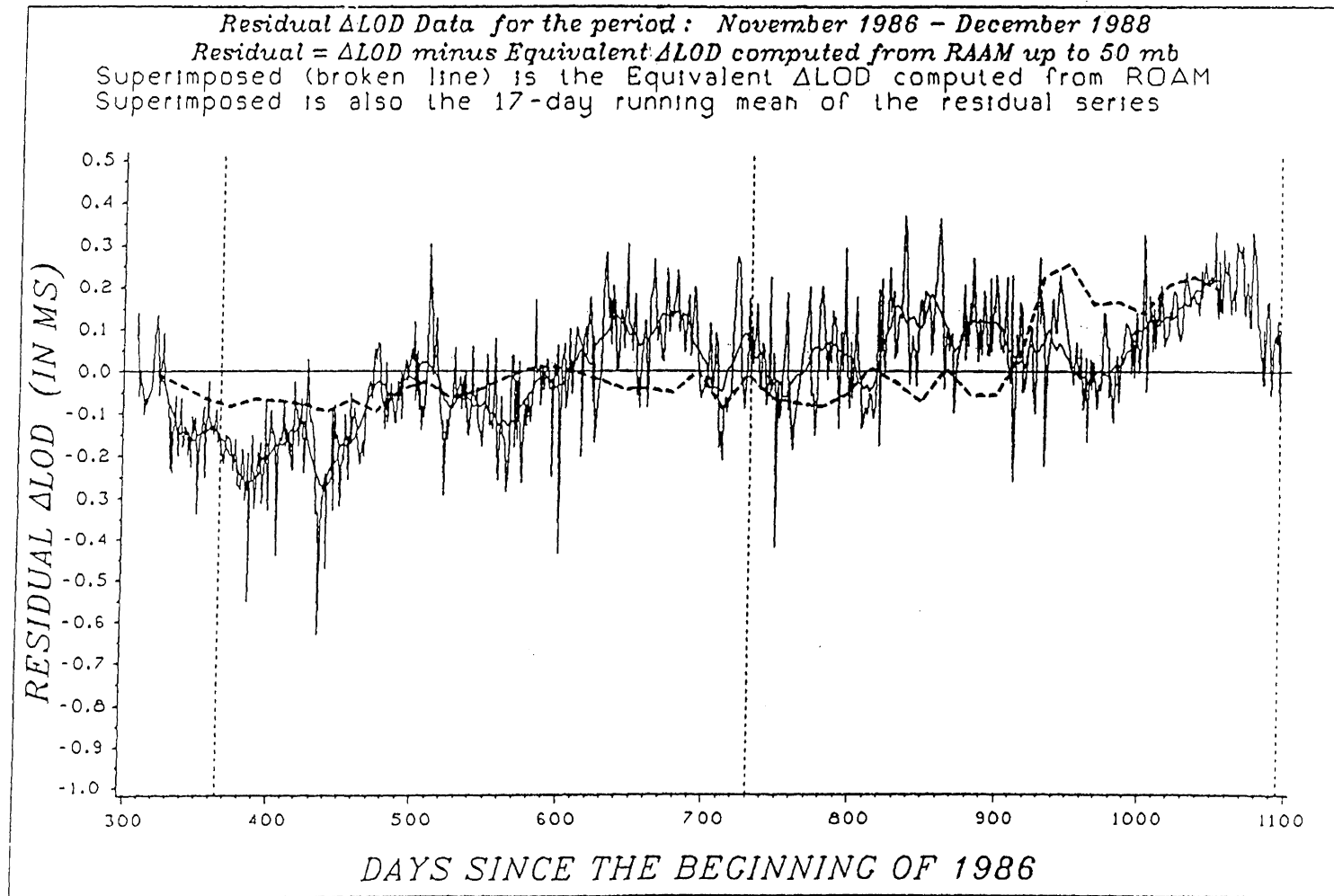


Fig. 8.3h

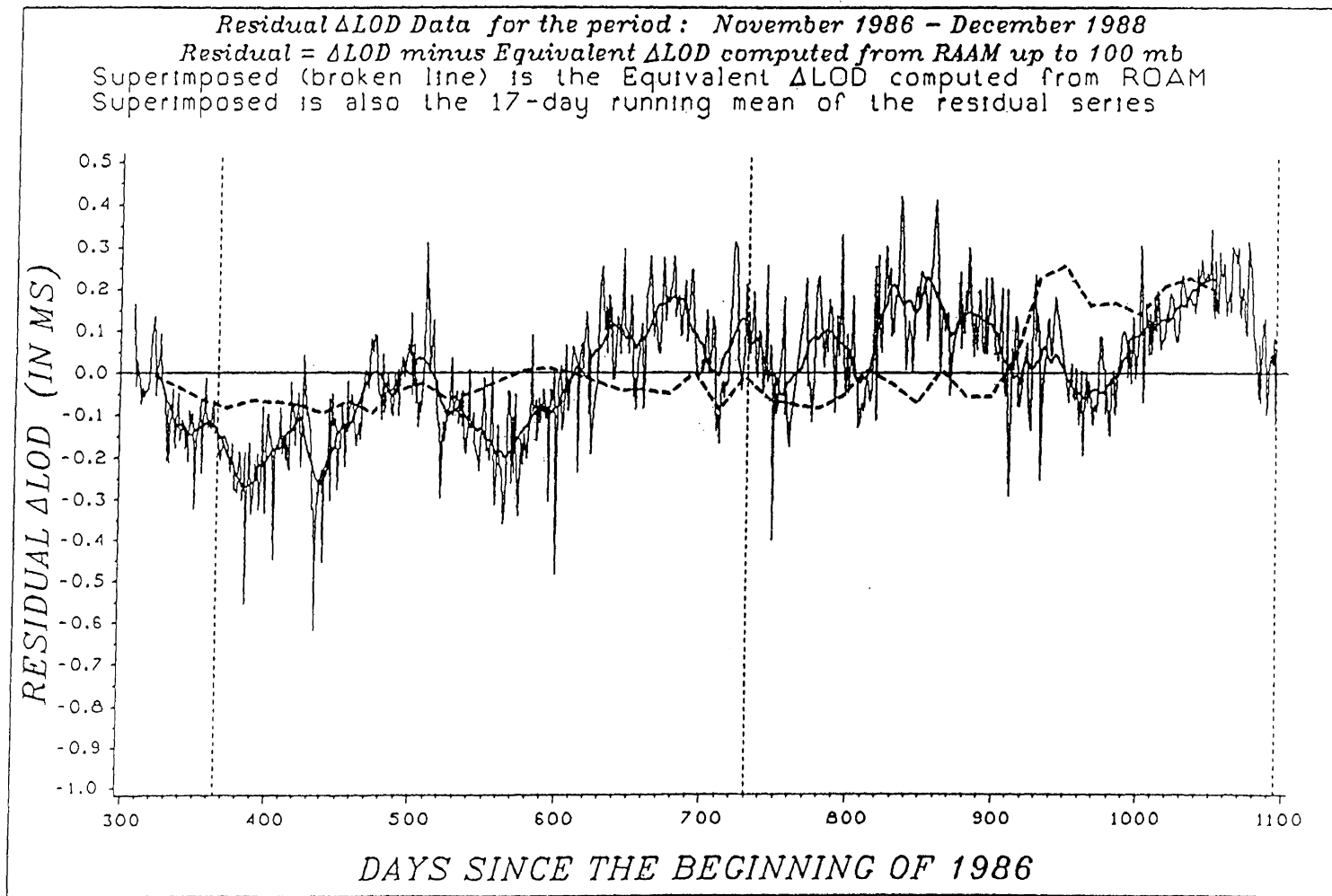


Fig. 8.3g

Several conclusions can be drawn from the visual comparison of the many series displayed in Figures 8.3 regarding the ROAM-inferred  $\Delta LOD$  time series. A first conclusion is that the ROAM-inferred  $\Delta LOD$  has a range of values of 0.1 ms. Although not shown in Figure 8.3c (but presented in Appendix II) the estimated standard deviation of the ROAM-inferred  $\Delta LOD$  is on the average  $\pm 0.033ms$ . As we have discussed in Chapters 6 and 7, from the standard deviation image time-frames we have estimated the associated standard deviations of the altimetry derived  $[u^*]$ -fields. These error estimates were propagated through equation (7.10) to produce formal  $\Delta ROAM$  error estimates.

The sudden increase in the ROAM-inferred  $\Delta LOD$  shown after day-915 is of the order of 0.2 ms. The residual  $\Delta LOD$  time series (Figure 8.3g) indeed shows changes of approximately the same magnitude occurring during this time. However, it is difficult to explain the source of such a change in the present ROAM analyses. We have discussed in Chapter 6 the general relation between the computed zonal ocean current fields and the SOI behaviour, and we have revisited the subject in Chapter 7, when the latitude structure of the  $\Delta ROAM$  was discussed in more detail. This oceanic behaviour remains to be further researched before it is conclusively accepted or dismissed.

Another comment regarding the ROAM-inferred  $\Delta LOD$  time series is its relation to the equivalent  $\Delta LOD$  generated by the difference  $\Delta RAAMW050$  minus  $\Delta RAAMW100$  (designated from here on as  $RAAMW_{100-50}$ ), i.e., the lower stratosphere contribution to  $\Delta LOD$ . The  $\Delta ROAM$  equivalent  $\Delta LOD$  experiences similar magnitude variations as the  $RAAMW_{100-50}$  equivalent  $\Delta LOD$ , as can easily be deduced from Figures 8.3d, 8.3e, and

8.3f. In fact, it appears that the  $\Delta ROAM$  equivalent is approximately the reflection of the  $RAAMW_{100-50}$  for most part of the time series.

In the rest of the comparisons, we will only consider the  $\Delta RAAMW_{050}$ -inferred  $\Delta LOD$  time series. It is conceivably the most appropriate data series, since it represents a larger portion of the atmosphere.

### 8.3.1. Frequency Domain Comparisons

To focus on the similarities and the connection between the different time series that we discussed previously, we have used frequency domain techniques of spectral analysis. The analysis technique we employed is known by the name “Least Squares Spectral Analysis” (LSSA). The theoretical and practical developments of the technique are described in *Vanicek* [1971] and *Wells et al.* [1985].

In brief, LSSA is an algorithm to compute the optimum least squares spectrum of an unequally (or equally) spaced, generally non-stationary and coloured time series, for which the structure of some of the contained systematic signals are known. Known constituents (systematic signals) can be either datum biases, linear or other shape trends, and periodic (harmonic) functions. In the LSSA context, a linear trend means that the “mean” value of the quantity represented in the time series changes linearly with time. This, of course, makes the series non-stationary.

The relationship of the least squares spectrum to other spectral functions has briefly been discussed in *Wells et al.* [1985]. The Fourier spectrum is a degenerate case of the general least squares spectrum.

We have used the LSSA technique to produce the least squares spectra of:

- (a) the raw time series;
- (b) the residual time series, i.e., the time series after the removal of contributions of certain periodic functions.

Of course, the mean value of each individual time series has been removed from the time series at an earlier stage.

Figures 8.4a, 8.4b, and 8.4c show the least squares spectra of the observed  $\Delta LOD$ , the  $\Delta RAAMW050$  -inferred  $\Delta LOD$ , and the  $\Delta ROAM$  -inferred  $\Delta LOD$ , respectively. For the same period, i.e., November 1986 to November 1988, we have analysed an additional time series. This data series is the Tahiti-Darwin SOI and has been presented earlier in Chapters 6 and 7. Figure 8.4d shows the least squares spectrum of this particular SOI.

Before we depart into commenting on these spectra, two explanations are necessary. First, the spectra shown in Figures 8.4 were obtained after removing a datum bias and a linear trend from the original time series. Any trend in a series (linear quadratic, exponential, step function, etc.) should be removed from the series to avoid erroneous spectral representations. It is thus the detrended time series that are analysed to produce the least squares spectra shown in Figures 8.4.

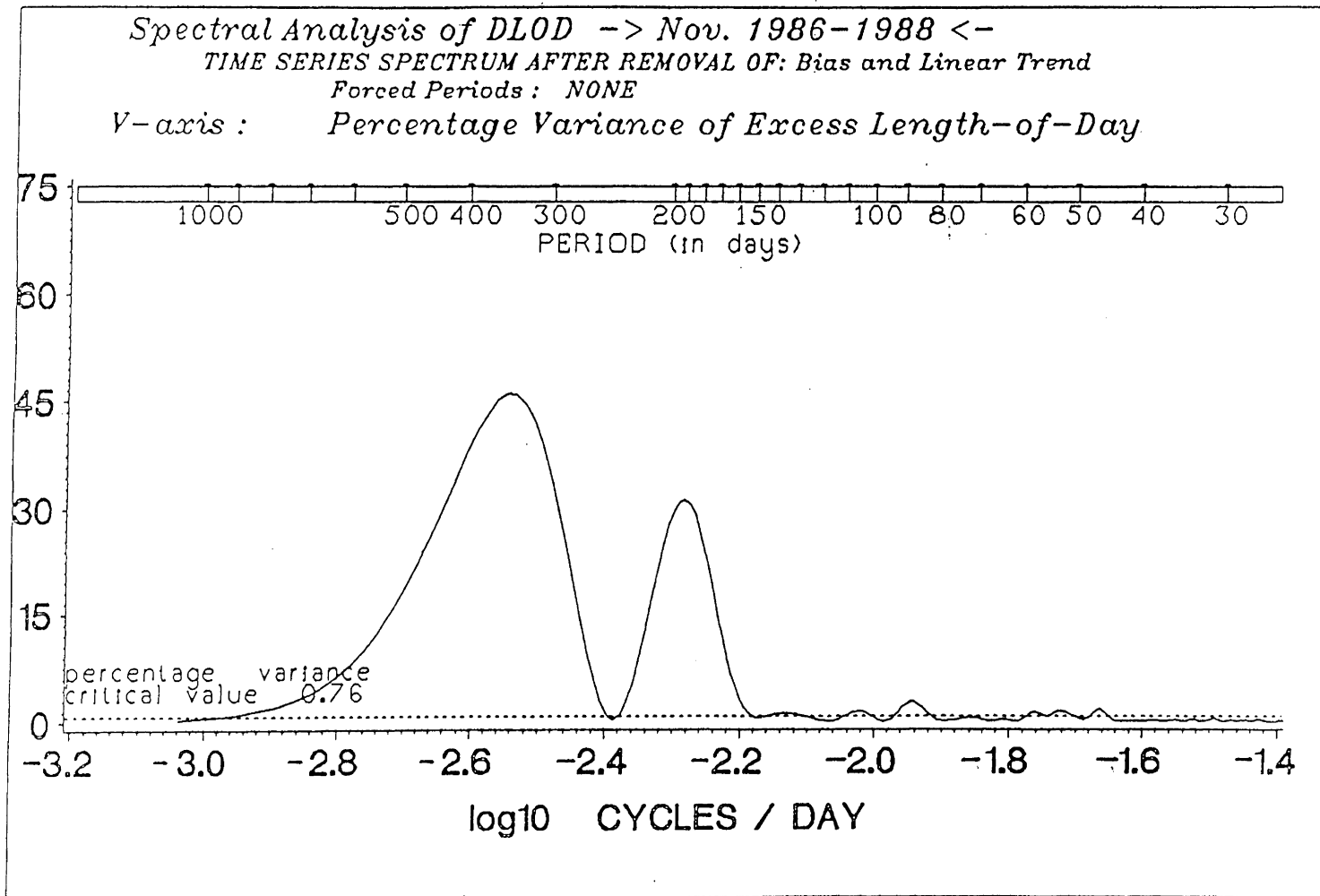


Fig. 8.4a

*Spectral Analysis of RAAMW050 Equivalent DLOD -> Nov. 1986-1988 <-*  
*TIME SERIES SPECTRUM AFTER REMOVAL OF: Bias and Linear Trend*  
*Forced Periods: NONE*  
*V-axis: Percentage Variance of RAAM Equivalent Excess Length-of-Day*

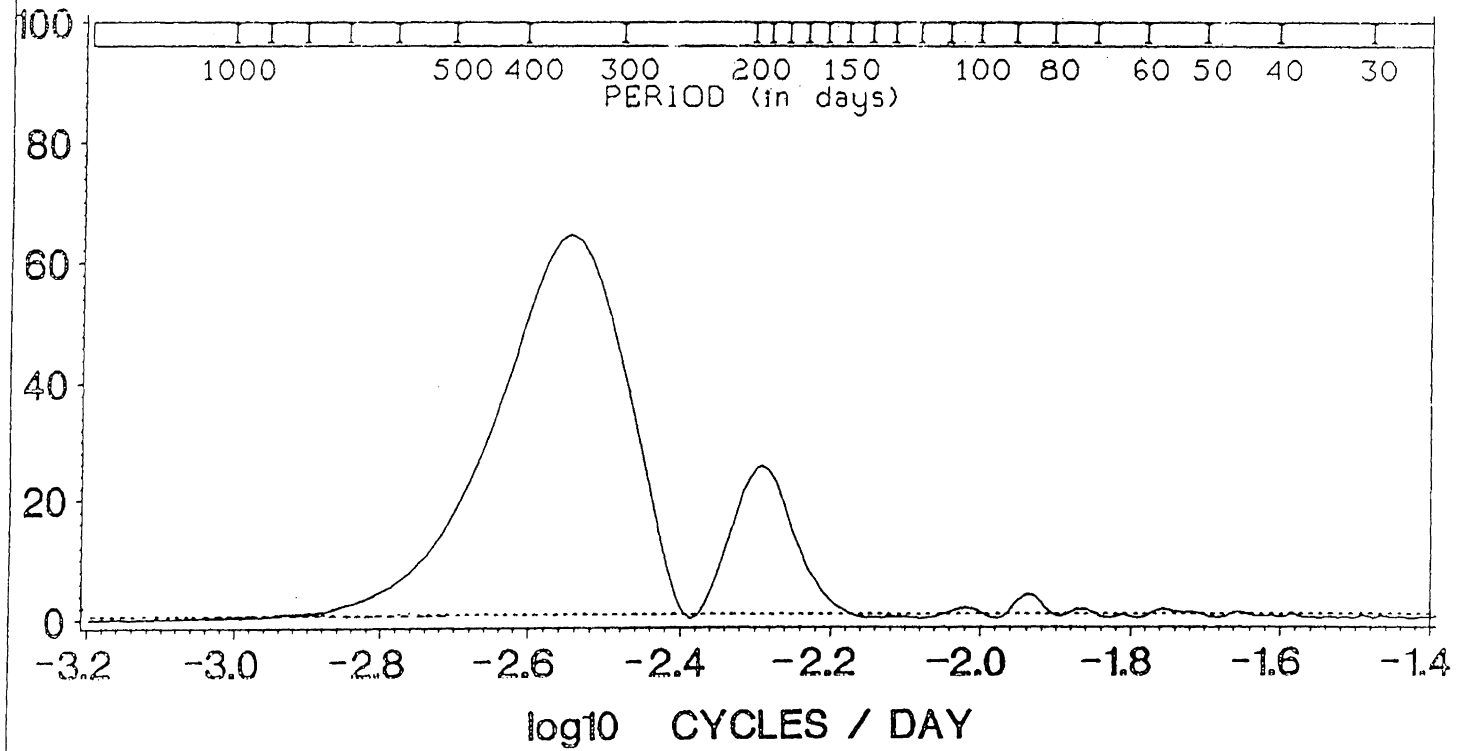


Fig. 8.4b

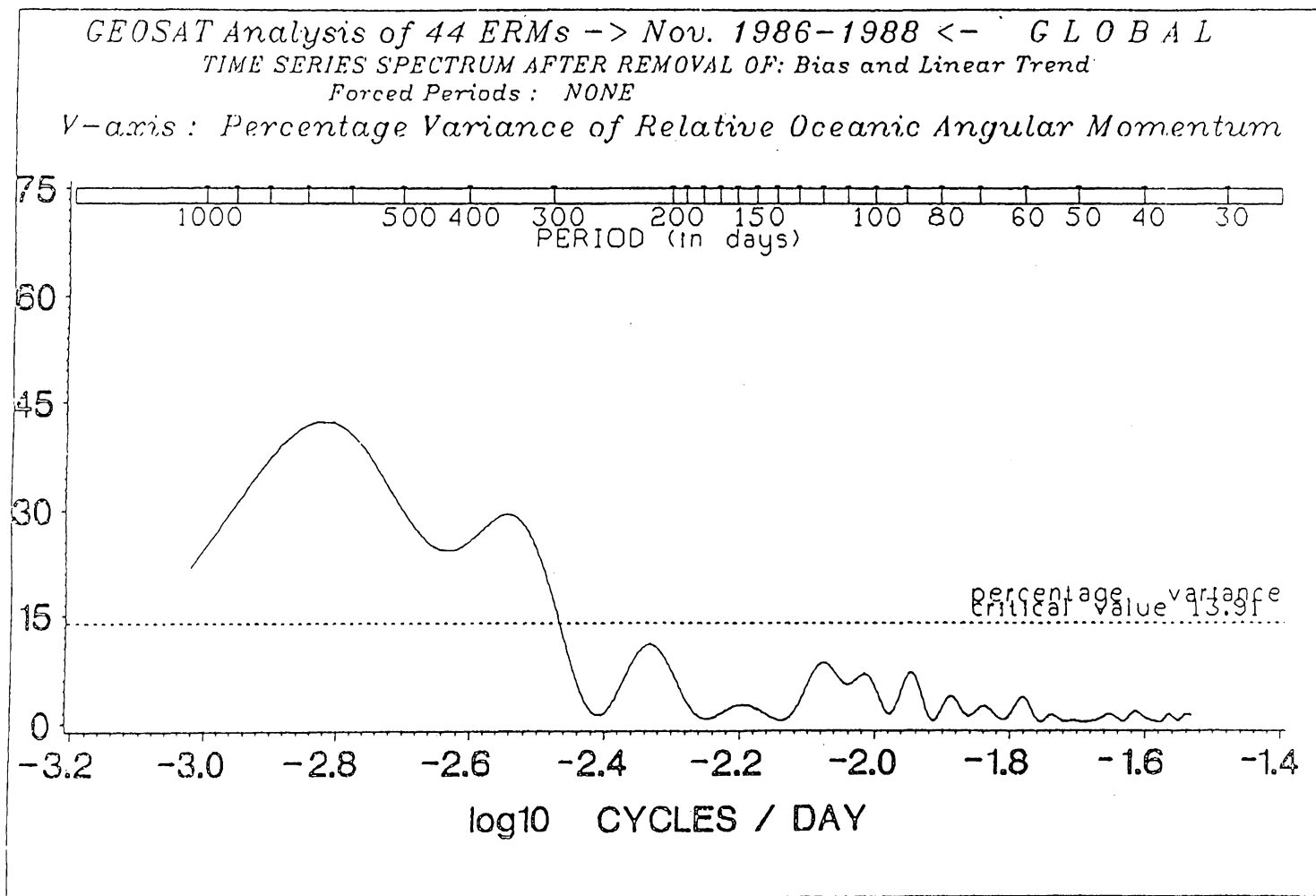


Fig. 8.4c



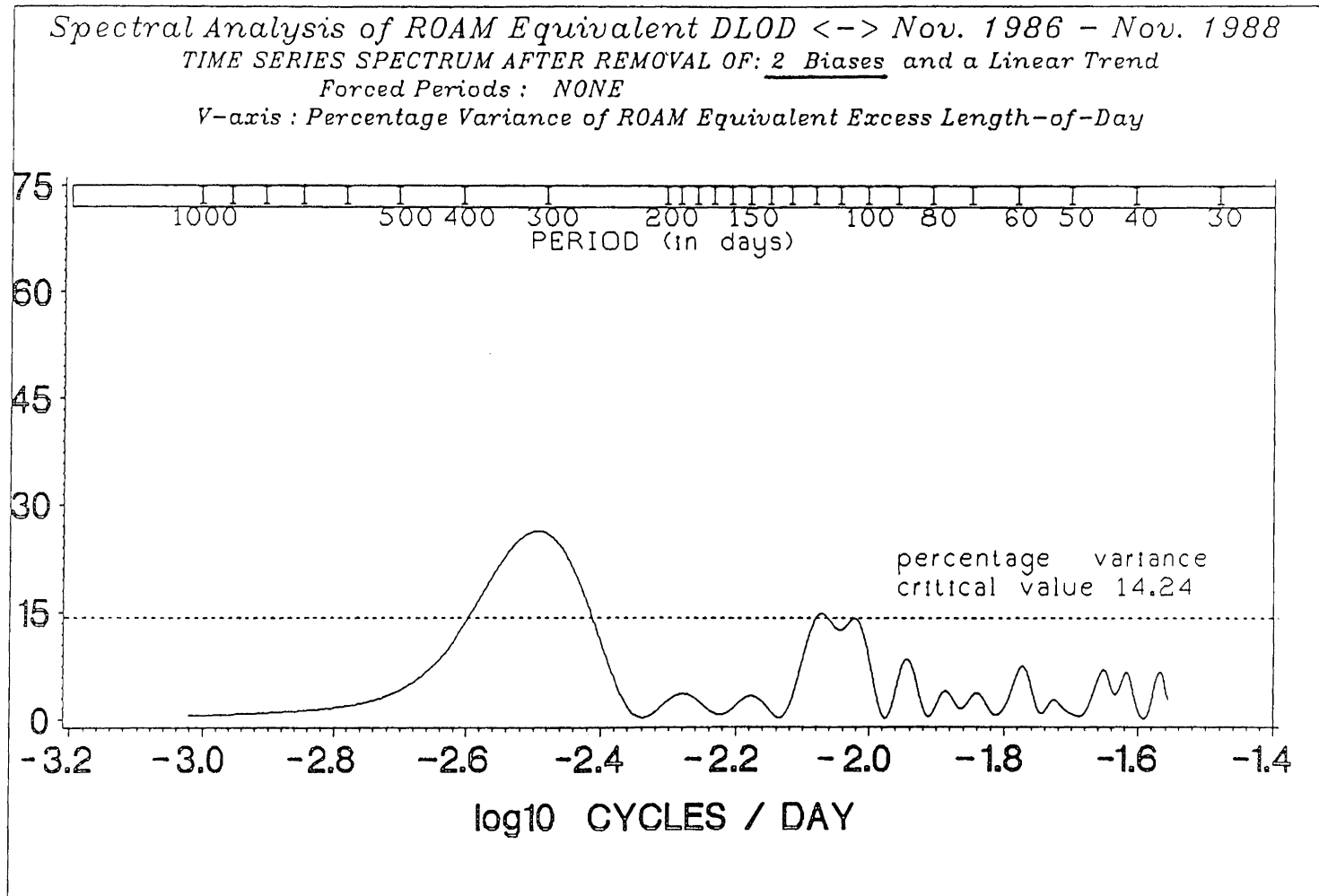


Fig. 8.4d

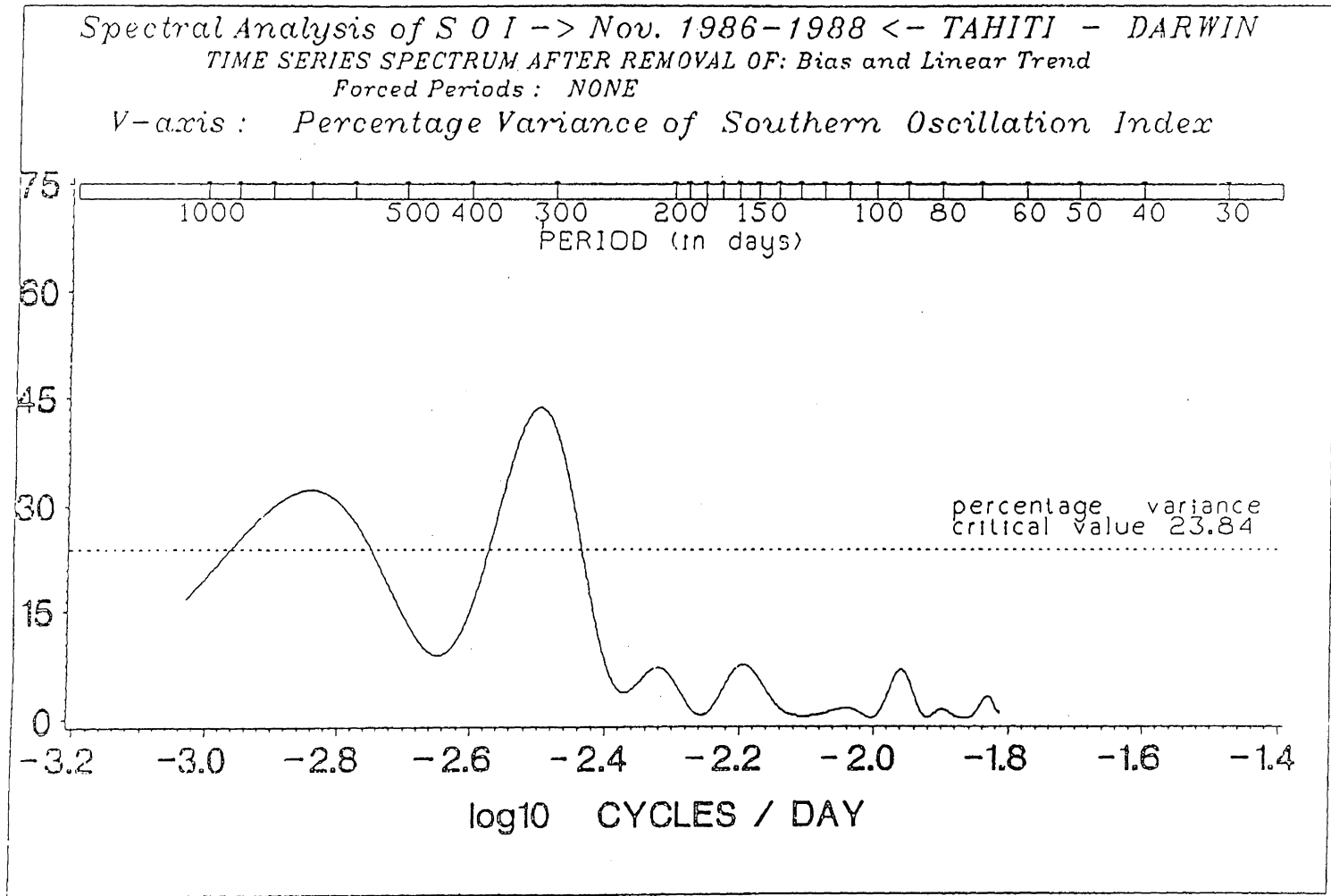


Fig. 8.4e

Second, the LSSA implementation provides outputs consisting of the residual time series and its norm, the estimates of the bias and trend functions, the amplitude and phases of any “known” periodic constituents that were (by user’s request) removed from the time series and their associated error estimates, and finally, the spectral values (in the form of percentage variance) of the input vector of periods (frequencies). A valuable output parameter from the LSSA algorithm is the critical percentage variance at a pre-selected confidence level (chosen in our analysis at 95%), for detecting significant peaks in the computed spectrum. The critical percentage variance value is also superimposed on the plots of the different spectra shown in Figures 8.4.

**Observed LOD Fluctuations.** From Figure 8.4a it is obvious that the annual and semi-annual frequencies dominate the least squares spectrum, i.e., most of the power is contained in these two periodic constituents. This is a well known fact and has been extensively discussed in the literature. In order to be able to investigate the remaining frequency content in the  $\Delta LOD$  time series, the overshadowing effect of the annual and semi-annual variations in the  $\Delta LOD$  have to be removed (forced out) from the time series. This will also allow us to estimate their amplitude and phase (see section 8.4).

**RAAM-inferred LOD Fluctuations** (Figure 8.4b). The comments we made for the observed  $\Delta LOD$  apply here as well. However, the temptation to repeat the statement that the atmosphere’s variable zonal wind is the protagonist in exciting length-of-day fluctuations is too large to avoid. Indeed, the annual and semi-annual, non-tidal, LOD variations are the work of the wind field upon the solid earth.

**ROAM-inferred LOD Fluctuations** (Figure 8.4c). To our knowledge, this is the first time that a spectrum of oceanic excitation of LOD variations appears in the literature. By default, there is nothing to compare it with, except from some speculations of what the role of the oceans should be, and what the discrepancies between the solid earth-atmosphere components currently are. Let us first examine the oceanic spectrum visually from Figure 8.4c.

The discussion that follows is based on the presumption that the event-like change in  $\Delta ROAM$  is legitimate. There appears to be an annual periodicity. Moreover, there is a strong presence of a lower frequency signal, which for the time being, we will label as a “2-year” or “biennial” periodicity. Both the “biennial” and annual peaks are above the percentage variance critical value, thus being significant peaks in the statistical sense. It can be argued that the “biennial” period is not a real signal, because the time series span only just over 2 years. Indeed, this is a very legitimate argument.

In any event, the point is that a very large portion of percentage variance is associated with the lower frequency end of the spectrum in Figure 8.4c and something must be done to reduce it, so as to allow us to investigate whether other higher frequencies are significant in the time series. The choice of a “biennial” peak looks like a valuable starting point and we will discuss more about it in due course.

Another important observation drawn from the  $\Delta ROAM$  spectrum displayed in Fig. 8.4c is that there is no indication of a significant semi-annual frequency. For the past 20 years or so, the discrepancies between the observed  $\Delta LOD$  and the

atmospherically excited  $\Delta LOD$  at the semi-annual frequency have been invariably interpreted as the lacking oceanic excitation contribution (see, e.g., *Lambeck* [1980]; *Eubanks et al.* [1984]; *Wahr* [1983]; etc.). The work of *Rosen & Salstein* [1985] on the contribution of the stratospheric winds towards  $\Delta LOD$  excitation, put more or less to rest, the subject of semi-annual discrepancies. They reached the conclusion (*ibid.*) that there is no need to invoke any other geophysical process to explain the discrepancies at the semi-annual frequency, since the stratospheric contribution is capable of explaining it both in terms of amplitude and phase. Looking at the  $\Delta ROAM$  least squares spectrum computed here, their statement seems to be supported to a very large extent. There is no convincing sign of a semi-annual frequency in the oceanic component.

Regarding the rest of the spectral characteristics of the oceanic component, we will examine them in more detail later on.

We have also computed the spectral properties of the  $\Delta ROAM$  equivalent  $\Delta LOD$  latitude structure, and the raw spectra are displayed in Appendix III. Comments on these spectra are reserved for future investigations. The only comment we make here is that there are some slightly different spectral characteristics associated with the different latitude belts.

We would like to return to the point made earlier regarding the event like change in the  $\Delta ROAM$  time series appearing around day 932 (cf. Fig. 8.3c). We have carried out additional spectral analysis studies by introducing a new datum, i.e., a second unknown bias to be determined through the least squares process at exactly day 932. This approach effectively removes the event-like feature occur-

ring in the  $\Delta ROAM$  time series. The introduction of the new datum at day 932 plays the role of estimating a step change in the time series and removing it before any spectra are computed. The results from this spectral analysis approach are shown in Figure 8.4d.

**Spectral Analysis of the Tahiti-Darwin SOI** (Figure 8.4e). We have already pointed out in the previous chapters some similarities between the oceanic zonal current variability and the SOI.

From the spectral analysis of the SOI time series it is obvious that the two significant peaks shown in Figure 8.4e are related to a “biennial” and an “annual” frequency.

An interesting observation in the SOI spectrum is that there is no convincing evidence for a semi-annual frequency. This observation can at least provide us with some speculative arguments to justify the spectral characteristics we saw in the  $\Delta ROAM$  equivalent  $\Delta LOD$  spectrum.

## 8.4 Spectral Analysis Results and Intercomparisons

To investigate further the concurrent time series, i.e., observed (IRIS/VLBI)  $\Delta LOD$ ,  $\Delta RAAMW050$ -inferred and  $\Delta ROAM$ -inferred  $\Delta LOD$ , each data set was studied separately by applying the LSSA technique to estimate the amplitude and phases of 730.50-day, 365.25-day, and 182.63-day constituents (forced periods) for the 2-year long period Nov'86-Nov'88. The results for the above three periodic components are summarized in Table 8.1 and reflect the time series displayed in Figure 8.3c without the removal of the event-like change in  $\Delta ROAM$ .

It should be pointed out that the tidal components up to 18.6 years have been a-priori removed from the observed  $\Delta LOD$  time series. Before making any comments on the summary of the results presented in Table 8.1, we present an additional table of results. This one refers to the spectral analysis of the differenced  $\Delta LOD$  time series and the oceanic inferred  $\Delta LOD$ . By differenced  $\Delta LOD$  time series, we mean the  $\Delta LOD$  remaining after we subtract the  $\Delta RAAMW050$ -inferred  $\Delta LOD$  from the observed  $\Delta LOD$ , or in the first approximation, solid earth minus atmosphere.

TIME SERIES	"Biennial"		Annual		Semi-annual	
	AMPL	PHASE	AMPL	PHASE	AMPL	PHASE
observed $\Delta LOD$	0.137	321.4°	0.421	33.1°	0.288	239.6°
	$\pm 0.009$	$\pm 0.6^\circ$	$\pm 0.009$	$\pm 0.2^\circ$	$\pm 0.009$	$\pm 0.2^\circ$
$\Delta RAAMW050$ inferred $\Delta LOD$	0.110	308.6°	0.441	36.2°	0.216	236.6°
	$\pm 0.008$	$\pm 0.6^\circ$	$\pm 0.008$	$\pm 0.1^\circ$	$\pm 0.007$	$\pm 0.2^\circ$
$\Delta ROAM$ inferred $\Delta LOD$	0.066	185.1°	0.052	260.1°	0.014	88.5°
	$\pm 0.011$	$\pm 1.8^\circ$	$\pm 0.011$	$\pm 1.5^\circ$	$\pm 0.009$	$\pm 5.5^\circ$

**Table 8.1 Individual Time Series Spectral Analysis Results:** Common periodic components removed from the three concurrent time series (Nov'86 - Nov'88). Amplitudes are in milliseconds and phases in degrees from the beginning of the year. Standard deviations of the estimated amplitudes and phases are also included in the table, and are estimated internally by the LSSA software, without recourse to the time series accuracies. (Based on the spectra displayed in Figure 8.4c).

TIME SE- RIES	"Biennial"		Annual		Semi-annual	
	AMPL	PHASE	AMPL	PHASE	AMPL	PHASE
differenced $\Delta LOD$	0.039	1.8°	0.031	266.3°	0.072	248.1°
	$\pm 0.005$	$\pm 1.4^\circ$	$\pm 0.006$	$\pm 0.2^\circ$	$\pm 0.005$	$\pm 0.6^\circ$
$\Delta ROAM$ inferred $\Delta LOD$	0.066	185.1°	0.052	260.1°	0.014	88.5°
	$\pm 0.011$	$\pm 1.8^\circ$	$\pm 0.011$	$\pm 1.5^\circ$	$\pm 0.009$	$\pm 5.5^\circ$

**Table 8.2** Differenced Time Series Spectral Analysis Results: Common periodic components removed from the differenced  $\Delta LOD$  time series ( $\Delta LOD$  minus  $\Delta RAAMW050$ ) and the  $\Delta ROAM$  inferred  $\Delta LOD$ . Amplitudes are in milliseconds and phases in degrees from the beginning of the year. Standard deviations of the estimated amplitudes and phases are also included in the Table. (Based on the spectra displayed in Figure 8.4c).

The phase estimates presented in Tables 8.1 and 8.2 correspond to the times of occurrence of the first maximum of the wave from the beginning of the year (360 degrees phase angle corresponds to 365 days).

The results of estimating the amplitudes and phases of annual and semi-annual constituents from the time series in the case of introducing a second datum bias at day 932 are respectively:



TIME SE- RIES	-		Annual		Semi-annual	
	AMPL	PHASE	AMPL	PHASE	AMPL	PHASE
$\Delta ROAM$	-	-	0.026	231.4°	0.006	342.5°
inferred $\Delta LOD$	-	-	$\pm 0.008$	$\pm 2.1^\circ$	$\pm 0.007$	$\pm 8.6^\circ$

**Table 8.3 Alternative Time Series Spectral Analysis Results:** Spectral analysis results of  $\Delta ROAM$  inferred  $\Delta LOD$  in the case of introducing a second datum bias in the time series at day 932 to remove the effect of the event-like feature in the time series. Amplitudes are in milliseconds and phases in degrees from the beginning of the year. Standard deviations of the estimated amplitudes and phases are also included in the Table. (Based on the spectra displayed in Figure 8.4d).

Spectral analysis of the  $\Delta ROAM$  time series containing only the results from the first 36 ERMs was also performed (i.e., up to day 915) and the results are as follows: (a) annual period amplitude  $0.029 \pm 0.008$  ms and phase  $235.0^\circ \pm 1.8^\circ$ ; (b) semi-annual period amplitude  $0.002 \pm 0.007$  ms and phase  $102.7^\circ \pm 37.3^\circ$ .

Finally, Figure 8.5 is a superposition plot of the spectra of the individual residual time series after the removal of the three periodic components, namely the 730.50-day, 365.25-day, and 182.63-day periods. Figure 8.6 displays the spectra

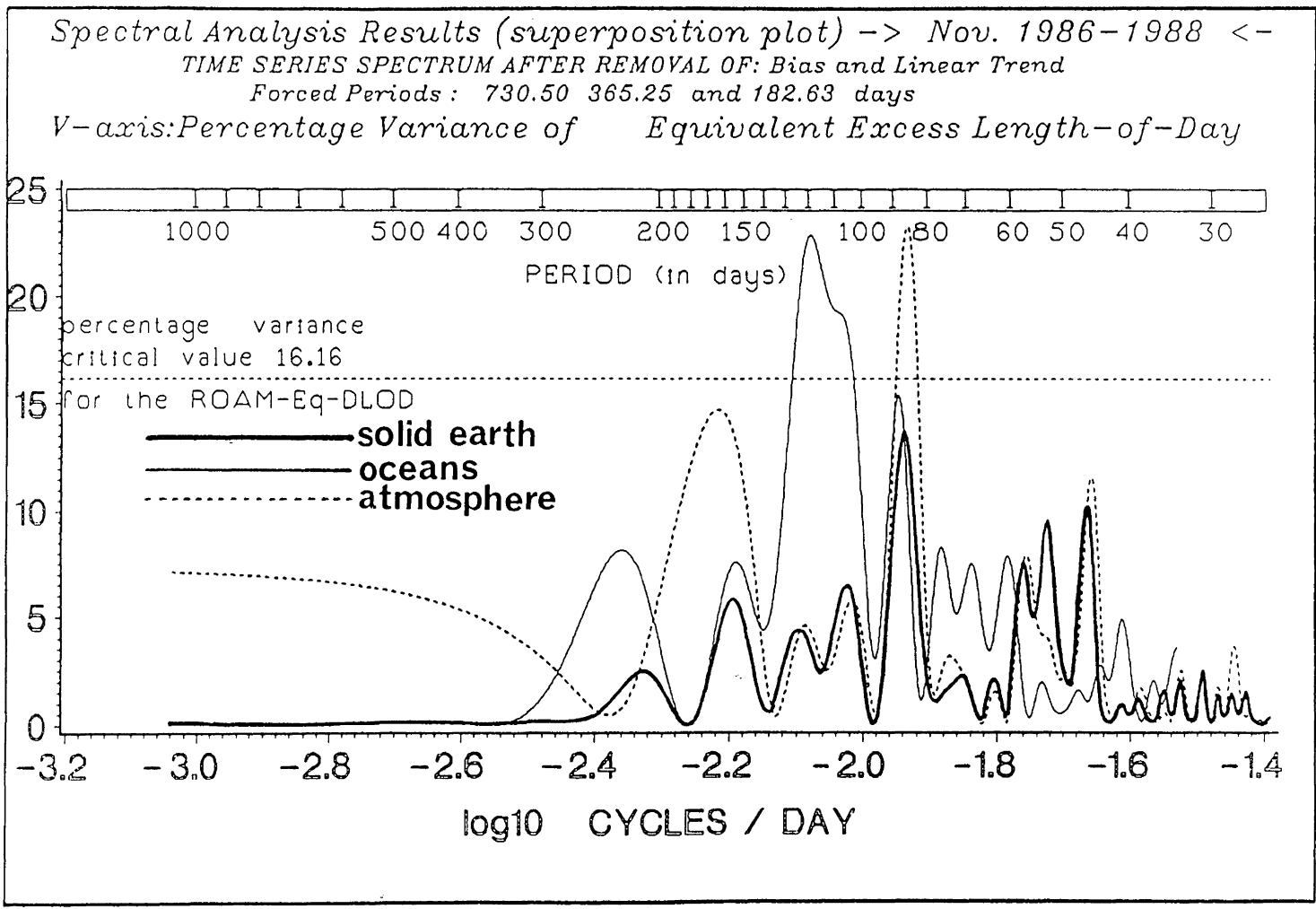


Fig. 8.5

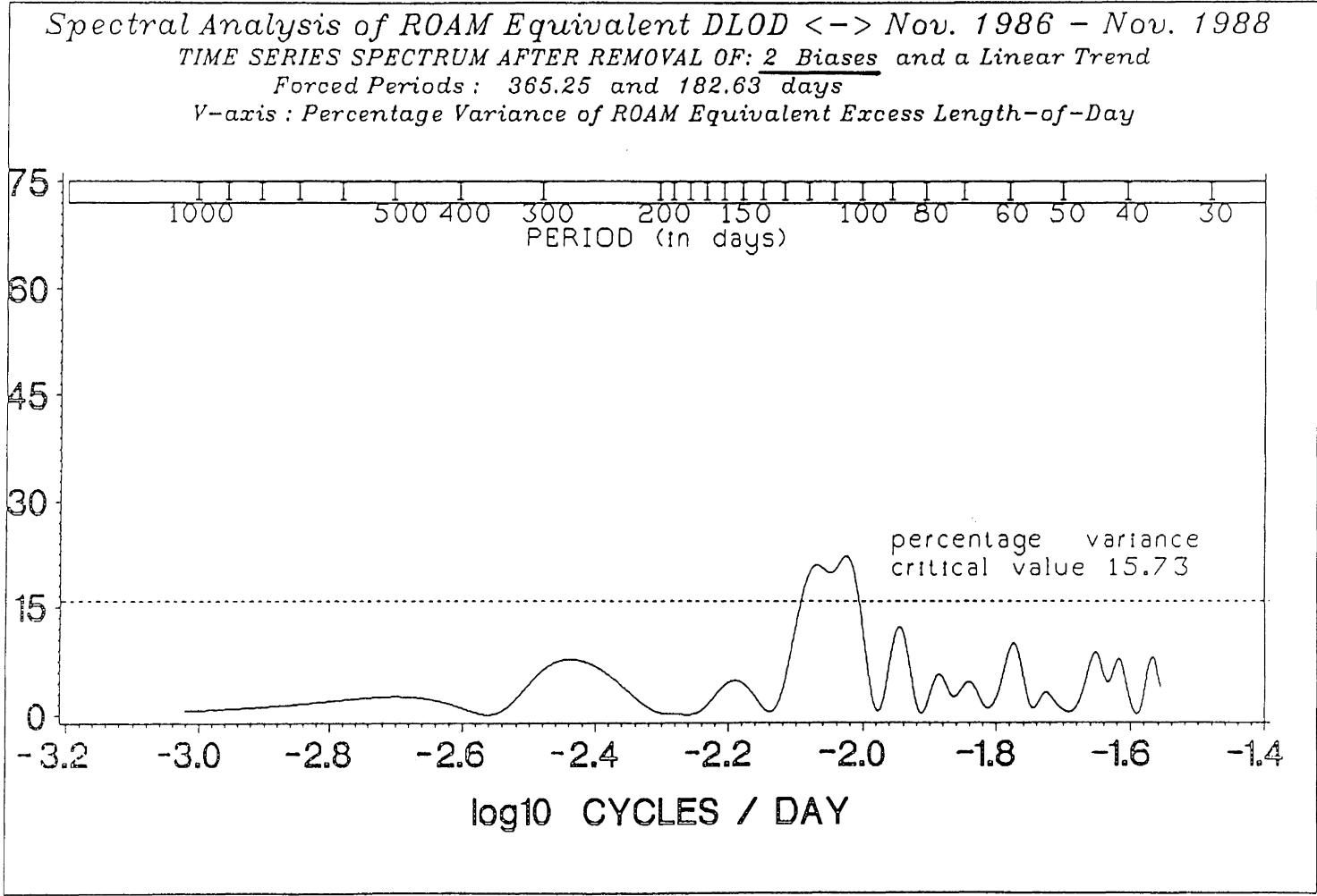


Fig. 8.6

of the  $\Delta ROAM$  time series with the additional datum bias imposed on the time series at day 932.

From Figure 8.3a and Table 8.1, it is obvious that the seasonal terms dominate the non-tidal variations in the observed LOD. The largest component is the annual cycle, with an amplitude of  $0.421 \pm 0.009ms$ . It reaches its maximum approximately on February 2<sup>nd</sup> – 3<sup>rd</sup> and its minimum approximately on August 3<sup>rd</sup> – 4<sup>th</sup>. The semi-annual component has approximately half the amplitude of the annual term, i.e.,  $0.288 \pm 0.009ms$ . What we have termed as “biennial” component is also present with half the amplitude of the semi-annual term, i.e.,  $0.137 \pm 0.009ms$ . All three components present in the  $\Delta LOD$  have been discussed previously in the literature and there is no need to carry on any further discussion here.

The atmosphere ( $\Delta RAAMW050$ -inferred  $\Delta LOD$ ), is undoubtedly the major source of seasonal excitation of LOD variations as can be seen from Table 8.1. However, there are discrepancies (see row 1 in Table 8.2) between the amplitudes of the three seasonal waves which indicate that there are other geophysical mechanisms that play a role in the earth’s variable rotation rate. From either Table 8.2 or 8.3 (last row) it is confirmed that the oceans can be the candidate geophysical excitation source needed to close the gap between the observed and the wind-inferred  $\Delta LOD$  at least at the annual frequency. It is also obvious that the thesis of *Rosen & Salstein* [1985] that the inclusion of the upper stratospheric winds (50 to 1 mbar) explains the remnant semi-annual amplitude (see Table 8.2, differenced time series) is supported by the results obtained here, since the oceans did not show any significant semi-annual variation. This contradicts the thesis

put forward by *Lambeck* [1980] and other researchers, that the oceans could be responsible for about 0.05 ms at the semi-annual frequency.

One thing is very clear from our analyses. The oceanic signal, both in amplitude and phase, from either spectral analysis (i.e., 1 bias or two datum biases), appears large enough to explain the discrepancy between the observed and the wind inferred  $\Delta LOD$  at the annual frequency during the period Nov'86-Nov'88. From Table 8.2 the longer than 1 year periodic signal (here we called it "biennial") that agrees relatively well in amplitude with the differenced  $\Delta LOD$  amplitude, but is  $180^\circ$  out of phase is very clear that is associated with the event-like feature presence or absence. When better quality and longer ROAM time series become available they will either confirm or dismiss its existence.

The weak semi-annual oceanic contribution is still somewhat of a surprise to us. Logically thinking, we might expect the ocean currents to experience semi-annual periodic fluctuations. This notion, however, is not supported by our numerical results. Not only that, but even from the latitude analysis of the estimated  $\Delta ROAM$ , we did not find convincing evidence for the presence of a significant semi-annual period. Also, it was found from the latitude analyses of  $\Delta ROAM$ , that most of the stronger oceanic fluctuations are associated with the low- and mid-latitude oceanic belts. The ACC's role in the  $\Delta ROAM$  budget seems to be small compared to the rest of the latitudinal bands, as far as amplitude variations are concerned. This statement should not be misinterpreted. What we mean here by ACC is the whole latitude band extending between  $65^\circ S$  and  $45^\circ S$ , and not just a certain area such as the Drake Passage.

There are many more interesting observations and conclusions coming out of our analyses. They can be deduced from the residual spectra displayed in Figure 8.5 (or Figure 8.6). It appears that the oceans' contributions to higher frequencies (higher than 0.5 cy/y) are worthwhile investigating. There is certainly statistically significant spectral information in the frequency band between 55 days and 155 days as shown in the spectral display (i. e., spectral peaks above the percentage variance critical value). From preliminary spectral analyses we have carried out, but not included here, the amplitudes of some of these statistically significant waves in the 55-155 days frequency band, are of the order of 0.020 to 0.025 ms. They may, therefore, be valuable in explaining higher frequency discrepancies between observed and wind inferred fluctuations in LOD. Detailed work in this spectral band is planned for the future.

Another interesting observation from the spectral analysis results obtained from the run without the removal of the event-like feature in the  $\Delta ROAM$  time series is that the estimated bias and linear trend of the differenced  $\Delta LOD$  and  $\Delta ROAM$ -inferred  $\Delta LOD$  are in very good agreement:

$$(a) \quad \text{bias} = -0.226ms \quad ; \quad \text{drift} = 0.330 \times 10^{-3}ms/day;$$

$$(b) \quad \text{bias} = -0.232ms \quad ; \quad \text{drift} = 0.336 \times 10^{-3}ms/day,$$

where (a) refers to the differenced  $\Delta LOD$  time series and (b) to the  $\Delta ROAM$  inferred  $\Delta LOD$  time series. It should be remembered that because the origin of the time axis is January 1, 1986, whereas the time series analysed begin in November of 1986, there is a non-zero intercept (datum bias) computed during the de-

trending of the time series. As we have said earlier, the version of the LSSA software we have been using in our analyses does not print the uncertainties of the estimated datum bias and drift parameters if they are less than 25% of the estimated values. In our runs there were no uncertainty values printed for the bias and drift estimates, which implies that their estimated values are at least 4 times larger than their respective formal error estimates.

The importance of such drift estimates lies in the fact that the oceans might be responsible for low frequency contributions towards LOD fluctuations [*Rosen et al.*, 1989], in which case the linear trend we see in this 2-year long period may indeed be indicative of such a behaviour. *Rosen et al.*, [1989] point to a positive slope in the differenced  $\Delta LOD$  they have computed (observed  $\Delta LOD$  minus  $\Delta RAAMW100$ -inferred  $\Delta LOD$ , Figure 13, *ibid.*) starting approximately at the end of 1986 - beginning of 1987 and lasting at least through 1988. This is exactly the period we have analysed in this research. If it is not just pure coincidence that the results we have computed and show in (a) and (b) above agree so well, then there are very interesting questions to answer in future research.

One last comment regarding the estimates of amplitudes and phases shown in Tables 8.1 and 8.2 is in order. Both the “biennial” and annual constituents of the oceanic contribution towards  $\Delta LOD$  are well above three standard deviations. However, the  $\Delta ROAM$  time series associated accuracies have not been considered in the numerical procedures that compute the amplitude and phase, simply because the LSSA computer algorithm does not make provisions for it. In possible future work, we plan to incorporate alternative spectral analysis techniques that

may offer the advantage of including in the estimation process of the spectrum the associated accuracies of the time series.

In conclusion, for the Nov'86-Nov'88 period, we have constructed ocean inferred  $\Delta LOD$  time series from GEOSAT satellite altimetry data. We have analysed concurrent time series of observed  $\Delta LOD$  from VLBI observations and wind inferred  $\Delta LOD$  from the NMC forecast analyses. We have found that there is a strong connection between all three time series at the annual period, both in amplitude and phase from either spectral analysis runs (including or removing the event-like feature at day 932). There is also evidence that the oceans may have a relatively strong signal at the 55-155 days spectral band. From the residual spectral display (Figures 8.5, 8.6) it is seen that there are ocean related periodicities at the 121-day, 107.5-day, 89-day and shorter periods.

Longer, and preferably finer temporal resolution oceanic time series will confirm whether the above noted periods are playing an important role in inducing LOD variations at these frequencies. The oceans' role in  $\Delta LOD$  has just begun to be seriously investigated. Realistic oceanic global data bases are now becoming available. The future promises both global numerical ocean models using real time data and increased ocean coverage both in space and time from space-based platforms, and hence better chances to study the effect of ocean current variability on the length-of-day variations.



## **Chapter 9: Discussion, Conclusions, Future Considerations**

In this research we have tried to adopt a global perspective regarding the space-time variations of the ocean circulation. We have also tried to put these variations in the context of global changes occurring within the oceans - solid earth - atmosphere composite system. Within this context, we have discussed the exchange of axial angular momentum between the three system components (Chapters 7 and 8). It is important to note that the angular momentum is a global parameter (i.e., an integral quantity) characterizing the dynamical behaviour of the composite earth system over specific time scales. Once such a geophysical setting is adopted (i.e., earth system), then numerical studies can progress if the pertinent data bases for each system component are available. So far, the oceans have been the least well known, observationally speaking, global medium. Their influence on the earth's variable rotation rate was undervalued because it was difficult to quantify. In this dissertation we have shown that it is feasible with today's space-based observational techniques, to obtain routine determinations of synoptic ocean surface dynamics for earth rotation studies. With appropriate analytical modelling and numerical techniques, it is more than certain that tomorrow we will be able to explore more connections between the earth system

components. It is only a matter of time before we start probing the oceanic vastness and its dynamical links with global climate and *Global Change* at many space and time scales.

## **9.1. Summary of Research Investigations**

In this thesis research, we mostly concentrated on geodesy and physical oceanography as the disciplines that can provide the essential observational information and estimation techniques for the determination of the oceanic  $\Delta LOD$  excitation.

The main objective of the research reported here was to investigate the global ocean current variability in space and time and its effect on the length-of-day fluctuations. We have succeeded in establishing connections between the variable oceanic circulation and the LOD fluctuations at time scales between two months and two years. Satellite altimetry observations from the GEOSAT/ERM and in-situ oceanographic data provided the information needed to monitor the synoptic ocean surface dynamics and the mean seasonal 3-dimensional structure of the global ocean circulation, respectively.

One of the key objectives of the research was the development of techniques for extracting ocean current variability (especially from satellite altimetry) and the demonstration of the capability to provide routine determinations of axial relative oceanic angular momentum time series, under certain assumptions. The most challenging problem along this line of investigation (i.e., routine determination of ROAM) was and still is, the conversion of the satellite derived surface ocean current variability into 3-dimensional information on ocean dynamics. Here, we postulated that the surface

ocean current variability reflects the dynamics of the top 250m of the ocean water column, hence assuming that only the surface oceanic layer above the main thermocline is participating in the space-time fluctuations. Although this is a poor assumption, at least at this state of research it is a working assumption, until global data assimilation techniques become readily available in numerical ocean circulation forecast models. Such models will also improve the needed time resolution of the ROAM operational time series.

While developing the ROAM long-term mean seasonal time series from the in-situ oceanographic data, we generated a series of dynamic topography maps that by themselves are very important for geodetic and oceanographic studies of the absolute sea surface topography field, both in 3-d space and time. The usefulness of the derived maps extends further from their application towards the LOD research we carried out here. The computed mean seasonal difference-maps are especially useful for the study of the long-term mean behaviour of the ocean and the definition of the marine geoid.

A solid body of knowledge has been produced from the investigations performed using the GEOSAT/ERM satellite altimetry data. A new technique for directly extracting ocean current variability was developed and implemented. The power of the technique is demonstrated by the fact that we have processed two years of altimetry data (44 ERMs) with relative ease, using software that was written from scratch. Several important issues regarding the different error sources and their space-time behaviour that arose during the satellite altimetry data processing were discussed.

In our view, however, the most important aspect of our GEOSAT/ERM altimetry data analyses was the generation of the zonal current variability time series maps. They can be labelled the ocean current *zonal index* maps. They are valuable in describing the latitudinal structure of the ocean current variability, the role of high latitudes and tropical latitudes in exchange processes, and the relationship to dynamic processes occurring in the atmosphere, whose latitude structure is much better known.

In order to provide a better view of the effect of ocean current variability on the LOD, we have brought together oceanic as well as atmospheric and solid earth concurrent  $\Delta LOD$  time series. To our knowledge, no such attempt has been tried before, simply because direct oceanic data bases were not available for analysis. Although the comparison studies in this thesis work have not exhausted all the possibilities, the basic conclusion is that we have established a real and solid connection between  $\Delta LOD$  and ocean current variability. The implications of our investigations and the results on the  $\Delta LOD$  are discussed below.

## **9.2. Discussion of the Derived $\Delta LOD$ Results**

The time resolution of the analysed in-situ oceanographic data was inadequate for the study of the influence of temporal variations in the ocean current fields on  $\Delta LOD$ . Only long-term mean seasonal estimates of ROAM could be obtained, given the data availability at the time. Although the oceanographic estimates were just marginally useful for time series analysis, they did provide us with a “reference frame” for numerically comprehensive ROAM estimates and not simply “back of the envelope” calculations of what the oceanic budget ought to be. In addition, the oceanography derived estimates

provided us with a mean seasonal latitudinal structure of the ROAM budget which is also useful for relative order of magnitude studies between the different oceanic regions.

As a result of our investigations, periodic as well as irregular variations in the satellite altimetry derived  $\Delta ROAM$  were identified and quantified at periods between two months and two years. The analysed oceanic, atmospheric, and solid earth  $\Delta LOD$  concurrent time series span the period between November 1986 and November 1988. The analysed RAAM time series refer to the 1000 to 50 mbar atmospheric layer, thus they include a portion of the lower stratosphere as well.

The comparison studies between the three concurrent time series are the first of that kind ever reported, using  $\Delta ROAM$  data series that have been derived from direct observations of oceanic variability. The comparisons showed that the discrepancy at the annual period between the observed non-tidal  $\Delta LOD$  and the atmospheric wind excitation of  $\Delta LOD$  can be explained by the oceanic contribution, both in amplitude and phase (see the results in Table 8.2). The atmospheric pressure contribution towards the  $m_3^{matter}$  term (see Chapter 2), has not been included in our AAM analyses simply because data were not available to us at the time of the comparisons. It will be interesting to include in future comparative studies the contributions from the pressure term so that we can look at the complete picture of the ES angular momentum budget.

Furthermore, the residual spectra of the three concurrent time series (see superposition plot of spectra, Chapter 8), after the removal of linear trends and three periodic seasonal components (i.e., “biennial”, annual, and semi-annual) exhibit some common

characteristics at other frequencies as well. Statistically significant spectral peaks in the oceanic excitation of  $\Delta LOD$  have been found at periods of 121, 107.5 and 89 days, with amplitudes of the order of  $0.025 \pm 0.009$  ms (preliminary analysis results). These periodicities do not really surprise us, since they fall within the expected time scales of intermediate scale oceanic eddy fields.

Another interesting observation from the spectral analyses of the time series is the linear trend of the oceanic excitation during the Nov. 1986 - Nov. 1988 period. It has the same magnitude and direction (i.e., positive) as the linear trend found in the differenced- $\Delta LOD$  (observed minus atmospheric wind excitation). This agreement of the linear trends from the 2-year long time series will have important ramifications regarding the long-term influence of the oceans on the variable LOD. Analysis of longer oceanic time series will confirm whether this is the case or not.

The periodicity which we have labelled in this dissertation as “biennial” is indeed in question. Longer oceanic time series are needed to confirm its real presence. The low frequency signal is the result of the irregular increase in  $\Delta ROAM$  that occurred about June - July of 1988. In any event, whether it is a periodic or irregular signal or an artifact even, longer oceanic time series will provide us with some answers.

In conclusion, the oceanic excitation of  $\Delta LOD$  was found to be of the order of 0.15 ms, i. e., at a level that is above the current  $\Delta LOD$  observational noise of 0.05 to 0.10 ms.

A relatively strong oceanic signal at the annual period was identified and quantified (  $0.052 \pm 0.011$  *ms* from Table 8.2 or  $0.026 \pm 0.008$  *ms* from Table 8.3) ) which is large enough to explain the discrepancy at this period between observed and atmospheric wind inferred  $\Delta LOD$ , and thus reassure us that the oceanic variable circulation is the most serious contender for the presently unexplained angular momentum imbalances between the solid earth - atmosphere components.

No strong evidence of a semi-annual variation was found in the oceanic excitation time series. This conforms with previous investigations that have reported on the explanation of the semi-annual imbalance due to the non-inclusion of the upper stratospheric winds in the RAAM budget.

From our analysis of the spectral content of the differenced- $\Delta LOD$  time series, it is evident that there is considerable percentage variance at a period of approximately 53 days. It is conceivable that this period may be explained by the lack of upper stratospheric winds in the RAAM budget. From the present oceanic time series there is no evidence for such periodicity.

Again, from the residual spectra of the oceanic time series, there appears to be a broad spectral peak at a period between 200 and 300 days but not statistically significant. It will be interesting to investigate this periodicity when longer oceanic time series become available.

Finally, the satellite altimetry derived  $\Delta ROAM$  leaves room for considerable future improvements, both in terms of time resolution, absolute magnitude and accuracy, as we shall see in the next and last section.

### 9.3. Future Research Issues

The research reported in this thesis work did not provide all the answers to the problem of oceanic excitation of  $\Delta LOD$ . On the contrary, we believe that our investigations generated more questions regarding the role of the oceans in  $\Delta LOD$  studies as well as in ocean dynamics and ocean - atmosphere coupling. We dare say that our results call for more vigorous and rigorous investigations of oceanic variability and its effect on the Earth System dynamics.

We have identified two major directions for future research. One deals with possible refinements of the techniques of data processing reported in this thesis, while the second deals with future advancements in the generation of oceanic data bases and their effective usage for  $\Delta LOD$  studies.

With regard to the refinements of the techniques and procedures developed in this dissertation, we see the following, immediately achievable goals:

- (a) Analysis of the whole 3-year long GEOSAT/ERM data base, i.e., from November 1986 till November 1989.
- (b) The 3-year long GEOSAT/ERM data base will allow the analysis of year-to-year ocean current variability and will provide us with a confir-



mation of low frequency signals in the oceanic  $\Delta LOD$  . In addition, the connection with SOI variations will be particularly interesting to investigate further.

- (c) For both steps (a) and (b) above, we recommend that the analysis of the altimetric data records be carried out using the GSFC/CCAR orbits instead of the NAG operational orbits included in the GDRs. Although the gradient technique we developed and applied to extract sea surface slope variability reduces most of the long wavelength orbital error, the GSFC/CCAR orbits are demonstrably more accurate and thus, we expect less influence on the sea surface slopes from the higher than 1 cy/rev orbital errors.
  
- (d) We also recommend the use of an alternative reference geoid surface, instead of the one embedded in the GEOSAT GDRs. A more precise reference geoid surface such as the SEASAT derived mean sea surface, is in our opinion required, since it reflects much closer the actual average geoid gradients. Moreover, the GEOSAT/ERM ground track was designed specifically to duplicate the SEASAT ground track; thus the SEASAT derived mean sea surface [Marsh *et al.*, 1986] is a very meaningful choice. Although, again, the use of a reference geoid surface is not required for oceanic variability determinations, we have used the reference geoid for many editing and screening criteria during pre-processing and processing of the altimetry data. Thus, we expect that the replacement of the reference

geoid surface will change the data rejection statistics in the sea surface slope “validation” processing step.

- (e) One of the serious problems we were faced with was the incomplete coverage of the  $1^{\circ}$  by  $1^{\circ}$  grid of ascending and/or descending SST average gradients. In order to salvage as much as possible of the single-track observed gradient information, we resorted to a crude interpolation procedure which utilized the basin-wide zonal average gradients (what we called a primitive objective analysis interpolation technique). More work along this line has to be done, to render useful the partially observed along track sea surface gradients.
- (f) A particular aspect of the work reported here is the ocean current velocity zonal average variability maps presented in Chapter 6 and Appendix I. One of the planned extensions of the present work for the near future is to use empirical orthogonal function (EOF) analysis techniques (see, for example, *Lau et al.* [1989]) in order to determine the space-time spectrum (wavenumber / frequency) of the two year long zonal current variability time series. We believe that the EOF results are going to be extremely interesting regarding the space-time principal normal modes of this data series (or of the 3-year long one).
- (g) A major assumption was made during the course of this study. Once the ocean current variability time-frames were computed, in order to use them as input files into the ROAM estimation process, we postulated that the

surface  $u^*$ -fields reflect the dynamics of the current velocity field of the top 250m thick oceanic surface layer. We have argued that this is a poor but generally reasonable assumption. However, this assumption has to be replaced in any future work. The transfer of surface observations to subsurface information is a crucial aspect not only for the broad scope problem of oceanic circulation prediction, but also for  $\Delta LOD$  studies. This subject leads to the second major direction of future research that we have identified and which is related to future advancements in oceanic data bases and improved numerical techniques to analyse these data bases.

Regarding the future advancements in oceanic data bases we would like to draw attention to the major oceanographic experiments scheduled for the early 1990s such as the TOPEX/POSEIDON altimetry mission and the concurrent WOCE oceanographic experiment. These major oceanic experiments will offer more accurate and comprehensive oceanic data sets than before. However, the forerunner GEOSAT/ERM data base and the interim SALT altimetry mission (scheduled between the GEOSAT and the TOPEX/POSEIDON mission), will allow 10-12 years of almost continuous ocean monitoring.

On the numerical front, the initial simulation studies of dynamic transfer of altimetry derived ocean surface data into subsurface information through the use of numerical ocean circulation models (see, for example, *Marshall* [1985], *Hurlburt* [1986], *Kindle* [1986], *Thomson* [1986], *Rao et al.* [1987], *Robinson & Walstad* [1987a; 1987b]), will give us a real chance to obtain the full 4-dimensional oceanic circulation picture very

soon. The subject of oceanic excitation of  $\Delta LOD$  is in my opinion just starting, with yet many undiscovered ramifications for the dynamics of the Earth System.

## REFERENCES

- Akima, H. [1978]. "A Method of Bivariate Interpolation and Smooth Surface Fitting for Irregularly Distributed Data Points", *ACM Transaction on Mathematical Software*, Vol. 4, 148-159.
- Anderson, A. J. and A. Cazenave, eds. [1986]. *Space Geodesy and Geodynamics*. Academic Press, London, G.B.
- Baker, D. J. [1982]. "A Note on Sverdrup Balance in the Southern Ocean", *Journal of Marine Research*, Vol. 40 (suppl.), 21-26.
- Baker, D. J., W. D. Nowlin, R. D. Pillsbury and H. L. Bryden [1977]. "Antarctic Circumpolar Current: Space and Time Fluctuations in the Drake Passage", *Nature*, Vol. 268, 696-699.
- Barnes, R. T. H., R. Hide, F. R. S. White and C. A. Wilson [1983]. "Atmospheric Angular Momentum Fluctuations, Length-of-Day Changes and Polar Motion", *Proceedings of the Royal Society of London, A*, 31-37.
- Born, G. H., D. M. Lame and J. L. Mitchell [1984]. "A Survey of Oceanographic Satellite Altimetric Missions", *Marine Geodesy*, Vol. 8, No. 1-4, 3-16.
- Born, G. H., P.C. Allen and A. Pino [1988]. "Orbit Analysis for the GEOSAT-ERM", *Journal of the Astronautical Sciences*, Vol. 36, No. 4, 425-446.
- Bradley, R. S., H. F. Diaz, G. N. Kiladis and J. K. Eischeid [1987]. "ENSO Signal in Continental Temperature and Precipitation Records", *Nature*, Vol. 327, 497-501.
- Brosche, P. and J. Sundermann [1985]. "The Antarctic Circumpolar Current and Its Influence on the Earth's Rotation", *Deutsche Hydrographische Zeitschrift*, Vol. 38, 1-6.

- Brown, G. S. [1977]. "The Average Impulse Response of a Rough Surface and Its Applications", *IEEE Journal of Oceanic Engineering*, Vol. OE-2, 67-74.
- Brown, G. [1979]. "Estimation of Surface Wind Speeds Using Satellite Borne Radar Measurements at Normal Incidence", *Journal of Geophysical Research*, Vol. 84, B8, 3974-3978.
- Bryden, H. L. and R. D. Pillsbury [1977]. "Variability of Deep Flow in the Drake Passage from Year-Long Current Measurements", *Journal of Physical Oceanography*, Vol. 7, 803-810.
- Capitaine, N. [1986]. "The Conceptual and Conventional Definitions of the Earth Rotation Parameters", in *Earth Rotation: Solved and Unsolved Problems*, A. Cazenave, ed., D. Reidel Publ. Co., Dordrecht.
- Carter, W. E. and D. S. Robertson [1984]. "IRIS Earth Rotation and Polar Motion Results", in *Proceedings of Int. Symp. Space Techniques for Geodynamics*, Sopron, Hungary.
- Carter, W. E., D. S. Robertson, J. E. Pettey, B. D. Tapley, B. E. Schutz, R. J. Eanes and Miao Lufeng [1984]. "Variations in the Rotation of the Earth", *Science*, Vol. 224, 957-961.
- Carter, W. E. and D. S. Robertson [1985]. "High Frequency Variations in the Rotation of the Earth", *IEEE Transactions on Geoscience and Remote Sensing*, Vol. GE-23, No. 4, 369-372.
- Carter, W. E. and D. S. Robertson [1986]. "Accurate Earth Orientation Time Series from VLBI Observations", in *Earth Rotation: Solved and Unsolved Problems*, A. Cazenave, ed., D. Reidel Publ. Co., Dordrecht.
- Carton, J. A. and E. J. Katz [1990]. "Estimates of the Zonal Slope and Seasonal Transport of the Atlantic North Equatorial Countercurrent", *Journal of Geophysical Research*, Vol. 95, No. C3, 3091-3100.
- Cazenave, A., ed. [1986]. *Earth Rotation: Solved and Unsolved Problems*. D. Reidel Publ. Co., Dordrecht.
- Chao, B. F. [1988]. "Correlation of Interannual Length-of-Day Variations with El Nino/Southern Oscillation, 1972-1986", *Journal of Geophysical Research*, Vol 93, B7, 7709-7715.

- Chao, B. F. [1989]. "Length-of-Day Variations Caused by El Nino/Southern Oscillation and the Quasi-Biennial Oscillation", *Science*, Vol. 243, 923-925.
- Chelton, D. B. [1988]. "World Ocean Circulation Experiment: WOCE/NASA Altimeter Algorithm Workshop", *United States WOCE Technical Report No. 2*, November.
- Chelton, D. B., K. J. Hussey and M. E. Parke [1981]. "Global Satellite Measurements of Water Vapour, Wind Speed, and Wave Height", *Nature*, Vol. 294, 529-532.
- Cheney, R. E. and B. C. Douglas [1990]. "GEOSAT Ends", *EOS, Transactions of the American Geophysical Union*, Vol. 71, No. 6.
- Cheney, R. E. and J. G. Marsh [1981]. "SEASAT Altimeter Observations of Dynamic Topography in the Gulf Stream Region", *Journal of Geophysical Research*, Vol. 86, 473-483.
- Cheney, R. E., J. G. Marsh and B. D. Beckley [1983]. "Global Mesoscale Variability from Collinear Tracks of SEASAT Altimeter Data", *Journal of Geophysical Research*, Vol. 88, 4343-4354.
- Cheney, R. E., B. C. Douglas, R. W. Agreen, L. Miller, D. L. Porter, and N. S. Doyle [1987]. "GEOSAT Altimeter Geophysical Data Record User Handbook", *NOAA TM NOS NGS-46*.
- Cheney, R. E., L. Miller, B. C. Douglas, and R. W. Agreen [1987]. "Monitoring Equatorial Pacific Sea Level with GEOSAT", Johns Hopkins APL, *Technical Digest*, Vol. 8, Number 2.
- Christou, N. [1984]. "On the Effect of Ocean Currents on the Length-of-Day", PhD thesis research proposal submitted to the Department of Surveying Engineering, University of New Brunswick, Fredericton, December.
- Christou, N. and R.B. Langley [1988]. "Estimates of the Angular Momentum of the Global Ocean Derived from Mean Seasonal Dynamic Topography Fields", paper presented at the American Geophysical Union Spring Meeting, Baltimore, MD, USA, 16-20 May (abstract: *EOS, Transactions of the American Geophysical Union*, Vol. 69, No. 16, pp. 327).
- Coleman, [1981]. "A Geodetic Basis for Recovering Ocean Dynamic Information from Satellite Altimetry", *UNISURV S-19*, University of New South Wales, Kensington, Australia.

- Colombo, O. [1984]. "Altimetry, Orbits and Tides", *NASA Technical Memorandum 86160*, Goddard Space Flight Center, Greenbelt.
- Dickey, J. O. [1989]. "Atmospheric Excitation of the Earth's Rotation", *JPL Geodesy and Geophysics Preprint Series, No. 180*, Jet Propulsion Laboratory, California Institute of Technology, Pasadena, California.
- Dickey, J. O. and T. M. Eubanks [1985]. "Earth Rotation and Polar Motion: Measurements and Implications", *IEEE Transactions on Geoscience and Remote Sensing, Vol. GE-23*, 373-384.
- Dickey, J. O. and T. M. Eubanks [1986]. "The Application of Space Geodesy to Earth Orientation Studies", in *Space Geodesy and Geodynamics*, A. J. Anderson and A. Cazenave, eds., Academic Press, London.
- Dickey, J. O., B. E. Schutz, S. R. Dickman, T. M. Eubanks, M. Feissel, T. A. Herring, I.I Mueller, R. D. Rosen, J. M. Wahr and C. R. Wilson [1989]. "Earth Rotation Reference Frames", Science Panel Position Paper, *JPL Geodesy and Geophysics Preprint Series, No. 176*, Jet Propulsion Laboratory, California Institute of Technology, Pasadena, California.
- Dickson, R. R., W J. Gould, P. A. Gurbutt and P. D. Killworth [1982]. "A Seasonal Signal in Ocean Currents to Abyssal Depths", *Nature, Vol. 295*, 193-198.
- Douglas, B. C., R. W. Agreen and D. T. Sandwell [1984]. "Observing Global Ocean Circulation with SEASAT Altimeter Data", *Marine Geodesy, Vol. 8, Nos. 1-4*, 67-83.
- Duing, W. [1978]. "Spatial and Temporal Variability of Major Ocean Currents and Mesoscale Eddies", *Boundary Layer Meteorology, Vol. 13*, 7-22.
- Duxbury, A. C. [1971]. *The Earth and its Oceans*. Addison - Wesley Publ. Co., Reading, Massachusetts.
- Eanes, R. J., B. E. Schutz and B. D. Tapley [1984]. "Earth Rotation from LAGEOS. The 1984 CSR System", *EOS, Transactions of the American Geophysical Union, Vol.65, No. 16*, 187-188.
- Engelis, T. [1987]. "Radial Orbit Error Reduction and Sea Surface Topography Determination Using Satellite Altimetry", Department of Geodetic Science and Surveying, *Report No. 377*, The Ohio State University, Columbus, Ohio.



- Engelis, T. and P. Knudsen [1989]. "Orbit Improvement and Determination of the Ocean Geoid and Topography from 17 Days of Seasat Data", *manuscripta geodaetica, Vol.14*, 193-201.
- Eubanks, T. M., J. O. Dickey and J. A. Steppe [1984]. "The Geophysical Significance of Systematic Errors in the Earth's Angular Momentum Budget", *Proceedings of the International Association of Geodesy Symposia, International Union of Geodesy and Geophysics (IUGG) XVIII-th General Assebly (Hamburg, F.R.G.)*, Vol. 2, 122-143.
- Eubanks, T. M., J. O. Dickey and J. A. Steppe [1986]. "The El Nino, the Southern Oscillation and the Earth's Rotation", in *Earth Rotation: Solved and Unsolved Problems*, A. Cazenave ed., D. Reidel Publ. Co., Dordrecht.
- Eubanks, T. M., J. A. Steppe, J. O. Dickey and P. S. Callahan [1985]. "A Spectral Analysis of the Earth's Angular Momentum Budget", *Journal of Geophysical Research, Vol. 90*, 5385-5404.
- Ewing, G. C., ed. [1965]. *Oceanography from Space*. Woods Hole Oceanographic Institute, Woods Hole, MA.
- Fedor, C. S., T. W. Godbey, J. F. R. Gower, R. Guphill, G. S. Hayne, C. L. Rufenach and E. J. Walsh [1979]. "Satellite Altimeter Measurements of Sea State - An Algorithm Comparison", *Journal of Geophysical Research, Vol. 84, B8*, 3991-4002.
- Fofonoff, N. P. [1962]. "Physical Properties of Sea Water", in *The Sea*, Vol. 1, M. N. Hill, ed., Wiley, New York.
- Fofonoff, N. P. and R. N. Millard Jr. [1983]. "Algorithms for Computation of Fundamental Properties of Sea Water", in *UNESCO Technical Papers in Marine Science, Vol. 44*.
- Fomin, L. M. [1964]. *The Dynamic Method in Oceanography*. Elsevier, Amsterdam.
- Frain, W. E., M. H. Barbagallo, and R. J. Harvey [1987]. "The Design and Operation of GEOSAT", Johns Hopkins APL, *Technical Digest, Vol. 8, Number 2*.
- Fu, L-L. [1983]. "On the Wavenumber Spectrum of Oceanic Mesoscale Variability Observed by the SEASAT Altimeter", *Journal of Geophysical Research, Vol. 88*, 4331-4341.

- Fu, L-L. and D. B. Chelton [1984]. "Observing Large-Scale Temporal Variability of Ocean Currents by Satellite Altimetry : With Application to the Antarctic Circumpolar Current", *Journal of Geophysical Research*, Vol. 90, 4721-4739.
- Georgi, D. T. and J. M. Toole [1982]. "The Antarctic Circumpolar Current and the Oceanic Heat and Fresh-Water Budgets", *Journal of Marine Research*, Vol. 40 (suppl.), 183-197.
- Gonella, J. A. [1986]. "Ocean-Atmosphere Coupling and Short Term Fluctuations of Earth Rotation", in *Earth Rotation: Solved and Unsolved Problems*, A. Cazenave, ed., D. Reidel Publ. Co., Dordrecht.
- Gonzalez, R. C. and P. Wintz [1987]. *Digital Image Processing*. Addison - Wesley Publ. Co., second edition.
- Gower, J. F. R., ed. [1981]. *Oceanography from Space*. Plenum Press, New York.
- Greenwood, J. A., A. Nathan, G. Neumann, W. J. Pierson, F. C. Jackson and T. E. Pease [1969]. "Oceanographic Applications of Radar Altimetry from a Spacecraft", *Remote Sensing Environment*, Vol. 1, 71-80.
- Gross, R. S., J. A. Steppe and J. O. Dickey [1989]. "The Yearly rms Difference between AAM and LOD During 1987-1988", paper presented at the NASA Crustal Dynamics Project Principal Investigators Meeting, October 24-25, Greenbelt, MD.
- Haines, B. J., G. H. Born, J. G. Marsh and R. Williamson [1988]. "Precise GEOSAT Orbits for the Exact Repeat Mission Using the GEM-T1 Gravity Solution", paper presented at the 1988 American Geophysical Union Fall Meeting, San Fransisco, CA.
- Harder, R. L. and R. N. Desmarais [1972]. "Interpolation Using Surface Splines", *Journal of Aircraft*, Vol. 9, 189-191.
- Hayne, G. S. and D. W. Hancock [1982]. "Sea-State Related Altitude Errors in the SEASAT Radar Altimeter", *Journal of Geophysical Research*, Vol. 87, C5, 3227-3231.
- Hide, R. [1985]. "Rotation of the Atmospheres of the Earth and Planets", *Phil. Trans. R. Soc. Lond., Series A., Vol. 313*, 107-121.
- Holland, W. R. and J. C. McWilliams [1987]. "Computer Modelling in Physical Oceanography from the Global Circulation to Turbulence", *Physics Today*, 51-57, October issue.

- Holland, W. R., D. E. Harrison and A. J. Semtner [1983]. "Eddy - Resolving Numerical Models of the Large - Scale Ocean Circulation", in *Eddies in Marine Science*, A. R. Robinson Edt., Springer - Verlag, Berlin.
- Huang, N. E., C. D. Leita0 and C. G. Parra [1978]. "Large - Scale Gulf Stream Frontal Study Using GEOS-3 Radar Altimeter Data", *Journal of Geophysical Research*, Vol. 83, C9, 4673-4682.
- Hurlburt, H. E. [1984]. "The Potential for Ocean Prediction and the Role of Altimeter Data", *Marine Geodesy*, Vol. 8, Nos. 1-4, 17-66.
- Hurlburt, H. E. [1986]. "Dynamic Transfer of Simulated Altimeter Data Into Subsurface Information by a Numerical Ocean Model", *Journal of Geophysical Research*, Vol. 91, C2, 2372-2400.
- Johns, C. M., R. J. Eanes and B. D. Tapley [1989]. "Recent Work on the Latitude Structure of the Atmospheric '40-60 Day' Oscillation", paper presented at the American Geophysical Union Fall Meeting, San Fransisco, CA.
- Johns, C. M., J. O. Dickey, T. M. Eubanks and J. A. Steppe [1987]. "The Role of the Antarctic Circumpolar Current in the Earth's Angular Momentum Budget", paper presented at the American Geophysical Union Fall Meeting, San Fransisco, CA, (abstract : *EOS, Transactions of the American Geophysical Union*, Vol. 68, No. 44, pp.1244).
- Johnson, M. A. [1989]. "Forcing the Volume Transport Through Drake Passage", *Journal of Geophysical Research*, Vol. 94, C11, 16115-16124.
- Kerr, R. A. [1988]. "La Nina's Big Chill Replaces El Nino", *Science*, Vol. 241, 1037-1038.
- Kindle, J. C. [1986]. "Sampling Strategies and Model Assimilation of Altimetric Data for Ocean Monitoring and Prediction", *Journal of Geophysical Research*, Vol. 91, C2, 2418-2432.
- Kort, V. G. [1962]. "The Antarctic Ocean", *Scientific American*, Vol. 207, 103-112.
- Lamb, H. H. [1972]. *Climate, Present, Past and Future*. Methuen, London.
- Lambeck, K. [1980]. *The Earth's Variable Rotation. Geophysical Causes and Consequences*. Cambridge University Press, London.

- Lambeck, K. and P. Hopgood [1982]. "The Earth's Rotation and Atmospheric Circulation: 1958-1980", *Geophysical Journal of the Royal Astronomical Society*, Vol. 71, 581-587.
- Langley, R.B., R. W. King and I. I. Shapiro, R. D. Rosen and D. A. Salstein [1981]. "Atmospheric Angular Momentum and the Length of the Day: A Common Fluctuation with a Period Near 50 Days", *Nature*, Vol. 294, 730-733.
- Lau, K.-M., In-Sik Kang and P. J. Sheu [1989]. "Principal Modes of Intraseasonal Variations in Atmospheric Angular Momentum and Tropical Convection", *Journal of Geophysical Research*, Vol. 94, No. D5, 6319-6332.
- Levitus, S., [1982]. "Climatological Atlas of the World Ocean", *NOAA Prof. Pap. No. 13*, U.S. Government Printing Office, Washington, DC, 173pp.
- Levitus, S. and C. J. Koblinsky [1989]. "Fourier Analysis of the Climatological Annual Cycle of Steric Sea Level (0-1000) of the World Ocean", preprint, (to be submitted to *Journal of Marine Research*).
- Luo, S., D. Zheng, D. S. Robertson and W. E. Carter [1987]. "Short Period Variations in the Length of Day. Atmospheric Angular Momentum and Tidal Components", *Journal of Geophysical Research*, Vol. 92, B11, 11657-11661.
- Lybanon, M. and R. L. Crout [1987]. "The NORDA GEOSAT Ocean Applications Program", Johns Hopkins APL, *Technical Digest*, Vol. 8, Number 2.
- MacArthur, J. L., P. C. Marth, and J. G. Wall [1987]. "The GEOSAT Radar Altimeter", Johns Hopkins APL, *Technical Digest*, Vol. 8, Number 2.
- Malanotte-Rizzoli, P. [1982]. "The Predictability Problem of Planetary Motions in the Atmosphere and the Ocean", in *Topics in Ocean Physics*, A. R. Osborne ed., *Proceedings of the International School of Physics "Enrico Fermi"*, Course LXXX, Varena on Lake Como, July 1980.
- Mamayev, O. I. [1975]. *Temperature Salinity Analysis of World Ocean Waters*. Elsevier, Amsterdam.
- Marchuk, G. I. and A. S. Sarkisyan [1989]. *Mathematical Modelling of Ocean Circulation*. Springer - Verlag, Berlin.
- Marsh, J. G., F. J. Lerch, C. J. Koblinsky, S. M. Klosko, J. W. Robbins, R. G. Williamson and G. B. Patel [1988]. "Dynamic Sea Surface Topography, Gravity

and Improved Orbital Accuracies from the Direct Evaluation of SEASAT Altimetry”, Draft Manuscript, Goddard Space Flight Center, Greenbelt, MD.

Marsh, J. G., A. C. Brenner, B. D. Beckley and T. V. Martin [1986]. “Global Mean Sea Surface Based on the SEASAT Altimeter Data”, *Journal of Geophysical Research*, Vol. 91, B3, pp. 3501-3506.

Marshall, J. C. [1985]. “Determining the Ocean Circulation and Improving the Geoid from Satellite Altimetry”, *Journal of Physical Oceanography*, Vol. 15, 330-349.

Maul, G. A., A. G. Mourad, P. Wilson, O. H. Shemdin, R. H. Estes and G. Weiffenbach [1980]. “Report on International Symposium on Interaction of Marine Geodesy and Ocean Dynamics”, *Marine Geodesy*, Vol. 3, No. 1-4, 3-24.

Mazegga, P. [1986]. “How Radial Orbit Errors Are Mapped in Altimetric Surfaces”, *Journal of Geophysical Research*, Vol. 91, C5, 6609-6628.

McCarthy, D. D. and A. K. Babcock [1985]. “The Length of Day since 1663”, Special Study Group 5-98: Atmospheric Excitation of the Earth's Rotation Bulletin No. 2, Jet Propulsion Laboratory, Pasadena, California.

McConathy, D. R. and C. C. Kilgus [1987]. “The Navy GEOSAT Mission : An Overview”, Johns Hopkins APL, *Technical Digest*, Vol. 8, Number 2.

McGoogan, J. T. [1975]. “Satellite Altimetry Applications”, *IEEE Transaction in Microwave Theory Techniques*, Vol. 23, 970-978.

McPhaden, M. J., S. P. Hayes and L. J. Magnum [1990]. “Variability in the Western Equatorial Pacific Ocean during the 1986-87 El Nino / Southern Oscillation Event”, *Journal of Physical Oceanography*, Vol. 20, 190-207.

McWilliams, J. C. [1984]. “A Concept of WOCE”, in *Large - Scale Oceanographic Experiments and Satellites*, C. Gautier and M. Fieux, eds., D. Reidel Publ. Co., Dordrecht.

Meinguet, J. [1979]. “Multivariate Interpolation at Arbitrary Points Made Simple”, *Journal of Applied Mathematics and Physics*, Vol. 30, 292-304.

Mignard, F. [1986]. “Tidal and Non Tidal Acceleration of the Earth's Rotation”, in *Earth Rotation: Solved and Unsolved Problems*, A. Cazenave, ed., D. Reidel Publ. Co., Dordrecht.

- Miller, L., R. E. Cheney and B. C. Douglas [1988]. "GEOSAT Altimeter Observations of Kelvin Waves and the 1986-87 El-Nino", *Science*, Vol. 239.
- Miller, L. and D. Hammond [1972]. "Objectives and Capabilities of the Skylab S-193 Altimeter Experiment", *IEEE Transactions in Geoscience and Electronics*, Vol. GE-10, 73.
- Mitchell, J. L., Z. R. Hallock and J. D. Thompson [1987]. "REX and GEOSAT : Progress in the First Year", Johns Hopkins APL, *Technical Digest*, Vol. 8, Number 2.
- Monin, A. S., V. M. Kamenkovich and V. G. Kort [1977]. *Variability of the Oceans*. John Wiley & Sons, New York.
- Montgomery, R. B. [1969]. "Comments on Oceanic Levelling", *Deep Sea Research*, Vol. 16 (suppl), 147-152.
- Morabito, D. D., T. M. Eubanks and J. A. Steppe [1986]. "Kalman Filtering of Earth Orientation Changes", paper presented at the IAU Symposium No 128, The Earth's Rotational Reference Frames for Geodesy and Geodynamics, Coolfont, W. Virginia, October 20-24.
- Morabito, D. D., T. M. Eubanks and J. A. Steppe [1988]. "Kalman Filtering of Earth Orientation Changes", in *The Earth's Rotation and Reference Frames for Geodesy and Geodynamics*, Proceedings of the 128-th Symposium of the IAU, Babcock and Wilkins, eds., Kluwer Academic Publishers, Dordrecht, 257-268.
- Morgan, P. J., R. W. King and I. I. Shapiro [1985]. "Length of Day and Atmospheric Angular Momentum: A Comparison for 1981-1983", *Journal of Geophysical Research*, Vol. 90, B14, 12645-12652.
- Moritz, H. and I. I. Mueller [1987]. *Earth Rotation: Theory and Observation*. Ungar, New York.
- Munk, W. H. and G. J. F. MacDonald [1960]. *The Rotation of the Earth*. Cambridge University Press, London.
- Neumann, G. and W. J. Pierson [1966]. *Principles of Physical Oceanography*. Prentice Hall Inc., Englewood Cliffs, New Jersey.
- NOAA [1985]. "Climatological Atlas of the World Ocean, Seasonal Five-Degree Square Statistics", *NODC Environmental Information Bulletin*, No. 85-1, U.S. Department of Commerce, Washington, DC.

- Nova University [1983]. "Satellite Data Relay and Platform Locating in Oceanography", Report of the In-situ Ocean Science Group, N.Y.I.T. Press, Fort Lauderdale, Florida.
- Nowlin, W. D. and M. Clifford [1982]. "The Kinematic and Thermohaline Zonation of the Antarctic Circumpolar Current at Drake Passage", *Journal of Marine Research*, Vol. 40 (suppl.), 481-507.
- Nowlin, W. D. and J. M. Klink [1986]. "The Physics of the Antarctic Circumpolar Current", *Reviews of Geophysics and Space Physics*, Vol. 24, No. 3, 469-491.
- Nowlin, W. D., T. Whitworth III and R. D. Pillsbury [1977]. "Structure and Transport of the Antarctic Circumpolar Current at Drake Passage from Short Term Measurements", *Journal of Physical Oceanography*, Vol. 7, 788-802.
- Oort, A. H. and J. P. Peixoto [1986]. "Global Angular Momentum and Energy Balance Requirements from Observations", in *Theory of Climate*, B. Saltzman, ed., Academic Press, New York.
- Ottmans, S. J. and J. London [1982]. "The Quasi-Biennial Oscillation in Atmospheric Ozone", *Journal of Geophysical Research*, Vol. 87, No. 11, 8981-8989.
- Paquet, P. [1986]. "How to Measure the Earth Rotation", in *Earth Rotation: Solved and Unsolved Problems*, A. Cazenave, ed., D. Reidel Publ. Co., Dordrecht.
- Parsons, C. L. [1979]. "GEOS-3 Wave Height Measurements: Assessment During High Sea State Conditions in the North Atlantic", *Journal of Geophysical Research*, Vol. 84, B8, 4011-4020.
- Pavlidis, T. [1982]. *Algorithms for Graphics and Image Processing*. Computer Science Press Inc., Rockville, MD.
- Peterson, R. G. [1988]. "On the Transport of the Antarctic Circumpolar Current Through Drake Passage and Its Relation to Wind", *Journal of Geophysical Research*, Vol. 93, C11, 13993-14004.
- Phillander, S. G. H. [1983]. "El Nino Southern Oscillation Phenomena", *Nature*, Vol. 302, 295-301.
- Pisacane, V. L. [1986]. "Satellite Techniques for Determining the Geopotential of Sea Surface Elevations", *Journal of Geophysical Research*, Vol. 91, C2, 2365-2371.

- Pond, S. and G. L. Pickard [1983]. *Introductory Dynamic Oceanography*. Pergamon Press, Oxford.
- Rao, D. B., S. D. Steenrod and B. V. Sanchez [1987]. "A Method of Calculating the Total Flow from a Given Sea Surface Topography", *NASA Technical Memorandum 87799*.
- Reid, J. L. [1986]. "On the Total Geostrophic Circulation of the South Pacific Ocean. Flow Patterns, Tracers and Transports", *Prog. Oceanogr.*, Vol. 16, 1-61.
- Rhines, P. B. [1979]. "Geostrophic Turbulence", *Annual Review of Fluid Mechanics*, Vol. 11, 401-441.
- Robertson, D. S., W. E. Carter, J. Cambell and H. Schuh [1985]. "Daily Earth Rotation Determinations from IRIS Very Long Baseline Interferometry", *Nature*, 316, 424.
- Robinson, A. R., ed. [1983a]. *Eddies in Marine Science*. Springer - Verlag, Berlin.
- Robinson, A. R., [1983b]. "Overview and Summary of Eddy Science", in *Eddies in Marine Science*. Robinson, ed., Springer - Verlag, Berlin.
- Robinson, A. R. and L. J. Walstad [1987a]. "The Harvard Open Ocean Model: Calibration and Application to Dynamical Process, Forecasting, and Data Assimilation Studies", *Journal of Applied Numerical Mathematics*, Vol. 3, 89-131.
- Robinson, A. R. and L. J. Walstad [1987b]. "Altimetric Data Assimilation for Ocean Dynamics and Forecasting", Johns Hopkins APL, *Technical Digest*, Vol. 8, Number 2, 267-271.
- Roemmich, D. and C. Wunsch [1982]. "On Combining Satellite Altimetry with Hydrographic Data", *Journal of Marine Research*, Vol. 40 (suppl.), 605-619.
- Rosborough, G. W. [1986]. "Satellite Orbit Perturbations Due to Geopotential", PhD Thesis, University of Texas, Austin.
- Rosen, R. D. [1986]. "Meteorological Data for Earth Rotation Studies", in *Earth Rotation: Solved and Unsolved Problems*, A. Cazenave, ed., D. Reidel Publ. Co., Dordrecht.
- Rosen, R. D. and D. A. Salstein [1983]. "Variations in Atmospheric Angular Momentum on Global and Regional Scales and the Length of Day", *Journal of Geophysical Research*, Vol. 88, C9, 5451-5470.



- Rosen, R. D. and D. A. Salstein [1985]. "Contributions of Stratospheric Winds to Annual and Semi-annual Fluctuations in AAM and the Length of Day", *Journal of Geophysical Research*, Vol. 90, 8033-8041.
- Rosen, R. D., D. A. Salstein and T. Wood [1989]. "Discrepancies in the Earth - Atmosphere Angular Momentum Budget", paper submitted to the Journal of Geophysical Research, (preprint).
- Sandwell, D. T. and B. Zhang [1989]. "Global Mesoscale Variability from the GEOSAT Exact Repeat Mission: Correlation with Ocean Depth", *Journal of Geophysical Research*, Vol. 94, C12, 17971-17984.
- Schmitz, W. J. [1978]. "Observations of the Vertical Distribution of Low Kinetic Energy in the Western North Atlantic", *Journal of Marine Research*, Vol. 36, 295-310.
- Schwiderski, E. W. [1980]. "On Charting Global Tides", *Reviews of Geophysics and Space Physics*, Vol. 18, 243-268.
- Stewart, R. H. [1981]. "Satellite Altimetric Measurements of the Ocean", Report of the TOPEX Science Working Group, NASA-JPL, Pasadena, California.
- Stewart, R. H. [1985]. *Methods of Satellite Oceanography*. University of California Press, Berkeley, CA.
- Stewart, R. H., L-L. Fu and M. Lefebvre [1986]. "Science Opportunities from the TOPEX - Poseidon Mission", *Jet Propulsion Laboratory Publication 86-18*, Pasadena, CA.
- Stommel, H. and F. Schott [1977]. "The Beta-Spiral and the Determination of the Absolute Velocity Field from Hydrographic Station Data", *Deep Sea Research*, Vol. 24, 325-329.
- Tai, C. K. and L-L. Fu [1986]. "On Crossover Adjustment in Satellite Altimetry and Its Oceanographic Implications", *Journal of Geophysical Research*, Vol. 91, 2549-2554.
- Tai, C. K. and C. Wunsch [1983]. "Absolute Measurement by Satellite Altimetry of the Dynamic Topography of the Pacific Ocean", *Nature*, 296, 408-410.
- Tapley, B. D. and G. W. Rosborough [1985]. "Geographically Correlated Orbit Error and its Effect on Satellite Altimetry Missions", *Journal of Geophysical Research*, Vol. 90, C6, 11817-11831.

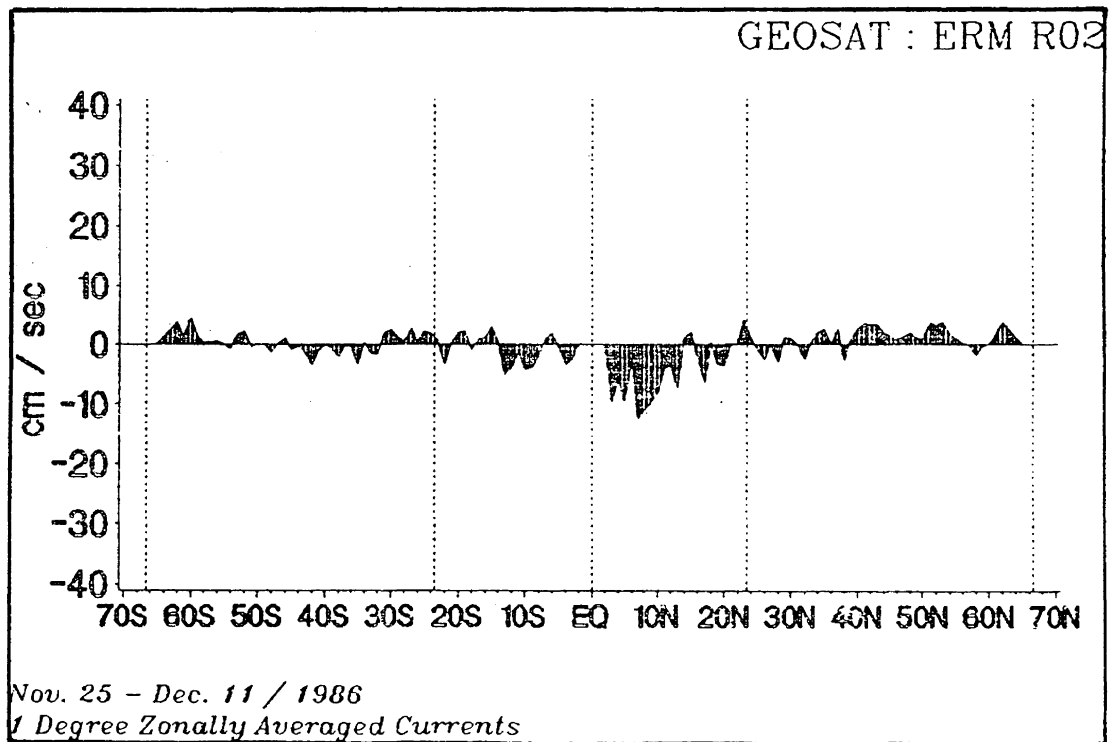
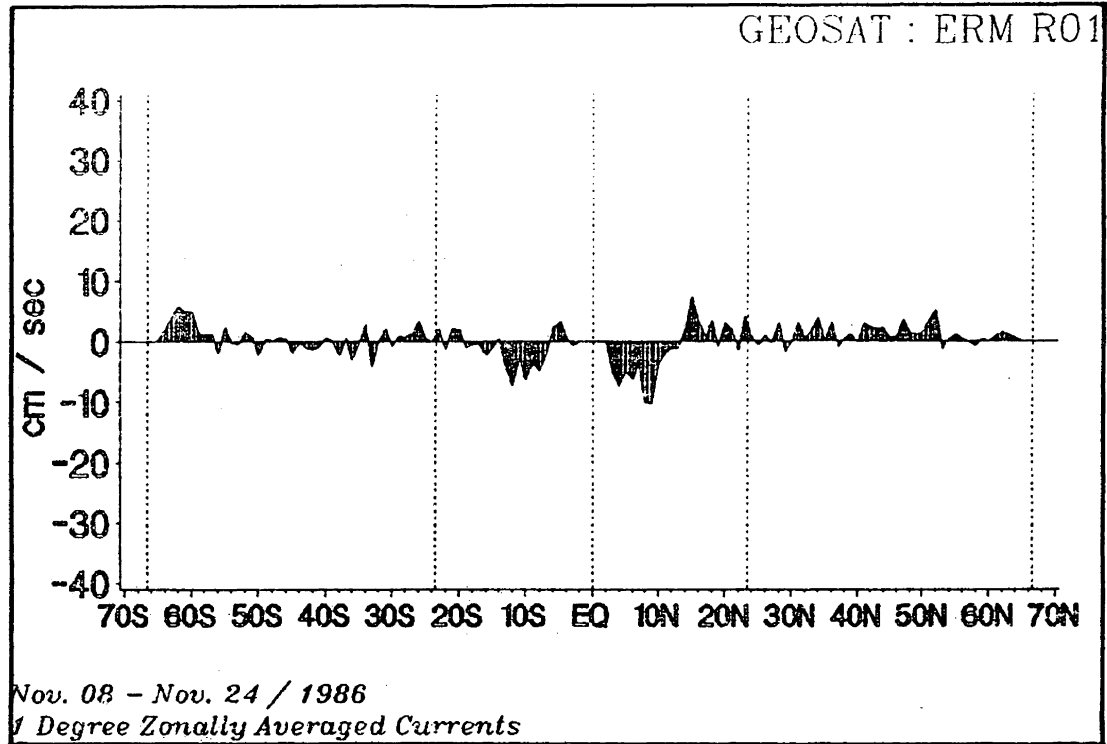
- Tapley, B. D., G. H. Born and M. E. Parke [1982]. "The SEASAT Altimeter Data and its Accuracy Assessment", *Journal of Geophysical Research*, Vol. 87, 3179-3188.
- Tapley, B. D., R. S. Nerem, C. K. Shum, J. C. Ries, and D. N. Yuan [1988]. "Determination of the General Ocean Circulation from a Joint Gravity Solution", *Geophys. Res. Lett.*, Vol. 15, 1109-1112.
- The Polar Group [1980]. "Polar Atmosphere - Ice - Ocean Processes: A Review of Polar Problems in Climate Research", *Reviews of Geophysics and Space Physics*, Vol. 18, No. 2, 525-543.
- Thomson, J. D. [1986]. "Altimeter Data and Geoid Error in Mesoscale Ocean Prediction: Some Results from a Primitive Equation Model", *Journal of Geophysical Research*, Vol. 91, C2, 2401-2417.
- Thomson, J. D., G. H. Born and G. A. Maul [1983]. "Collinear Track Altimetry in the Gulf of Mexico from SEASAT: Measurements, Modelling and Surface Truth", *Journal of Geophysical Research*, Vol. 88, C3, 1625-1636.
- UNESCO, [1981]. "The Practical Salinity Scale 1978 and the International Equation of State of Sea Water 1980", *UNESCO Technical Papers in Marine Science No. 36*, 25 pp.
- Van Loon, H. [1971]. "A Half-Yearly Variation of the Circumpolar Surface Drift in the Southern Hemisphere", *Tellus*, Vol. 23, 511-516.
- Van Loon, H. [1972]. "Half-Yearly Oscillation in the Drake Passage", *Deep Sea Research*, Vol. 19, 527-529.
- Vanicek, P. [1971]. "Further Development and Properties of the Spectral Analysis by Least Squares", *Astrophysics and Space Physics*, Vol. 17, 357-367.
- Wagner, C. A. [1985]. "Radial Variations of a Satellite Orbit Due to Gravitational Errors: Implications for Satellite Altimetry", *Journal of Geophysical Research*, Vol. 90, B4, 3027-3036.
- Wahr, J. M. [1983]. "The Effects of the Atmosphere and Oceans on the Earth's Wobble and on the Seasonal Variations in the Length of Day - II. Results", *Geophys. J. Roy. Astron. Soc.*, Vol. 74, 451-487.
- Wahr, J. M. [1985]. "The Earth's Rotation Rate", *American Scientist*, Vol. 73, 41-46.

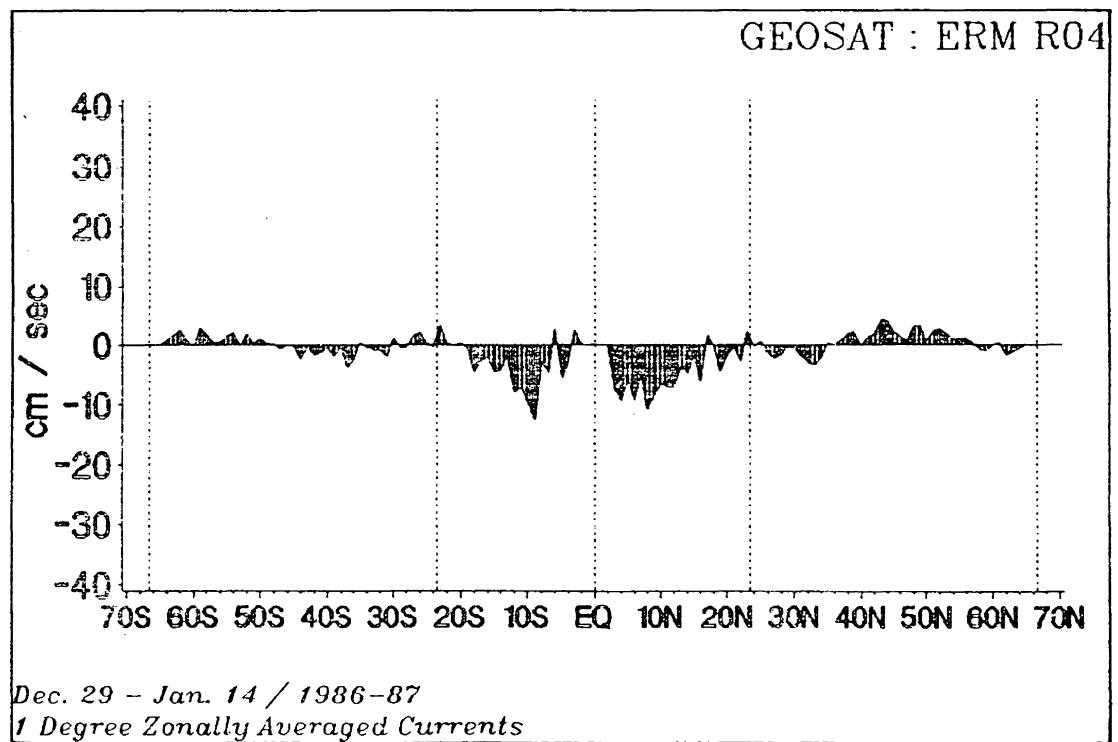
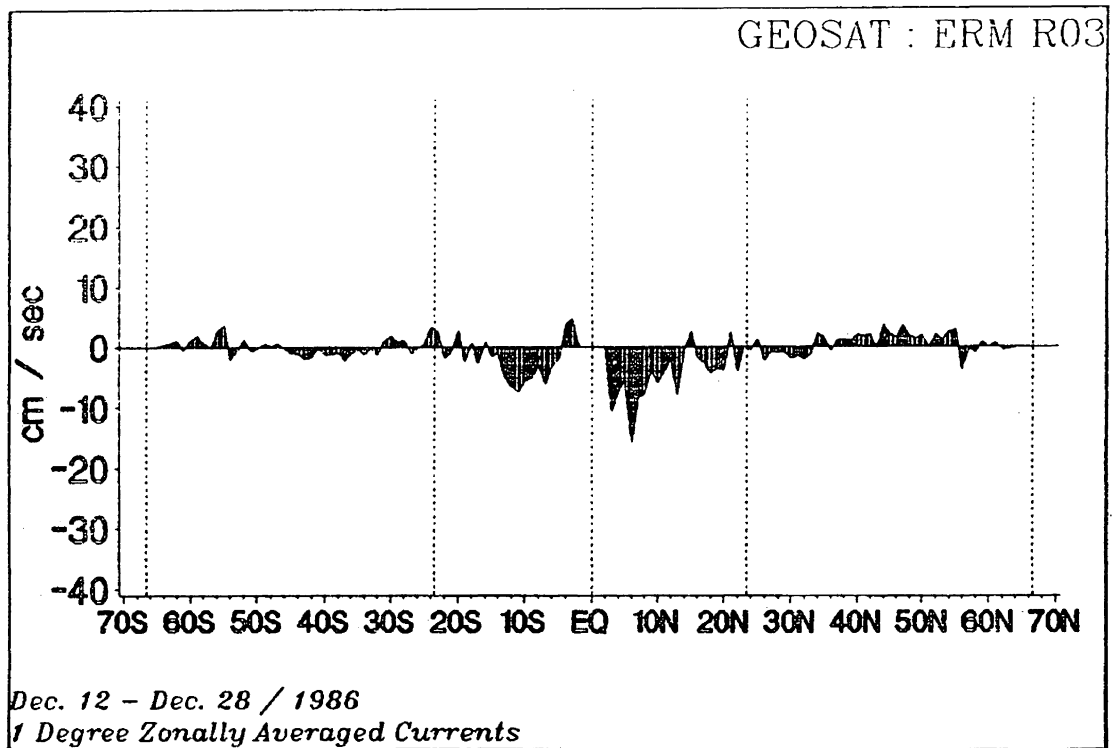
- Wahr, J. M. [1988]. "The Earth's Rotation", *Ann. Rev. Earth Planet. Sci.*, Vol. 16, 231-248.
- Walsh, E. J. [1974]. "Analysis of Experimental NRL Radar Altimeter Data", *Radio Science*, Vol. 9, 711-722.
- Walsh, E. J. [1979]. "Extraction of Ocean Wave Height and Dominant Wavelength from GEOS-3 Altimeter Data", *Journal of Geophysical Research*, Vol. 84, B8, 4003-4010.
- Webster, F. and M. Fieux [1984]. "TOGA Overview", in *Large - Scale Oceanographic Experiments and Satellites*, C. Gautier and M. Fieux Edts., D. Reidel Publ. Co., Dordrecht.
- Wells, D. E., P. Vanicek and S. Pagiatakis [1985]. "Least Squares Spectral Analysis Revisited", Department of Surveying Engineering, *Technical Report No. 84*, University of New Brunswick, Fredericton.
- Whitworth, T. [1983]. "Monitoring the Transport of the Antarctic Circumpolar Current at Drake Passage", *Journal of Physical Oceanography*, Vol. 13, 2045-2057.
- Whitworth, T. and R. G. Peterson [1985]. "Volume Transport of the Antarctic Circumpolar Current from Bottom Pressure Measurements", *Journal of Physical Oceanography*, Vol. 15, 810-816.
- Wilkins, G. A., ed. [1980]. *Project MERIT*. Joint Working Group on the Rotation of the Earth, IAU/IUGG.
- Wilkins, G. A. [1983]. "Report on the Second MERIT Workshop and on Other Activities in 1983", Royal Greenwich Observatory, Herstmonceux, U.K.
- Wunsch, C. [1978]. "The North Atlantic General Circulation West of 50W Determined by Inverse Methods", *Reviews of Geophysics and Space Physics*, Vol. 16, No. 4, 583-620.
- Wunsch, C. and E. M. Gaposchkin [1980]. "On Using Satellite Altimetry to Determine the General Circulation of the Ocean With Application to Geoid Improvement", *Reviews of Geophysics and Space Physics*, Vol. 18, No. 4, 725-745.
- Wyrcki, K. [1974]. "The Dynamic Topography of the Pacific Ocean and its Fluctuations", *Report HIG-74-5*, Hawaii Institute of Geophysics.

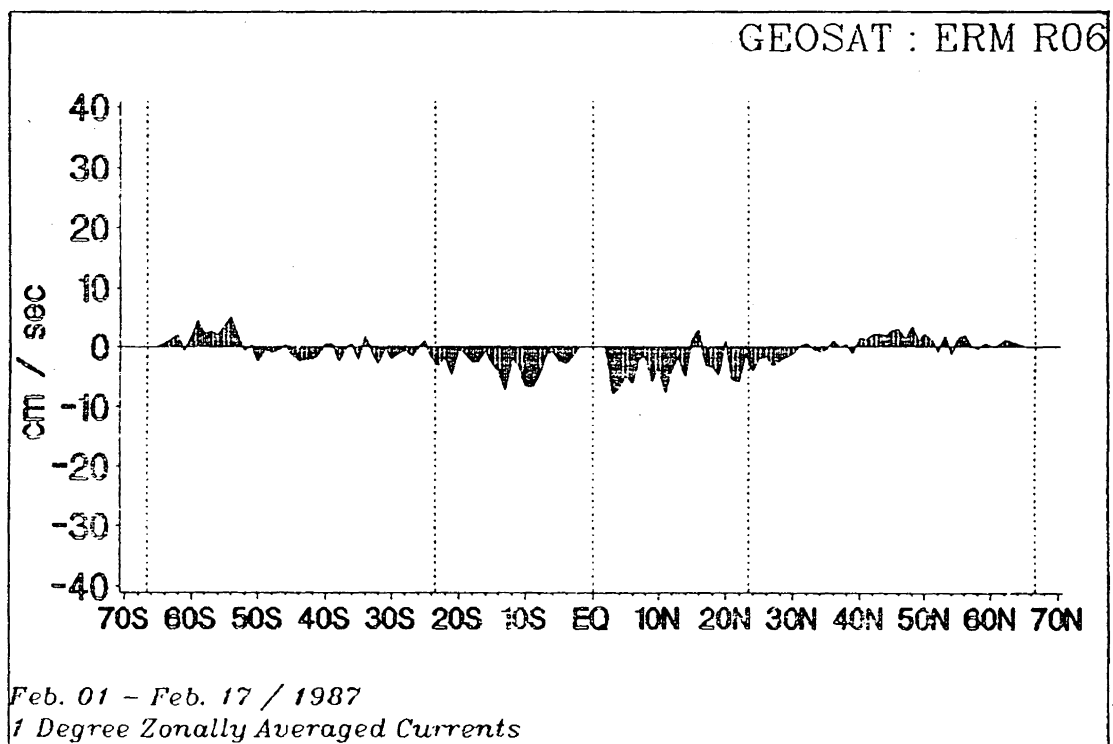
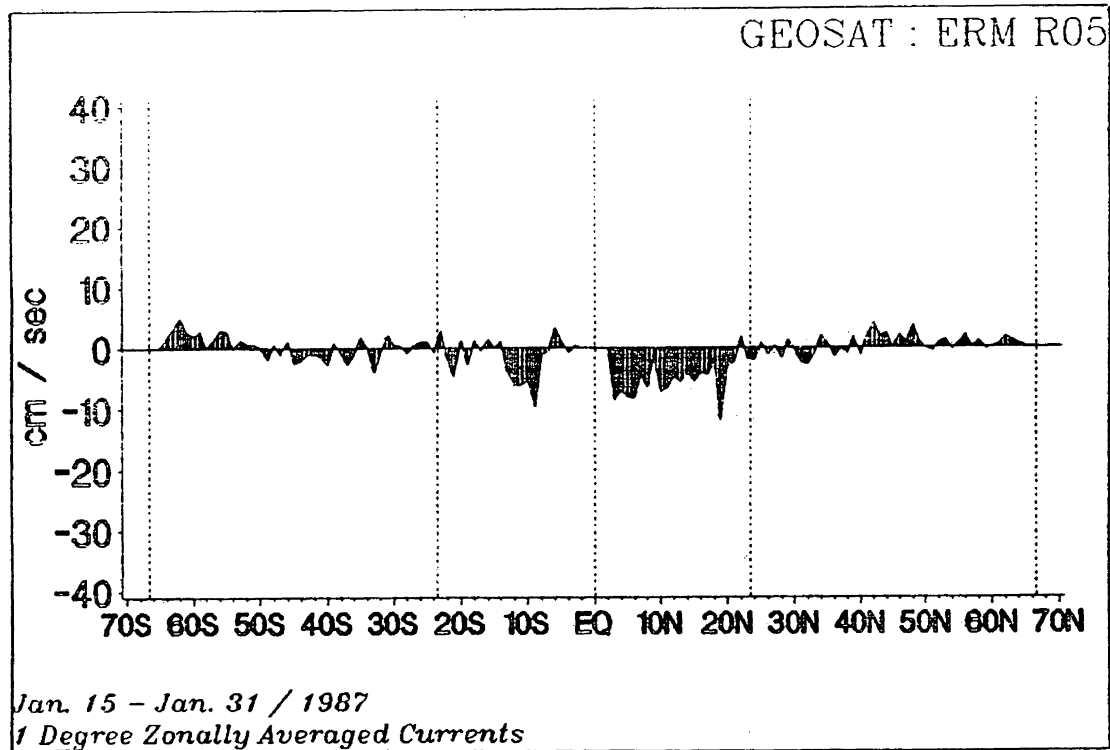
- Wyrcki, K. [1975]. "Fluctuations of Dynamic Topography in the Pacific Ocean", *Journal of Physical Oceanography*, Vol. 5, 450-459.
- Wyrcki, K. [1985]. "Sea Level Fluctuations in the Pacific During the 1982-83 El Nino", *Geophysical Research Letters*, Vol. 12,, 125-128.
- Yoder, C. F., J. G. Williams and M. E. Parke [1981]. "Tidal Variations of Earth Rotation", *Journal of Geophysical Research*, Vol. 86, 881-891.
- Yoder, C. F., J. G. Williams, J. O. Dickey, B. E. Schutz, R. J. Eanes and B. D. Tapley [1983]. "Secular Variation of the Earth's Gravitational Harmonic  $J_2$  Coefficient from LAGEOS and Non-tidal Acceleration of the Earth's Rotation", *Nature*, Vol. 303, 757-762.
- Zwally, H. J., J. A. Major, A. C. Brenner, and R. A. Bindshadler [1987]. "Ice Measurements by GEOSAT Radar Altimetry", Johns Hopkins APL, *Technical Digest*, Vol. 8, Number 2.

## Appendix I

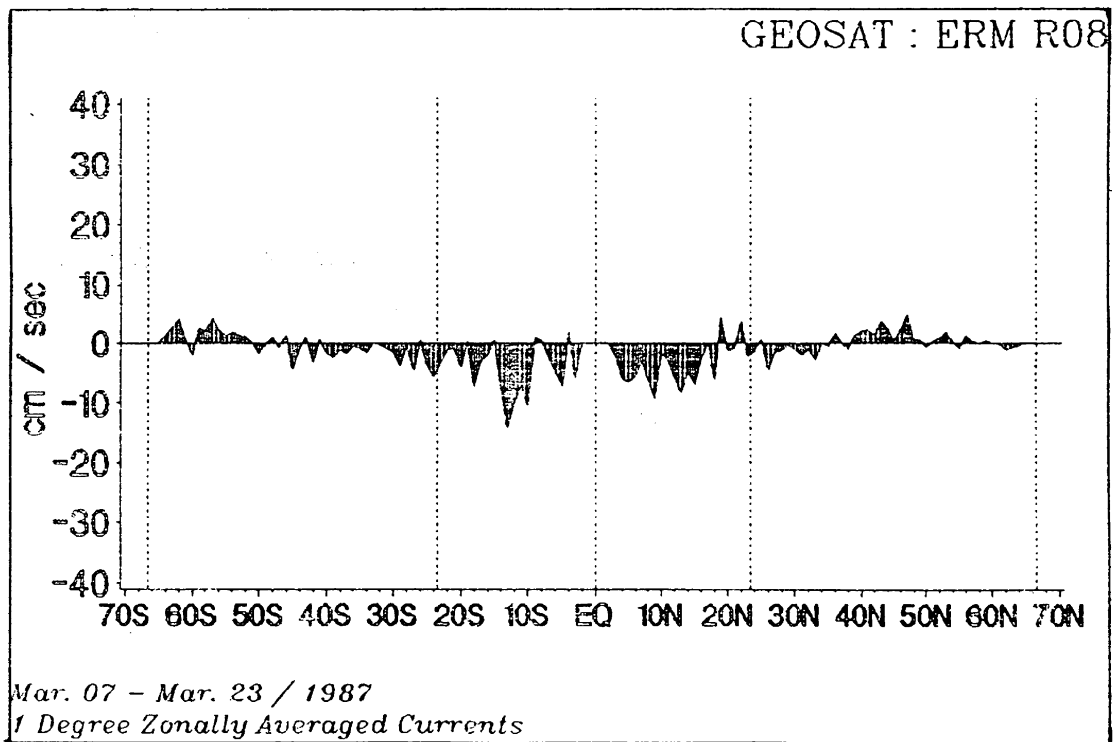
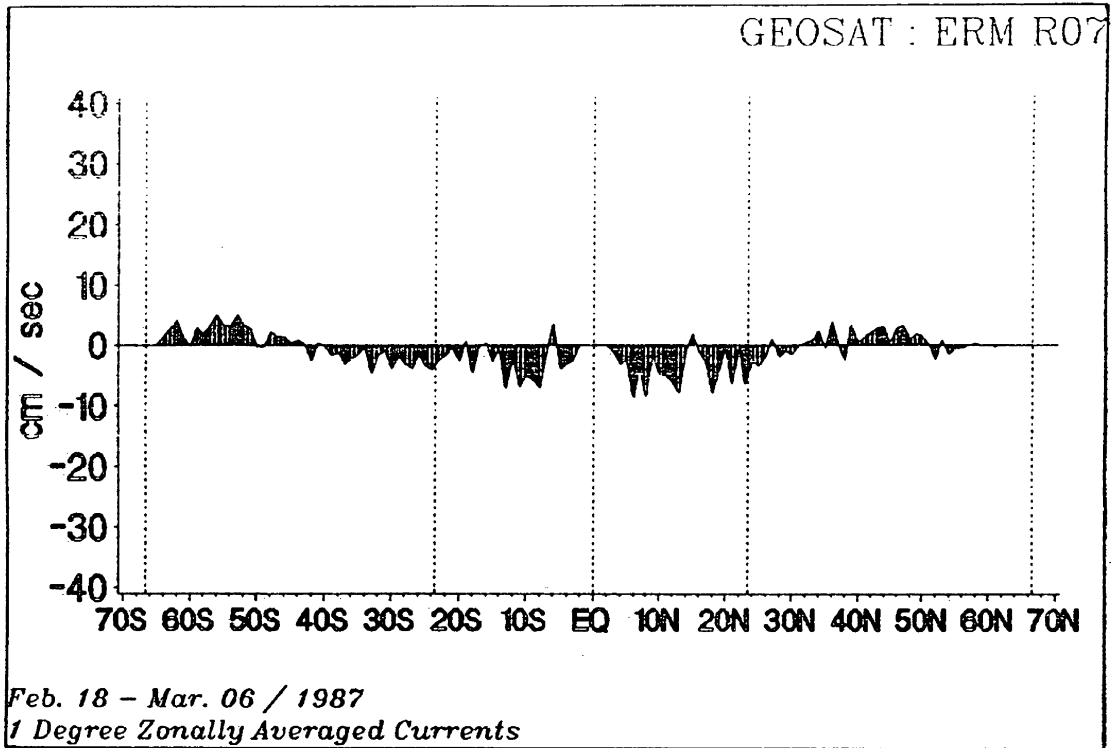
This Appendix contains two-dimensional plots of  $1^\circ$  zonally averaged ocean current variability from the first 44 cycles of the GEOSAT Exact Repeat Mission. Each plot represents a 17-day average zonal current variability with respect to the 2-year long mean (between November 08, 1986 and November 24, 1988) computed from all 44 analysed ERM's.

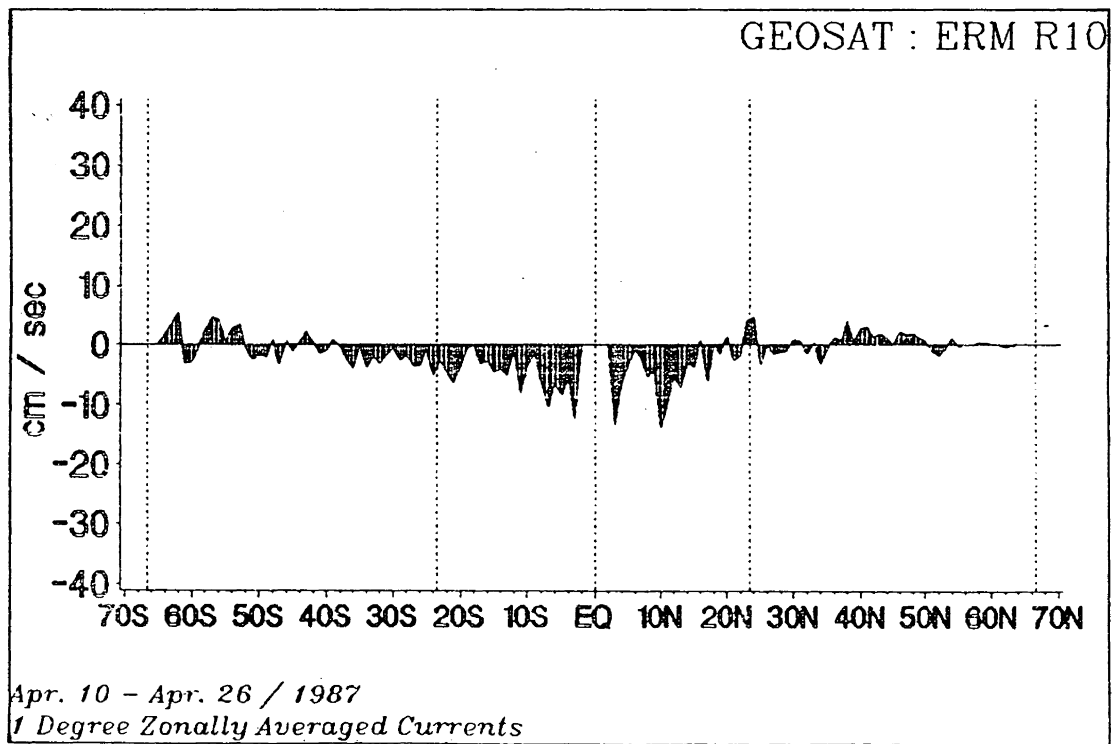
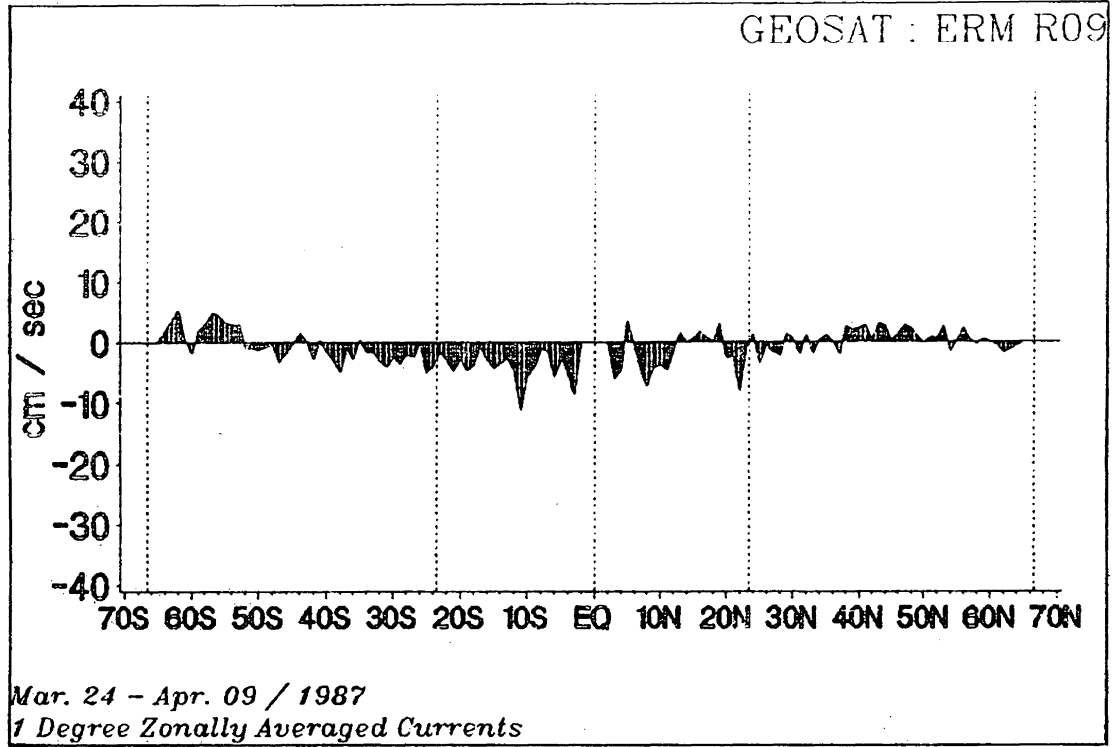


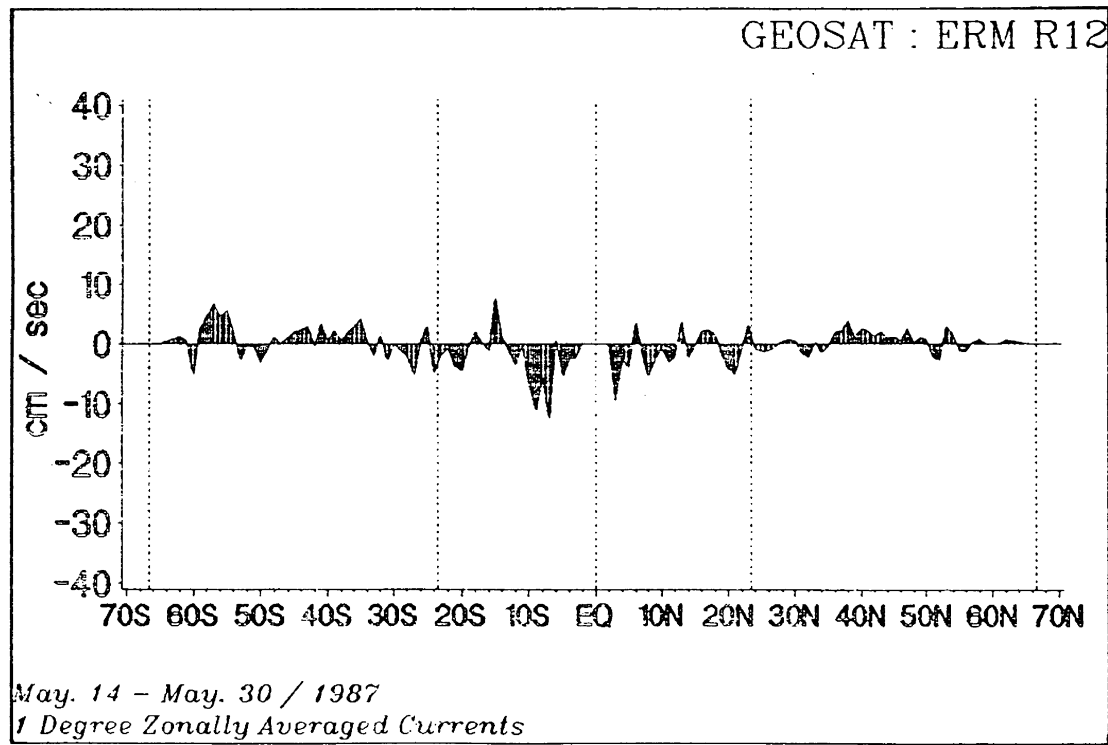
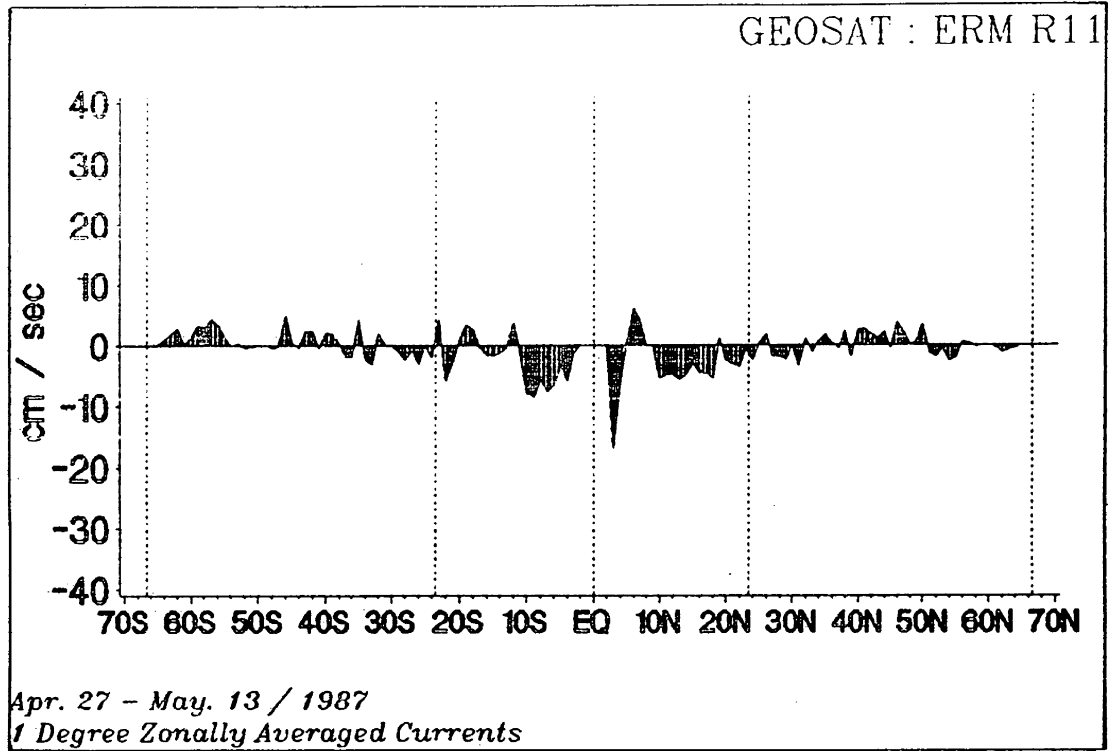


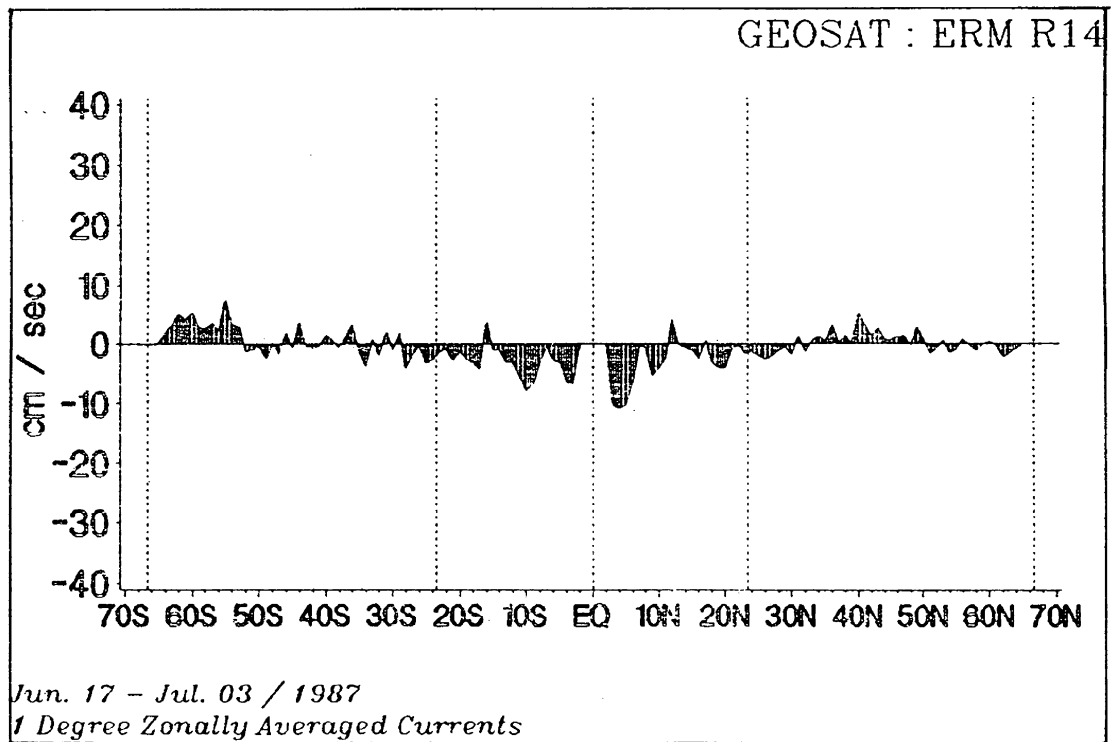
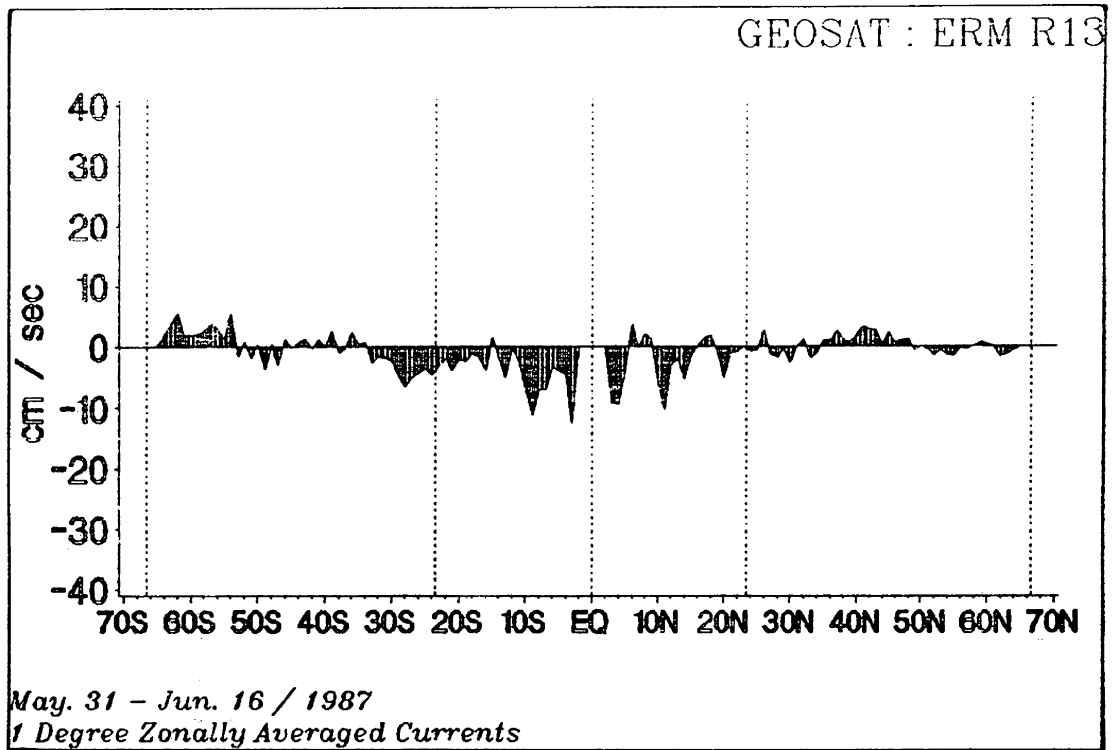


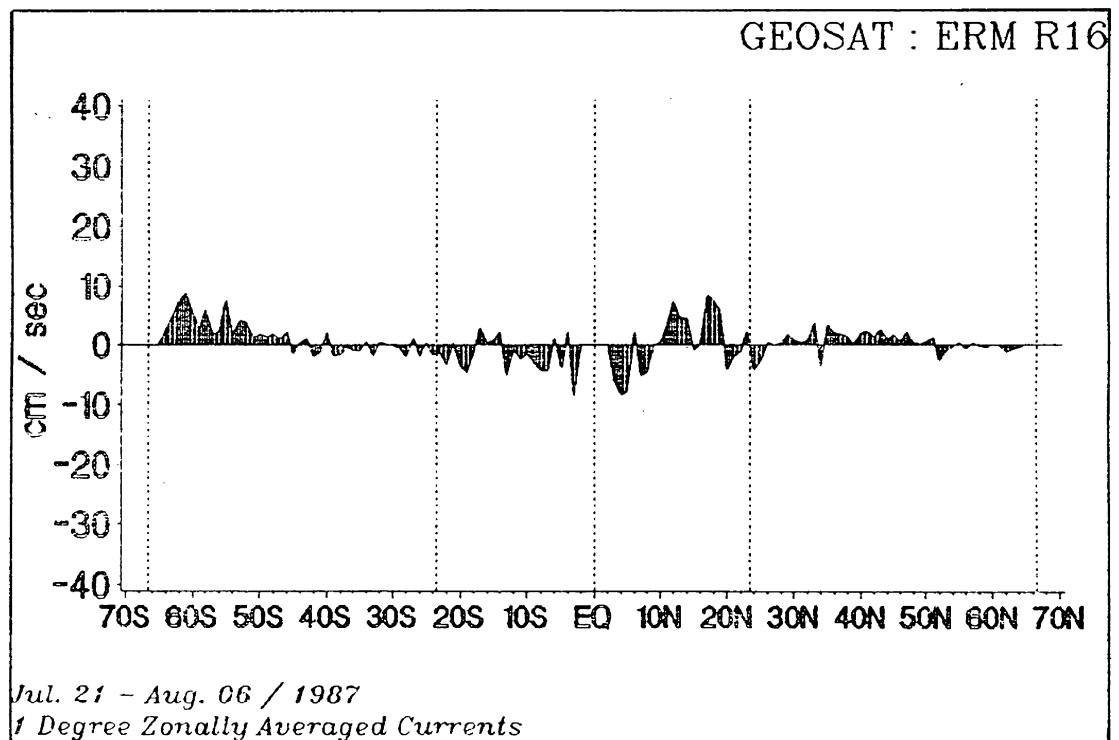
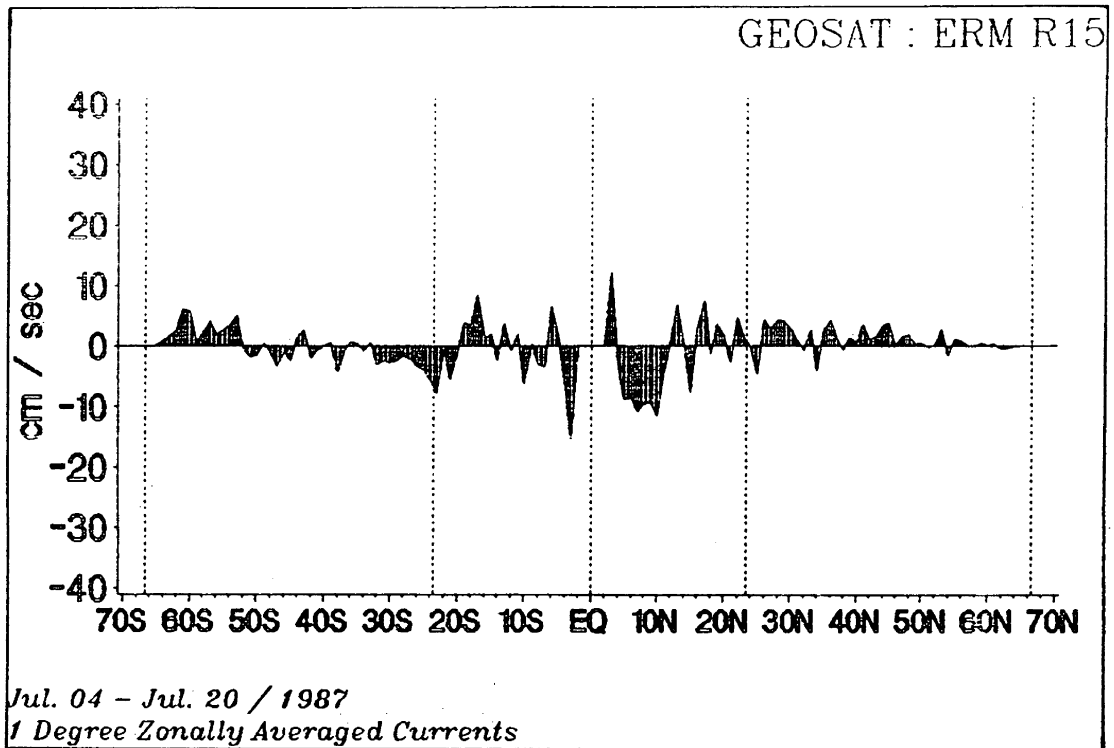


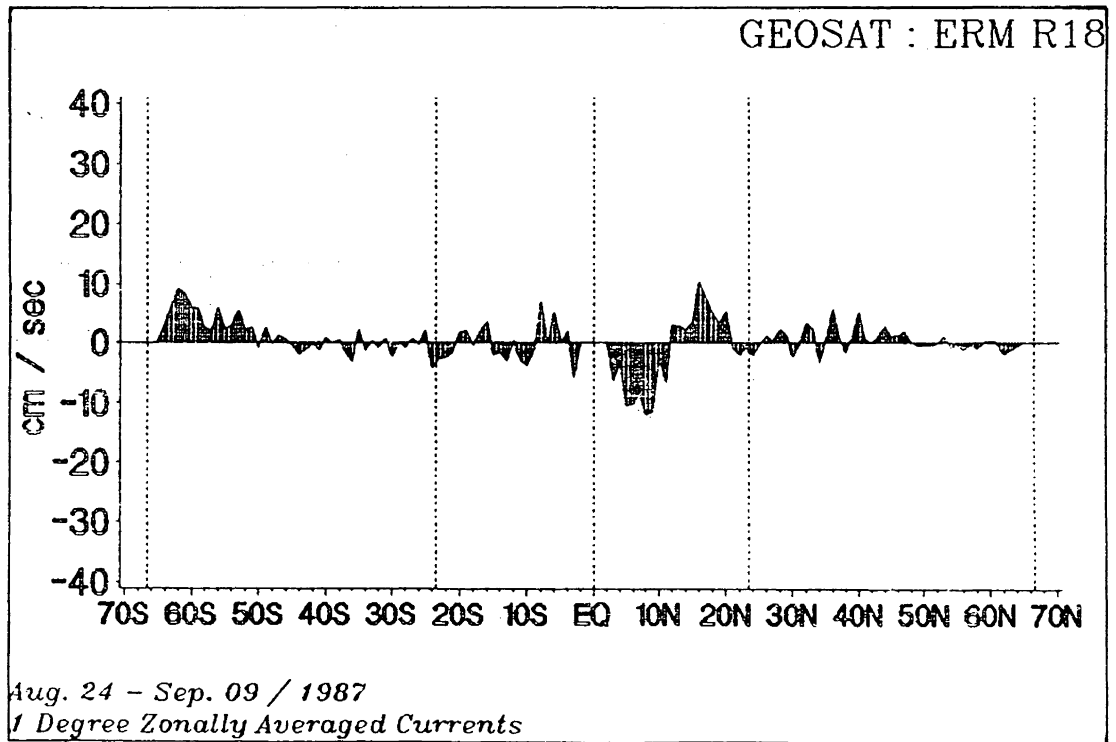
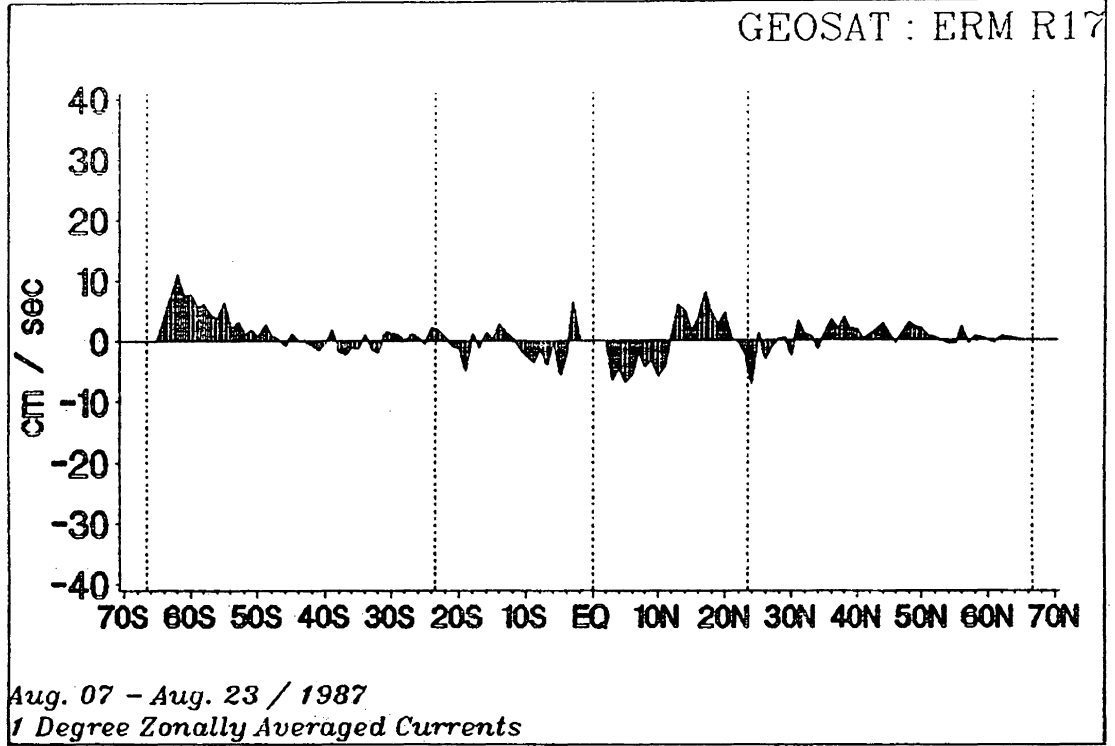


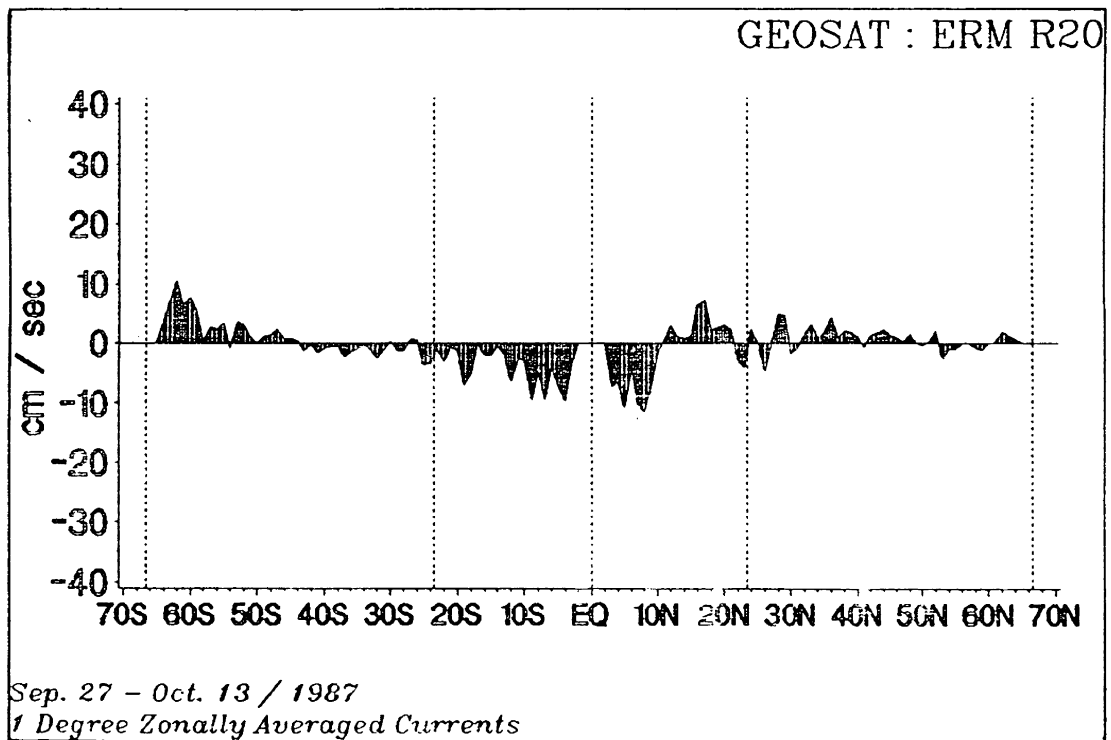
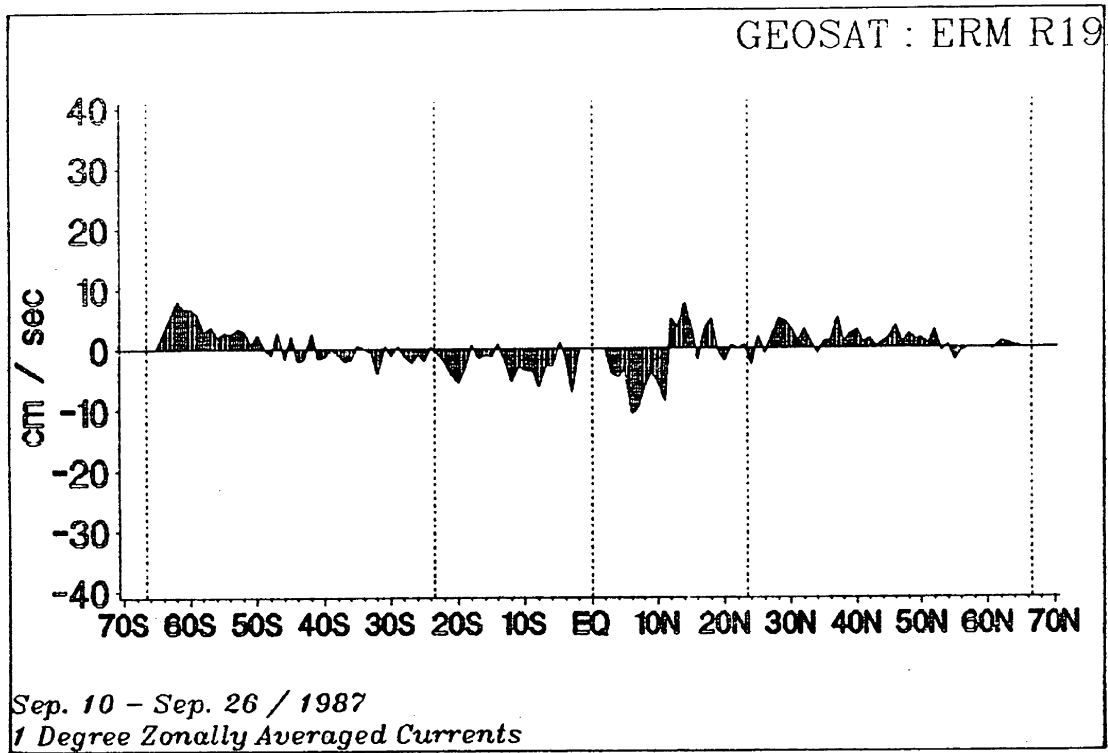


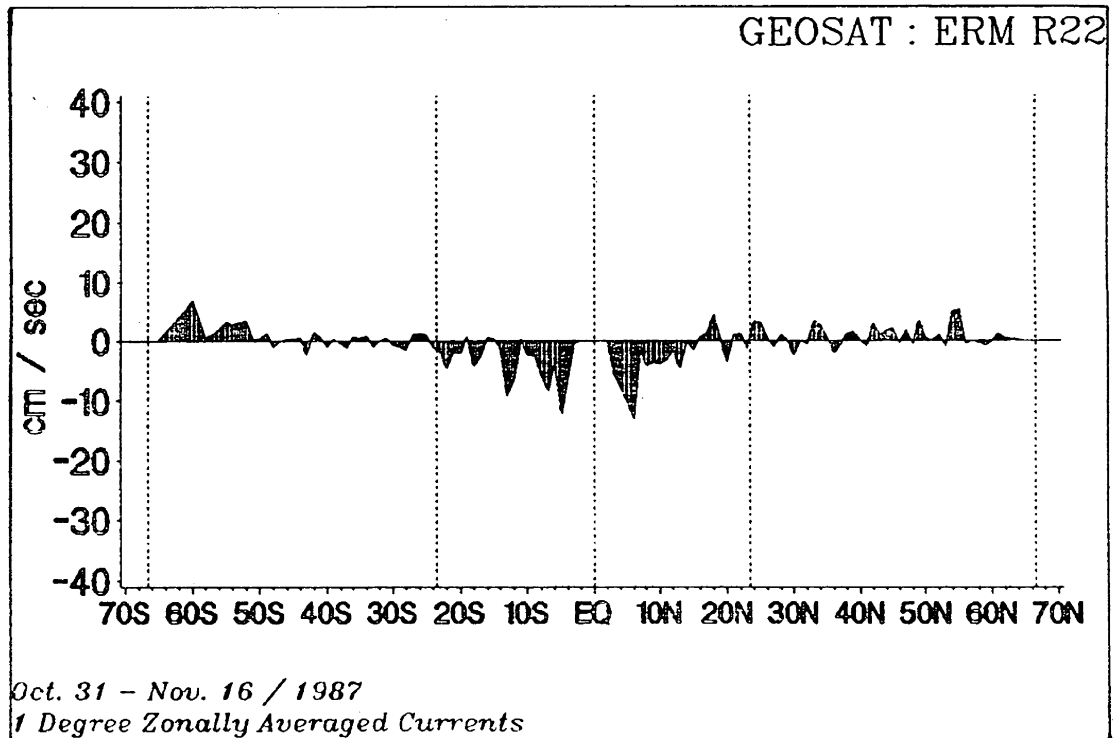
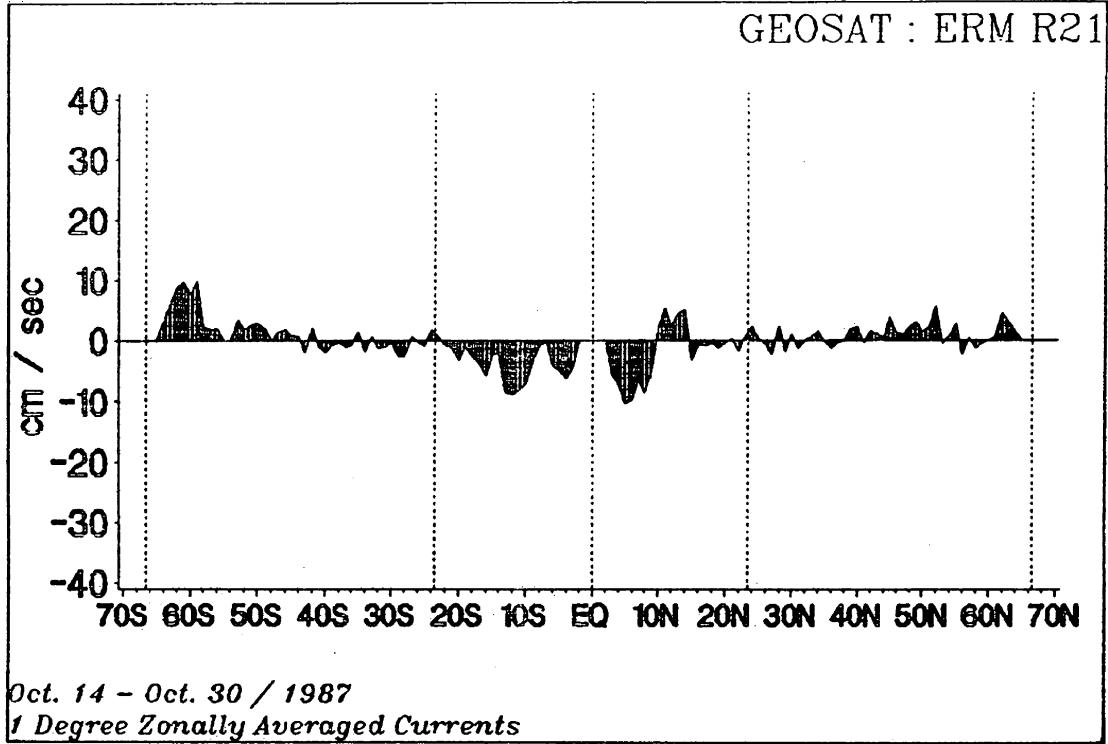




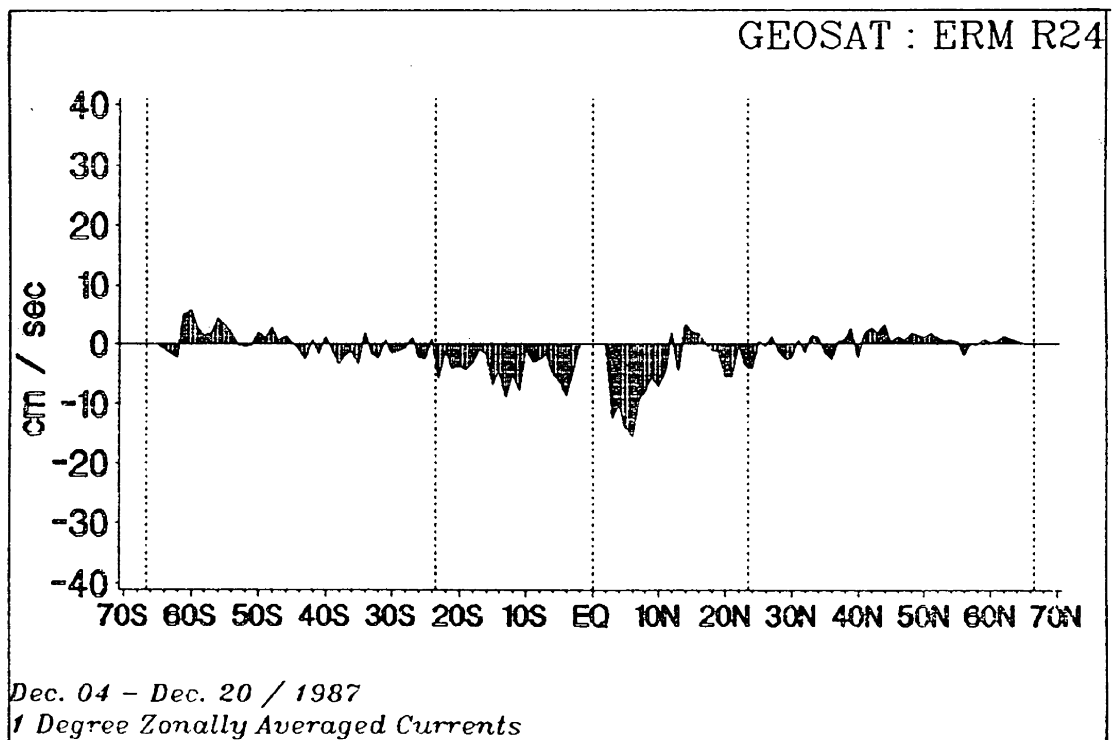
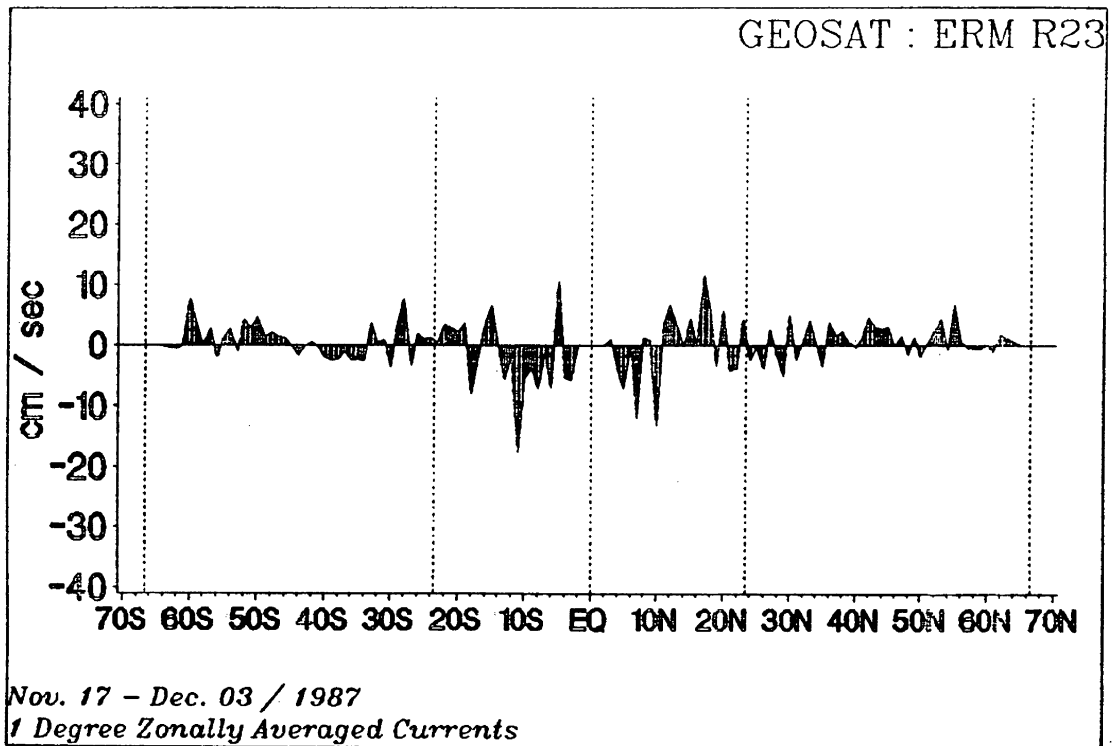


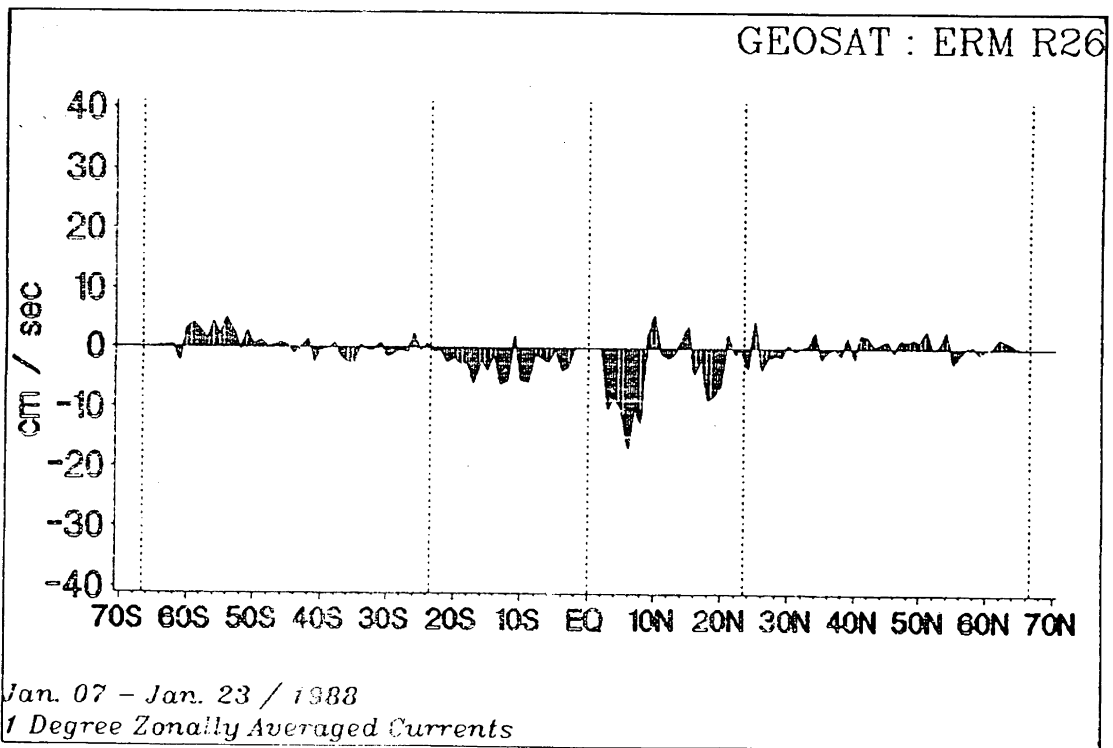
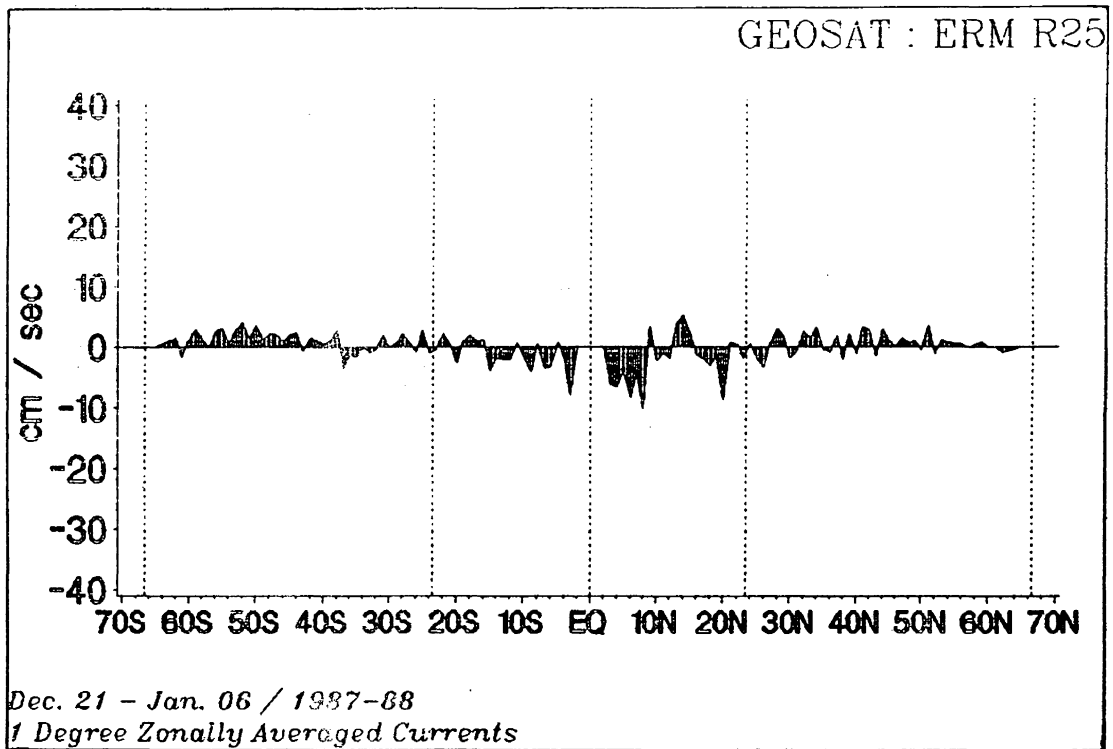


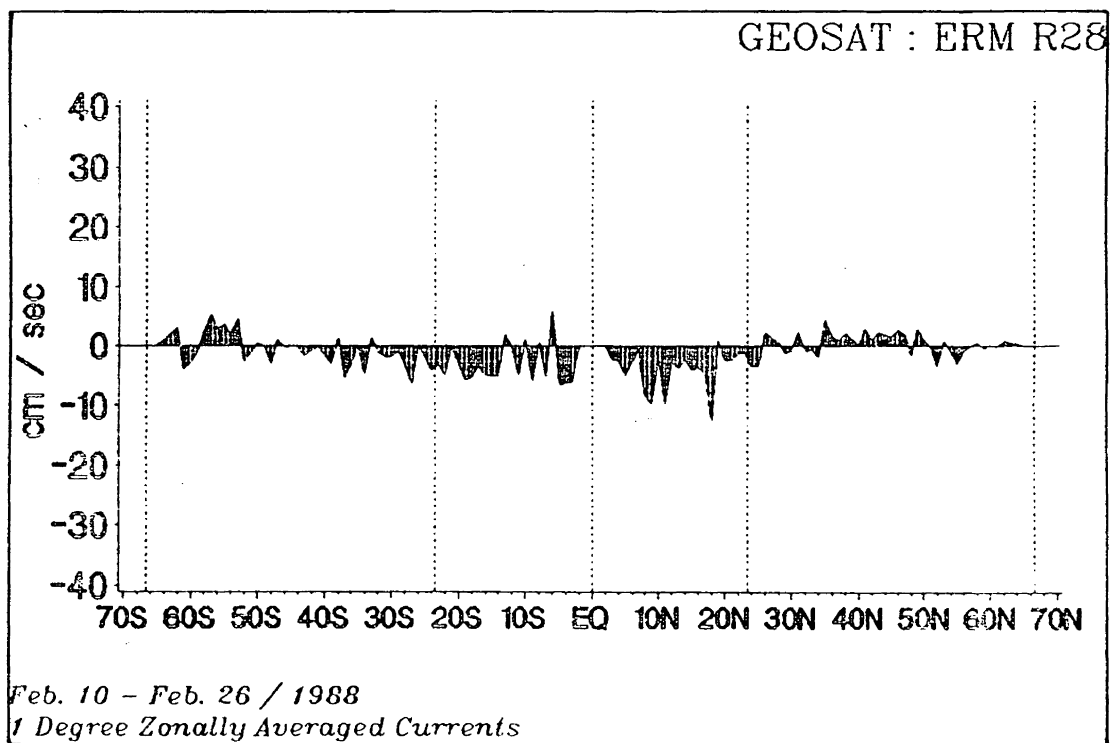
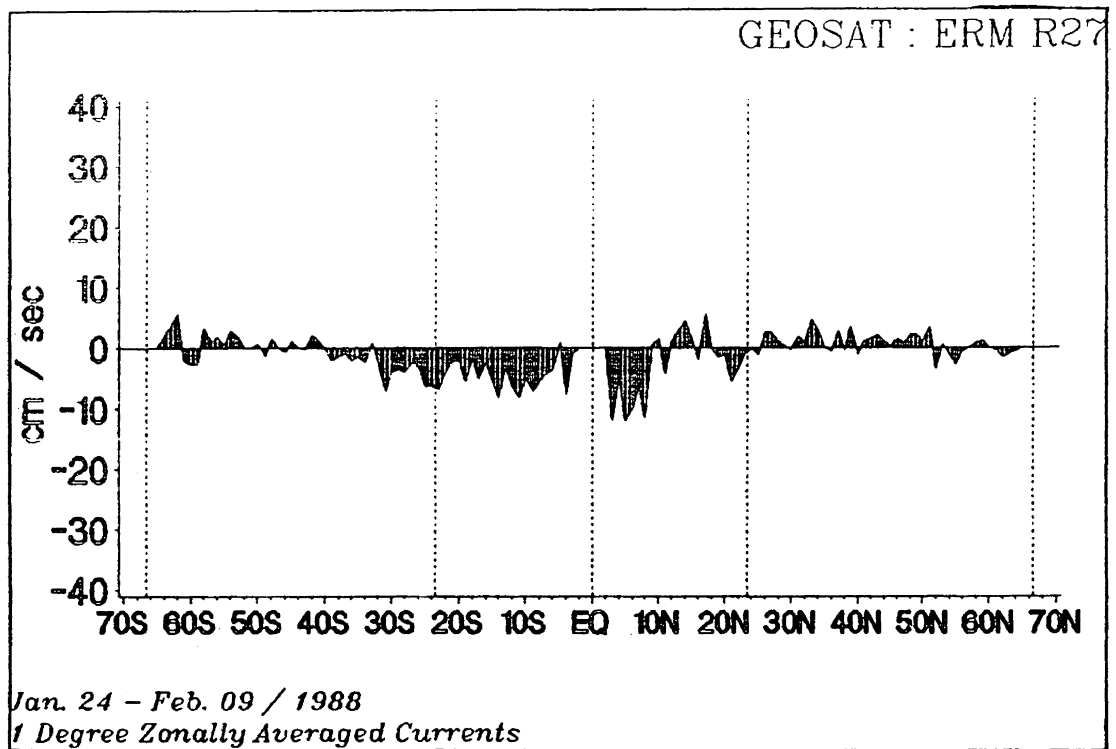


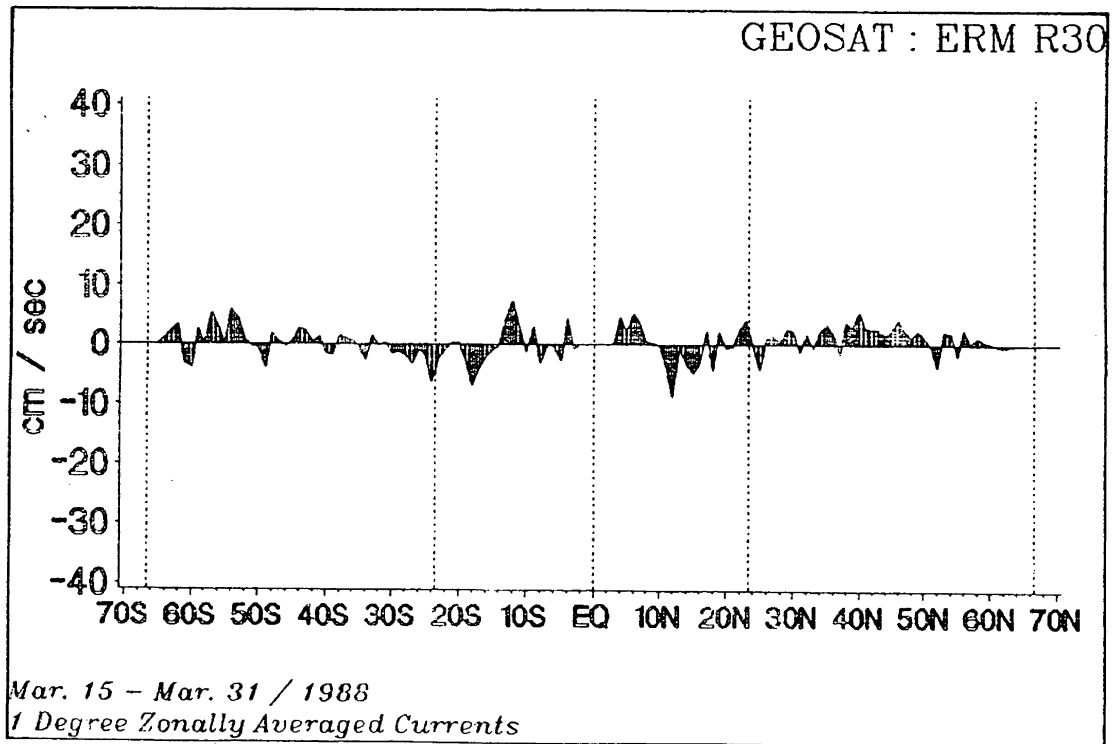
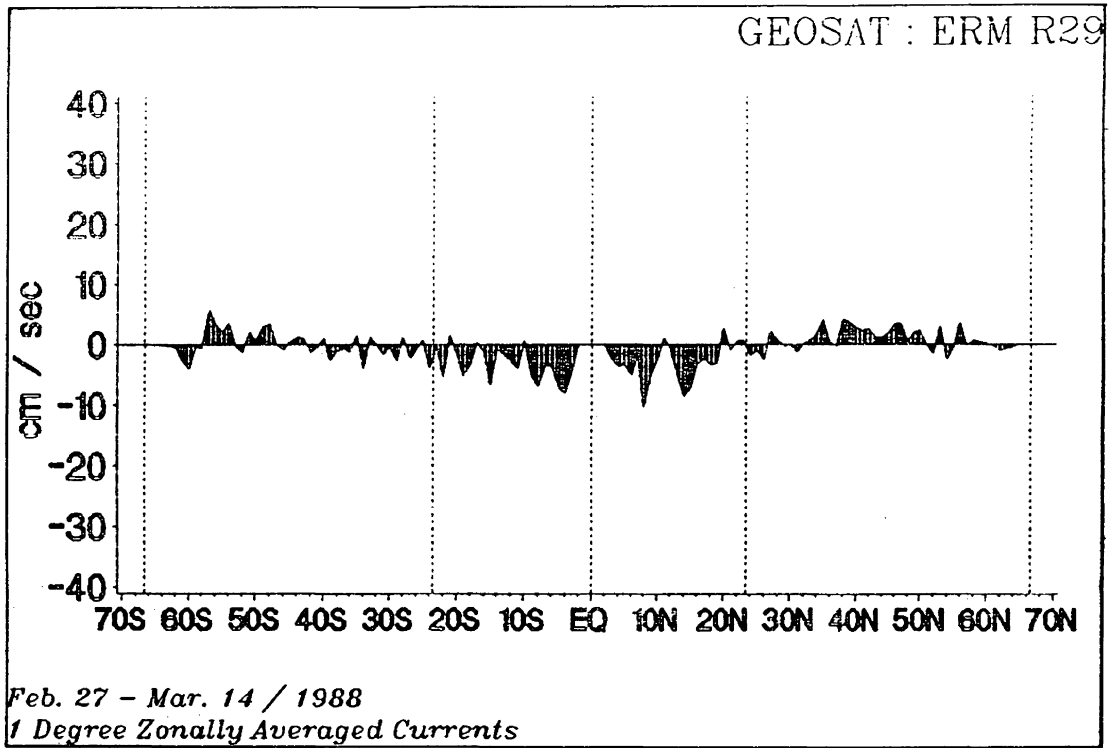


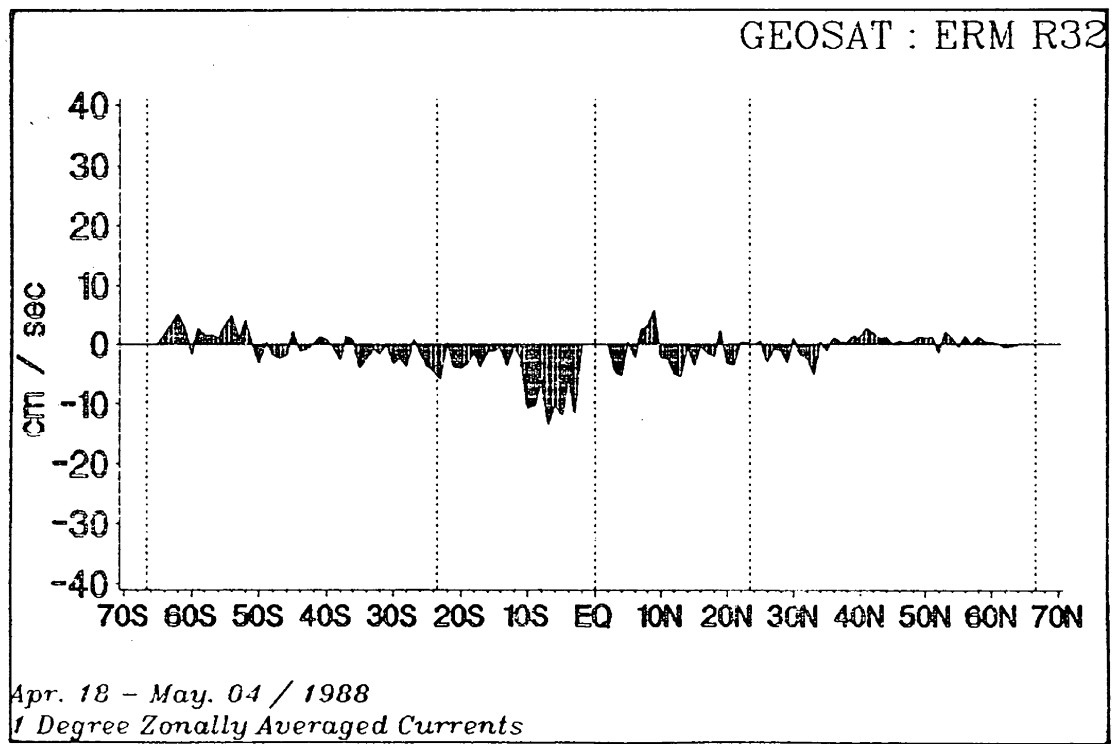
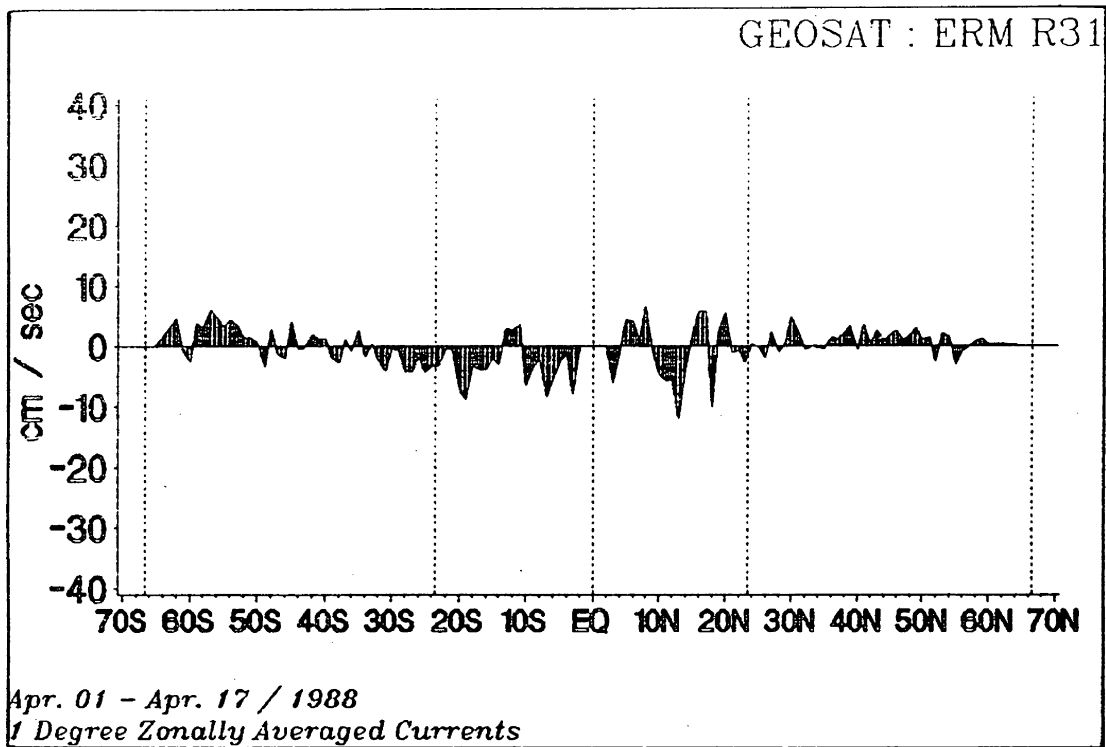


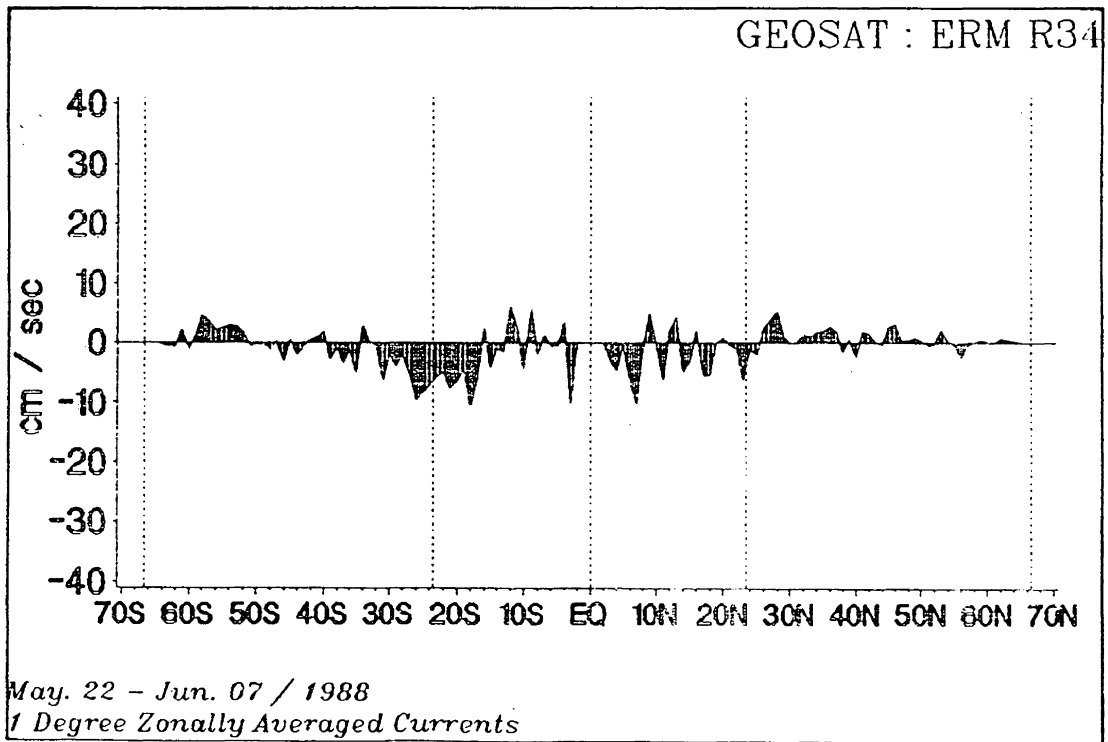
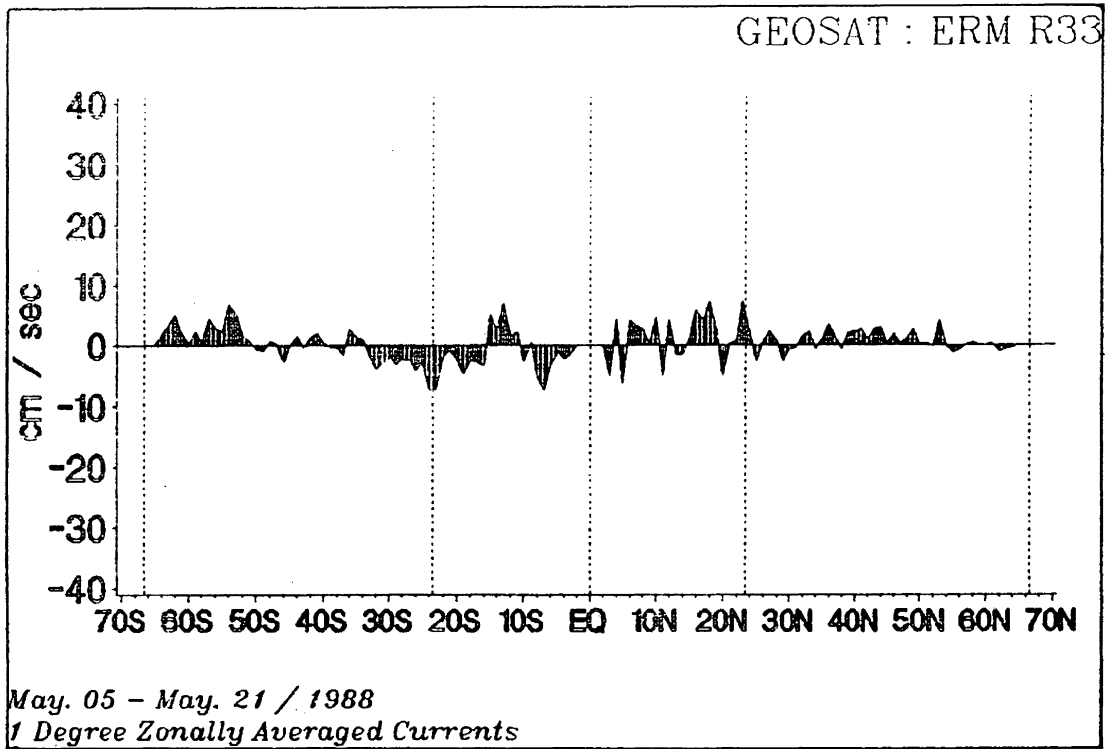


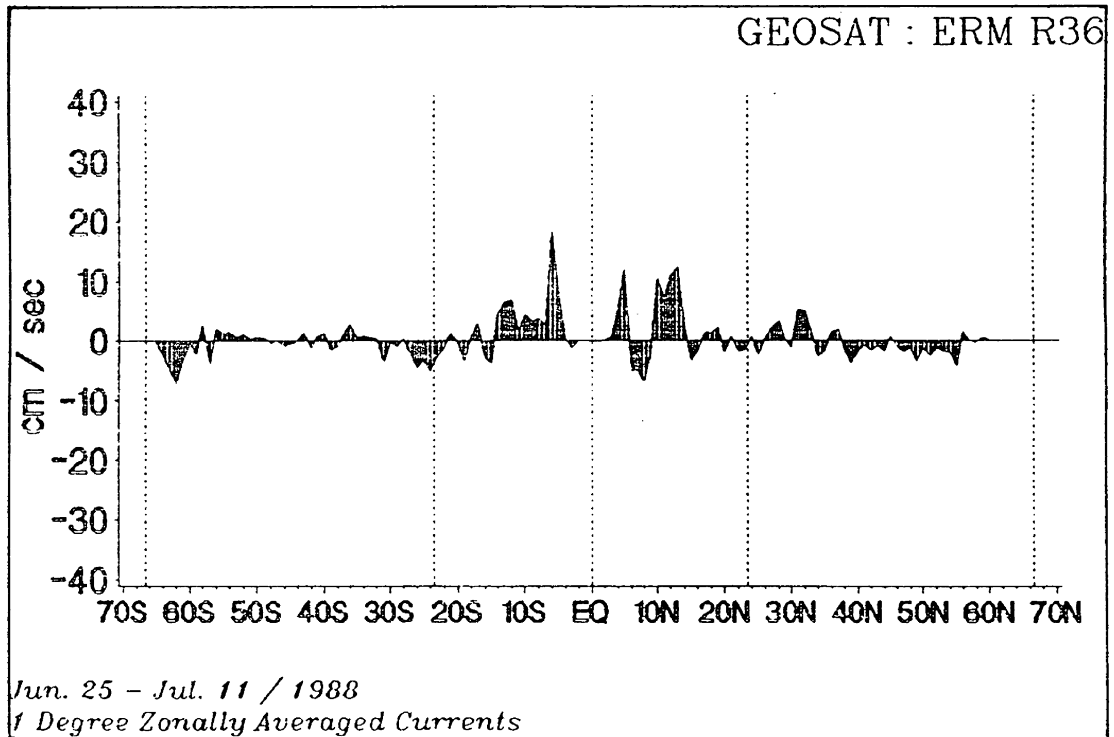
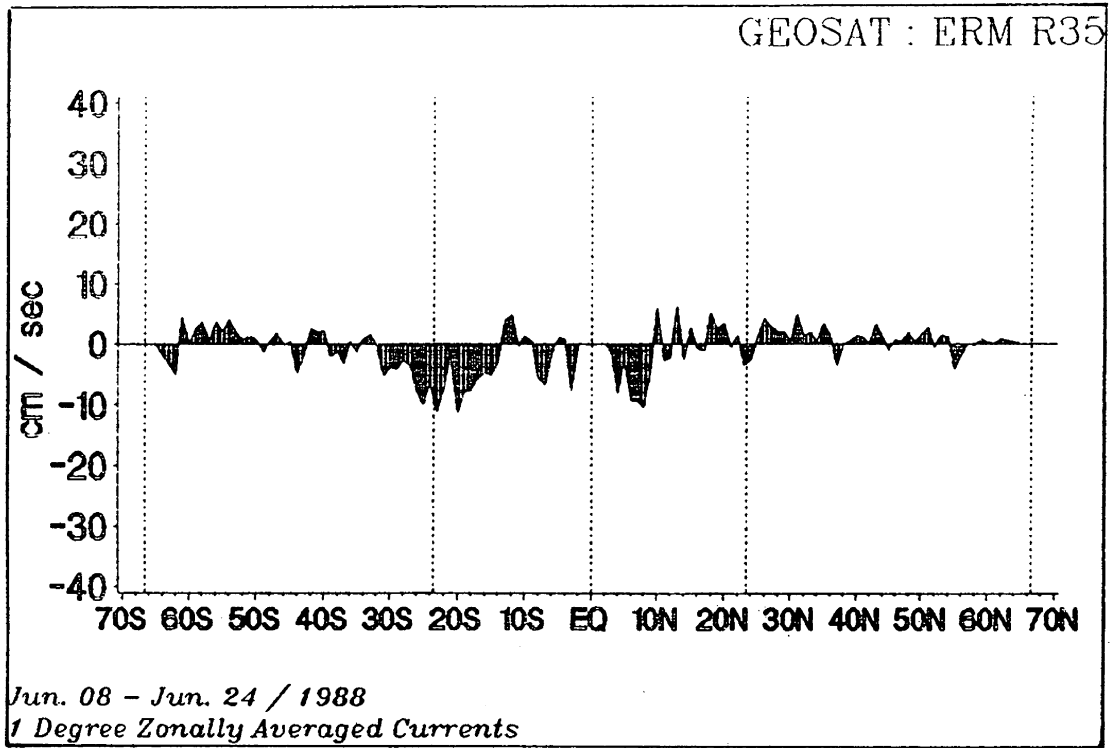


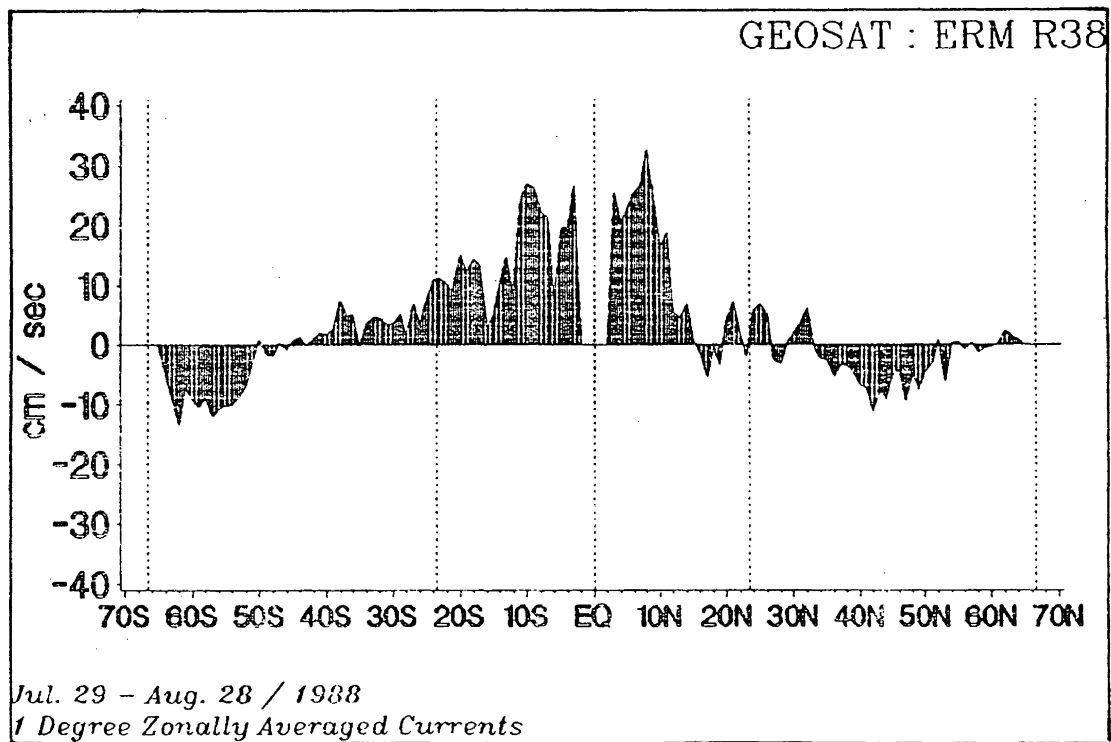
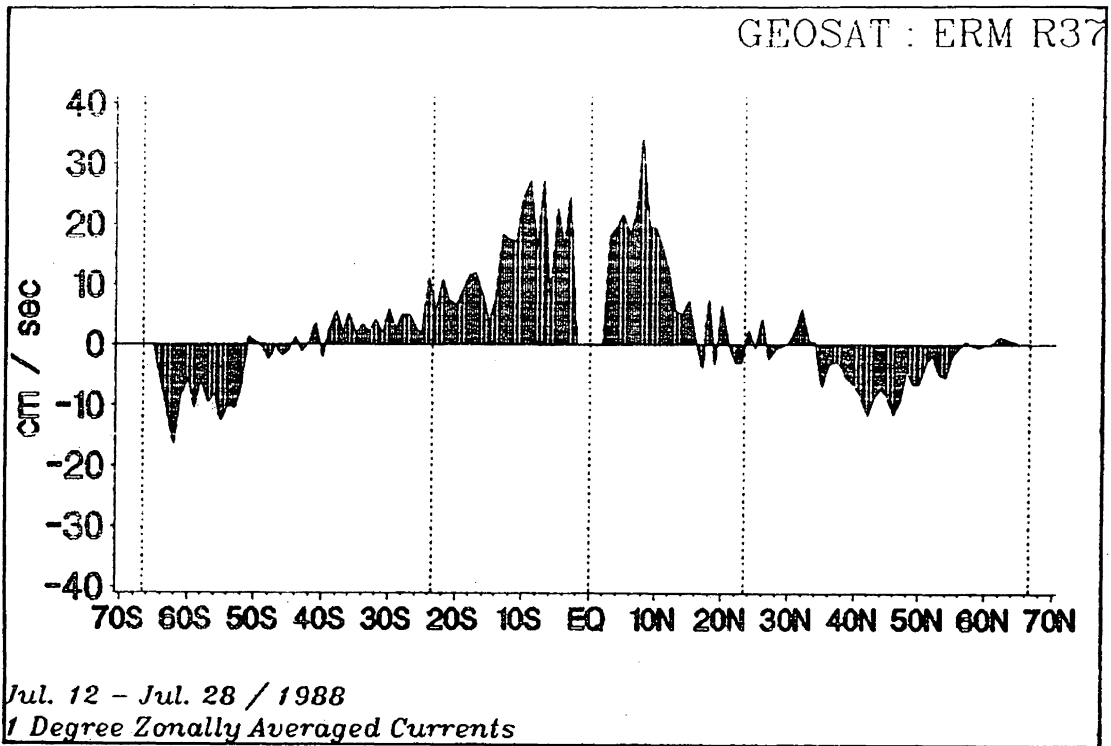




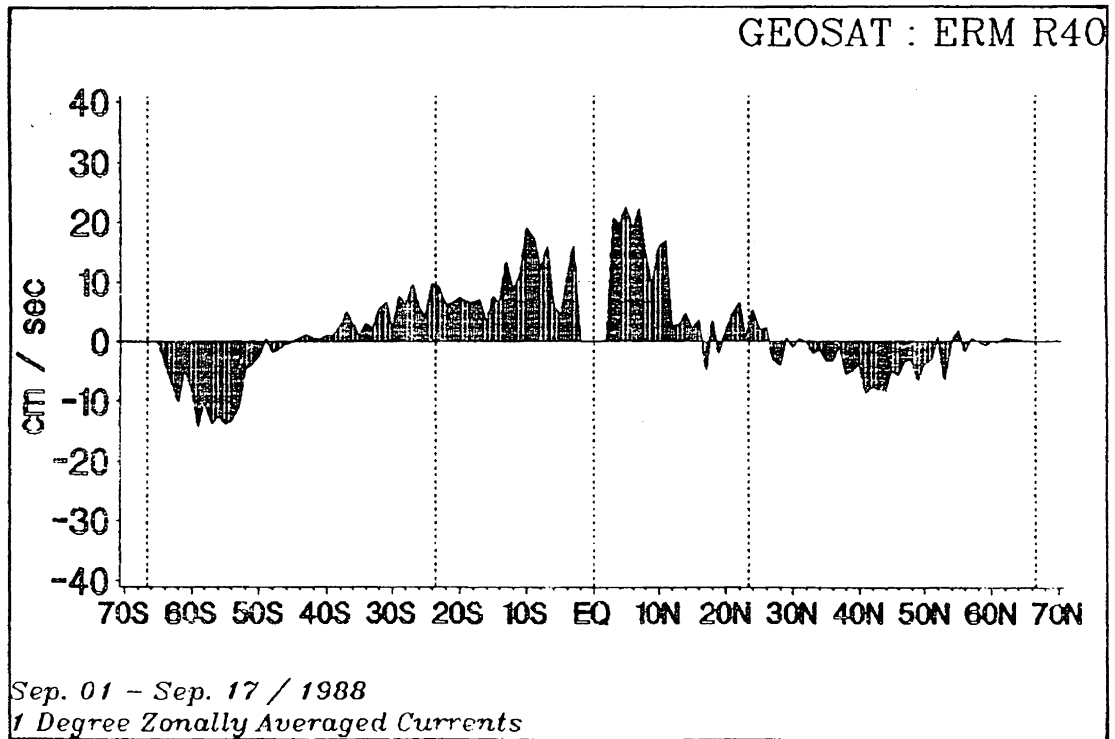
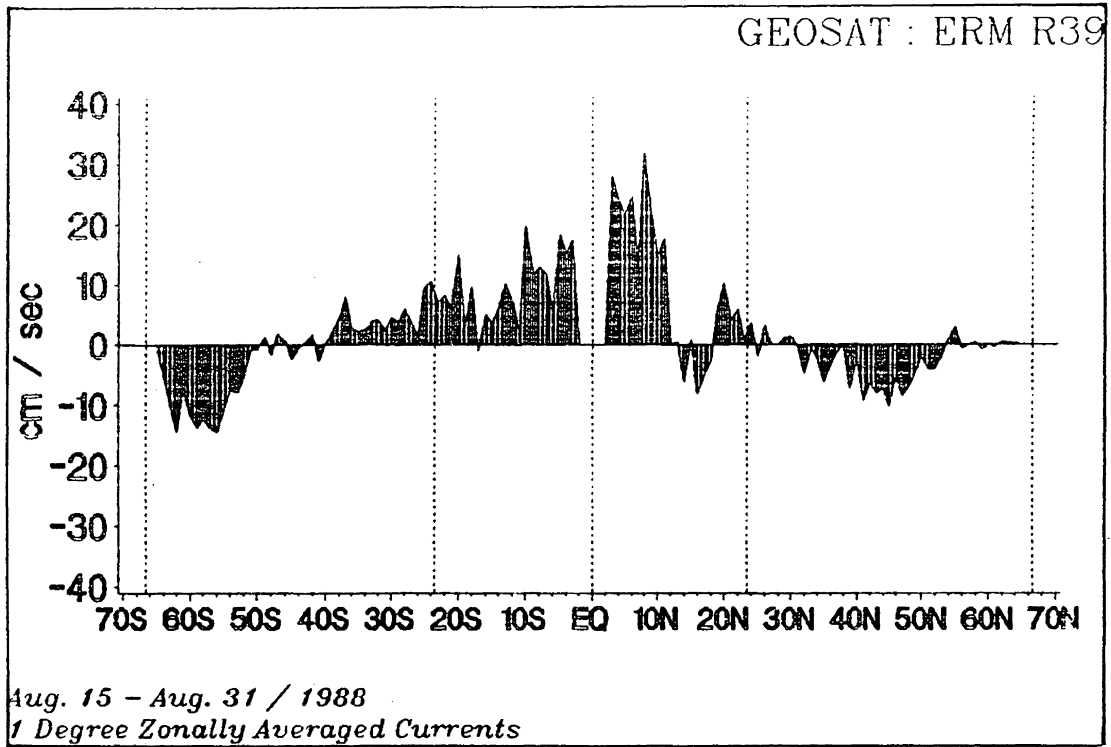


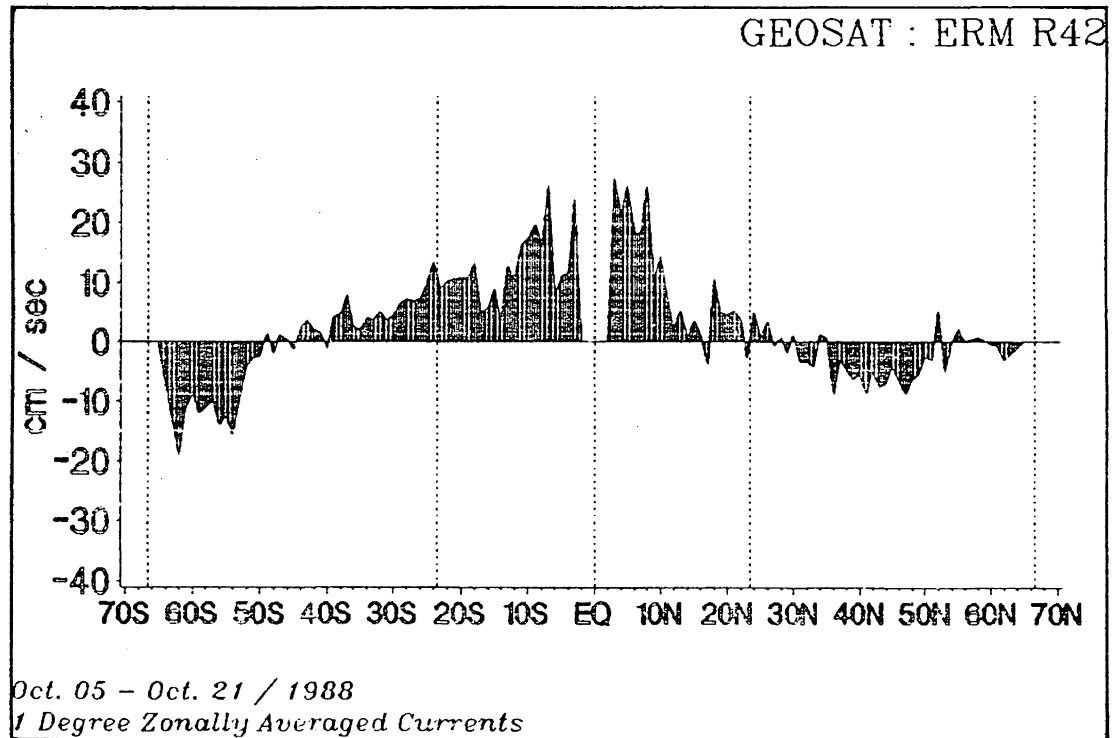
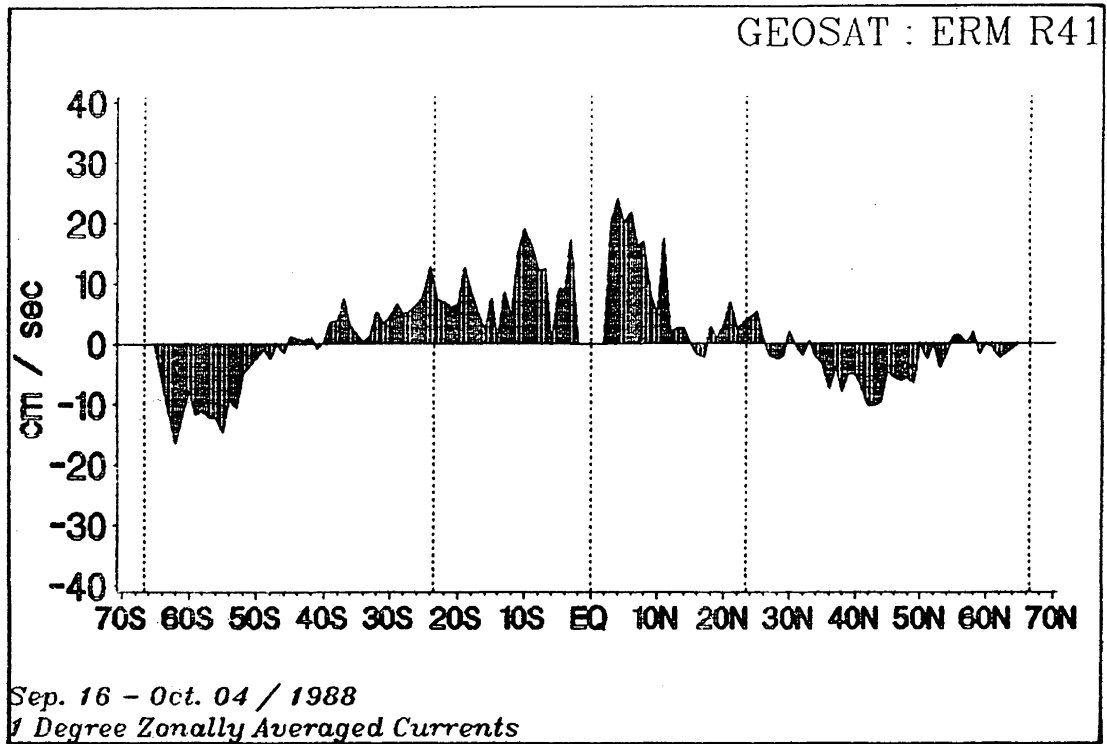


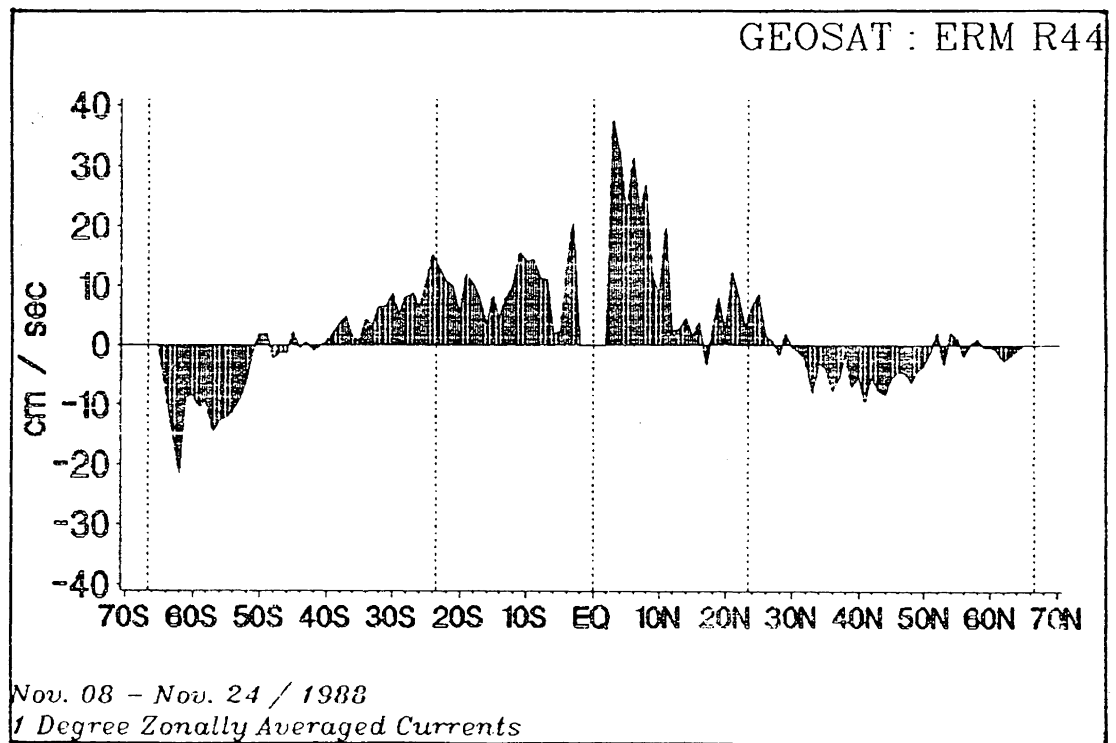
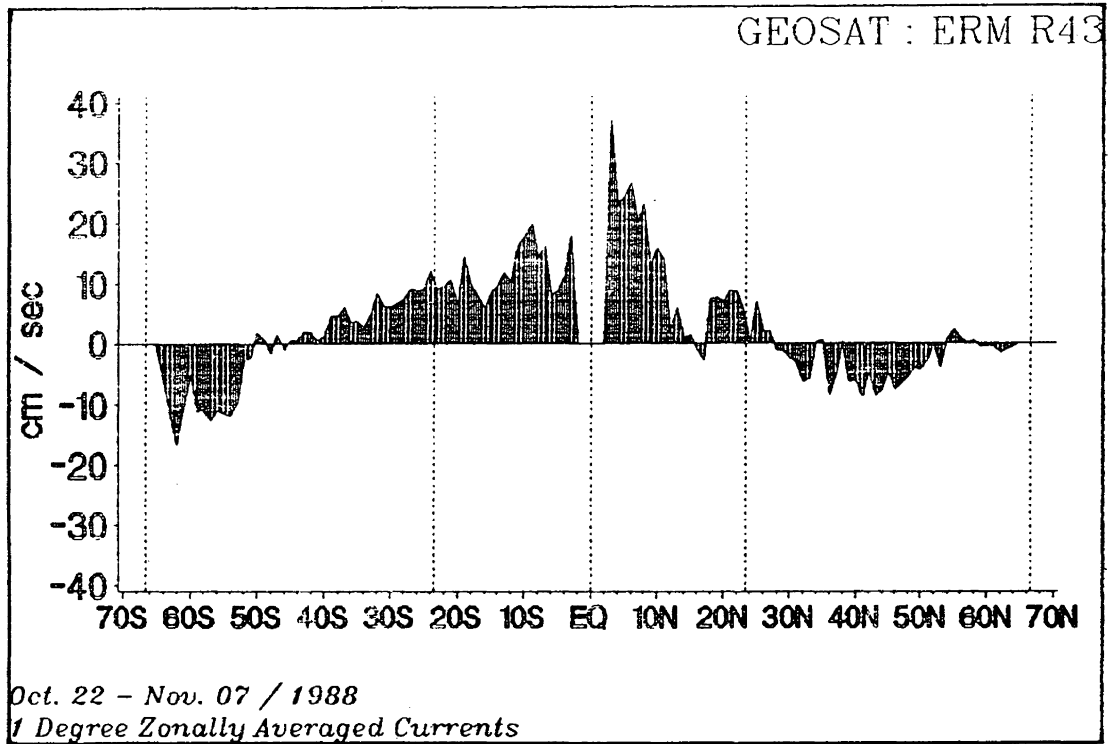












## Appendix II

This Appendix presents the tabular values of the computed equivalent oceanic  $\Delta LOD$  time series for the period Nov' 86 - Nov' 88. The first column represents the time-axis in days since the beginning of 1986 (day 1 is January 01, 1986). The values of computed equivalent oceanic  $\Delta LOD$  represent 17-day averages and their time-tag is centred at the middle of the 17-day interval. The equivalent oceanic  $\Delta LOD$  values are given in units of milliseconds together with their associated standard deviations (column three in the table) also expressed in units of milliseconds. These results have been computed using the formulation given in equation (7.11). The assumptions used to compute the axial relative oceanic angular momentum variations ( $\Delta h_3^{ocean}$ ) are given in Chapter 7. It should be noted that these results reflect an one-sided integration of the variable ocean current fields over 250 metres of oceanic depth (cf. detailed explanation in Section 7.3).

days since 1/1/86	oceanic $\Delta$ LOD (ms)	sigma (ms)
320.00	-0.007662	0.0333
337.00	-0.036052	0.0332
354.00	-0.065782	0.0325
371.00	-0.084312	0.0329
388.00	-0.066908	0.0329
405.00	-0.071069	0.0327
422.00	-0.078847	0.0328
439.00	-0.096330	0.0331
456.00	-0.069352	0.0329
473.00	-0.096349	0.0332
490.00	-0.043034	0.0319
507.00	-0.026319	0.0331
524.00	-0.063913	0.0329
541.00	-0.049579	0.0334
558.00	-0.021365	0.0360
575.00	0.003185	0.0341
592.00	0.010285	0.0330
609.00	-0.001489	0.0342
626.00	-0.021937	0.0341
643.00	-0.043005	0.0333
660.00	-0.042358	0.0338
677.00	-0.051022	0.0331
694.00	-0.000474	0.0407
711.00	-0.090504	0.0338
728.00	-0.009311	0.0324
745.00	-0.064536	0.0336
762.00	-0.077783	0.0353
779.00	-0.085947	0.0344
796.00	-0.056541	0.0331
813.00	0.005948	0.0335
830.00	-0.028242	0.0336
847.00	-0.073263	0.0322
864.00	0.005866	0.0339
881.00	-0.057171	0.0361
898.00	-0.057965	0.0366
915.00	0.034281	0.0363
932.00	0.228251	0.0341
949.00	0.256133	0.0350
966.00	0.160285	0.0372
983.00	0.166355	0.0310
1000.00	0.137397	0.0333
1017.00	0.207309	0.0330
1034.00	0.225762	0.0327
1051.00	0.197365	0.0339

## Appendix III

This Appendix contains the computed spectra of the GEOSAT/ERM derived ROAM results for different latitude belts. The ROAM results have been obtained by varying the domain of integration in latitude in equation (7.9) or equivalently the summation in equation (7.10).

Northern Hemisphere corresponds to:  $4^{\circ}N < \phi < 65^{\circ}N$ .

Northern Tropics correspond to:  $4^{\circ} < \phi < 23^{\circ}N$ .

Northern Midlatitudes correspond to:  $25^{\circ}N < \phi < 45^{\circ}N$ .

Southern Hemisphere corresponds to:  $4^{\circ}S < \phi < 65^{\circ}S$ .

Southern Tropics correspond to:  $4^{\circ}S < \phi < 23^{\circ}S$ .

Southern Midlatitudes correspond to:  $25^{\circ}S < \phi < 45^{\circ}S$ .

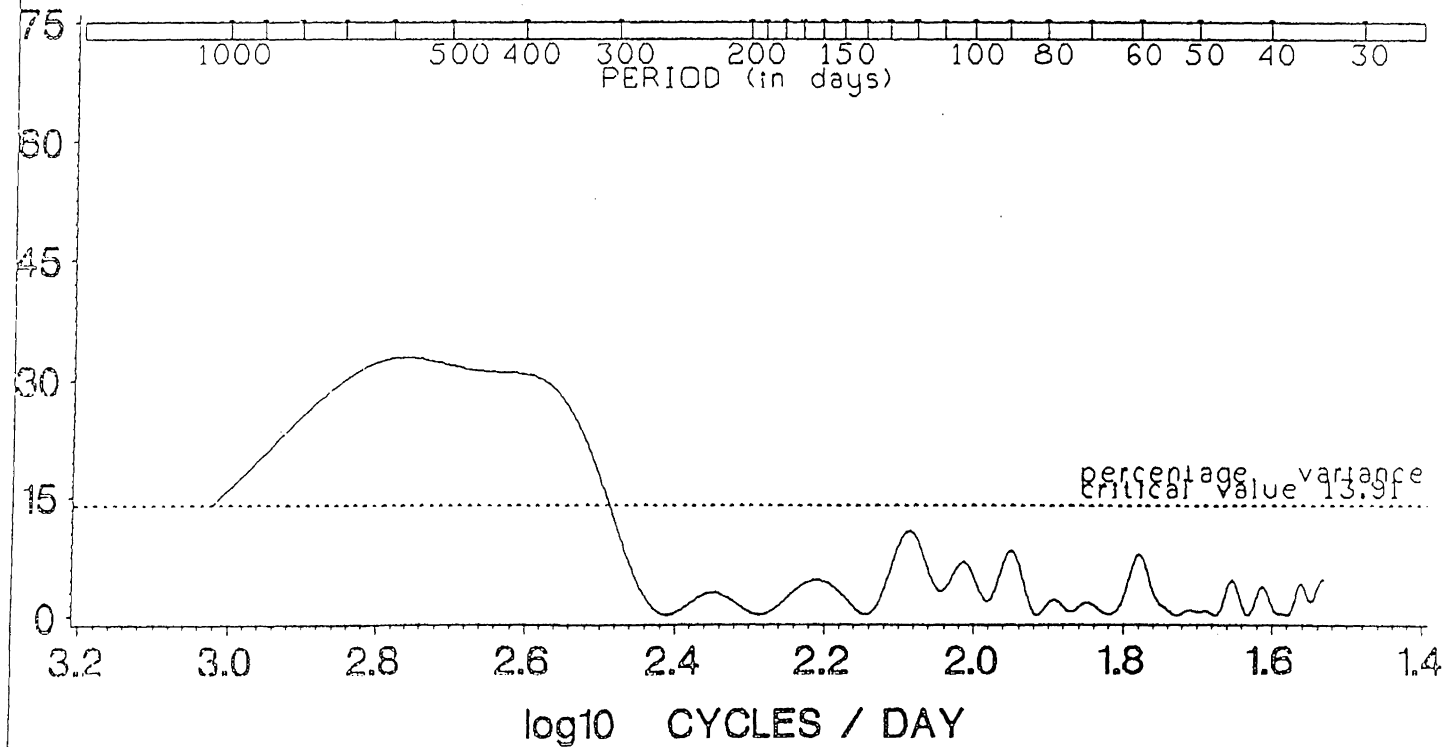
Antarctic Circumpolar Current (ACC) corresponds to:  $45^{\circ}S < \phi < 65^{\circ}S$ , i.e., the mid-axis of the current was assumed to lie at  $55^{\circ}S$ .

GEOSAT Analysis of 44 ERM's -> Nov. 1986-1988 <- N. HEMISPHERE

TIME SERIES SPECTRUM AFTER REMOVAL OF: Bias and Linear Trend

Forced Periods: NONE

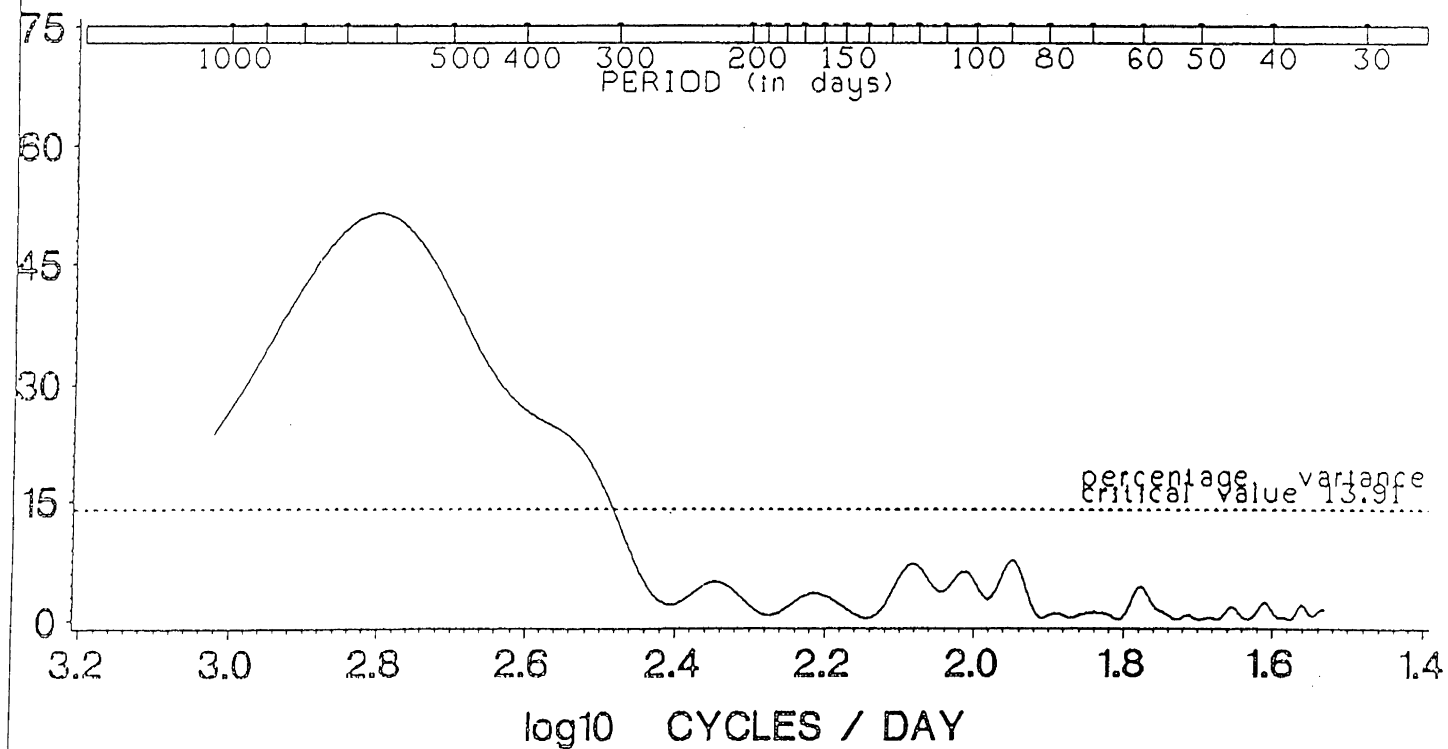
Y-axis: Percentage Variance of Relative Oceanic Angular Momentum



GEOSAT Analysis of 44 ERMs -> Nov. 1986-1988 <- N. T R O P I C S  
TIME SERIES SPECTRUM AFTER REMOVAL OF: Bias and Linear Trend

Forced Periods : NONE

Y-axis : Percentage Variance of Relative Oceanic Angular Momentum

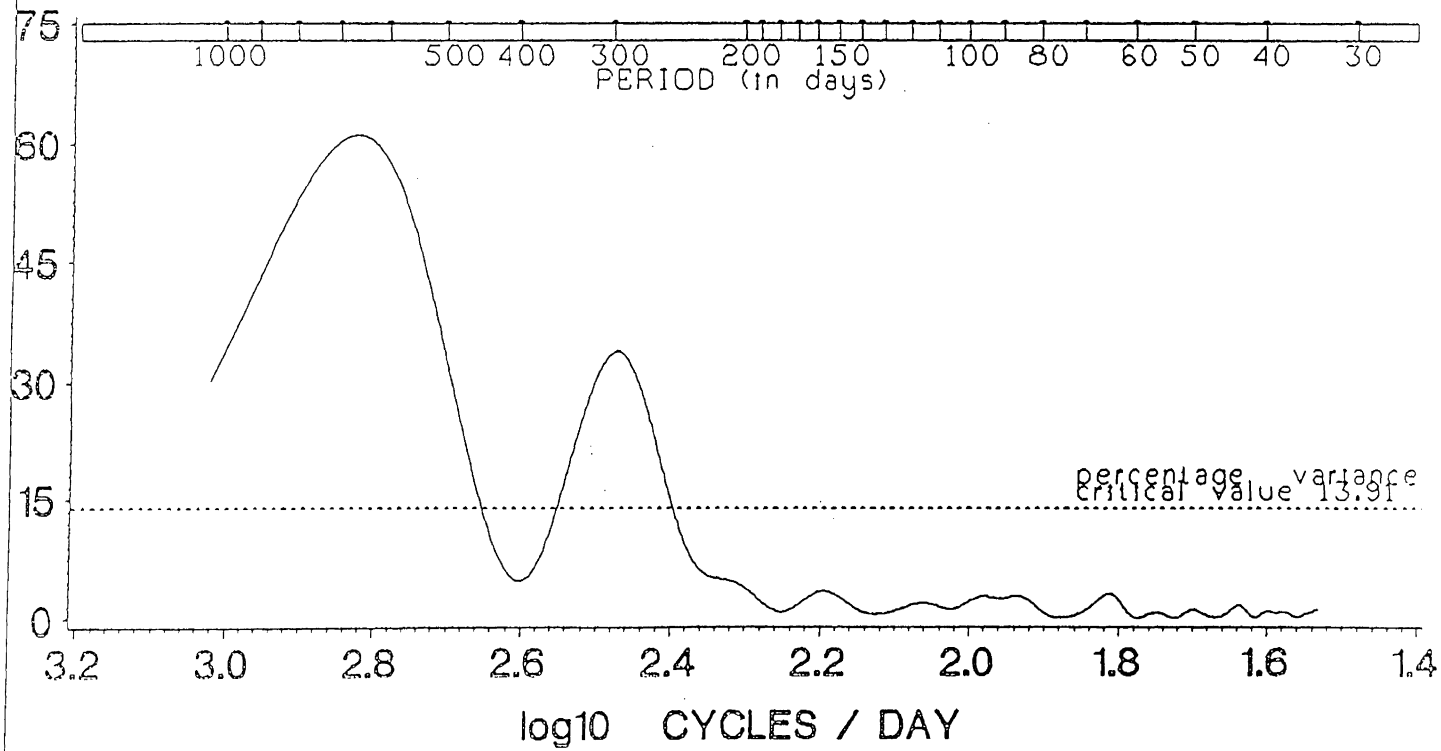




GEOSAT Analysis of 44 ERM's -> Nov. 1986-1988 <- NORTH 25 to 45  
TIME SERIES SPECTRUM AFTER REMOVAL OF: Bias and Linear Trend

Forced Periods : NONE

Y-axis : Percentage Variance of Relative Oceanic Angular Momentum

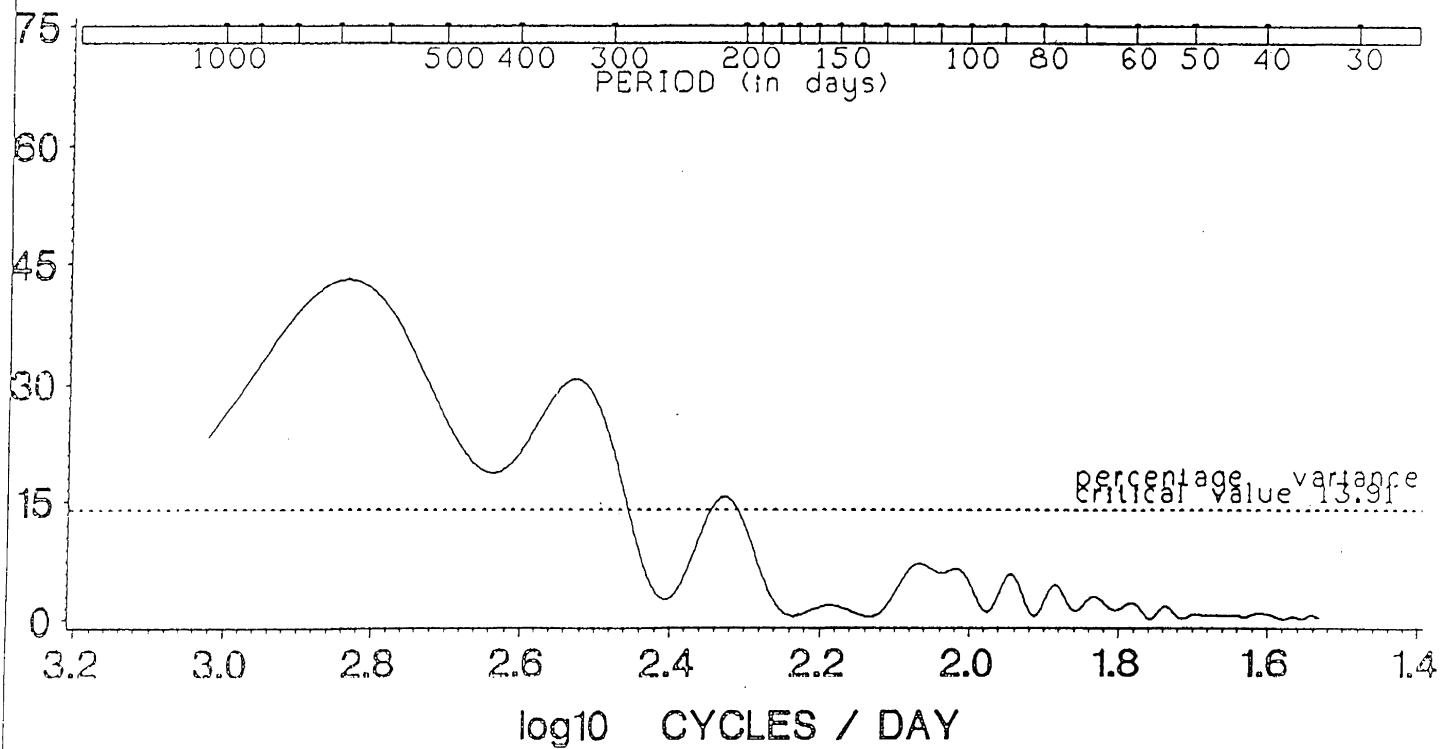


*GEOSAT Analysis of 44 ERMs -> Nov. 1986-1988 <- S. HEMISPHERE*

*TIME SERIES SPECTRUM AFTER REMOVAL OF: Bias and Linear Trend*

*Forced Periods : NONE*

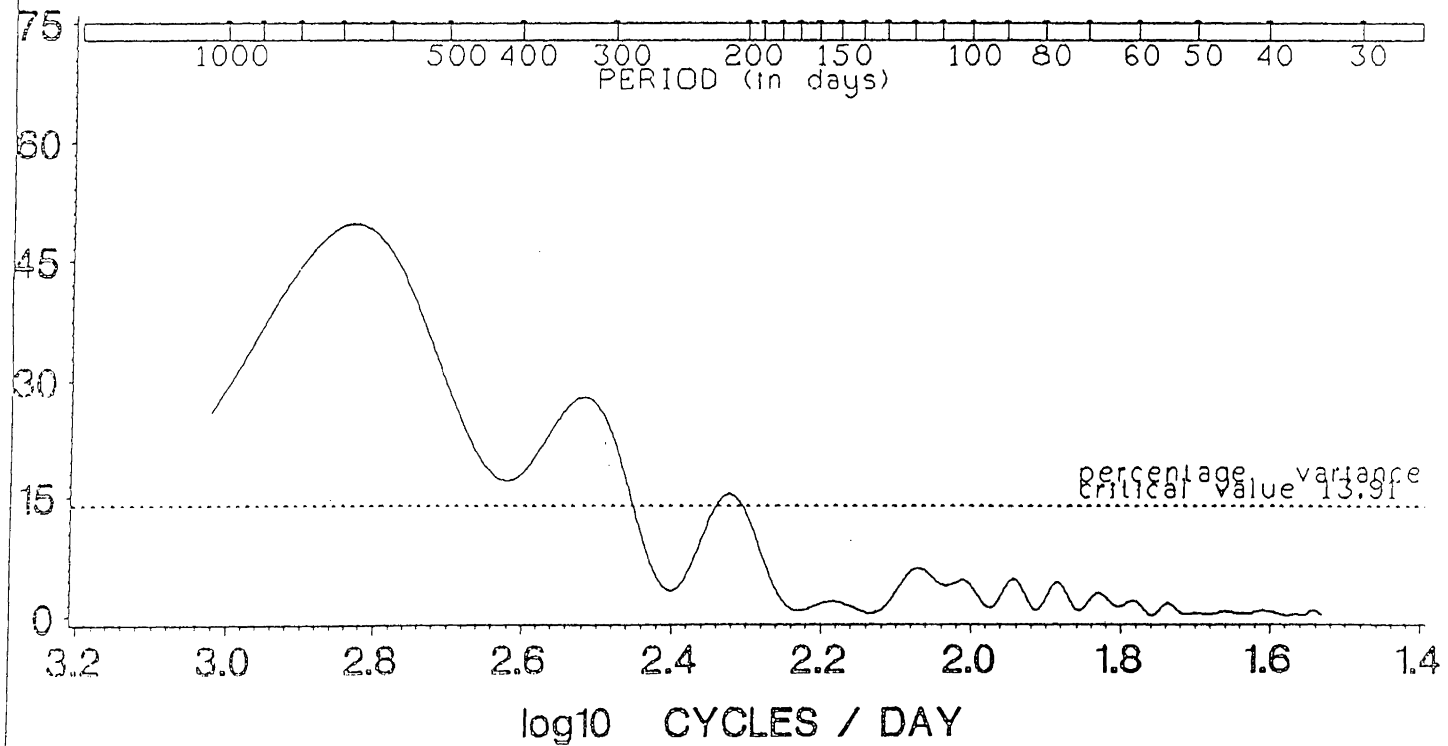
*Y-axis : Percentage Variance of Relative Oceanic Angular Momentum*



*GEOSAT Analysis of 44 ERM's -> Nov. 1986-1988 <- S. T R O P I C S  
TIME SERIES SPECTRUM AFTER REMOVAL OF: Bias and Linear Trend*

*Forced Periods : NONE*

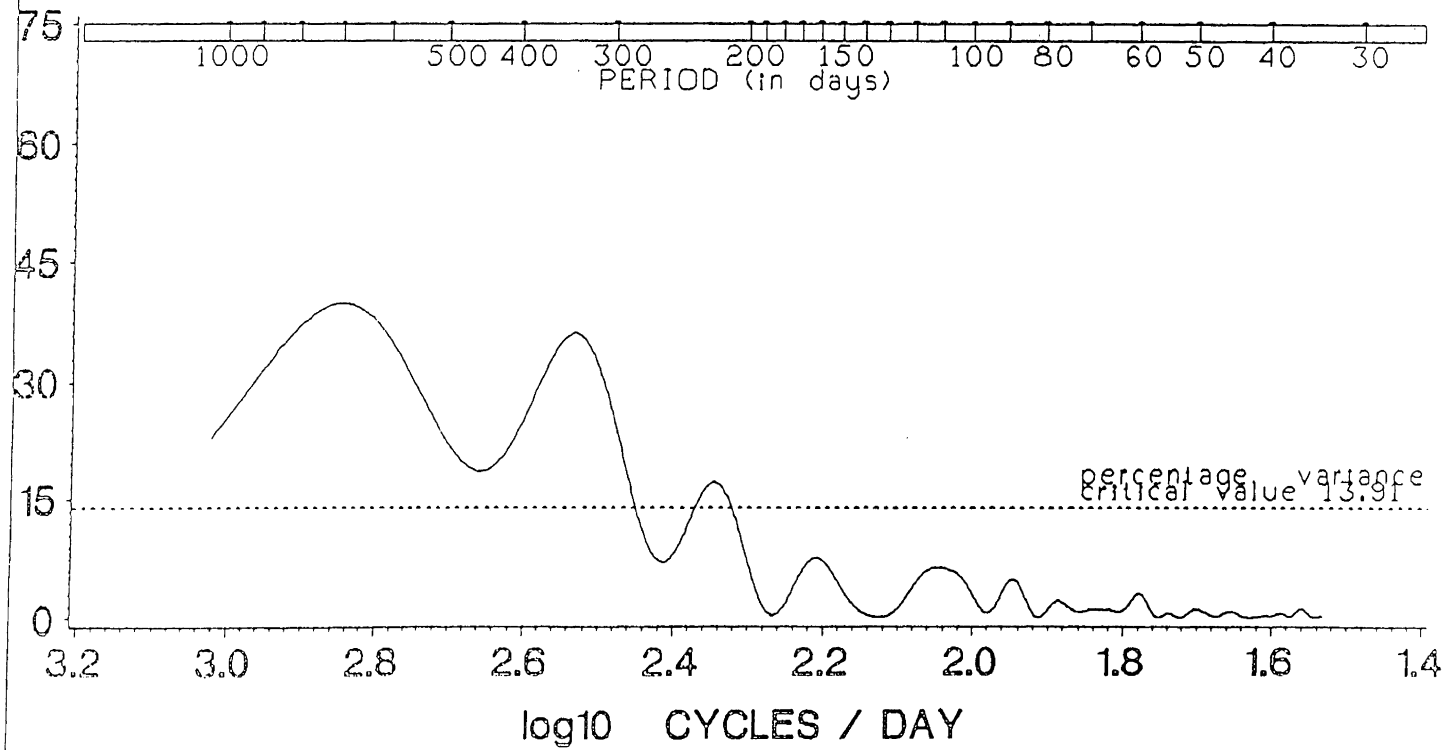
*Y-axis : Percentage Variance of Relative Oceanic Angular Momentum*



*GEOSAT Analysis of 44 ERMs -> Nov. 1986-1988 <- SOUTH 45 to 25  
TIME SERIES SPECTRUM AFTER REMOVAL OF: Bias and Linear Trend*

*Forced Periods : NONE*

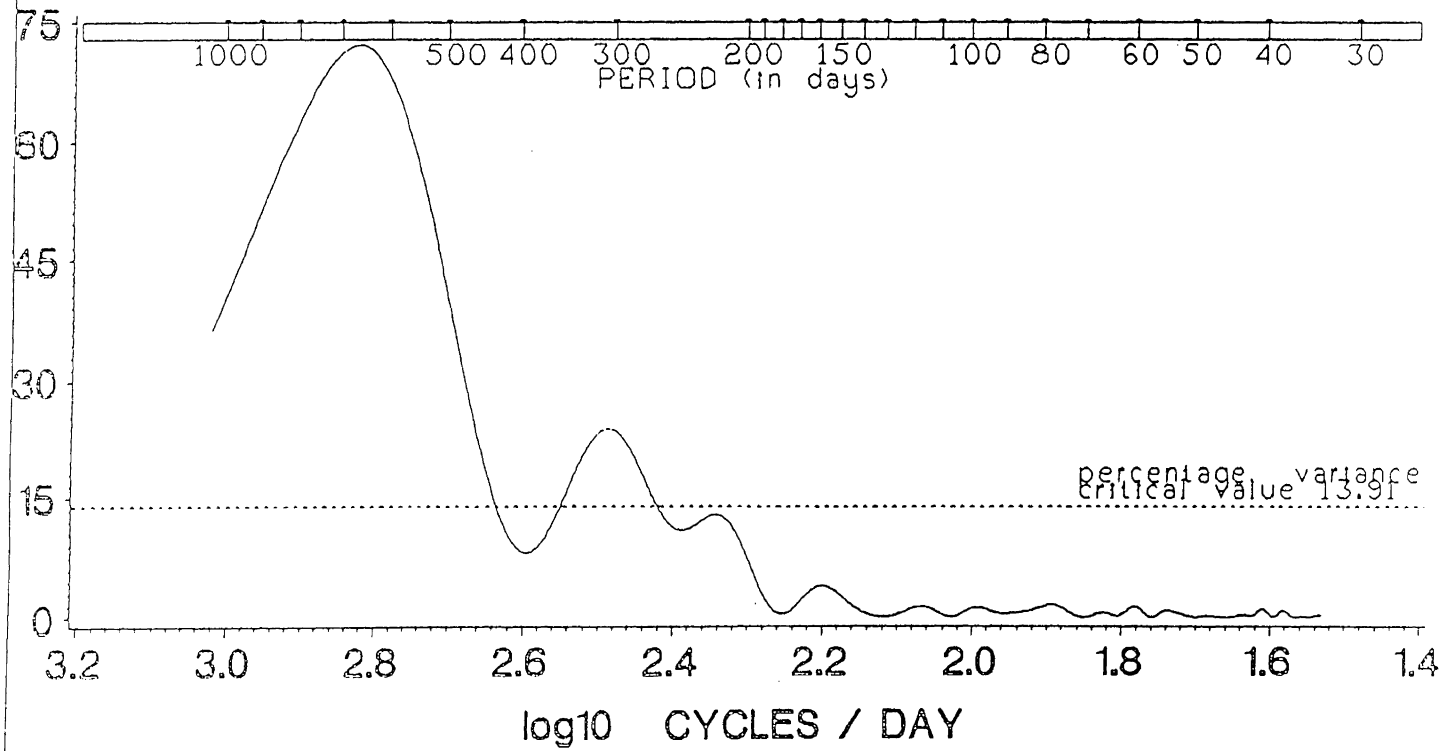
*V-axis : Percentage Variance of Relative Oceanic Angular Momentum*



*GEOSAT Analysis of 44 ERMs -> Nov. 1986-1988 <- A C C 65S to 45S  
TIME SERIES SPECTRUM AFTER REMOVAL OF: Bias and Linear Trend*

*Forced Periods : NONE*

*Y-axis : Percentage Variance of Relative Oceanic Angular Momentum*



## VITA

Candidate's full name: Nikolaos Theodoros Christou

Place and date of birth: Athens, Greece  
May 06, 1956

Permanent address: 17 Olympos Street Kifissia, Athens GREECE 145-62

Universities attended: National Technical University of Athens (NTUA), Faculty of Rural and Surveying Engineering  
1974-1979 *Dipl. Ing.*.

University of New Brunswick, Department of Surveying Engineering,  
Fredericton, N. B.  
1980-1983 *M. Sc. E.*.

University of New Brunswick, Department of Surveying Engineering,  
Fredericton, N. B.  
1983-1990 *Ph. D.* candidate.

## PUBLICATIONS

- Christou, N. (1990). "Seasonal Mean Dynamic Topography Maps of the Global Ocean for Oceanography, Geodesy and Geodynamics." (submitted to *EOS, Transactions of the American Geophysical Union.*)
- Christou, N., P. Vaníček and C. Ware (1989). "Geoid and Density Anomalies." *EOS, Transactions of the American Geophysical Union, Vol. 70, No. 22, May 30*
- Vaníček, P., A. Kleusberg, R-G. Chang, H. Fashir, N. Christou, M. Hofman, T. Kling and T. Arsenault (1988). The Canadian Geoid. Department of Surveying Engineering, *Technical Report No. 129*, University of New Brunswick, Fredericton.
- Yazdani, R., N. Christou and E. Derenyi (1987). "Potential Applications of Digital Image Analysis Systems for Displaying Satellite Altimetry Data." *Photogrammetric Engineering and Remote Sensing, Vol. 53, No. 11*, pp. 1545-1548.
- Christou, N., A. Kleusberg, J. Mantha and S. Pagiatakis (1987). Satellite Altimetry Applications for Marine Gravity: Software. Department of Surveying Engineering, *Technical Memorandum TM-17*, University of New Brunswick, Fredericton.
- Vaníček, P., D.E. Wells, E. Derenyi, A. Kleusberg, R. Yazdani, T. Arsenault, N. Christou, J. Mantha and S. Pagiatakis (1987). Satellite Altimetry Applications for Marine Gravity. Department of Surveying Engineering, *Technical Report No. 128*, University of New Brunswick, Fredericton.
- Chang, R-G., N. Christou and H. Fashir (1986). Software for Geoid Computations. Department of Surveying Engineering, *Technical Memorandum TM-10*, University of New Brunswick, Fredericton.
- Yazdani, R., N. Christou and E. Derenyi (1986). "Processing of SEASAT Altimetry Data on a Digital Image Analysis System." *Proceedings of The Tenth Canadian Symposium on Remote Sensing*, Edmonton, Alberta, Canada, May.

Christou, N. (1983). Evaluation of Mathematical Models for Gyrocompass Behaviour: Error Modelling and Applications. Department of Surveying Engineering, *Technical Report No. 100*, University of New Brunswick, Fredericton.

Christou, N. (1982) " High Latitude Behaviour of the Gyrocompass: Its Performance and Its Deviations. " *Proceedings of the National Marine Meeting*, The Institute of Navigation, Cambridge, Massachusetts, USA, 27-29 October.

Nakos, A., S. Pagiatakis and N. Christou (1980). Time Variations of Gravity in the Area of Dionysos-Athens. Department of Geodesy, Faculty of Rural and Surveying Engineering, *Technical Report*, National Technical University of Athens, Athens, Greece, (in Greek).

#### CONFERENCE PRESENTATIONS

Christou, N. and R.B. Langley (1988). "Estimates of the Angular Momentum of the Global Ocean Derived from Mean Seasonal Dynamic Topography Fields." Presented at the American Geophysical Union Spring Meeting, Baltimore, MD, USA, 16-20 May (abstract: *EOS, Transactions of the American Geophysical Union, Vol. 69, No. 16, pp. 327*).

Christou, N., P. Vaníček, and C. Ware (1988). "Can the Geoid Add Anything to Our Knowledge of the Lithosphere?" Presented at the Canadian Geophysical Union 15th Annual Meeting, University of Saskatchewan, Saskatoon, Canada, 8-11 May.

Christou, N. and R. Yazdani (1986). "Processing of SEASAT Adjusted Altimetry Data." Presented at the Canadian Geophysical Union 13th Annual Meeting, Carleton University, Ottawa, Canada, 19-21 May.